THE UNIVERSITY *of* EDINBURGH

Enhancing glycosylated triterpenoid production in *Saccharomyces cerevisiae*

Jess Tallis

Thesis presented for the degree of Doctor of Philosophy

Institute of Quantitive Biology, Biochemistry and Biotechnology

The University of Edinburgh

2023

Declaration

I declare that this thesis was composed by myself and that the work presented is my own, except where otherwise stated. This thesis has not been submitted for any other academic degree or professional qualification. The publication in Appendix A is my own work in collaboration with the other authors who are indicated and whose individual contributions are outlined within the publication.

Jess Tallis

29th September 2023

Table of Contents

Abstract

Glycosylated triterpenoids are secondary metabolites found in plants with numerous potential applications in medicine, food, agriculture, and household cleaning products. These compounds are produced through the cyclisation of 2,3-oxidosqualene by oxidosqualene cyclases. The resulting triterpenes can be further modified and oxidised by cytochrome P450 enzymes to form triterpenoids. Triterpenoids are then glycosylated by UDP-glycosyltransferases, resulting in the formation of glycosylated triterpenoids, commonly known as saponins. The diverse nature of these compounds allows for various modifications that are essential for their bioactivity. The industrial potential of glycosylated triterpenoids is extensive and encompasses a wide range of applications in home and personal care products, medicine, cosmetics and food. However, the production of glycosylated triterpenoids for industrial purposes poses significant challenges. In plants, the yield is low, and obtaining glycosylated triterpenoids can be influenced by factors such as seasonal growth and associated expenses. Synthetic production of these compounds is also exceedingly difficult due to their chiral nature and the sheer diversity of glycosylated triterpenoids. As a result, it has been established in the field to produce these compounds using microbial hosts, such as *Saccharomyces cerevisiae.* Although *S. cerevisiae* is a suitable host for glycosylated triterpenoid production, the yield of the desired product remains insufficient for industrial applications.

This study focuses on escin, a medically relevant glycosylated triterpenoid, currently unattainable in *S. cerevisiae* due to its inherent toxicity at elevated concentrations. There are well-known interactions of escin with cholesterol, leading to cell membrane disruption. This led us to investigate its potential analogous toxicity to the yeast membrane sterol, ergosterol. Our findings support this hypothesis, emphasising the need for identifying suitable *S. cerevisiae* sterol mutants as hosts for escin production. Importantly, this research demonstrates the potential of sterol biosynthesis mutants as chassis for glycosylated triterpenoid production. The key findings provide insights into

escin toxicity mechanisms, paving the way for developing robust microbial hosts for enhanced glycosylated triterpenoid production.

Lay Summary

Plant chemicals have significant potential for applications in medicine, food production, and cleaning products. However, plants produce these chemicals in limited quantities, which slows down their commercial use. Therefore, there is a need to explore alternative methods for producing these plant chemicals. One promising approach involves using baker's yeast as a production host by incorporating the necessary plant DNA into the yeast genome. This allows the yeast to make the desired plant chemicals. Yeast offers several advantages, including the ability to multiply quickly and good growth all year round. Nevertheless, certain plant chemicals, such as escin, remain challenging to produce in yeast due to their complex structure and toxicity to the yeast. This research aims to overcome these obstacles and develop a commercially viable method for producing escin, a toxic plant chemical, in baker's yeast.

List of Figures

List of Tables

Abbreviations

ACT	Acyltransferase
βAS	β-amyrin synthase
BAHD	Benzyl alcohol *O*-acetyltransferase, anthocyanin *O*-hydroxycinnamonyltransferase, N-hydroxycinnamoyl/benzoyltransferase, Deacetylvinoline 4-*O*-acetyltransferase
CBC	Chair-boat-chair conformation
CCC	Chair-chair-chair conformation
COX	Cyclooxygenase
CPR	NADPH-cytochrome P450 reductase
CSM	Complete synthetic media/minimal media
CYP	Cytochrome P450 monooxygenase
DCW	Dry cell weight
DIC	Differential interference constant
DMAPP	Dimethylallyl pyrophosphate
EIC	Extracted ion chromatogram
ER	Endoplasmic reticulum
Erg10p	Acetoacetyl-CoA thiolase
Erg11p	Lanosterol 14-alpha-demethylase
Erg12p	Mevalonate kinase
Erg13p	3-hydroxy-3-methylglutaryl-CoA (HMG-CoA) synthase
Erg19p	Mevalonate pyrophosphate decarboxylase
Erg20p	Farnesyl pyrophosphate synthetase
Erg25p	C4 methyl sterol oxidase
Erg26p	C3 sterol dehydrogenase
Erg27p	3-keto sterol reductase
Erg29p	Protein of unknown function
Erg2p	C8 sterol isomerase
Erg3p	C5 sterol desaturase
Erg4p	C24(28) sterol reductase

Erg5p	C22 sterol desaturase
Erg6p	Delta(24)-sterol *C*-methyltransferase
Erg7p	Lanosterol synthase
Erg8p	Phosphomevalonate kinase
Erg9p	Squalene synthase
Ex/em	Excitation/emission
FPP	Farnesyl pyrophosphate
G418	Geneticin
GCMS	Gas chromatography-Mass spectrometry
GFP	Green fluorescent protein
GPP	Geranyl pyrophosphate
IPP	Isopentyl pyrophosphate
HMG-CoAp	*3-hydroxy-3-methylglutaryl coenzyme A*
HR	Homologous recombination
Idi1p	Isopentenyl diphosphate dimethylallyl diphosphate isomerase
ITC	Isothermal titration calorimetry
Ka	Binding affinity
LCMS	Liquid chromatography-Mass spectrometry
LoFlo	Low fluorescence media
LUV	Lipid unilamellar vesicles
MEV	Mevalonate pathway
MIC	Minimum inhibitory concentration
MCC domain	Membrane compartment of Can1 domain
MPL	Monophosphoryl lipid A
NHEJ	Non-homologous end joining
OD	Optical density
OSC	Oxidosqualene cyclase
PI	Propidium iodide
PCR	Polymerase chain reaction
PM	Plasma membrane
RT-qPCR	Real-time quantitative-PCR
SCPL	Serine carboxypeptidase-like ACTs
UDP	Uridine diphosphate

UGT	UDP-glycosyltransferase
WT	Wild type
YPD	Yeast peptone dextrose/rich media

Chapter 1: - Introduction

1.1 Glycosylated triterpenoids in nature

1.1.1 Diversity and Abundance

Traditional herbal medicine, which has existed for thousands of years, harnesses the capacity of plants to synthesise and accumulate small molecules, known as natural products (Croteau *et al*., 2000; Firenzuoli & Gori, 2007). These natural products play crucial roles in various physiological and ecological processes of plants while offering significant benefits to humans. With advances in our understanding of the production and pathway regulation of these small molecules, natural products derived from plants have emerged as high-value commodities in fields such as medicine, household and cleaning products, cosmetics, fragrances, food additives, and colourants. Plant natural products can be categorised into groups such as alkaloids, flavonoids, lignans, and terpenoids (Croteau *et al*., 2000).

Among these natural products, terpenoids stand out as a remarkable class, comprising more than 80,000 compounds. They represent the largest group of secondary metabolites and are characterised by immense chemical and structural diversity, encompassing substances like steroids and carotenoids (Ashour *et al*., 2010; Christianson, 2017). Terpenoids originate from terpenes, which, in turn, are synthesised from the 5-carbon compound isoprene. The classification of terpenes depends on the number of isoprenoid units present in their structure (Table 1), which correlates with the quantity of carbons they contain. This classification results in mono- (two isoprenoid units, C10), sesqui- (three isoprenoid units, C15), di- (four isoprenoid units, C20), sester- (five isoprenoid units, C25), tri- (six isoprenoid units, C30), sesqua- (seven isoprenoid units, C35), and tetra-terpenes (eight isoprenoid units, C40) (Ashour *et al*., 2010). Terpenes can be subject to modifications that yield terpenoids, and further alterations can lead to the formation of glycosylated terpenoids (also referred to as

saponins) (Thimmappa *et al*., 2014). In this thesis, our primary focus will be on triterpenes, and consequently triterpenoids and glycosylated triterpenoids.

Table 1: - Classification of terpenes based on number of isoprene units and carbon atoms.

Isoprene units	Carbon atoms	Name	Examples	Reference
1	5	Hemiterpene	Isoprene, Tiglic acid, Angelic acid	Ludwiczuk *et al*., 2017
2	10	Monoterpene	Linalyl acetate, Menthol, Thymol	Trombetta *et al*., 2005
3	15	Sesquiterpene	Polygodial, Artbasin, Helenalin, Artemesinin	Paddon & Keasling, 2014; Ludwiczuk *et al*., 2017
4	20	Diterpene	Paclitaxel, Phytol, Sclareol	Ashour *et al*., 2010; Mosquera *et al*., 2021
5	25	Sesterterpene	Santonin, Hippolide E, Manoalide	Ashour *et al*., 2010; Ludwiczuk *et al*., 2017
6	30	Triterpene	Squalene, β-amyrin, Oleanolic acid	Ludwiczuk *et al*., 2017
7	35	Sesquaterpene	Tetraprenyl-β-curcumene	Sato *et al*., 2011; Sato, 2013; Mosquera *et al*., 2021
8	40	Tetraterpene	β-carotene; Lycopene, Zeaxanthin.	Ludwiczuk *et al*., 2017
9 - 30,000	> 40	Polyterpene	Rubber	Ashour *et al*., 2010; Ludwiczuk *et al*., 2017

Triterpenes comprise one of the most extensive classes of plant natural products, with over 20,000 reported variations (Hill & Connolly, 2013; Thimmappa *et al*., 2014), underscoring the vast diversity inherent in plants (Thimmappa *et al*., 2014). Triterpenoids have a ubiquitous presence across all domains of life. Among eukaryotes, they manifest as sterols, saponins, steroid hormones, and sterol analogues (Mallory *et al*., 1963; Stocco & Clark, 1996; Thimmappa *et al*., 2014; Hillier

& Lathe, 2019). Prokaryotes have hopanoids which act as sterol analogues, as well as carotenoids (Maoka, 2020). Archaea possess membranes composed of isoprenoid chains, analogous to terpenoids (Jain *et al*., 2014). These terpenoids exhibit diverse structures and functions, with some, like hopanoids and tetrahymanol, stabilising cell membranes, while others, such as cucurbitacins, act as defence mechanisms (Mallory *et al*., 1963b; Kaushik *et al*., 2015; Sáenz *et al*., 2015).

The realm of triterpenes covers over 100 distinct scaffolds, each giving rise to a vast spectrum of structures. More than 700 modified triterpene structures derived from these scaffolds have been identified, highlighting the remarkable diversity in triterpenoid molecules (Xu *et al*., 2005; Thimmappa *et al*., 2014; Hill & Connolly, 2020). These scaffolds undergo further modifications such as glycosylation, expanding the array of structures with extensive structural variation (Thimmappa *et al*., 2014).

Plant triterpenes, triterpenoids, and glycosylated triterpenoids (Figure 1) constitute secondary metabolites in plants and play diverse roles in plant growth, development, and defence mechanisms (Thimmappa *et al*., 2014). Triterpenes and triterpenoids are widespread across various plant kingdoms, including angiosperms (flowering plants), gymnosperms (conifers and ginkgoes), ferns (non-flowering vascular plants), bryophytes (mosses), algae (macroalgae such as seaweeds), lichens, and non-vascular plants (liverworts and hornworts) (Moses *et al*., 2014b). In contrast, glycosylated triterpenoids are primarily found in angiosperms, where they serve as secondary metabolites with a multitude of ecological functions, which are discussed in 1.1.2. However, they may also be present, albeit to a lesser extent, in marine invertebrates such as starfish (*Culcita* and *Asteroidea*) and sea cucumbers (*Holothuroidea*) (Williams & Gong, 2007; Bordbar *et al*., 2011; Liu *et al*., 2008; Osbourn *et al*., 2011; Moses *et al*., 2014b; Nakayasu *et al*., 2021).

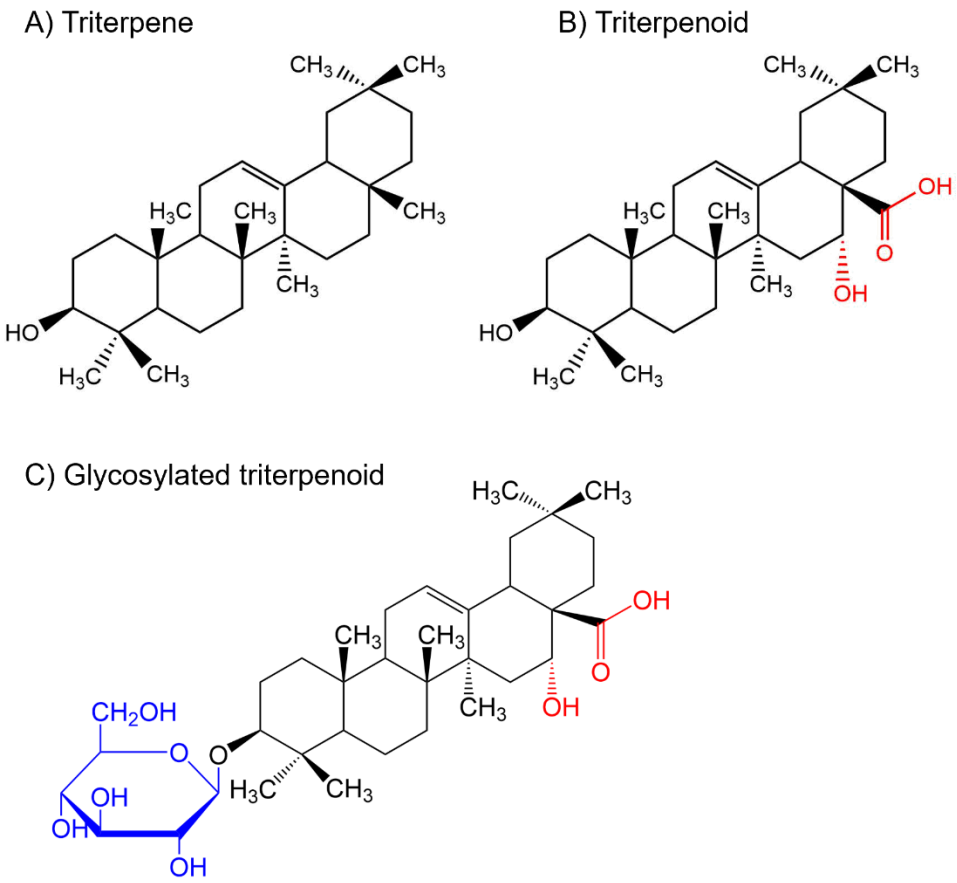

Figure 1: - The structures of a pentacyclic triterpene, triterpenoid and glycosylated triterpenoid. A) The triterpene shown is β-amyrin; B) the triterpenoid shown is echinocystic acid; C) the glycosylated triterpenoid shown is echinocystic acid-3-glucoside. Hydroxyl and carboxyl groups shown in red, glucose shown in blue.

Plants typically produce triterpenoids and glycosylated triterpenoids in relatively low concentrations. Take ginsenosides, for instance, which are glycosylated triterpenoids found in various parts of *Panax ginseng,* including the roots, leaves, stems, and fruit (Shi *et al*., 2007; Chung *et al*., 2016). Ginsenosides account for approximately 4 % of the root dry-cell weight and 7 % of the leaf dry-cell weight (Shi *et al*., 2007; Goodwin & Best, 2023). While these figures might initially appear significant, it's essential to note that ginsenosides encompass approximately 30 different structural variations within the same plant (Shi *et al*., 2007; Christensen, 2008; Goodwin & Best, 2023). This diversity significantly diminishes the dry-cell weight value for each ginsenoside.

This presents a significant challenge for the commercialisation of glycosylated triterpenoids. The inherently low concentration of these compounds in the plant,

combined with extended cultivation periods (typically 4-6 years for *P. ginseng*), results in very limited overall yields. The yield is roughly 4 % of the root dry weight, and 7 % of the leaf dry weight (Shi *et al*., 2007; Goodwin & Best, 2023).

1.1.2 Functional role of terpenoids, triterpenoids and glycosylated triterpenoids

Terpenoid biosynthesis in plants is intricately regulated due to its many roles in development and overall plant growth (Tholl, 2006; Nagegowda, 2010). Notably, terpenoid biosynthesis often occurs within specific plant tissues, demonstrated by specialised glandular trichomes dedicated to the synthesis of terpenoids intended for secretion and believed to serve as protective agents for the plant (Lange & Turner, 2013). For instance, *Arabidopsis thaliana* has specialised tissues that secrete volatile terpenoids, which not only attract pollinators but may also act as a defence mechanism against microbial pathogens, all while protecting the plant against photooxidative stress (Sharkey & Yeh, 2001; Loreto *et al*., 2004; Tholl, 2006).

Furthermore, certain terpenoids play vital roles in plant development, functioning as phytohormones or essential photopigments. Carotenoids, for instance, are tetraterpenoids that serve as pigments crucial for photo-protection, antioxidation, colour attractants, and as precursors to plant hormones. These compounds achieve this by capturing light energy and subsequently transferring it to chlorophyll, providing essential photo protection (Maoka, 2020).

Triterpenoids and glycosylated triterpenoids, being secondary metabolites, primarily play functional roles within the domain of plant defence mechanisms but have been shown to have some role in plant development as well. These metabolites predominantly serve as deterrents to pests and herbivores through mechanisms such as imparting a bitter taste or disrupting the cell membranes of potential attackers. This defensive function is notably observed in the fruits of bitter melon (*Momordica charantia*), which contain triterpenoids known as cucurbitacins. These compounds are

responsible for the fruit's bitter taste, a result of the unique ester bridge formation between positions C5 and C9 of the triterpenoid backbone (Figure 2; Takase et al., 2019).

Studies have shown that several glycosylated triterpenoids can slow down food passage through the gut, increase larval mortality, and decrease progeny per female in *Spodoptera littoralis (*Adel *et al*., 2000). Notably, the glycosylation of these triterpenoids also influenced their insecticidal activity, as the aglycones of the same compounds were found to exhibit lower toxicity in comparison (Nozzolillo *et al*., 1997; Adel & Sammour, 2012).

Studies on the glycosylated triterpenoid avenacin from oat root have demonstrated its significance in resisting soil-borne pathogens, such as the fungal pathogen *Gaeumannomyces graminis var. avenae*. Mutants affected in avenacin biosynthase lose their protection against these pathogens, highlighting the role of glycosylated triterpenoids in defence-related processes (Papadopoulou *et al*., 1999; Lambert *et al*., 2011). The anti-fungal properties of avenacins are thought to be attributed to their ability to form complexes with membrane sterols, compromising membrane integrity (Morrissey & Osbourn, 1999). Resistance to avenacins has been observed, where *G. graminis* produces an extracellular avenacinase that removes glucose from the sugar moiety of the glycosylated triterpenoid, underscoring the importance of the glycolic region in avenacin's defence against pathogens (Turner, 1960; Crombie *et al*., 1986).

Another example of the role of glycosylated triterpenoids in plant defence mechanisms come from *Barbarea vulgaris* R. Br. with 3-*O*-β-cellobiosyloleanolic acid. This glycosylated triterpenoid plays a crucial role in resisting *Plutella xylostella* (diamondback moth). In new leaves, a high concentration of 3-*O*-β-cellobiosyloleanolic acid provides resistance to diamondback moth larvae during the spring, but as the plant ages, the concentration decreases, and the leaves lose their resistance to diamondback moth feeding (Agerbirk *et al*., 2003; Badenes-Perez *et al*., 2014).

Triterpenes also play a significant role in plant development, as demonstrated by the presence of β-amyrin in oats. In oat plants, the presence of β-amyrin in the roots has been shown to influence their length and morphology. Elevated levels of β-amyrin in the roots lead to the development of shorter roots with a more densely-haired phenotype (Kemen *et al*., 2014). This, in turn, alters the fate of the root epidermis and consequently impacts overall plant development (Moses *et al*., 2014b).

Due to their highly toxic nature, glycosylated triterpenoids have attracted significant commercial interest as potential anti-pathogenic agents. This interest has led to the discovery that these compounds have diverse applications, ranging from medicinal uses to home care products, foodstuffs, and cosmetics. An example of this is found in medicine with Carbosan gel. This gel, designed for treating mouth and stomach ulcers, derives its main component from liquorice root, featuring the triterpenoid carbenoxolone as the active ingredient. It is synthesised by refluxing glycyrrhetic acid with an organic acid in the presence of an organic solvent and then neutralised by sodium hydroxide (Pindado *et al.,* 1996). Research has demonstrated that carbenoxolone stimulates mucous membranes, facilitating the protection of ulcers and expediting their healing process (Doll *et al.,* 1962; Pindado *et al*., 1996).

Beyond pharmaceuticals, plant metabolites contribute to the food industry, where glycyrrhizic acid has been used as a natural sweetener (Yang *et al.,* 2019). As well as in the cosmetic sector, where lupeol has found application as a skin-protective agent in moisturisers (Saleem *et al*., 2001; Saddique & Saleem, 2011). Due to these products being high value and produced in a low volume, the need for them in these different industries is warranted.

1.2 Glycosylated triterpenoid biosynthesis in plants

1.2.1 The Mevalonate pathway and production of 2,3-oxidosqualene

Glycosylated triterpenoids, have a triterpenoid backbone and are glycosylated with various sugar molecules, including glucose, fructose, and galactose. The synthesis of triterpenoids starts from terpene precursors, composed of repeating units of isopentenyl pyrophosphate (IPP) and dimethylallyl pyrophosphate (DMAPP), to produce a linear terpene backbone (Figure 2A), which is then cyclised to a triterpene (Figure 2B) (Wagner & Elmadfa, 2003; Thimmappa *et al*., 2014). Eukaryotes utilise the mevalonic acid pathway (MVA), while prokaryotes use the non-mevalonate pathway (MEP) to supply these precursors, and plants employ both MVA and MEP pathways.

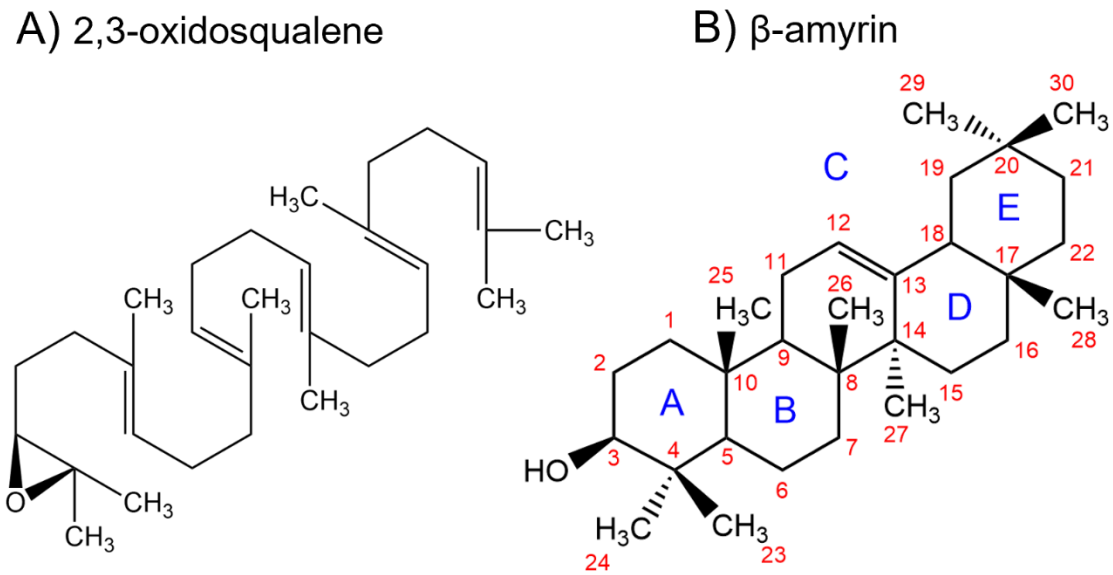

Figure 2: - Linear 2,3-oxidosqualene and cyclised β-amyrin. A) The linear structure of 2,3-oxidosquelene. B) The numbering and labelling convention for cyclised triterpenes. Carbons are numbered in red, and the rings are labelled in blue The triterpene shown is β-amyrin

Triterpenes undergo subsequent modifications through the action of cytochrome P450 monooxygenases (CYPs), leading to the formation of triterpenoids. These

triterpenoids are further altered by UDP-glycosyltransferases (UGTs) (Thimmappa *et al*., 2014). These modifications can occur at various positions along the triterpene backbone, resulting in a wide array of diverse triterpenoid structures (Moses *et al*., 2014). The following section provides an in-depth overview of the biosynthesis of glycosylated triterpenoids.

Biosynthesis of triterpenes, and in turn triterpenoids and glycosylated triterpenoids begins with two acetyl-CoA molecules. First two acetyl-CoA molecules are used in the mevalonate pathway (Figure 3). One of these proteins is acetylacetyl-CoA thiolase which transfers the acetyl group from acetyl-CoA to another molecule, producing acetoacetyl-CoA. This molecule is then converted to 3-hydroxy-3-methylglutaryl-CoA (HMG-CoA) by 3-hydroxy-3-methylglutaryl-CoA synthase. HMG-CoA is further reduced to mevalonate by HMG-CoA reductase (HMGRp; Hampton *et al*., 1996; Feldmann, 2012.), and this step is tightly regulated through negative feedback control.

Mevalonate is then utilised for the biosynthesis of farnesyl pyrophosphate (FPP), a process that occurs in the cytosol. FPP biosynthesis begins with the activation of mevalonate by mevalonate kinase, resulting in the production of mevalonate 5-phosphate. This is rapidly converted to mevalonate 5-pyrophosphate by phosphomevalonate kinase (Liao *et al*., 2016). These reactions rely on phosphate groups donated by ATP. Next, mevalonate pyrophosphate decarboxylase removes a carbon atom from the six-carbon mevalonate 5-pyrophosphate, introducing a double bond and yielding isopentenyl diphosphate (IPP; C5) (Miziorko, 2011; Liao *et al*., 2016). IPP serves as the foundation for all subsequent reactions in triterpene production (Liao *et al*., 2016). Isopentenyl diphosphate isomerase catalyses the isomerisation of IPP to dimethylallyl diphosphate (DMAPP; C5) (Moses *et al*., 2014; Kirby & Keasling, 2009). Then, farnesyl pyrophosphate synthetase facilitates the formation of farnesyl pyrophosphate (FPP) units. This occurs through the initial condensation of IPP and DMAPP to form geranyl pyrophosphate (GPP; C10), followed by the condensation of DMAPP to GPP to generate FPP (C15). Two FPP molecules are then converted to squalene (C30) via squalene synthase (SQS) and then to 2,3-oxidosqualene via squalene epoxidase (SQE) (Phillips *et al*., 2006; Liao *et al*., 2016).

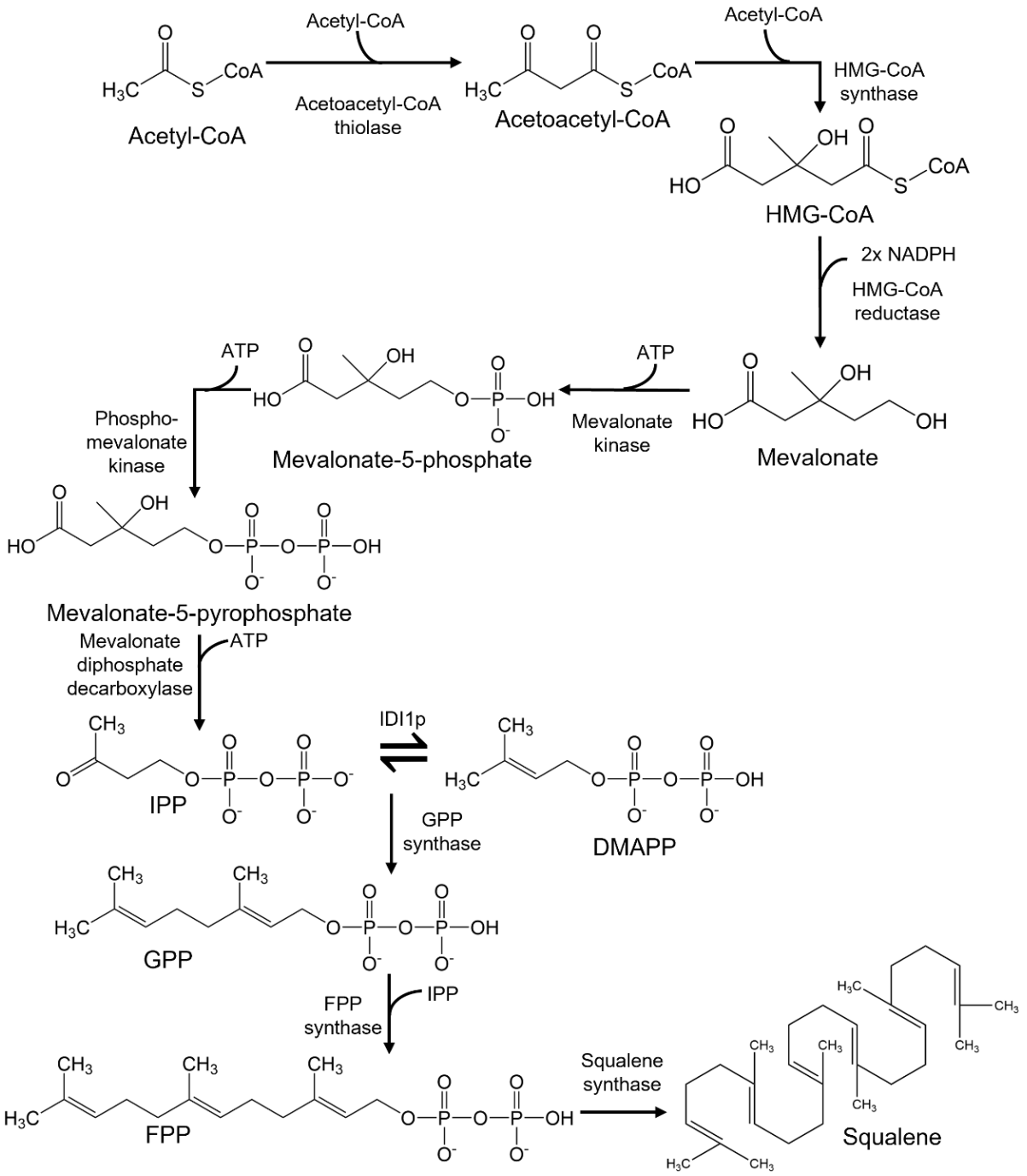

Figure 3: - Generation of farnesyl pyrophosphate from acetyl-coenzyme A (acetyl CoA) via the mevalonate pathway. The mevalonate pathway converts acetyl-CoA to isopentenyl pyrophosphate (IPP), a 5-carbon molecule, via 3-hydroxy-3-methylglutaryl coenzyme A (HMG-CoA) and mevalonate. In triterpenoid biosynthesis, mevalonate is used to produce IPP, which undergoes isomerisation to dimethylallyl pyrophosphate (DMAPP; 5C). GPP synthase joins the two molecules, forming geranyl pyrophosphate (GPP; 10C), and then adds another IPP to generate farnesyl pyrophosphate (FPP; C15).

1.2.2 Cyclisation of 2,3-oxidosqualene to triterpenes

The biosynthesis of triterpenes is catalysed by oxidosqualene cyclases (OSCs) in eukaryotes. These cyclise 2,3-oxidosqualene to produce either sterol or triterpene backbones (Augustin *et al*., 2011). In prokaryotes, non-oxidised squalene is cyclised to form a triterpene backbone alone (Volkman, 2005). The specific backbone produced depends on the orientation of cyclisation, with the chair-chair-chair (CCC) conformation leading to specialised triterpenes and the chair-boat-chair (CBC) conformation leading to sterols (Hoshino *et al*., 2012; Thimmappa *et al*., 2014) (Figure 4).

In animals and fungi, lanosterol synthase catalyses the cyclisation of 2,3-oxidosqualene, yielding lanosterol. This compound is subsequently converted into cholesterol in animals or ergosterol in fungi. On the other hand, in plants, cycloartenol synthase transforms 2,3-oxidosqualene into cycloartenol, which serves as the precursor for phytosterols (Thimmappa *et al*., 2014). Triterpene biosynthesis, including sterols, can be differentiated by the conformation of the first three rings during cyclisation. In triterpene biosynthesis, these rings adopt the chair-chair-chair (CCC) conformation, while in sterol biosynthesis, they adopt the chair-boat-chair (CBC) conformation (Thimmappa *et al*., 2014).

The initial cyclisation step in oxidosqualene cyclases (OSCs) is determined by whether they function as triterpene or sterol synthases. During this step, the OSC binds 2,3-oxidosqualene, which adopts either the CCC or CBC conformation (Thimmappa *et al*., 2014). An aspartate residue within the OSC catalyses the protonation of the epoxide group in 2,3-oxidosqualene, initiating the cyclisation process (Hoshino, 2017). This complex cyclisation involves multiple rounds of ring formation, subsequent ring expansion, and skeletal rearrangements, leading to various carbocation intermediates (Thimmappa *et al*., 2014; Hoshino, 2017). The deprotonation of the carbocation serves as the termination point for triterpene reactions, determining the resulting structure. This intricate process underscores the immense diversity of triterpenes. Numerous carbocations aren't depicted in Figure 4, contributing to the vast array of triterpene products (Thimmappa *et al*., 2014).

The protonation of 2,3-oxidosqualene initiates the formation of the A ring in triterpenes, which also incorporates a hydroxyl group derived from the epoxide in 2,3-oxidosquelene (Hoshino, 2017). Subsequently, the B, C, D and E rings form sequentially. Each ring generation involves the creation of a five-membered ring, followed by ring expansion yielding a six-membered ring (Hoshino, 2017). As the rings form, protonation shifts throughout the structure, giving rise to diverse carbocation intermediates. Consequently, each intermediate can result in a distinct triterpene, featuring varying ring sizes, positions of double bonds, and methyl group placements (Thimmappa *et al*., 2014; Hoshino, 2017).

The reaction terminates after deprotonation, leading to the formation of a double bond or the addition of a second hydroxyl group (Thimmappa *et al*., 2014). For instance, the cyclisation of 2,3-oxidosqualene in the CCC conformation produces the dammarenyl cation, featuring three 6-carbon rings and one five-carbon ring. Further expansion of the 5-carbon ring and generation of the 6-carbon ring led to the lupyl cation, which, upon deprotonation, yields the triterpene lupeol (Thimmappa *et al*., 2014; Hoshino, 2017). The oleanyl cation gives rise to β-amyrin, derived from five 6-carbon rings through the expansion of the germanicyl cation and a structural rearrangement to the oleanyl cation. Deprotonation ultimately results in β-amyrin formation (Thimmappa *et al*., 2014).

OSCs are categorised as mono- or multifunctional, with monofunctional OSCs producing a single triterpene and multifunctional OSCs generating multiple triterpenes. This classification is based on their ability to effectively terminate specific carbocation reactions. Ineffective termination can lead to the generation of multiple carbocations and, consequently, different triterpene products (Thimmappa *et al*., 2014). An instance of a multifunctional OSC is found in apples (*Malus domestica*), where the gene MdOSC4 encodes an OSC-producing germanicol, β-amyrin, and lupeol (Andre *et al*., 2016).

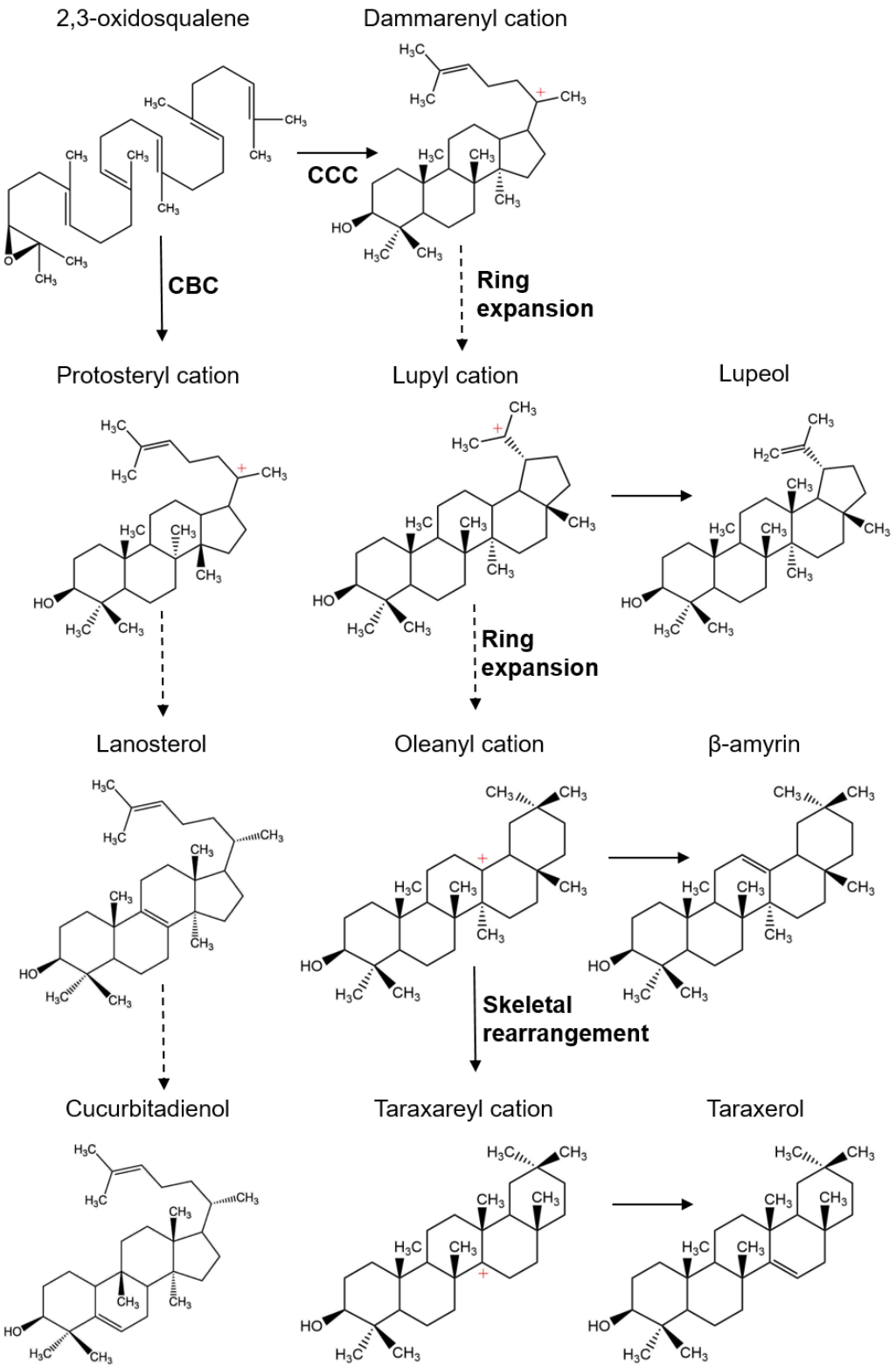

Figure 4: - 2,3-oxidosqualene cyclisation to produce triterpenes. 2,3-oxidosqualene can either form sterols via the chair-boat-chair (CBC) conformation or triterpenes via the chair-chair-chair (CCC) conformation. Dashed arrows represent multiple reactions.

1.2.3 Oxygenation of triterpene backbones

Following cyclisation, triterpenes undergo enzymatic modifications, such as oxygenation catalysed by cytochrome P450-dependent monooxygenases (CYPs). CYPs play a pivotal role in the biosynthesis of specific triterpenoids, facilitating the oxidation of the carbon backbone and yielding a diverse spectrum of triterpenoids (Fukushima *et al*., 2011; Fukushima *et al*., 2013; Thimmappa *et al*., 2014; Moses *et al*., 2014; Moses *et al*., 2014c; Ghosh, 2017; He *et al*., 2019) (Figure 5).

CYPs are conventionally categorised into families based on amino acid sequence identity; this grouping occurs when sequence identity is ≥ 40%. Subfamily members are further distinguished for those with ≥ 55% sequence identity (Bak *et al*., 2011; Nelson, 2011). The nomenclature for CYPs follows a specific pattern: the family is indicated by the first numeral after the CYP name, while the subfamily is denoted by the initial letter that follows (Nelson, 2009; Nelson, 2011).

Cytochrome P450 monooxygenases catalyse many reactions and are ubiquitously present across vertebrates, insects, fungi bacteria, archaea and viruses and are particularly abundant in plants, forming the largest family of biosynthetic enzymes (Nelson & Werck-Reichhart, 2011; Sezutsu *et al*., 2013). CYP-mediated catalysis (Figure 6) relies on activating and heterolytically cleaving molecular oxygen, incorporating one oxygen atom into the substrate while reducing the other to water (Bak *et al*., 2011). CYPs feature a catalytic centre comprising a haem moiety with iron coordinated to a cysteine residue's thiolate (Werck-Reichhart & Feyereisen, 2000; Graham & Peterson, 1999). For plant CYPs, the reaction necessitates electrons, which are supplied by NADPH-cytochrome P450 reductases (CPRs). These enzymes accept electrons from NADPH, channelling them to the CYP haem group (Werck-Reichhart & Feyereisen, 2000; Bak *et al*., 2011). Thus, CYPs require i) molecular oxygen, ii) cofactors like NADPH and haem and iii) CPR.

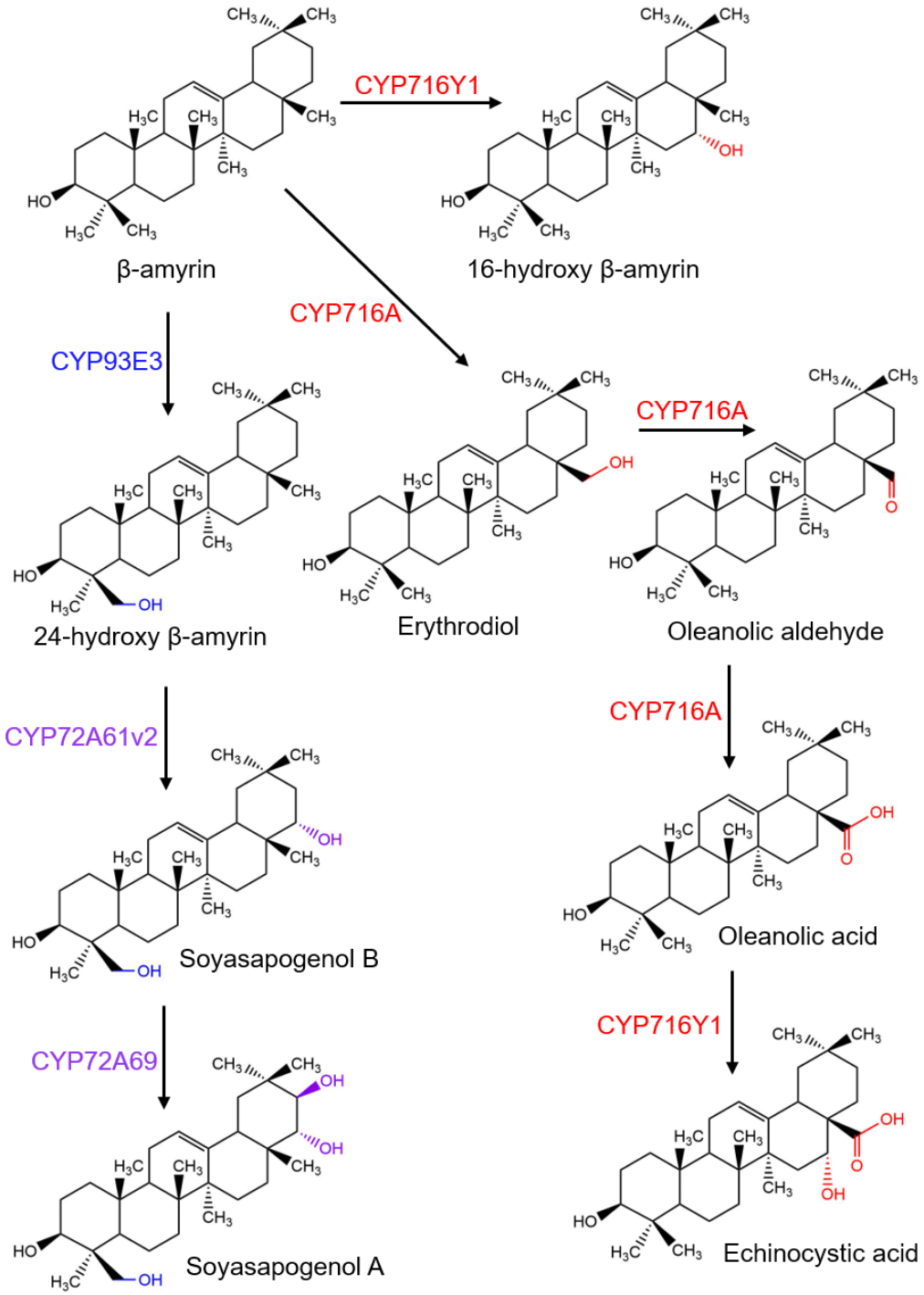

Figure 5: - Triterpenoid diversity. Oxygenation of β-amyrin by different cytochrome P450s. The oxygenation of triterpenes happens in multiple positions. Colours indicate the enzymes of the same group, CYP71; red, discovered in *Bupleurum falcatum*, and *Medicago trunculata*, CYP72; purple, discovered in *Medicago trunculata* and *Glycine max* and CYP93; blue, discovered in *Phaseolus vulgaris*.

CYPs exhibit regiospecificity, mediating alterations such as carboxylation, hydroxylation, epoxidation, and addition of aldehyde groups etc. on the triterpene backbone (Augustin *et al*., 2011; Geisler *et al*., 2013; Thimmappa *et al*., 2014; Miettinen *et al*., 2018). The modification of triterpenoids frequently involves multiple CYPs acting on the same triterpene backbone, resulting in numerous modifications (Moses *et al*., 2014; Arendt *et al*., 2017). Many CYPs possess multifunctional capabilities, overseeing multiple reactions. The entire family of the C28 oxidase family of CYPs possess multifunctional capabilities (Ghosh, 2017). For instance, *CYP716AL1* from *Catharanthus roseus* acts as a C28 oxidase, sequentially oxidising the C28 position of triterpenes and triterpenoids. Starting with α-amyrin, *CYP716AL1* oxidises the C28 position to yield uvaol and can further oxidise the same position to generate ursolic aldehyde and ursolic acid (Huang *et al*., 2012). Another example is CYP716A which hydroxylates the C28 position of β-amyrin to produce erythrodiol which in turn can be further oxidised twice to produce oleanolic aldehyde and oleanolic acid (Figure 5) (Ghosh, 2017). Additionally, CYPs can target various regions of the triterpene backbone; an instance is *CYP716A2* from *A. thaliana*, which hydroxylates β-amyrin at three distinct positions: C16, C22, and C28. Hence, a single CYP can produce multiple triterpenoids (Yasumoto *et al*., 2016).

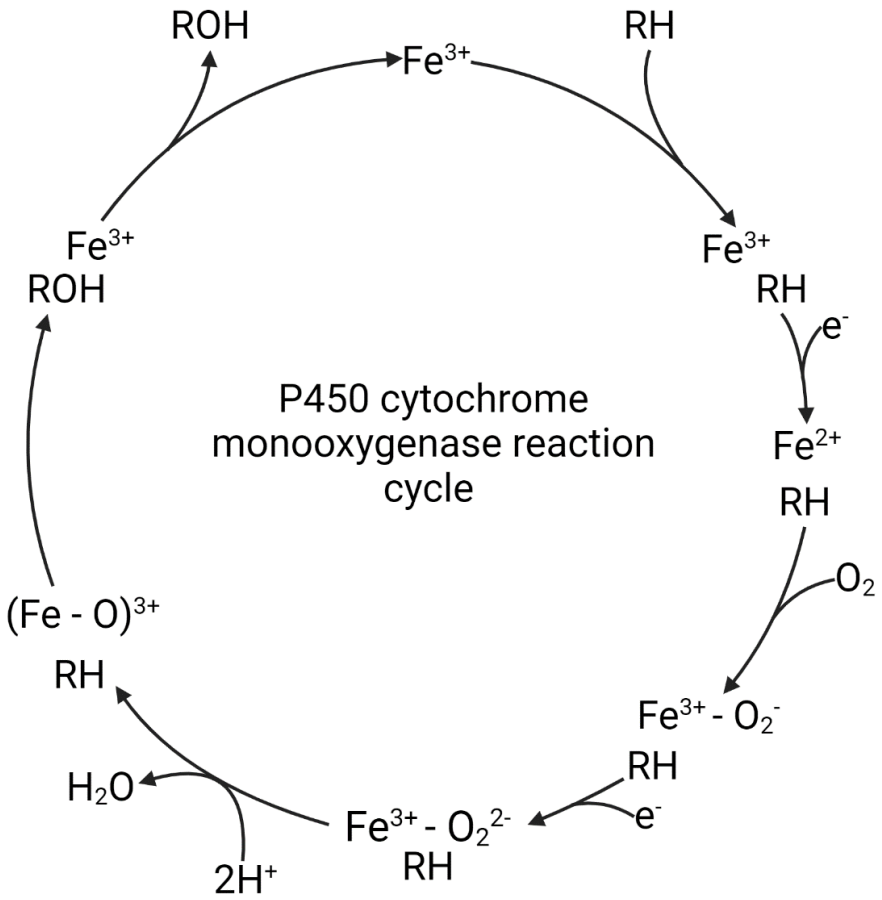

Figure 6: - The P450 cytochrome monooxygenase reaction cycle. The substrate, represented here as RH, is a triterpene molecule. The cycle starts with the binding of the substrate to the enzyme's active site, resulting in a reduction of the redox potential and necessitating an electron (e^-) donation from NADPH. This electron transfer alters the spin state of the haem iron within the active site. Subsequently, Fe^{3+} is reduced to Fe^{2+} through the donation of an electron from NADPH, facilitating the binding of oxygen (O_2) to Fe^{2+} to generate Fe^{3+} and O_2^-. The iron is then once again reduced, by another electron from NADPH. The oxygen molecule bound to the iron is subsequently cleaved, and it reacts with nearby protons to form water, resulting in the formation of $(Fe + O)^{3+}$. The oxygen ligated to the iron is then transferred to the triterpene substrate, leading to the creation of a hydroxylated triterpenoid, as depicted in this case. Following the formation of the triterpenoid, it is released from the active site, and the enzyme resets to its initial state (Hamdane et al., 2008). This figure was created using BioRender.com.

1.2.4 Glycosylation of triterpenoid backbones

Numerous functional groups introduced by CYPs can serve as targets for subsequent modifications, such as acetyltransferases and UDP-glucuronosyltransferases (UGTs) (Thimmappa *et al*., 2014; Moses *et al*., 2014). Glycosylation, catalysed by UGTs, contributes further diversity to triterpenoid products, yielding glycosylated triterpenoids, which are found exclusively in photosynthetic organisms (Pączkowski & Wojciechowski, 1994). The glycosylation process uses UDP-sugar donors to modify the triterpenoid substrate (Thimmappa *et al*., 2014). Monosaccharides are sequentially added, with common donors including UDP-arabinose, UPD-galactose, -glucose, -glucuronic acid, -rhamnose, and -xylose (Thimmappa *et al*., 2014; Augustin *et al*., 2011).

In pentacyclic triterpenoids, glycosylation primarily targets the C3 position (originating from the epoxide group in 2,3-oxidosqualene) or the CYP-modified C28 position typically featuring a carboxyl group (Thimmappa *et al*., 2014). In the C28 glycosylated triterpenoids, prior modification by a CYP from the CYP716A subfamily is necessary for the initial carboxylation of C28, which can then be glycosylated (Moses *et al*., 2014). The appended sugar moieties can exhibit linear or branched structures, generally encompassing 2-5 monosaccharides. Monodesmosidic glycosylated triterpenoids contain a single sugar chain, often glycosylated at the C3 region, while bidesmosidic counterparts have two sugar chains, situated at both the C3 and C28 positions. Examples of monodesmosidic glycosylated triterpenoids include escin, glycyrrhizin, lessonioside, avenacin (Figure 7A). Bidesmosidic glycosylated triterpenoids include soyasaponin Aa (Figure 7B), leiyemudanoside A and ginsenoside. Glycosylated triterpenoids with three sugar chains, known as tridesmosidic, are less common and include 3-O-β-D-xylopyranosyl-6-Oβ-D--glucopyranosyl-16-O-β-D-glucopyranosyl-3β,6α,16β, 24 (S)-25-pentahydroxycycloartane (Figure 7C) (Oleszek *et al*., 1992; Vincken *et al*., 2007; Augustin *et al*., 2011; Augustin *et al*., 2012; Owatworakit *et al*., 2013; Katano *et al*., 2015; Rehan *et al*., 2020).

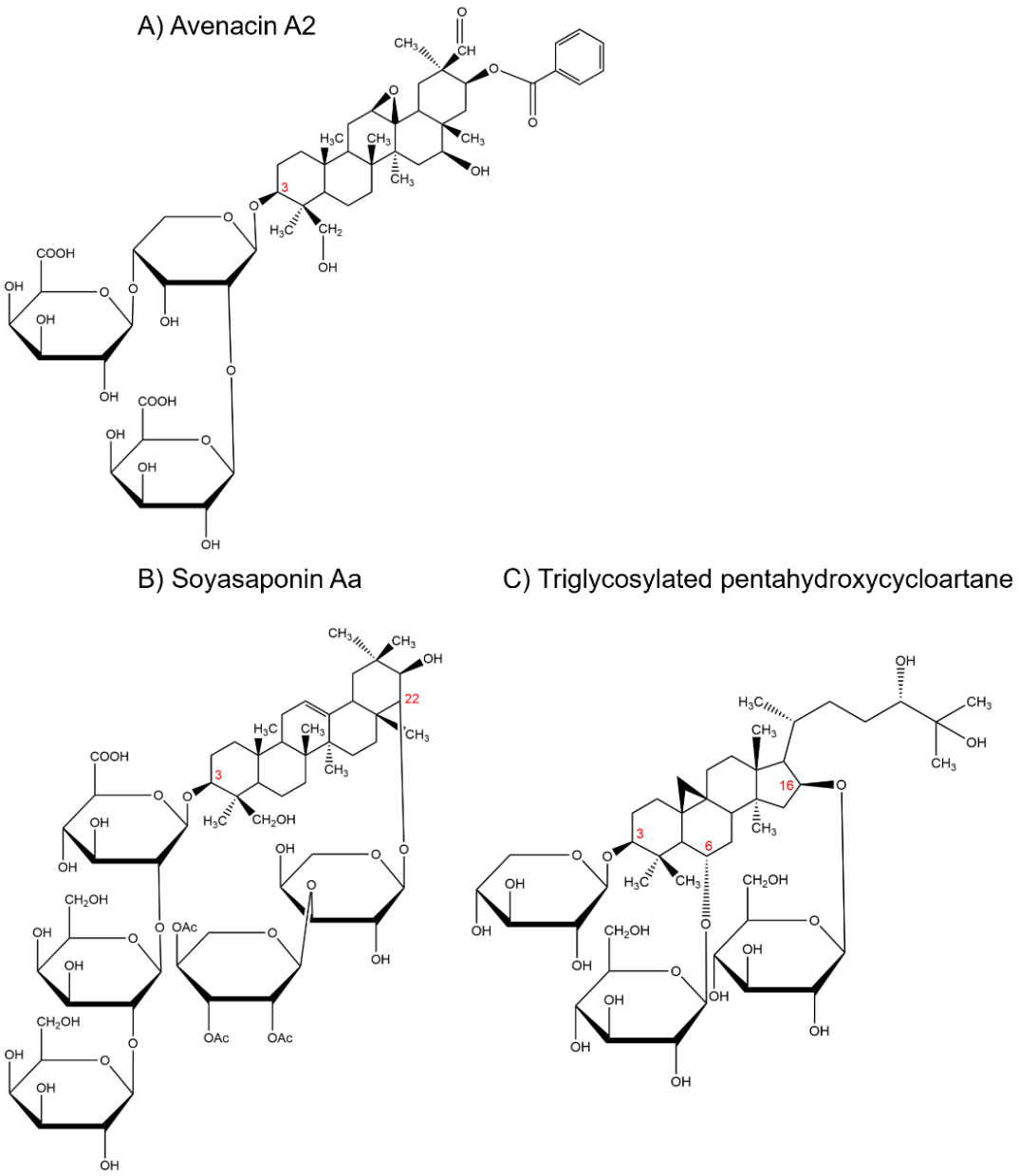

Figure 7: - Glycosylated triterpenoids with differing numbers of sugar moieties. A) The monodesmosidic glycosylated triterpenoid avenacin A2, with a single chain of arabinose and two glucose moieties branching from the C3 position of the triterpenoid backbone. B) The didesmosidic glycosylated triterpenoid soyasaponin Aa with two sugar chains branching from positions C3 and C22. Soyasaponin Aa contains glucose, glucuronic acid, arabinose and acetyl xylose C) The tridesmosidic glycosylated triterpenoid 3-O-β-D-xylopyranosyl-6-Oβ-D--glucopyranosyl-16-O-β-D-glucopyranosyl-3β,6α,16β, 24 (S)-25-pentahydroxycycloartane which contains sugar moieties at position C3, C6 and C16. This glycosylated triterpenoid contains glucose and xylose.

An example of triterpenoid glycosylation from a single precursor to produce multiple products is glycyrrhetinic acid glycosylation (Figure 8). Cellulose-synthase-derived glycosyltransferases (CSyGTs), identified in various plants, add a glucuronic acid to the C3 position of glycyrrhetinic acid, forming glycyrrhetinic acid 3-*O*-monoglucuronide. This intermediate can undergo further modification by UGT73P12, adding another glucuronic acid to yield glycyrrhizin. Alternatively, UGT73F13 can modify glycyrrhetinic acid to produce glycyrrhetinic acid 3-*O*-monoglucoside, with a glucose moiety at C3 rather than glucuronic acid (Chung *et al*., 2020).

Like CYPs, UGT families are categorised based on amino acid sequence similarity; families feature an amino acid sequence identity of > 40 %, and subfamilies exhibit > 60 % amino acid sequence identity (Augustin *et al*., 2011).

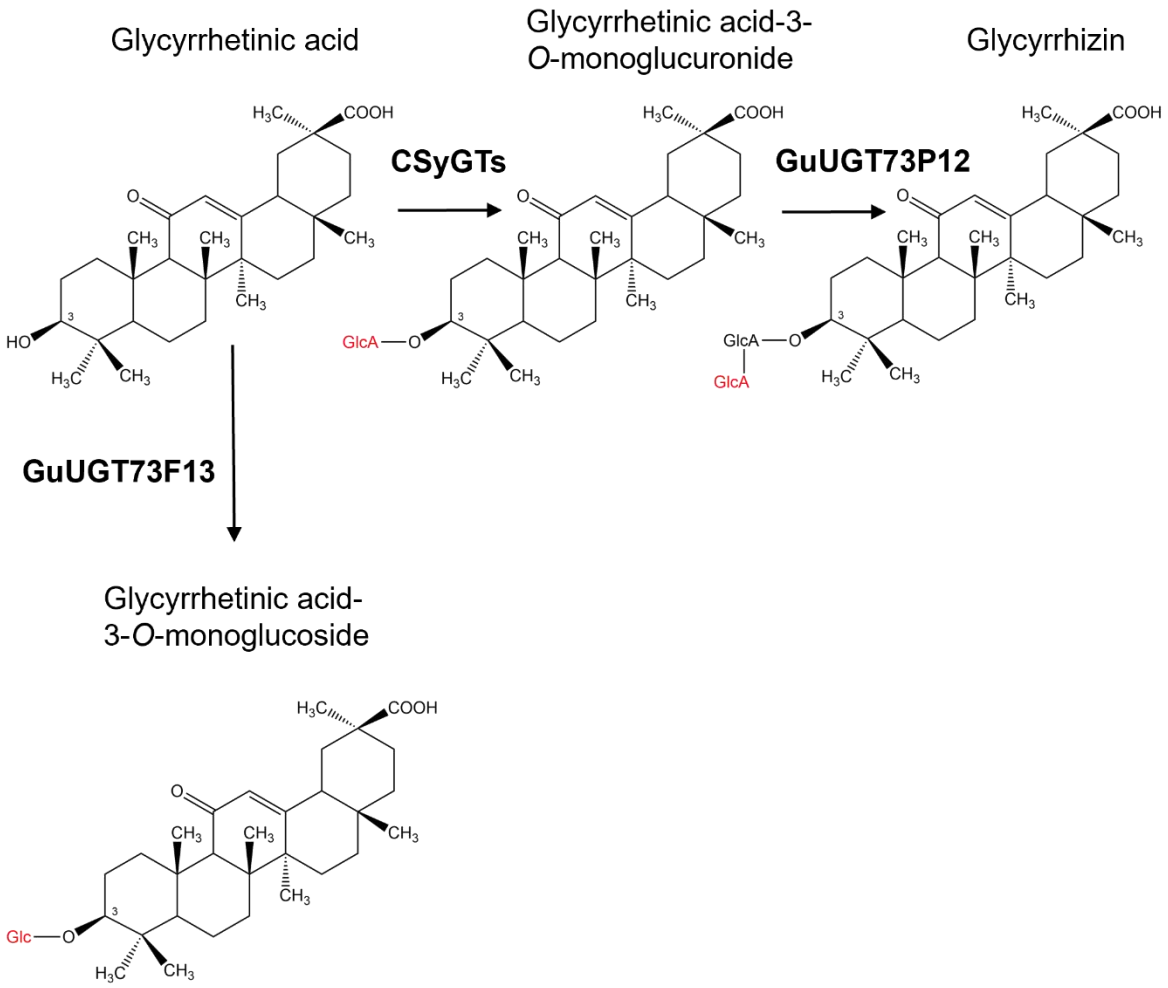

Figure 8: - Glycosylation patterns of triterpenoids. Glycosylation reactions involving glycyrrhetinic acid are depicted, including the attachment of a glucuronic acid via cellulose-synthase-derived glucosyltransferase (CSyGT) and *Glycyrrhiza uralensis* UGT73P12 (GuUGT73P12), resulting in the formation of glycyrrhizin. An alternate glycosylation pathway mediated by *G. uralensis* UGT73F13 (GuUGT73F13) involves the addition of a glucose moiety, yielding Glycyrrhetinic acid 3-O-monoglucoside. Figure adapted from Chung *et al.,* 2020.

1.2.5 Other modifications of the triterpenoid backbone

In addition to glycosylation, further modifications, such as acylation, methylation, malonylation, and epoxide hydrolysis, can also occur (Moses *et al*., 2014; Itkin *et al*., 2016; Cárdenas *et al*., 2019). Acylation can take place on sugar chains or the aglycone, and it has been shown to significantly impact the bioavailability and bioactivity of glycosylated triterpenoids (Ragupathi *et al*., 2011; Chan, 2007; Al Qathama *et al*., 2020). Plant acylation is mediated by acyltransferases (ACTs), which belong to two distinct families differing in their acyl donors and subcellular localisation. The first family, known as BAHDs, utilise acyl-CoA thioesters as acyl donors and are located in the cytosol. The second family, serine carboxypeptidase-like ACTs (SCPLs), employ acyl-sugar derivatives as acyl donors and are confined to the vacuole (Milkowski & Strack, 2004; Bontpart *et al*., 2015).

Acylation can occur at various positions along the aglycone backbone, including C16, C22, C23, and/or C25, leading to vast structural diversity. For instance, over 80 glycosylated triterpenes with C16 acylation have been identified (Figure 9A). Twenty-seven have been found to have C23 acylation, and an additional 15 possess multiple acyl groups on the triterpene backbone (Figure 9B) within the Holothuroidea genus alone (Bahrami & Franco, 2016). Escin is another illustrative example of a triterpenoid featuring both glycosylation and acylation (Figure 9C). It is characterised by a glucuronic acid at the C3 position and the addition of two other sugars, along with acyl groups, commonly located at either positions C21 or C22 (Savarino *et al*., 2023).

Another intriguing example of a triterpenoid with diverse modifications is irpeksolactin F (Figure 9D). This triterpenoid possesses a hydroxyl group at position C16 and a branched side chain at position C17. Additionally, it features a 5,8-endoperoxy moiety, further contributing to the wide array of structures that can be produced (Tang *et al*., 2019). Other CYPs, such as CYP51H10 from *Avena spp*. have been shown to both hydroxylate at C16 and introduce an epoxide group at positions C12(13) on β-amyrin (Geisler *et al.,* 2013).

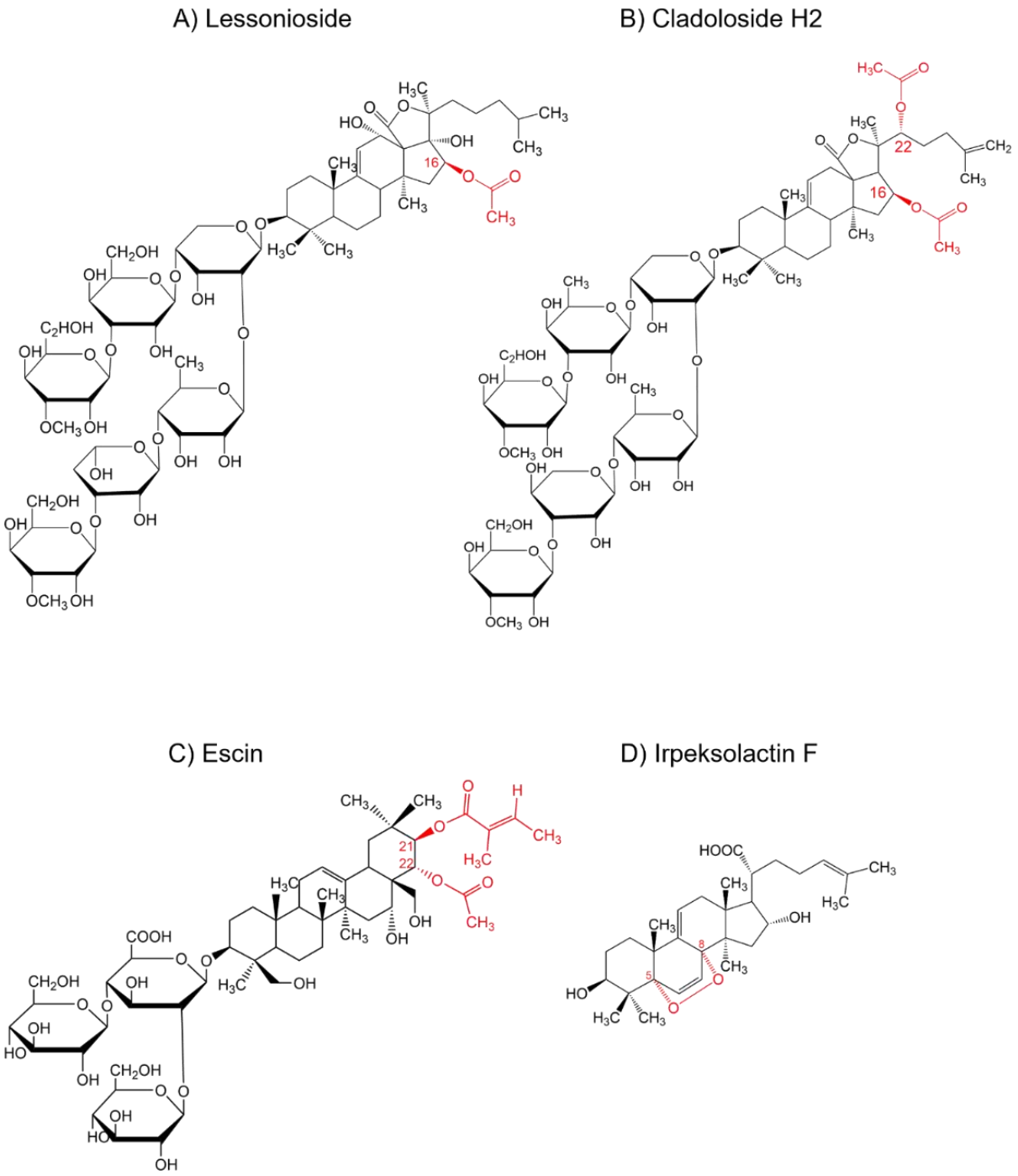

Figure 9: - Further modifications of triterpenoids. A) Lessonioside, a glycosylated triterpenoid with an acyl group modification at position C16. B) Cladoloside, a glycosylated triterpenoid with acyl group modifications at positions C16 and C22. C) Escin, a glycosylated triterpenoid with an acyl group modification at position C22 and a tiglic acid at position C21. D) Irpeksolactin F, a triterpenoid with an unusual endoperoxy bond at positions C5 and C8. Red in the figure represents the different modifications, attached acyl groups, acid groups and epoxide groups.

1.3 Commercial interest in triterpenoids

Triterpenoids and glycosylated triterpenoids are commercially very valuable. They have a wide range of uses in many different fields, from cosmetics (Malinowska *et al*., 2021), home care products (Chen *et al*., 2020b; section 1.3.1), healthcare (section 1.3.2) and gelling agents (Ghiulai *et al*., 2020). Moreover, these compounds find practical utility as feed additives, bacterial and vegetal growth regulators, soil remediation agents, foaming agents, and emulsifiers in water-based beverages across diverse industries (Cheeke, 2000; Roy *et al*., 1997; Martín & Briones, 2000). Notably, certain glycosylated triterpenoids, like tomatine and digitonin, contribute to healthier dairy products by removing cholesterol content (Micich *et al*., 1992). The high potential of triterpenoids and glycosylated triterpenoids as bulk surfactants and in medicine are reported in more depth below.

1.3.1 Triterpenoids as bulk surfactants

It is increasingly evident that the sustainable production of chemicals without relying on fossil fuels is a pressing priority across all scientific fields. The urgency to shift away from fossil fuel-based production towards more environmentally friendly alternatives is vital. The 2016 Paris Agreement is the commitment of all countries to reduce their carbon emissions and work together to reduce the impact of climate change. It states that the global average temperature increase should not exceed 1.5 ºC compared to pre-industrial levels (Paris Agreement). During the most recent United Nations Climate Change Conference (COP27) the progress made towards this goal was deemed insufficient with the current efforts to reduce the global temperature through the use of more sustainable alternative fuels (United Nations Climate Change). Therefore, there is a high priority for the reduction of greenhouse gas emissions and in this field, one way we can do this is by reducing our dependence on fossil fuels. Currently, surfactants are derived from both petrochemicals and oleochemicals and are extensively used in laundry detergents (41 % of the total production), industrial cleaners (18 %), hard surface household cleaners (11 %), dishwash household

products (11 %), domestic maintenance products (10 %), soaps (5 %) and domestic bleach products (4 %) (Karsa, 2006). However, this reliance on crude oil is unsustainable due to its decreasing global supply and the volatile nature of compounds released when in production (Hibbs, 2006). Glycosylated triterpenoids can act as surfactants (Figure 10A), which are compounds which display both hydrophobic and hydrophilic regions due to both polar and apolar areas of the molecule (Figure 10B). While plant-based alternatives, such as glycosylated triterpenoids, have been known for decades, their large-scale industrial production remains untapped.

When glycosylated triterpenoids are present in aqueous media, surfactants decrease the surface tension between the two phases. This is because in aqueous solution, the surfactant molecules will gather at the substrate (such as clothing) to minimise the contact of the hydrophobic region with water, forming micelles (Figure 10C; Figure 10E). The hydrophilic head groups stay in contact with the water, but the hydrophobic regions stay in contact with each other, and can be cylindrical, lamellar or spherical. Therefore, in aqueous media, the hydrophobic domains solubilise the substrate, removing it from the surface (Figure 10F) (Karsa, 2006).

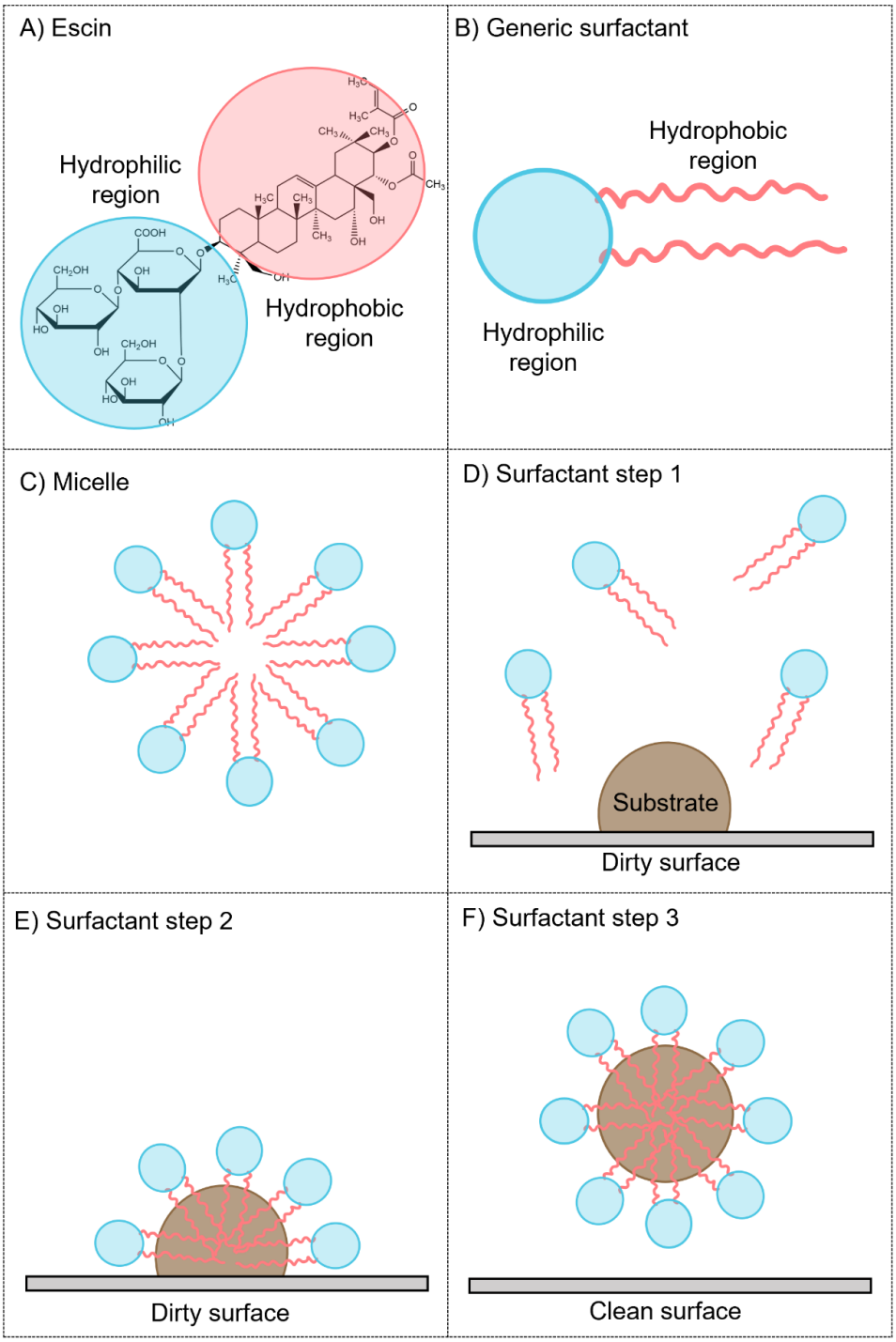

Figure 10: - Micelle formation. A) Escin and the hydrophilic and hydrophobic regions which correlates with B) showing the generic surfactant structure. C) Shows micelle formation with the hydrophobic regions joining together and the hydrophilic regions in contact with the aqueous environment. D) Surfactant solution in the presence of a dirty surface. E) The surfactant hydrophobic regions are absorbed by the substrate due to the difference in polarity, leaving the hydrophilic regions to contact the aqueous environment. F) Micelle formation with substrate removed from the surface.

Glycosylated triterpenoids present valuable products with surfactant properties that can be harnessed and produced in biological systems. Their amphiphilic nature, with a hydrophobic triterpenoid backbone and hydrophilic glycosidic region, enables the formation of micelles that effectively remove dirt from surfaces and clothing (Dargel *et al*., 2019). Additionally, glycosylated triterpenoids offer a more environmentally friendly and biodegradable alternative to conventional commercial surfactants, making them highly desirable (Schmitt *et al*., 2014; Honda *et al*., 2019).

1.3.2 Triterpenoids as Pharmaceuticals

In addition to their surfactant properties, glycosylated triterpenoids showcase remarkable biological activities, encompassing over 45 distinct effects. These effects span antifungal, antiparasitic, chemopreventive, neuroprotective, and sedative properties (Lacaille-Dubois & Wagner, 1996; Milgate & Roberts, 1995; Francis *et al*., 2002; Güçlü-Üstündağ & Mazza, 2007).

A pharmaceutically relevant glycosylated triterpenoid is from *Quillaja saponaria*, which produces a blend of bidesmosidic glycosylated triterpenoids, glycosylated at both C3 and C28 positions. While historically employed as a detergent, these compounds have gained traction as food additives, cosmetic industry components and pharmaceuticals. These glycosylated triterpenoids exhibit antiviral, antifungal, antibacterial, antiparasitic, anti-inflammatory, hypocholesterolemic, and haemolytic attributes (Sen *et al*., 1998; Roner *et al*., 2007; Holtshausen *et al*., 2009; Dixit *et al*., 2010; Tam & Roner, 2011; Fleck *et al*., 2019). The antimicrobial effects stem from the interaction of glycosylated triterpenoids with cholesterol, leading to cholesterol removal from membranes and subsequent cell lysis (Holtshausen *et al*., 2009; Cheeke, 2000). Moreover, the surfactant properties of these glycosylated triterpenoids disrupt bacterial cell membranes, compromising their integrity and rendering them more susceptible to antibiotics. Their application has extended to the treatment of skin disorders and scalp diseases (Fleck *et al*., 2019).

Reports highlight that QuilA, a vaccine adjuvant derived from the crude mixture of glycosylated triterpenoids in *Q. saponaria*, plays a crucial role in stimulating the

immune system to elicit a robust response in pharmaceutical vaccines (Pulendran *et al*., 2021). QS-21 is a fraction of QuilA (Figure 11), distinguished by a more hydrophobic region due to acyl chain attachment to a sugar moiety. This hydrophobic modification has paved the way for its significant contributions to vaccine development. For example, AS01, a vaccine adjuvant system incorporating QS-21 and 3-O-desacyl-4'-monophosphoryl lipid A (MPL), demonstrated efficacy in mice infected with malaria antigens and underwent clinical trials. These trials unveiled that AS01 induced the innate immune response, thereby enhancing vaccine efficiency by fostering antigen-specific responses (Coccia *et al*., 2017). Beyond its role as a vaccine adjuvant, QuilA and QS-21 exhibit anti-tumour potential, as its interactions with cholesterol, resulting in compromised cell membranes and subsequent lysis (Fleck *et al*., 2019). To address its toxicity toward healthy cells, specific fractions of the glycosylated triterpenoid mixture, as opposed to the crude extract, have been employed, along with binding it to cholesterol on nanoparticles (Hu *et al*., 2010).

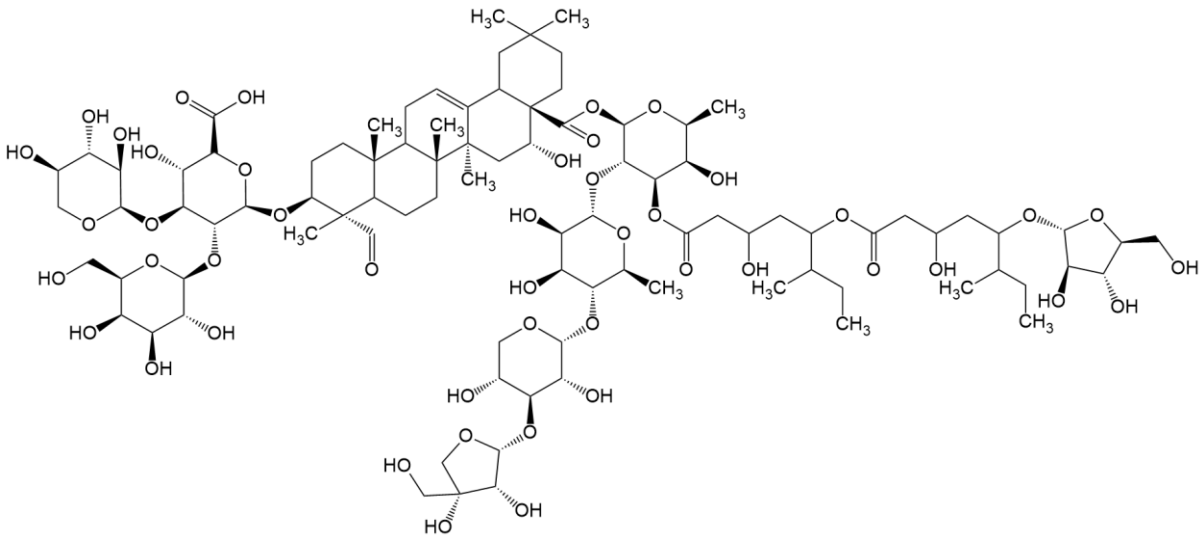

Figure 11: - The QS-21 fraction of QuilA. The acyl chain is prominent which gives the QS-21 more hydrophobicity and in turn enables it to interact with cholesterol of tumour cells more freely. Sugar moieties include glucuronic acid, xylose, galactose, fucose, rhamnose and arabinose.

Another glycosylated triterpenoid of significant pharmaceutical relevance is glycyrrhizin, synthesised by *Glycyrrhiza glabra*. It is a monodesmosidic glycosylated triterpenoid, featuring glucuronic acid (GlcA) as its attached sugar moiety. Glycyrrhizin has demonstrated antiviral, antibacterial, and anticancer effects, akin to the mechanisms mentioned for QS-21. Additionally, it has hepatoprotective properties. Studies have indicated that the consumption of glycyrrhizin alongside alcohol results in no elevation of liver function enzymes, which typically surge with alcohol intake. Consequently, glycyrrhizin protects against alcohol-induced liver toxicity, culminating in enhanced liver function and overall health when contrasted with alcohol consumption alone (Chigurupati *et al*., 2016).

Furthermore, glycyrrhizin exhibits potent anti-inflammatory properties. It effectively modulates the secretion of cytokines (immune response molecules that trigger inflammation) by macrophages. The slowed cytokine release leads to diminished inflammation. This anti-inflammatory capacity of glycyrrhizin is attributed to its ability to bind with cholesterol, hindering the formation of cholesterol-rich lipid rafts that are pivotal for toll-like receptor 4 (TLR-4) binding in the plasma membrane. This disrupts TLR-4 translocation, which initiates the cascade of the inflammatory pathway upon pathogen recognition (Fu *et al*., 2014; Graebin, 2018).

1.4 Approaches to triterpenoid production

1.4.1 Extraction of glycosylated triterpenoids

Given their broad range of biological activities and industrial applications, glycosylated triterpenoids represent a promising area for further exploration and utilisation. As previously mentioned, glycosylated triterpenoids are plant products, and the extraction from plants can be inefficient, requiring pretreatment of the samples, such as drying and grinding, to increase surface area and reduce particle size. Typically, a solvent is used for extraction due to the apolar nature of these compounds, which allows for easier dissolution and extraction from the plant cells (Güçlü-Üstündağ & Mazza, 2007).

To enhance efficiency, other technologies like microwave (Vongsangnak *et al*., 2004; Le *et al*., 2018) and ultrasound (Wu *et al*., 2001) have been employed to further disrupt the cell structure and facilitate the extraction of intracellular products. However, the choice of extraction method and solvent can influence the composition of the glycosylated triterpenoid extract, as different glycosylated triterpenoids have varying solubilities (Du *et al*., 2004). Following extraction, the glycosylated triterpenoids need to be purified and a common method involves partitioning between aqueous extracts and a water-immiscible solvent, followed by further purification through chromatography (Güçlü-Üstündağ & Mazza, 2007).

It is essential to consider that plants typically produce glycosylated triterpenoids in low amounts and in response to stress, leading to challenges in terms of long growing times, seasonal variations, low yield and complex mixtures of glycosylated triterpenoids. While synthetic production of these compounds is attempted, the complex stereochemistry of glycosylated triterpenoids often renders chemical synthesis too expensive or even impossible (Dale *et al*., 2020). These limitations underscore the significance of efficient extraction and purification processes from plant sources and highlight the need for alternative approaches to enhance the production and utilisation of these valuable compounds.

1.4.2 Production of triterpenoids in *S. cerevisiae*

Glycosylated and non-glycosylated triterpenoids hold significant promise in biotechnology, but their large-scale production through traditional plant cultivation faces challenges due to their low abundance, seasonal cycles, many structural analogues and complex process (Farhi *et al*., 2013; Sun *et al*., 2019). Moreover, the complexity and chirality of these compounds make chemical synthesis a daunting task (Zhu *et al*., 2008). However, a promising solution lies in using the yeast *S. cerevisiae* as a host system, circumventing the need for synthetic chemical production and reducing reliance on plants for triterpenoid production (Farhi *et al*., 2013; Arendt *et al*., 2017). Recent advancements in plant genomics and transcriptomics have enabled the

identification of the plant enzymes responsible for synthesising glycosylated and non-glycosylated terpenoids (Miettinen *et al*., 2018).

S. cerevisiae naturally produces ergosterol, an analogue of cholesterol, from 2,3-oxidosqualene. By introducing heterologous oxidosqualene cyclases (OSCs) from plants, we can generate glycosylated triterpenoid precursors within the yeast. Furthermore, producing biosurfactants from glycosylated triterpenoids in systems like *S. cerevisiae* offers advantages over chemical synthesis using petroleum or harsh chemicals, as glycosylated triterpenoids pose a lower environmental risk (Scheibel, 2004; Song *et al*., 2008). Likewise, the ability to selectively produce the specific glycosylated triterpenoid of interest, rather than yielding a complex mixture requiring subsequent separation, offers significant advantages of using *S. cerevisiae* to produce these compounds.

S. cerevisiae is the preferred choice for these industrial applications due to its simple nutritional requirements, robust growth at low pH, and flexibility in genetic manipulation techniques. The capacity to thrive in low pH environments is highly advantageous for the fermentation process, a critical technique widely employed in industrial applications. As fermentation advances, the medium undergoes gradual acidification owing to the generation of carbon dioxide and acids by the yeast (Maicas, 2020). Low pH also reduces the potential for contamination as other micro-organisms are less well adapted to the acidic environment. The pH is also important in this case as the change in pH can alter the chemistry of the compounds produced. For example, the glycosylated triterpenoid escin is affected by pH. An increase in pH increases its solubility by deprotonating the sugar moiety (Geisler *et al*., 2020) as well as the migration of acetyl groups present on the backbone. In high pH, the acetyl groups present on escin move to a different position, generating a different isomer which has different properties (this is discussed in more detail in Chapter 5) (Wu *et al*., 2010). Consequently, microorganisms capable of enduring acidic conditions, such as *S. cerevisiae* exhibit better performance in industrial settings and the glycosylated triterpenoids produced will be more stable. There is lots of flexibility in genetically modifying *S. cerevisiae* and is a relatively straightforward process which is facilitated by the modularity of parts and the abundance of accessible strains. Additionally, this yeast species has been comprehensively characterised and is genetically tractable,

therefore, engineering their native metabolism to redirect metabolic flux towards heterologous pathways is possible (Moses *et al*., 2013). The yeast system also allows for heterologous enzyme expression with the potential for post-translational modifications, a feature not available in other model organisms like *Escherichia coli* (Hammer & Avalos, 2017; Dale *et al*., 2020). Thus, *S. cerevisiae* is well-suited for large-scale industrial production of high-value compounds. While bacterial systems, such as *E. coli*, could theoretically produce triterpenoids, the membrane-bound nature of CYPs required for triterpenoid production poses challenges in expressing them in systems lacking an endoplasmic reticulum (Kim *et al*., 2019). Yeast systems exhibit better activity than their prokaryotic counterparts in this regard (Bill, 2014). Additionally, bacterial triterpenoid analogues use squalene as a precursor instead of 2,3-oxidosqualene, necessitating additional steps involving SQE to produce the desired precursor (Taylor, 1984).

Progress in the identification and characterisation of CYPs and UGDs has opened new possibilities for heterologous expression of these genes in biological systems, like yeast, to produce specific triterpenoids and other terpenoids with immense industrial potential. For example, artemisinic acid, a sesquiterpene and precursor used in artemisinin-based malaria therapies, can now be produced in yeast by integrating genes from *Artemisia annua* L., including an amorphadiene synthase gene (*ADS*) and a cytochrome P450 monooxygenase (*CYP71AV1*). This yeast-based production achieves artemisinic acid comparable to *A. annua* but in a fraction of the time (5 days compared to months). As a result, synthetic biology has successfully employed *S. cerevisiae* to produce the precursor for the antimalarial drug artemisinin. Chemical synthesis is used for the final stages due to the well-established high-yielding conversion of artemisinic acid to artemisinin (Acton & Roth, 1992; Ro *et al*., 2006; Paddon *et al*., 2013).

1.4.3 Increasing flux to triterpenoid production in *S. cerevisiae*

Extensive research has been dedicated to the heterologous expression of plant genes in yeast (Farhi *et al*., 2011; Liu *et al*., 2019; Lv *et al*., 2019). The yeast membrane sterol, ergosterol has the same 2,3-oxidosquelene precursor needed for triterpenoid biosynthesis, but previous studies have shown that completely terminating the ergosterol pathway is not feasible due to its essential role in cell viability, contributing to cell membrane fluidity, mitochondrial respiration, and endocytosis (Bagnat *et al*., 2000; Heese-Peck *et al*., 2002; Altmann & Westermann, 2005; Abe & Hiraki, 2009). The ergosterol pathway initiates with 2,3-oxidosqualene, and lanosterol synthase (Erg7p) produces the ergosterol precursor, lanosterol. An alternative approach involving an *erg7Δ* mutant and supplementation with ergosterol is expensive and not ideal for industrial applications (Kirby *et al*., 2008). Due to this field being relatively well established, there have been multiple efforts to increase terpenoid and glycosylated terpenoid production in *S. cerevisiae*. Table 2 displays just some of the methods used to increase the yield and the fold change achieved by some terpenes and terpenoids.

To enhance flux through the mevalonate pathway, it is well-established that overexpression of a truncated form of 3-hydroxy-3-methyl-glutaryl-coenzyme A reductase (Hmgrp) is effective. Hmgrp is natively inhibited by mevalonate and farnesyl pyrophosphate (FPP) at the N-terminal domain, leading to reduced pathway flux through negative feedback inhibition. Truncating the protein (tHmgrp) at the N-terminus eliminates this inhibition, enabling continuous production of mevalonate and FPP (Donald *et al*., 1997; Kirby *et al*., 2008).

The upregulation of pivotal genes involved in mevalonate synthesis is a common strategy in engineering *S. cerevisiae* to enhance triterpenoid biosynthesis. In many instances, genes like *tHMGR*, *ERG9*, and *ERG1* are reintroduced to amplify the production of FPP (a precursor that is converted into 2,3-oxidosqualene) and this

increased pool of precursors results in an elevated triterpenoid output (Dale *et al*., 2020).

Another approach to redirect flux towards triterpenoid biosynthesis in yeast involves coupling the overexpression of genes responsible for acetyl-CoA production with the deletion of competing pathways that consume acetyl-CoA. For instance, in *S. cerevisiae*, a 200 % increase in β-amyrin production was achieved through the overexpression of alcohol dehydrogenase (*ADH2*), acetaldehyde dehydrogenase (*ALD6*), acetyl-CoA synthase (*ACS*), ATP-citratelyase (*ACL*), phosphoketolase (*PK*), acetylating aldehyde dehydrogenase (*A-ALD*), and phosphotransacetylase (*PTA*). These genes collectively contribute to the generation of acetyl-CoA from both glucose and pyruvate, thus leading to a heightened availability of acetyl-CoA and subsequently elevating β-amyrin production (Liu *et al*., 2019). Furthermore, in the same yeast strain, an impressive 330 % increase in β-amyrin production in *S. cerevisiae* was achieved by eliminating competing pathways that consume acetyl-CoA. This was accomplished by deleting malate synthase (*MLS1*) and citrate synthase (*CIT2*), enzymes responsible for producing malate and citrate from acetyl-CoA derived from glucose. The removal of these pathways resulted in a substantial boost in β-amyrin production compared to the original β-amyrin-producing strain without carbon flux redirection (Liu *et al*., 2019).

Another approach used to enhance the production of triterpenoids in *S. cerevisiae* involves the engineering of promoters. An example of this involves the modification of promoters for β-amyrin synthesis to incorporate Upc2p binding activity. Upc2p serves as a transcription factor that triggers the upregulation of the sterol biosynthesis pathway by interacting with promoters harbouring UPC2 binding domains. Consequently, upon activation of Upc2p (induced by sterol depletion, a consequence of triterpenoid synthesis that uses 2,3-oxidosqualene), it binds to the promoters of β-amyrin synthesis genes, effectively activating their expression (Zhang *et al*., 2011).

Table 2: - Examples of some methods for the overproduction of essential terpene products or precursors of glycosylated terpenoids. Full legend on next page.

Target	Technique used	Fold change	Reference
Amorphadiene	Targeting FDP synthase and amorphadiene synthase to the mitochondria	20x increase	Farhi *et al*., 2011
Amorpha-4,11-diene	Relocalisation of amorpha-4,11-diene synthase to the mitochondria	16x increase	Yuan and Ching, 2016
Artemisinic acid	Expression of CYB5, ADH1, ALDH	10x increase	Paddon *et al*., 2013
β-amyrin	Truncation of HMGR and and expression of AaβAS and downregulation of ERG7	1.5x increase	Kirby *et al*., 2008
β-amyrin	Coupling of endogenous and heterologous acetyl-CoA synthesis pathways to β-amyrin production, and removal of competing acetyl-CoA using pathways	3.3x increase	Liu et al., 2019
β-amyrin	Use of cyclodextrin to sequester β-amyrin out of the cell	1.6x increase	Moses *et al*., 2014
β-amyrin	Introduction of heterologous squalene monooxygenase and introduction of tHMGR	49x increase	Zhang *et al*., 2015
β-amyrin	Overexpression of UPC2.1 (transcription factor for sterol biosynthesis) combined with the above technique	69x increase	Zhang *et al*., 2015
Betulinic acid	Excess ethanol and nitrogen limitation fermentations	5x increase	Czarnotta *et al*., 2017
Betulinic acid	Increasing triterpenoids by decreasing flux to competing fatty acid biosynthesis pathway	39x increase	Li and Zhang, 2014
Carotenoid (tetraterpenoid)	Mutations in ERG20 (Y95S) and ERG12 (W186R)	11x increase	Jakočiūnas *et al*., 2018
Ginsenoside compound K	Balancing fatty acid and betulinic acid producing pathways and tHMGR overexpression	5x increase	Yan *et al*., 2014
Isoprene	Cytoplasmic and mitochondrial targeting of the MVA pathway	2.1x increase	Lv *et al*., 2016
Medicagenic-28-O-glucoside and others	ER expansion by disruption of PAH1	16x increase	Arendt *et al*., 2017
Oleanolic acid	Optimal CqβAS used	24x increase	Dale *et al.,* 2020
Oleanolic acid	Improvement of pairing efficiency between cytochrome P450 monooxygenase and reductase	1.6x increase	Zhao *et al*., 2018
Protopanaxadiol	ER expansion by overexpression of INO2	8x increase	Kim *et al*., 2019
Squalene (triterpenoid precursor)	Overexpression of truncated HMGR	10x increase	Donald *et al*., 1997

Table 2: - Examples of some methods for the overproduction of essential terpene products or precursors of glycosylated terpenoids. AaBAS, Artemisia annua β-amyrin synthase; ADH1, artemisinic alcohol dehydrogenase; ALDH1, aldehyde dehydrogenase; CqBAS, *Chenopodium quinoa* β-amyrin synthase; *CYB5*, cytochrome b5; ER, endoplasmic reticulum; *ERG7,* lanosterol synthase; *ERG12,* mevalonate kinase; *ERG20*, Farnesyl pyrophosphate synthase gene; FPP, farnesyl pyrophosphate synthase; HMGR, 3-Hydroxy-3-MethylGlutaryl-coenzyme a reductase; *INO2,* Inositol requiring transcription factor; MVA, mevalonate; *PAH1*, phosphatidic Acid phosphohydrolase; tHMGR, truncated 3-Hydroxy-3-MethylGlutaryl-coenzyme a reductase.

1.4.4 Engineering cell structure

Enhancing terpene and triterpenoid productivity can be achieved through organelle engineering of the endoplasmic reticulum (ER), as the latter stages of the biosynthetic pathway (SQS, SQE, βAS and all CYPs) are channelled toward this cellular organelle (Kim *et al*., 2019). Research demonstrates that disruption of phosphatidic acid phosphatase (*PAH1*) leads to ER expansion, resulting in a remarkable 16-fold increase in glycosylated triterpenoid production compared to the control strain (Arendt *et al*., 2017).

Furthermore, an alternative avenue for achieving this enhancement involves the overexpression of *INO2*, a pivotal transcription factor governing ER size regulation. Overexpression of *INO2* triggers an expansion of the ER in comparison to normal cells. This expanded ER capacity heightens the synthesis potential for both endogenous and heterologous proteins associated with the ER, thereby substantially increasing squalene production (the precursor to 2,3-oxidosqualene, which serves as the triterpene precursor) (Kim *et al*., 2019). This highlights another promising strategy for the elevated production of glycosylated triterpenoids.

An alternative technique employed in cell engineering involves localising mevalonate pathway genes to the mitochondria, which harbours more acetyl CoA than the rest of the cell. By incorporating mitochondrial localisation sequences (MLS) onto MVA

proteins, researchers were able to guide their transportation to the mitochondria. Erg10p, Hmgrp, Erg12p, Pmkp, Mvd1p, and Idi1p were all equipped with the MLS, along with reporter proteins for easy identification. By channelling these proteins to the mitochondria, the surplus acetyl-CoA available facilitated a 2.1-fold increase in isoprene production, a precursor to both triterpenes and triterpenoids (Lv *et al*., 2016).

1.4.5 Enzyme optimisation

Another engineering technique used is the modification and optimisation of enzymes needed for triterpenoid biosynthesis. Mutant strains of *S. cerevisiae* carrying alterations in *ERG20* (encoding farnesyl pyrophosphate synthase/Erg20p) and *ERG1* (encoding squalene monooxygenase/Erg1p) have proven beneficial for triterpenoid production (Foresti *et al*., 2013; Jakočiūnas *et al*., 2018). For example, the Y95S mutation in Erg20p of *S. cerevisiae*, which replaces a tyrosine with serine at position 95, has been shown to increase carotenoid (tetraterpenoid) production by 5-fold. This mutation is believed to improve the ligand binding pocket of Erg20p without altering its overall 3D structure, enhancing its ability to bind a catalyse FPP from GPP (Jakočiūnas *et al*., 2018).

Likewise, mutations in *ERG1* (squalene epoxidase) have also been found to boost the production of triterpenoid precursors. The K311R mutation, which replaces lysine at position 311 with arginine, reduces the impact of Doa10, an E3 ubiquitin ligase involved in the ER-associated degradation pathway. Doa10 attaches a ubiquitin tag to proteins which thus labels them for degradation. Therefore, the mutation in Erg1p stops Doa10 tagging it with ubiquitin, and so it is not degraded. This increases the concentration of the terpene precursor 2,3-oxidosqualene inside the cell (Foresti *et al*., 2013).

1.4.6 Overcoming the toxic burden of triterpenoids

A common challenge in synthetic biology and biotechnology concerns the toxic load imposed on microbial hosts by the products they synthesise. For instance, the

hydrophobic nature of triterpenoids means there is accumulation intracellularly or within the membrane, this could be a significant drawback as it might be detrimental to the cell but also may cause negative feedback inhibition for the beginning of the pathway (Sun *et al*., 2019b). In response to this challenge, research endeavours have been dedicated to harnessing the potential of cyclodextrins (CDs). CDs, cyclic oligosaccharides with a toroidal configuration composed of glucopyranoside units, have a pronounced ability to solubilise drugs due to their hydrophobic interior juxtaposed with a hydrophilic exterior (Stella & He, 2008; Moses *et al*., 2014). Methyl-β-cyclodextrin (MβCD), a specific type of CD, has been effectively employed to sequester triterpenes from yeast cells, facilitating their relocation into the surrounding media (Moses *et al*., 2014). This innovative approach involves the synthesis of triterpenes within the cell, followed by their secretion into the media via MβCD, only possible by its unique toroidal structure. This dual action not only limits intracellular accumulation but also mitigates growth inhibition by eliminating feedback inhibition products (Sun *et al*., 2019b).

Collectively, the interventions mentioned harbour the potential to elevate triterpenoid production by redirecting pathway inhibition, using more efficient enzymes, amplifying cofactor availability, and mitigating the toxic overload of intracellular product accumulation.

1.4.7 Production of triterpenoids in other yeast strains

Other yeast hosts can also be harnessed for triterpenoid production, including *Yarrowia lipolytica*. Many triterpenoids exert a toxic effect on cell viability, making alternative yeast systems like *Y. lipolytica* advantageous due to their high lipid content (Zhang *et al*., 2020). To achieve high concentrations of toxic terpenoids, such as lycopene, in *S. cerevisiae*, increasing lipid droplet size has been shown to yield the highest reported production (2.37 $g.L^{-1}$), enabling *S. cerevisiae* to tolerate higher lycopene concentrations (Ma *et al*., 2019). This tolerance is attributed to the lipophilic nature of terpenes, which accumulate in lipid droplets, storing them without causing cellular damage (Larroude *et al*., 2018; Zhang *et al*., 2020). *Y. lipolytica,* an oleaginous

yeast, harbours substantial lipid reserves stored as intracellular lipid droplets (Bhutada *et al*., 2018), making it suitable for enhanced terpene production, such as lycopene (Matthäus *et al*., 2014), β-carotene (Gao *et al*., 2017), and lupeol (Zhang *et al*., 2020).

While *Y. lipolytica* appears promising for terpene production, there are challenges associated with working with this genus. *Y. lipolytica* is an obligate aerobe (Coelho *et al*., 2010), unlike *S. cerevisiae*, which is a facultative anaerobe. Strict aerobes can be challenging to control in an industrial setting, as maintaining precise oxygen levels is crucial; excessive oxygen leads to excessive growth but insufficient product production and vice versa (Coelho *et al*., 2010; Kar *et al*., 2012; Park & Ledesma-Amaro, 2023). Higher oxygen requirements also result in excessive foam formation, necessitating antifoaming agents that increase production costs and reduce productivity (Kar *et al*., 2012; Snopek *et al*., 2021). Additionally, there is insufficient foundational knowledge; despite several *Yarrowia* strains having annotated genomes, functional and biochemical studies on these strains remain limited (Park & Ledesma-Amaro, 2023). Furthermore, there is a lack of adequate engineering tools, *Y. lipolytica* primarily employs nonhomologous end joining (NHEJ) rather than homologous recombination (HR) for DNA repair, making targeted deletions or integrations challenging (Schwartz *et al*., 2017; Park & Ledesma-Amaro, 2023).

Another yeast host used for triterpenoid production is *Pichia pastoris*, which has been engineered to produce the tetracyclic triterpenoid dammarenediol-II (Liu *et al*., 2015). *P. pastoris* is an established host for industrial protein production and can efficiently secrete heterologous proteins into the media (Karbalaei *et al*., 2020). The production of dammarenediol-II in *P. pastoris* reached 1.073 $mg.g^{-1}$ dry cell weight (DCW) and while this is promising, further development is needed to increase the yield (Liu *et al*., 2015). Lycopene has also been produced in *P. pastoris*, with higher yields observed when the lycopene pathway genes were expressed in the peroxisome (Bhataya *et al*., 2009; Zhang *et al*., 2020b). However, drawbacks include the lack of selectable marker genes for strain transformation and yields like those obtained in *S. cerevisiae* (Karbalaei *et al*., 2020; Zhang *et al*., 2020b).

Therefore, triterpenoid production in *S. cerevisiae* remains a focus. However, leveraging the advantages of these diverse yeast hosts may enhance triterpenoid

yields. For instance, directing triterpenoid pathway genes to the peroxisome, which increased lycopene production in *P. pastoris* (Bhataya *et al*., 2009), or enhancing *S. cerevisiae's* intracellular lipid bodies to resemble those of *Y. lipolytica* (Matthäus *et al*., 2014; Ma *et al*., 2019).

1.5 The glycosylated triterpenoid Escin

1.5.1 Chemical and functional characterisation of escin

An industrially important glycosylated triterpenoid is escin, also referred to as aescin or aescine. Escin is a mixture of glycosylated triterpenoids that has garnered significant interest in the pharmaceutical and home-care industries. It is derived from the seeds of horse chestnut trees *(Aesculus hippocastanum L.*) and has various industrial applications, in pharmaceuticals and as surfactants. Escins exhibit natural insecticidal properties due to them being bitter and thus deterrents for insects such as *Drosophila* (Freeman *et al*., 2014). Additionally, it acts as a repellent against the invasive pest *Cameraria ohridella* (horse chestnut leafminer moth) (Ferracini *et al*., 2010).

Escin possesses a wide range of pharmaceutical applications as an anti-inflammatory agent, which can be administered both orally and topically (Cravotto *et al*., 2011; Gallelli *et al*., 2021). Its primary use lies in the treatment of various vascular disorders, with extensive research conducted in this field. Escin is believed to exert its effects by acting as a glucocorticoid-type steroid, akin to cortisol, which binds to glucocorticoid receptors (GR). These receptors facilitate the transcriptional activation of genes involved in suppressing inflammation (Gallelli *et al*., 2021). The structural backbone of escin closely resembles that of hydrocortisone (cortisol), leading to the hypothesis that escin functions similarly. Unlike other anti-inflammatory drugs such as ibuprofen, which block cyclooxygenase (COX) to inhibit prostaglandin synthesis, escin operates through a distinct mechanism (Bushra & Aslam, 2010; Gallelli *et al*., 2021). Prostaglandins are responsible for inducing the pain and swelling associated with

inflammation. The anti-inflammatory response of escin reduces the permeability of small blood vessels, thereby mitigating swelling (Gallelli *et al*., 2021). In addition to its use in inflammation, escin has been investigated for its efficacy in treating other vascular disorders, including haemorrhoids (Sirtori, 2001; Zhang *et al*., 2010), varicose veins (Lichota *et al*., 2019), and chronic venous insufficiency (Zhang *et al*., 2010; Yu & Su, 2013). The availability of different anti-inflammatory drugs that target distinct pathways is highly beneficial, considering individual patient variations in drug response. Escin and its biotechnological production hold promising potential for developing diverse anti-inflammatory agents with varying modes of action. This allows for personalised treatment options tailored to individual patient needs.

1.5.2 Biosynthesis of escin

The precise biosynthesis mechanism of escin remains unknown, although several enzymes crucial for β-amyrin hydroxylation and subsequent modifications leading to escin production have been identified, albeit not exhaustively. Presently, our understanding encompasses multiple cytochrome P450 enzymes (CYPs) and acyltransferases (ACTs) responsible for orchestrating C21, C22, C28, and C16 hydroxylation, followed by further alterations to attach acetyl groups on C21 and C22 positions. Subsequent glycosylation of the C3 position, mediated by UDP-glycosyltransferases (UGTs), culminates in the formation of escin (Unpublished data presented in the PhD thesis of Eliot Jan-Smith, 2023, John Innes Centre).

1.6 Aims

The primary goal of this thesis is to enhance the production of glycosylated triterpenoids in *S. cerevisiae* by investigating their interactions with the yeast and finding ways to overcome their toxic effects. We focus on escin and aim to understand its mechanism of action on *S. cerevisiae* and identify and develop a tolerant yeast strain that can produce escin-like compounds in high quantities without being compromised by toxicity or production burden. To achieve this, we use sterol biosynthesis mutants that exhibit higher tolerance to glycosylated triterpenoids

compared to the wild-type *S. cerevisiae*, and we employ this mutation in production strains to determine if an increase in yield is observed.

Chapter 2: - Materials and Methods

2.1 Materials

2.1.1 *S. cerevisiae* growth media

OD_{600nm} measurements were conducted using a WPA Biowave CO8000 cell density meter and all media was autoclaved (121 ºC for 15 minutes) before use.

CSM + 2% (w/v) galactose: 6.9 $g.L^{-1}$ yeast nitrogen base, 0.77 $g.L^{-1}$ complete synthetic media, 2% (w/v) galactose

CSM agar: 6.9 $g.L^{-1}$ yeast nitrogen base, 0.77 $g.L^{-1}$ complete synthetic media, 2% (w/v) D-glucose, 20 $g.L^{-1}$ agar

CSM: 6.9 $g.L^{-1}$ yeast nitrogen base (Sigma Y0626), 0.77 $g.L^{-1}$ complete synthetic media (Formedium DCS0019), 2% (w/v) D-glucose

SC-HIS-LEU: 6.9 $g.L^{-1}$ yeast nitrogen base, 0.77 $g.L^{-1}$ complete synthetic media -HIS -LEU (Formedium DCS0469), 2% (w/v) D-glucose

SC-URA agar: 6.9 $g.L^{-1}$ yeast nitrogen base, 0.77 $g.L^{-1}$ complete synthetic media -URA, 2% (w/v) D-glucose, 20 $g.L^{-1}$ agar

SC-URA: 6.9 $g.L^{-1}$ yeast nitrogen base, 0.77 $g.L^{-1}$ complete synthetic media -URA (Formedium DCS0169), 2% (w/v) D-glucose

YPD agar: 10 $g.L^{-1}$ yeast extract, 2 $g.L^{-1}$ peptone, 2% (w/v) D-glucose, 20 $g.L^{-1}$ agar (Oxoid LP0011)

YPD: 10 $g.L^{-1}$ yeast extract (Acros Organics 84604-16-0), 2 $g.L^{-1}$ peptone (Millipore 70173-500G), 2% (w/v) D-glucose (media kitchen)

YPG: 10 $g.L^{-1}$ yeast extract, 2 $g.L^{-1}$ peptone, 2% (w/v) galactose (media kitchen)

2.1.2 *E. coli* growth media

OD_{600nm} measurements were conducted using a WPA Biowave CO8000 cell density meter and all media was autoclaved (121 ºC for 15 minutes) before use.

LB agar: 10 $g.L^{-1}$ tryptone, 5 $g.L^{-1}$ yeast extract, 1 $g.L^{-1}$ NaCl, 20 $g.L^{-1}$ agar

LB: 10 $g.L^{-1}$ tryptone (Formedium TRP03), 5 $g.L^{-1}$ yeast extract, 1 $g.L^{-1}$ NaCl (Fisher Chemical 7647-14-5)

2.1.3 Antibiotics

Ampicillin: 100 $\mu g.mL^{-1}$ in 70% ethanol working concentration

Chloramphenicol: 40 $\mu g.mL^{-1}$ in 99% ethanol working concentration

Geneticin: 50 $mg.\ mL^{-1}$ in dH_2O working concentration

Hygromycin B: 100 $mg.\ mL^{-1}$ in dH_2O working concentration

Kanamycin: 50 $\mu g.mL^{-1}$ in dH_2O working concentration

Spectinomycin: 100 $\mu g.mL^{-1}$ in dH_2O working concentration

2.1.4 Molecular biology

10X T4 DNA ligase buffer: (NEB B0202S)

6X Orange DNA Loading Dye: (Thermo Scientific R0631)

E.Z.N.A Plasmid mini kit I, (Q-spin): (Omega Bio-Tek D694245759-111)

Escin fractions: Gifted from Unilever. Dissolved in HPLC grade methanol to a stock of 40 $mg.mL^{-1}$

Escin: (Sigma E1378-1G) dissolved in HPLC grade methanol to a stock concentration of 40 $mg.mL^{-1}$

OneTaq: OneTaq® Quick-Load® 2X Master Mix with Standard Buffer. NEB

Q5: 5X Q5 Reaction Buffer, 2 mM dNTPs (Invitrogen 09733739), 2 $U.\mu L^{-1}$ Q5 High-Fidelity DNA Polymerase. (NEB MO491L)

Restriction enzymes: (NEB)

T7 DNA ligase: (NEB M0318)

TAE (1X): 40 mM Tris, 20 mM acetate, 1 mM EDTA

TFB1 buffer: 30 mM CH_3COOK, 100 mM RbCl, 10 mM CaCl2, 50 mM MnCl2, 15 % (v/v) glycerol; pH adjusted to 5.8 with acetate; filter sterilised (0.22 µm)

TFB2 buffer: 10 mM MOPS (pH 6.5), 75 mM CaCl2, 10 mM RbCl, 15 % (v/v) glycerol; pH adjusted to 6.5 with KOH; filter sterilised (0.22 µm)

Thiozole orange: (Sigma 390062-1G)

UltraPure Agarose: (ThermoFisher 16500500)

Zymoclean Gel Recovery Kit: (Zymo Research D4002)

2.1.5 Yeast transformation

Lithium Acetate (1 M): (Sigma L6883-250G)

PEG 3350, 50 % (w/v): 50 g PEG 3350 (Sigma 88276) dissolved in 100 mL dH_2O

Salmon sperm DNA (10 $mg.mL^{-1}$): (Invitrogen 15632-011)

2.1.6 Yeast gDNA extraction (bust n’ grab)

Lysis buffer: (2 % Triton X-100, 1 % SDS, 100 mM NaCl, 10 mM Tris-HCl at pH 8, and 1 mM EDTA at pH 8)

2.1.7 Metabolite Extractions for Gas Chromatography-Mass Spectrometry (GC-MS)

Coprostan-3-ol: (Sigma C7578) dissolved in 100 % ethanol to a concentration of 2.57 mM (-20 °C)

Ethyl acetate (anhydrous, 99.8 %): Sigma (270989)

GeneVac EZ-2 Elite evaporator

Lysis Buffer: 20 % KOH (SLS CHE3000); 50 % ethanol; 80 nmol.mL^{-1} coprostan-3-ol (Sigma C7578)

N-Hexane (99 %): Sigma (32292-M)

2.1.8 Metabolite Extractions for Liquid Chromatography-Mass Spectrometry (LC-MS)

Acid-washed glass beads (425-600 µm): Sigma (G8772)

Butan-1-ol (≥ 99 %): (Acros Organics 167695000).

Echinocystic acid-glucoside: (Extrasynthase 0110S)

YeastBuster: (Millipore 71186)

2.1.9 GC-MS and LC-MS

1.1 ml autosampler vials: 1.1 ml microliter crimp neck vial ND11, 32 x 11.6 mm, clear glass, 1st hydrolytic class; Gerstel (093640-121-00)

Crimp caps: 11 mm autosampler vial crimp caps with rubber or silicone liner (Thermo Scientific 11-MC-8RT1 or Thermo Scientific 11-MC-ST15)

MSTFA (*N*-Methyl-*N*-(trimethylsilyl) trifluoroacetamide with 1% trimethylchlorosilane): (Sigma 69478)

Pyridine (anhydrous, 99.8 %): (Sigma 270970)

2.1.10 Microplate assays

96 well plates: (Thermo Scientific 167008)

Micropore tape: (Micropore 1530-1)

2.1.11 Quantitive Reverse Transcription-polymerase chain reaction (qRT-PCR)

Buffer RLT + β-mecaptoethanol: 10 µL of β-mecaptoethanol for every 350 µL Buffer RLT (provided in QIAgen RNeasy mini kit)

Buffer Y1: 1 M sorbitol (Acros Organics 50-70-4), 0.1 M EDTA (Acros Organics 6381-92-6), pH 7.4. Before use add 0.1 % β-mecaptoethanol (Sigma 60-24-2) and 10 $U.\mu L^{-1}$ lyticase (Sigma L2524)

DEPC-treated water: (Ambion AM9915G)

dNTPs: (Invitrogen 09733739)

E. coli RNase H: (Invitrogen 18021071)

MicroAmp EnduraPlate Optical 96-well Fast Blue Reaction plate: (Thermo Fisher 4483486)

Microseal B adhesive sealer: (Bio-Rad MSB-1001)

Oligo$(dT)_{20}$ primer: Integrated DNA Technologies

QIAgen RNeasy plant mini kit: (QIAGEN 74904)

RiboLock RNase Inhibitor (40 $U.\mu L^{-1}$): (Thermo Scientific EO0381)

RNase-Free DNase Set: 1500 U DNase I (RNase-free, lyophilised) in 550 µL buffer RDD (QIAGEN 79254)

RNaseZAP: (ThermoFisher Scientific AM9780)

SuperScript IV First-Strand Synthesis System: (Invitrogen 18091200)

2.1.12 Propidium Iodide Assays

Brassicasterol: (Sigma 474-67-9) dissolved in HPLC grade methanol at a concentration of 13 mM

Chambered slides: (Ibidi 80807)

Concanavalin A: (Sigma C2010), 2 $mg.mL^{-1}$

Ergosterol: (Sigma m45480-10G-F) dissolved in HPLC grade methanol at a concentration of 13 mM

Leica DMi8 inverted microscope

Propidium iodide: (Invitrogen P3566)

Treatment media: 400 uL PBS, 1.25 % methanol, varying escin concentrations

2.1.13 Confocal Microscopy

Alpha Plan Apochromat objective

Chambered slides: (Ibidi 80807)

Concanavalin A: (Sigma C2010), 2 $mg.mL^{-1}$

Treatment media: 400 uL PBS, 1.25 % methanol, varying escin concentrations

Zeiss LSM 880 (Airyscan) Microscope

2.1.14 Membrane permeability

Hanna conductivity meter: (H199300)

0.5 mm glass beads: (Sigma Z250465-1PK)

2.2 Methods

2.2.1 Storage of *S. cerevisiae* and *E.coli*

The long-term storage of both wild-type and produced strains of *S. cerevisiae* involved preservation at -80 °C in a solution containing 20% (w/v) glycerol. For shorter-term storage, these strains were streaked onto agar plates and maintained at 4 °C. In contrast, *E. coli* strains which were used for plasmid cloning were preserved for the long term at -80 °C in a 40% (w/v) glycerol solution, while for shorter-term storage, they were also streaked onto agar plates and kept at 4 °C.

The process of preparing yeast glycerol stocks began with the inoculation of 5 mL of YPD medium with the appropriate yeast strain, followed by incubation at 30 °C for a minimum of 24 hours (up to 48 hours) with continuous shaking at 200 rpm. Subsequently, 750 µL of yeast culture was combined with 250 µL of cold 80 % glycerol and stored at -80 °C. In the case of *E. coli* glycerol stocks, the procedure began by inoculating 5 mL of LB medium (with the appropriate antibiotic, if necessary) with the *E. coli* strain, followed by overnight incubation at 37 °C (approximately 16 hours) with continuous shaking at 200 rpm. Afterwards, 500 µL of the *E. coli* culture was mixed with 500 µL of cold 80 % glycerol and stored at -80 °C.

2.2.2 Preparing competent *E.coli*

Competent cells were prepared using a method involving RbCl. Initially, *E. coli* TOP10 was inoculated in 5 mL of LB medium and allowed to grow overnight, approximately 16 hours, at 37 °C with continuous shaking at 200 rpm. Subsequently, the culture was diluted by a factor of 1:400 into 200 mL of pre-warmed LB medium supplemented with

20 mM $MgSO_4$. The culture was then incubated at 37 °C with continuous shaking (200 rpm) until the optical density at 600 nm (OD600nm) reached approximately 0.5. Following this, the bacterial cells were carefully transferred to a 50 mL falcon tube and allowed to incubate on ice for 10 minutes, ensuring that the cells remained cold throughout this process. The cultures were then subjected to centrifugation at 4 °C, with a relative centrifugal force (RCF) of 3750 for 5 minutes, resulting in the formation of a pellet. This pellet was subsequently resuspended in 20 mL of cold TFB1 buffer and incubated on ice for an additional 5 minutes. Following another round of centrifugation, this time at 4 °C with an RCF of 1350 for 10 minutes, a new pellet was formed. This pellet was then resuspended in 2 mL of cold TFB2 buffer, and the culture was once again incubated on ice, this time for 15 minutes. Finally, 200 µL aliquots of the prepared competent cells were rapidly frozen using liquid nitrogen and stored at -80 °C for future use.

2.2.3 Plasmid preparation

A 5 mL volume of LB medium was inoculated with a single colony of *E. coli* containing the desired plasmid, and this culture was grown overnight at 37 °C, approximately for 16 hours while being agitated at 200 rpm. Subsequently, plasmid extraction was carried out using the E.Z.N.A. Plasmid Mini Kit I, following the manufacturer's instructions. The elution step involved using 30 µL of deionised water (dH_2O) to recover the extracted plasmid.

2.2.4 Polymerase Chain Reaction (PCR)

PCRs were employed to generate DNA fragments for subsequent cloning into the pYTK001 vector, utilising Q5 DNA polymerase as the enzyme of choice. The reaction mixture consisted of 1X Q5 reaction buffer, 0.2 mM dNTPs, 0.5 µM of both forward and reverse primers, 1 µL of template DNA, and 1 unit of Q5 High-fidelity DNA polymerase.

The thermal cycling program for the PCR reactions involved an initial denaturation step at 98 °C for 30 seconds, followed by 30 cycles consisting of denaturation at 98 °C for 10 seconds, annealing for 30 seconds at a temperature 3 °C above the melting temperature of the lowest primer, and extension at 72 °C for 2 minutes. The reaction was then concluded with a hold at 4 °C. The extension time during the cycling was adjusted to 30 seconds per kilobase (kb) of the expected PCR product length. Following the PCR amplification, the resultant products were subjected to purification through gel extraction.

2.2.5 Restriction digest

For plasmid minipreps, a restriction digestion procedure was used. This involved the combination of 1000 ng of plasmid DNA, 0.5 µL of each respective restriction enzyme from New England Biolabs (NEB), and 1 µL of 1X CutSmart buffer (NEB) to attain a final volume of 20 µL. The mixture was then subjected to incubation at the specific optimal temperature for each enzyme for a minimum duration of 3 hours. Following incubation, the digested products were subsequently analysed using agarose gel electrophoresis.

2.2.6 Agarose gel electrophoresis

For restriction digests and PCR reactions, the samples were mixed with 6X Orange DNA Loading Dye and then loaded onto a 1% agarose-TAE gel containing thiazole orange. However, for PCR reactions utilising OneTaq, they were directly loaded onto the gel.

The gel electrophoresis was conducted by running the gel at a voltage of 100 V in 1X TAE buffer for 30 minutes. Subsequently, the gel was subjected to imaging using a Gel Doc™ XR+ Gel Documentation System manufactured by BioRad.

2.2.7 Gel extraction

The PCR reactions were subjected to analysis on agarose-TAE gels and subsequently purified using the QIAquick Gel Extraction Kit, following the guidelines provided by the manufacturer. The purified DNA fragments were eluted in a final volume of 30 µL of dH_2O.

2.2.8 Sanger sequencing

Plasmids were sequenced by MRC PPU DNA Sequencing and Services (University of Dundee) using the Sanger sequencing method.

2.2.9 Plasmid construction

The assembly of all plasmids was carried out using the MoClo-YTK method as described by Lee *et al*., (2015). The process involved the cloning of individual genetic parts, such as promoters, open reading frames, and terminators, into a part plasmid entry vector known as pYTK001, which included a GFP dropout part. Transcriptional units, comprising promoter-ORF-terminator sequences, were constructed by further cloning these parts into a transcriptional unit vector. Pathways were formed by assembling multiple transcriptional units into a destination vector, which contained transcriptional units, destination homology arms*, E. coli* markers, origin sequences, and *S. cerevisiae* markers. Most of the genes were synthesised previously in the Rosser Lab, designed by Dr Matthew Dale, Dr Emily Johnston, and Dr Tessa Moses, and codon-optimised using GeneArt, Gen9, or IDT. All these genetic parts were cloned into the MoClo-YTK entry vector pYTK001.

To prepare the genetic parts for cloning, PCR was performed to introduce appropriate BsmBI restriction sites. The resulting PCR products were then cloned into pYTK001. This cloning process involved mixing the PCR product with 20 fmol of pYTK001, 1500

U of T7 DNA ligase (NEB), 1X T4 DNA ligase buffer (NEB), and 5 U of BsmBI (NEB), resulting in a final volume of 10 µL. The thermocycler program for this reaction included the following steps: 42 °C for 2 minutes, 16 °C for 5 minutes (25 cycles), 60 °C for 10 minutes, and 80 °C for 10 minutes, followed by a hold at 16 °C. Similar assemblies into transcriptional unit vectors followed the same procedure, except with the addition of 20 fmol of each plasmid (the transcriptional unit vector and the parts in pYTK001), and using 5 U of BsaI (NEB) as the restriction enzyme. Assemblies into destination vectors were conducted in a manner identical to that for transcriptional unit vectors, except that 5 U of BsmBI (NEB) was used as the restriction enzyme.

The assembled constructs were transformed into *E. coli* TOP10 cells. In this process, 5 µL of the reaction mixture was added to 50–200 µL of chemically competent cells, which were subsequently incubated on ice for 30 minutes, followed by a heat shock at 42 °C for 30 seconds and another ice incubation for 2 minutes. Next, 400 µL of super optimal broth with catabolite repression media (SOC media) was added, and the cells were incubated at 37 °C for 90 minutes with shaking at 200 rpm. A 100 µL aliquot of the transformed cells was plated onto LB-agar containing the appropriate antibiotic, which included 40 $\mu g.mL^{-1}$ chloramphenicol for assemblies into pYTK001, 100 $\mu g.mL^{-1}$ ampicillin for transcriptional unit vectors, and 200 $\mu g.mL^{-1}$ spectinomycin for destination vectors. The transformed *E. coli* cells were incubated at 37 °C until colonies had formed, typically overnight or for approximately 16 hours.

The plasmids were extracted using a miniprep method with the E.Z.N.A Plasmid Mini Kit I and subsequently verified through restriction digest analysis and Sanger sequencing by the DNA Sequencing and Services facility at the University of Dundee. Miniprep involved centrifuging the culture at 10,000 g for 1 minute at room temperature. Following this, 250 µL of Solution I/RNaseA was added to the pellet and vortexed for thorough mixing. Subsequently, 250 µL of Solution II was gently added and mixed by inverting the tube, followed by the addition of 350 µL of Solution III with further gentle inversion until a precipitate formed. The culture and solution mixture were then centrifuged at 13,000 g for 10 minutes, and the supernatant was transferred to a HiBind® DNA Mini Column, followed by centrifugation at 13,000 g for 1 minute.

This step discarded the filtrate unless otherwise specified. Next, 500 µL of HBC Buffer was added and centrifuged at 13,000 g for 1 minute, followed by the addition of 700 µL of DNA Wash Buffer and another centrifugation at 13,000 g for 1 minute. The column was then dried by centrifuging for 2 minutes at 13,000 g and transferred to a microfuge tube. Finally, 50 µL of sterile dH_2O was added to the column, allowed to rest for 1 minute, and then centrifuged at 13,000 g for 1 minute to elute the DNA. The filtrate was not discarded. DNA concentration was measured using a nanodrop.

Verification by restriction digest involved using 500 ng of DNA, digesting it with 1 µL of the appropriate restriction enzyme, 1 µL of the appropriate restriction enzyme buffer, and adding water to reach a final volume of 10 µL. This mixture was incubated at the designated temperature for the respective restriction enzyme and visualized on a 1% agarose-TAE gel. The gel electrophoresis was run at 100 V in 1X TAE buffer and imaged using a Gel Doc™ XR+ Gel Documentation System from BioRad.

2.2.10 Yeast transformation

To generate production strains for JEscin, destination vectors encoding transcriptional pathways were introduced into yeast cells. In the case of JEscin production discussed in Chapter 6, the parent strain utilised was TME90. TME90 had been previously constructed in the Rosser lab, originating from the background strain TME04. TME04 was created by integrating pMGSE0IS(LEU2)-MEV2, which was constructed by Dr. Matthew Dale and consisted of a destination plasmid with LEU2 homology, enabling galactose-inducible expression of tHMG1, ERG9, and mERG1(K311R), into the BY4741*Δgal80* strain. TME90, on the other hand, was developed by chromosomally integrating TM94, a destination plasmid with URA3 homology that encoded galactose-inducible expression of AaBAS, CYP716A75, and ATR2, into the TME04 background.

For JEscin production, various JEscin strains were transformed using either high copy number plasmids or destination plasmids for chromosomal integration. Specifically, in transient JEscin production, TME90 was transformed with plasmids containing the transcriptional units of the genes of interest. These plasmids included components

such as BfCYP716Y1, MtCYP72A61v2, PvCYP93E9, and HHS (a high copy number plasmid with a spectinomycin resistance gene), among others. In the case of chromosomal integration for JEscin production, TME90 was transformed with specific constructs involving 308a homology sequences, which allowed for galactose-inducible expression of genes like HsUGT1A3, AtUGD1, and GmCYP72A69, ultimately producing a strain denoted as JTE09. For JEscin strains with *erg3Δ*, TME90 underwent a two-step transformation process. First, it was transformed with pE381, which encoded a spacer disrupting the *erg3* gene, leading to the creation of strain JTE06. Subsequently, JTE06 was further transformed with pJT019, another construct featuring 308a homology sequences and encoding HsUGT1A3, AtUGD1, and GmCYP72A69, resulting in the production of strain JTE11.

2.2.11 Yeast genomic DNA (gDNA) extraction

To prepare yeast samples, either 1.5 mL of liquid yeast culture grown overnight at 30 °C was utilised, or a sizable colony from an agar plate was selected. For the liquid culture, it was pelleted via centrifugation at 14,000 rpm for 2 minutes. Subsequently, the pelleted cells or the agar plate colony were re-suspended in 200 µL of lysis buffer composed of 2% Triton X-100, 1% SDS, 100 mM NaCl, 10 mM Tris-HCl at pH 8, and 1 mM EDTA at pH 8. The resulting mixture was then frozen at -80 °C for 10 minutes. This was followed by transferring the mixture to a 95 °C heat source for 1 minute, completing a freeze-thaw cycle. Freeze-thawing was repeated twice. The cells were then vortexed for 30 seconds, and 200 µL of chloroform was added, followed by an additional 2-minute vortexing step.

The next stage involved centrifuging the mixture at 14,000 rpm for 3 minutes. Following centrifugation, the upper aqueous phase was carefully transferred to a clean Eppendorf tube, where it was combined with 400 µL of cold ethanol and gently mixed by inversion. This mixture was then incubated at -20 °C for 5 minutes. Afterwards, the cold tube was once again subjected to centrifugation for 5 minutes at 14,000 rpm, and the supernatant was removed without disturbing the DNA pellet.

To further purify the DNA pellet, it was washed with 500 µL of 70% ethanol, and the pellet was allowed to air-dry at 60 °C for 10 minutes. Finally, the dried pellet was re-suspended in 30 µL of water, and the concentration of DNA was determined using a nanodrop spectrophotometer. This protocol follows the methodology outlined by Harju *et al*., (2004).

2.2.12 Yeast strain verification

To extract genomic DNA (gDNA) from individual colonies obtained after transformation, two different methods were employed. In one approach, gDNA extraction was performed using 20 µL of 20 mM NaOH by heating the sample at 95 °C for 10 minutes. Alternatively, the Bust n' Grab protocol, as detailed previously, was utilised for gDNA extraction.

Subsequently, the gDNA extracts were subjected to analysis through colony PCR, employing a touch-down protocol. The reaction setup included the following components: 0.5 µL of each primer at a concentration of 10 mM, 2 µL of the gDNA extract, 12.5 µL of OneTaq Quick Load 2X Master Mix with Green Buffer (NEB M0486), and 9.5 µL dH_2O. The thermal cycling program for the colony PCR consisted of the following steps: an initial denaturation at 94°C for 30 seconds, followed by 20 cycles of denaturation at 94 °C for 30 seconds, annealing at 70 °C for 45 seconds (with a gradual decrease of 1 °C per cycle), and extension at 68 °C for 1 minute. Subsequently, an additional 15 cycles were carried out, including denaturation at 94 °C for 30 seconds, annealing at 55 °C for 45 seconds, and extension at 68 °C for a duration calculated based on the size of the expected DNA fragment (1 minute per kilobase of DNA expected). The final step involved a 68 °C extension for 5 minutes. The entire PCR reaction was subsequently analysed using agarose gel electrophoresis to verify the presence and size of the DNA fragments.

2.2.13 Triterpenoid extraction

To prepare pre-cultures, 50 mL Falcon tubes were used, and the process involved inoculating 5 mL of YPD or CSM with the desired yeast strain. These pre-cultures were then incubated at 30 °C for 24 hours with shaking at 200 rpm. Subsequently, the pre-cultures were diluted to an OD_{600nm} of 0.25 in 5 mL of YPG within a Falcon tube and incubated at 30 °C for 72 hours with continuous shaking at 200 rpm.

For the extraction process, the OD_{600nm} of the yeast culture was first measured. Then, 1 mL of the yeast culture was transferred to a microtube and centrifuged at 14,000 rpm for 1 minute. The resulting pellet was re-suspended in 500 µL of lysis buffer, which consisted of 20 % KOH, 50 % ethanol, and 80 nM coprostanol. This suspension was incubated at 100 °C for 10 minutes, with the lids of the microtubes kept open to facilitate the evaporation of ethanol. Next, the cells were subjected to extraction procedures, which involved two rounds of extraction with 500 µL of hexane and two rounds with 500 µL of ethyl acetate. In each extraction step, 500 µL of the respective solvent (hexane or ethyl acetate) was added to the cell suspension, followed by vortexing at maximum speed for 10 seconds. Afterwards, the microtubes were centrifuged at 14,000 rpm for 1 minute, and the organic phase was carefully transferred to separate microtubes. During each extraction, 400 µL of the organic phase was removed, and these fractions were pooled together to yield a total of 1600 µL of extract. Subsequently, 600 µL of the extract was transferred to a 1.1 mL autosampler vial and subjected to evaporation using a GeneVac EZ-2 Elite evaporator, using the Low BP Mix program at 40 °C. The vials were then sealed with crimp caps, and the evaporated extracts were stored at room temperature until they were ready for analysis.

2.1.14 Glycosylated triterpenoid extraction

To initiate pre-cultures, 5 mL of YPD medium was inoculated with the desired yeast strain within 50 mL Falcon tubes. These pre-cultures were incubated at 30 °C for 24

hours with continuous shaking at 200 rpm. Subsequently, the pre-cultures were diluted to an OD_{600nm} of 0.25 in 20 mL of YPG medium within a conical flask and incubated at 30 °C for one week, while being subjected to shaking at 200 rpm.

For the extraction process, the OD_{600nm} of the yeast culture was first measured, following which 1 mL of the yeast culture was transferred to a microtube and pelleted at 14,000 rpm for 1 minute. The resulting pellet was then re-suspended in a solution comprising 10 µL of 4 mM echinocystic acid-glucoside and 50 µL of Yeast Buster. Approximately 100 µL of acid-washed glass beads were added to the microtube, followed by vortexing for 1 minute. This mixture was allowed to incubate at room temperature for 1 hour to facilitate cell lysis. Following the incubation period, the microtube was vortexed again for 1 minute. In parallel, 500 µL was withdrawn from the initial yeast culture supernatant and supplemented with 10 µL of 4 mM echinocystic acid-glucoside to prepare the supernatant for further processing.

Subsequently, both the lysed cells and the supernatant were subjected to extraction, each with two rounds of 500 µL butan-1-ol. In each extraction step, 500 µL of butan-1-ol was added, followed by a brief 10-second vortexing at maximum speed and subsequent centrifugation at 14,000 rpm for 1 minute. The resulting organic phases were transferred to separate microtubes. During each extraction, 400 µL of the organic phase was collected, and these fractions were combined to yield a total of 800 µL of extract. Following extraction, 600 µL of the extract was transferred to a 1.1 mL autosampler vial and sealed with caps. These extracts were stored at 4 ºC until they were ready for analysis.

2.1.15 Yeast sterol extraction

To initiate cultures, 5 mL of YPD or CSM medium was inoculated with the desired yeast strain within 50 mL Falcon tubes. These cultures were incubated at 30 °C for 24 hours while shaking at 200 rpm. The cultures were subjected to a washing process involving

two rinses with 5 mL of dH_2O. For each wash, the pellet was vortexed in water and subsequently centrifuged at 4000 rpm for 2 minutes. After centrifugation, the pellet was re-suspended in 1.5 mL of dH_2O. Following the washing steps, the cultures were diluted to an OD_{600nm} of 2.7, which corresponds to approximately 36.9 x 10^6 cells in 1.5 mL of culture. For the subsequent extraction, 1.5 mL of the yeast culture was pelleted at 14,000 rpm for 1 minute. The resulting pellet was re-suspended in 500 µL of lysis buffer consisting of 20 % KOH, 50 % ethanol, and 80 nM coprostanol. This suspension was then incubated at 100 °C for 10 minutes, with the lids left open to facilitate the evaporation of ethanol.

The cells were then subjected to a series of extractions with 500 µL of hexane, repeated thrice. In each extraction step, 500 µL of hexane was added, followed by vortexing for 10 seconds at maximum speed, centrifugation at 14,000 rpm for 1 minute, and removal of the organic phase to a separate microtube. Each extraction step collected 500 µL of the organic phase, and these fractions were combined to yield a total of 1500 µL of extract. Subsequently, 1 mL of the extract was transferred to a 1.1 mL autosampler vial and subjected to evaporation using a GeneVac EZ-2 Elite evaporator with the Low BP mix program at 40 °C. The vial was then sealed with crimp caps, and the evaporated extracts were stored at room temperature until they were ready for analysis.

2.1.16 GC-MS

Triterpenoid extracts were analysed using an Agilent 7200 gas chromatogram (GC) coupled to an Agilent 7890B quadrupole time-of-flight mass spectrometer (Q-TOF) with Gerstel Multi-Purpose Sampler (MPS) for automated sample derivatisation. Samples were trimethylsilylated by adding 50 µL MSTFA: pyridine (4:1) to the dried extract, vortexed for 30 s at 3000 rpm, and incubated at 37 °C for 60 min with shaking at 750 rpm. Samples were derivatised sequentially, with each sample being injected immediately after derivatisation. 1 µL of the derivatised sample was injected at a 10:1 split ratio into an Agilent DB-5ms column (30 m with 10 m guard x 250 µm x 0.25 µm). The GC parameters were as follows: constant helium flow of 1 mL/min; the inlet was

set to 250 °C; the oven was initially held at 100 °C for 1 minute, then increased to 300 °C at a rate of 60 °C/minute, then held at 300 °C for 25 minutes. Electron ionisation (EI) was performed at a source temperature of 230 °C, 35 µA filament current, 70 eV electron energy, and the mass range of 60-900 *m/z* was scanned at an acquisition rate of 4 spectra/s with a solvent delay of 10 minutes. Total ion chromatograms and mass spectra were analysed using the Agilent MassHunter Qualitative Analysis B.10.00 software. Many thanks to EdinOmics for devolving this protocol and machine operations.

2.1.17 LC-MS

Glycosylated triterpenoid extracts were subjected to analysis using an Agilent 6560 IM Q-TOF LC-MS system, which was coupled to an Agilent 1290 Infinity II UHPLC. The analytical procedure involved the injection of samples at a volume of 5 µL onto an ACE C18 PFP column, measuring 100mm in length and 2.1mm in diameter, with a particle size of 1.8 µm. During the analysis, a gradient elution method was employed, the details of which are outlined in Table 3. Specifically, Buffer A consisted of H_2O with 0.1 % formic acid, while Buffer B was composed of methanol with 0.1 % formic acid. The column was maintained at a temperature of 30 °C, and a constant flow rate of 0.3 ml/min was sustained throughout the procedure. For ionisation, electrospray ionisation (ESI) was employed. The acquisition mode was ion mobility-QTOF, and the analysis was conducted in positive ion mode. The mass spectrometer settings were configured as follows: the gas temperature was set at 325°C, the drying gas flow rate was maintained at 13 L per minute, the nebuliser operated at 20 psig, the sheath gas temperature and flow rate were 275°C and 12 L/min, respectively. Other settings included a VCap of 3500 V, a nozzle voltage of 700 V, a fragmenter voltage of 400 V, a collision energy of 65 V, a mass range spanning from 100 to 1600 *m/z*, and an acquisition rate of 1 frame per second. Data generated during the analysis, including total ion chromatograms and mass spectra, were processed and analysed using the Agilent MassHunter Qualitative Analysis B.10.00 software. It's important to

acknowledge EdinOmics for their contributions to protocol development and machine operation guidance.

Table 3: - Gradient of buffers for LC-MS analysis. Buffer A is H_2O with 0.1 % formic acid and buffer B is methanol with 0.1 % formic acid.

Time (min)	Buffer A %	Buffer B %
0	70	30
1	64	36
4	60	40
5	56	44
11	50	50
12	44	56
15	42	58
16	10	90
20	6	94
21	0	100
21.1	70	30

2.1.18 Microplate assays

To initiate pre-cultures, 5 mL of YPD or CSM medium was inoculated with the desired yeast strain within 50 mL Falcon tubes. These pre-cultures were then incubated at 30 °C for 24 hours while being shaken at 200 rpm. Subsequently, the OD_{600nm} of the pre-culture was measured, and the culture was diluted to an OD_{600nm} of 0.2 in 1 mL of YPD within a microtube. A stock solution of 40 $mg.mL^{-1}$ complete escin (or escin isomer) was diluted to the desired concentration in the same microtube, and methanol was added to maintain a uniform concentration of 1.25 %. The control sample consistently contained 1.25 % methanol.

Following these preparations, 100 µL of the culture with complete escin (or escin isomer) at an OD_{600nm} of 0.2 was pipetted into 96-well plates. A lid was placed on the plate and sealed with micropore tape. OD_{595nm} measurements were taken using a Tecan Sunrise plate reader at 30 °C, with a shaking mode set to "inside" and shaking intensity set to "high." Measurements were recorded at 15-minute intervals over 48 hours. The resulting data was exported into Microsoft Excel and subsequently

analysed using GraphPad Prism. Data was normalised to the endpoint values of the 0 $\mu g.mL^{-1}$ escin control, unless otherwise specified. Averages were calculated and plotted along with standard deviation for further analysis.

2.1.19 RNA Extraction

To maintain RNA integrity, the laboratory bench and all pipettes were thoroughly decontaminated with RNaseZAP (ThermoFisher Scientific AM9780).

Pre-cultures were prepared as previously described. The pre-cultures were diluted to an OD_{600nm} of 0.4 in 5 mL of YPD and incubated at 30 °C with shaking at 200 rpm for 5 hours. Subsequently, the OD_{600nm} was recorded, and specific treatments were administered. These treatments included 100 $\mu g.mL^{-1}$ of escin suspended in water, 75 $\mu g.mL^{-1}$ escin suspended in water, 100 $\mu g.mL^{-1}$ escin 1b dissolved in methanol, 100 $\mu g.mL^{-1}$ isoescin 1a dissolved in methanol, or methanol only (adjusted to 1.25 %). The treated cultures were then further incubated at 30 °C with shaking at 200 rpm for an additional 2 hours. Following this incubation, 1.5 mL of culture from each treatment (in triplicate) was used for total RNA extraction.

To extract RNA, 1.5 mL of culture was pelleted in a 1.5 mL Eppendorf tube at room temperature through centrifugation at 4000 g for 5 minutes, with the supernatant being discarded. The resulting pellets were flash-frozen using dry ice and subsequently stored at -80 °C until RNA extraction. Total RNA was isolated using the QIAgen RNeasy mini kit (QIAGEN 74104). Initially, the cell pellets were removed from the -80 °C freezer and lysed using 100 µL of Buffer Y1. The lysate was then incubated at 30 °C for 30 minutes at 200 rpm. Following this incubation, 350 µL of Buffer RLT with β-ME (β-mecaptoethanol) was added and vigorously vortexed. Next, 250 µL of 100 % ethanol was added and mixed via pipetting. The resulting sample was then transferred to an RNeasy spin column placed within a 2 mL collection tube and centrifuged for 15 seconds at 13,000 rpm. The flow-through was discarded unless otherwise specified.

Subsequently, 350 µL of Buffer RW1 was added to the column, and the centrifugation step was repeated. Then, 80 µL of DNase I in RDD was directly pipetted onto the membrane column and incubated at room temperature for 15 minutes. After incubation, 350 µL of Buffer RWI was added to the column and centrifuged for 15 seconds at 13,000 rpm. Following this step, 500 µL of Buffer RPE was added to the column and centrifuged for 15 seconds at 13,000 rpm. This process was repeated, but the centrifugation was extended to 2 minutes at 13,000 rpm. The column was then transferred to a new 2 mL collection tube and centrifuged at 13,000 rpm for 2 minutes. Subsequently, the column was moved to a new microfuge tube, and 50 µL of DEPC-treated water was added. A final centrifugation step at 13,000 rpm for 1 minute was performed to elute the RNA, which was collected without discarding. The concentration of RNA was measured using a nanodrop, and 500 ng of total RNA was analysed by agarose gel electrophoresis (1 % agarose-TBE) to verify RNA integrity. The RNA was then stored at -80 °C for future use.

2.1.20 cDNA synthesis

To ensure RNA integrity, the laboratory bench and all pipettes were meticulously cleaned and decontaminated with RNaseZAP (ThermoFisher Scientific AM9780).

For cDNA synthesis, RNA was retrieved from the -80 °C freezer and processed using the SuperScript IV First-Strand Synthesis System (Invitrogen 18091200). Initially, 500 ng of RNA was combined with 1 µL of 50 µM Oligo $d(T)_{20}$, 1 µL of 10 mM dNTP, and DEPC-treated water (Ambion AM9915G) to achieve a total volume of 13 µL. This mixture was then incubated at 65 °C for 5 minutes, followed by a transfer to ice for at least 1 minute. Next, the 5x SSIV buffer provided in the kit was briefly vortexed, and 4 µL of this buffer was added to 1 µL of 100 mM DTT, 1 µL of RiboLock (ThermoScientific EO0381), and 1 µL of SuperScript IV Reverse Transcriptase. Negative control samples received 1 µL of DEPC-treated water in place of the reverse transcriptase. The resulting mixture was then added to the RNA reaction mix and incubated at 50 °C for 10 minutes, followed by an additional incubation at 80 °C for 10 minutes. Subsequently, 1 µL of RNase H (Invitrogen 18021071) was added, and the mixture

was incubated for 20 minutes at 37 °C. The prepared cDNA samples were then stored at -20 °C for future use.

2.1.21 Quantitive Reverse Transcription polymerase chain reaction (qRT-PCR)

For quantitative reverse transcription PCR (qRT-PCR) analysis, 4 µL of cDNA was combined with 5 µL of PowerUp SYBR Green master mix and 0.5 mM of each primer. This mixture was placed into a MicroAmp EnduraPlate Optical 96-well Fast Blue Reaction plate and securely sealed with a Microseal B seal, resulting in a total volume of 10 µL per well. The plate was then subjected to centrifugation for 1 minute at 3000 rpm. The thermocycling program consisted of the following steps: initial denaturation at 95 °C for 20 seconds, followed by 40 cycles of denaturation at 95 °C for 3 seconds and annealing/extension at 60 °C for 30 seconds. Subsequently, a melt curve analysis was conducted, involving steps at 95 °C for 15 seconds, 60 °C for 1 minute, and 95 °C for 15 seconds. The qRT-PCR data obtained from the instrument was exported and subjected to analysis using Microsoft Excel. Graphs representing the results were generated using GraphPad Prism.

2.1.22 Propidium iodide (PI) assays

In each well of an Ibidi chambered slide (Ibidi 80807), 100 µL of concanavalin A was carefully pipetted, allowed to incubate for 30 seconds and then aspirated off. Subsequently, the wells were meticulously washed with water three times to ensure proper preparation. Yeast pre-cultures were grown in 5 mL CSM for 24 hours and then re-suspended in 5 mL of fresh CSM. Yeast cultures were cultivated until they reached an OD_{600nm} of 0.4. Following this, 400 µL of the yeast culture was transferred to each well. After a 5-minute incubation period, the culture was gently aspirated, and the wells were washed three times with treatment media, which consisted of 400 µL of PBS containing 1.25 % methanol and varying escin concentrations. This setup was then incubated for 1 hour at 30 °C with constant shaking at 200 rpm in a dark environment.

Subsequently, the cells were washed three times with 400 µL of PBS containing 5 $\mu g.mL^{-1}$ of propidium iodide (PI) and incubated for 20 minutes under the same conditions as before (30 °C, 200 rpm, in the dark). After this incubation, the cells were again washed three times with 400 µL of PBS. The prepared samples were then imaged using a Leica DMi8 inverted microscope, using an excitation/emission wavelength range of 540-580/592-668 nm.

2.1.23 Confocal microscopy

On the day of experimentation, chambered slides were prepared by treating them with concanavalin A (ConA). A volume of 45 µL of conA was carefully pipetted into each well and evenly spread across the surface using a sterile inoculation loop. The slides were then incubated at 30°C for 15 minutes. Subsequently, the conA solution was aspirated from each well, and thorough washing was performed with 500 µL of sterile water, repeated three times. These prepared slides could be stored at room temperature and used on the same day.

For the experimental setup, a 5 mL preculture of *S. cerevisiae* expressing sur7m-RFP and nce102-GFP in minimal media lacking uracil and histidine (ura-his-SD) was diluted to an OD_{600nm} of 0.2 on the day of the experiment. The diluted culture was allowed to grow until it reached the exponential phase (OD_{600nm} 0.4), and it was then vigorously vortexed. Subsequently, 400 µL of the cultured cells were pipetted into each well of the prepared chambered slides. The wells were covered with their respective lids and placed in a dark incubator for 20 minutes at 30°C with continuous shaking at 200 rpm. After the 20-minute incubation, the remaining cell suspension was aspirated from the wells, and each well was washed twice with ura- his- SD. Following the second wash, 400 µL of fresh media was added to each well.

Images were acquired at the Centre Optical Instrumentation Laboratory (COIL) using a Zeiss LSM 880 (Airyscan) microscope with an Alpha Plan Apochromat 100x/1.46 oil DIC M27 Elyra objective. Images were captured before any treatment, immediately

after the addition of media containing escin, and again after 1 hour. These steps were carried out in staggered intervals to ensure consistent exposure to escin across all samples. To analyse the confocal images, a Fiji plugin developed by Dr David Kelly from the COIL facility at the University of Edinburgh was used. This plugin analysed the fluorescence along the cell's circumference and generated histograms based on this data. The histograms were employed to identify the regions of the brightest fluorescence, providing insights into the localisation of the GFP-tagged proteins.

2.1.24 Membrane permeability

A preculture of WT *S. cerevisiae* was initially prepared by culturing it in 5 mL of CSM for 24 hours at 30 °C with continuous shaking at 200 rpm. The following day, this culture was diluted to an OD_{600nm} of 0.1, and yeast cells were subsequently grown until they reached an OD_{600nm} of 0.4, all in CSM.

The grown cultures were then subjected to centrifugation at 4,800 rpm for 1 minute, and the resulting pellet was re-suspended in water. The resuspension process was carried out to concentrate the yeast cells to an OD_{600nm} of 0.7. The culture was then divided into separate Falcon tubes, and escin was introduced to achieve final concentrations of either 0 $\mu g.mL^{-1}$ (in the presence of 1.25 % methanol), 31.25 $\mu g.mL^{-1}$, or 62.5 $\mu g.mL^{-1}$. For the positive control, escin was not added and mechanical lysis was used. The culture was instead subjected to two freeze-thaw cycles, involving freezing at -80 °C for 5 minutes and then thawing at 50 °C for 1 minute. Subsequently, sterile 0.5 mm glass beads were added to the culture, which was vortexed for 1 minute, and allowed to rest for 1 minute, and this vortex-rest cycle was repeated twice. Measurements were recorded at specific time points: at the moment of escin addition or mechanical lysis, at the 2-hour mark, and after a total incubation period of 24 hours. The data collected was then analysed using Microsoft Excel and presented using GraphPad Prism.

2.3 List of yeast strains

List of yeast strains generated or gifted, and the compound produced.

Strain	Genotype	Compound engineered to produce	Notes
S. cerevisiae BY4741	*MATa;* his3Δ1; leu2Δ0; met15Δ0; ura3Δ0		Wild-Type
S. cerevisiae BY4741 Δgal80	BY4741; YML051w::KanMX4		Galactose independent
S. cerevisiae BY4741 erg2Δ	BY4741; YMR202w::kanMX4		*erg2Δ* mutant
S. cerevisiae BY4741 erg3Δ	BY4741; YLR056w::kanMX4		*erg3Δ* mutant
S. cerevisiae BY4742 erg4Δ	BY4742; MATα; his3Δ1; leu2Δ0; lys2Δ0; ura3Δ0; YGL012w::kanMX4		*erg4Δ* mutant
S. cerevisiae BY4741 erg5Δ	BY4741; YMR015c::kanMX4		*erg5Δ* mutant
S. cerevisiae BY4741 erg6Δ	BY4741; YML008c::kanMX4		*erg6Δ* mutant
S. cerevisiae sur7m-RFP nce102-GFP			Gifted by Dr Jan Milinsky. RFP-tagged membrane protein Sur7p and GFP-tagged membrane protein Nce102p.
TME90	BY4741 *Δgal80; LEU2 5'[PGAL10-tHMG1-TENO2; PGAL1-ERG9-TTDH1; PGAL7-mERG1(K311R)-TPGK1]LEU2*	Erythrodiol	Gifted by Tessa Moses. Inducible mevalonate and erythrodiol.

	3' ; URA3 5'[PGAL1-AaBAS-TTDH1; PGAL10-CYP716A75-TENO2; PGAL3-ATR2-TPGK1] URA3 3'		
JTE01	TME90*;* p*MGS SEHHS[pGAL1-BfCYP716Y1-tTDH1]*	16-hydroxy-erythrodiol	Transient expression of 16-hydroxy-erythrodiol.
JTE02	TME90*;* p*MGS SEHHS[PGAL1-BfCYP716Y1-TTDH1; PGAL10v1-MtCYP72A61v2-TENO1]*	16, 22-dihydroxy-erythrodiol	Transient expression of 16, 22-dihydroxy-erythrodiol.
JTE03	TME90*;* p*MGS SEHHS[PGAL1-BfCYP716Y1-TTDH1; PGAL7-PvCYP939E-TADH1]*	16, 24-dihydroxy-erythrodiol	Transient expression of 16, 24-dihydroxy-erythrodiol.
JTE04	TME90*;* p*MGS SEHHS[PGAL1-BfCYP716Y1-TTDH1; PGAL10v1-MtCYP72A61v2-TENO1; PGAL7-PvCYP939E-TADH1]*	16, 22, 24-trihydroxy-erythrodiol	Transient expression of 16, 22, 24-trihydroxy-erythrodiol.
JTE05	TME90*;* p*MGS SEHHS[PGAL1-BfCYP716Y1-TTDH1; PGAL10v1-MtCYP72A61v2-TENO1; PGAL7-PvCYP939E-TADH1];* p*MGS SELHS[PGAL7-GmCYP72A69-TADH1]*	16, 21, 22, 24-tetrahydroxy-erythrodiol	Transient expression of 16, 21, 22, 24-tetrahydroxy-erythrodiol.
JTE06	TME90*;* YLR056w::spacer	Erythrodiol	Inducible mevalonate and erythrodiol, *erg3Δ* knockout.

JTE09	TME90; 308a 5' *[PGAL1-HsUGT1A3-TTDH1; PGAL10v1-AtUGD1-TENO1; PGAL7-GmCYP72A69-TADH1]* 308a 3'	glycosylated 21-hydroxy-erythrodiol	Inducible mevalonate and glycosylated 21-hydroxy-erythrodiol.
JTE11	JTE06; 308a 5' *[PGAL1-HsUGT1A3-TTDH1; PGAL10v1-AtUGD1-tENO1; PGAL7-GmCYP72A69-TADH1]* 308a 3'	glycosylated 21-hydroxy-erythrodiol	Inducible mevalonate and glycosylated 21-hydroxy-erythrodiol, *erg3Δ* knockout.

The sterol biosynthesis mutants were obtained from the yeast repository EUROSCARF.

2.4 List of primers

List of primers used; all primers provided by Integrated DNA Technologies (IDT).

Primer	Sequence	Notes
oJT075	TTGGTTTCTCCAGGTTACACTC	Used for qPCR of *ERG11* (Yang *et al*., 2015b)
oJT076	CGGAATAAGAGGAGGCAGAATC	Used for qPCR of *ERG11* (Yang *et al*., 2015b)
oJT081	CGAAGCTGACCGAAGTTCTG	Used for qPCR of *UPC2*
oJT082	ACTGAATGCCAACAAAGCGT	Used for qPCR of *UPC2*
oJT085	GACGGATGATATGGCCAGGA	Used for qPCR of *LAM4*
oJT086	TACTTTGTTGTACCGGGCCT	Used for qPCR of *LAM4*
oJT093	CATTTGGTGCTGTCAAGGCT	Used for qPCR of *ARE2*
oJT094	CGGTAGTGCCCCATTTCAAG	Used for qPCR of *ARE2*
oJT100	CGACGTCTTTTGCATCGCTA	Used for qPCR of *ERG3*
oJT101	CCATGGAACGGTCAACATCG	Used for qPCR of *ERG3*
oJT106	TTGGTACTGAAGGGCACACA	Used for qPCR of *ERG2*
oJT107	CCTGGCATGCTGTATTGCTT	Used for qPCR of *ERG2*
oJT108	TGATCGGGTTTCCACTGCTA	Used for qPCR of *ERG4*
oJT109	CCTTTTGTCCAAATCCCGGG	Used for qPCR of *ERG4*
oJT110	GGTGCAGGGAGAGGAGAAAA	Used for qPCR of *ERG4*
oJT111	ATCCACGATTCACCAGCCTT	Used for qPCR of *ERG4*
oJT114	AATAACTACGAGCCCCAGGT	Used for qPCR of *ERG5*
oJT115	TGGCCATGTCTGCAGTTTTC	Used for qPCR of *ERG5*
oJT116	CCTGGCGGACAATGATGATG	Used for qPCR of *ERG6*
oJT117	AACCAACCGCAGCATTTTCT	Used for qPCR of *ERG6*
oEJ157	CAAACCGCTGCTCAATCTTCT	Used for qPCR of *ACT1* (positive control) Gifted by Dr Emily Johnston
oEJ158	AATACCGGCAGATTCCAAACC	Used for qPCR of *ACT1* (positive control) Gifted by Dr Emily Johnston

Chapter 3: - Verification of *Saccharomyces cerevisiae* sterol mutants

3.1 Sterols

The plasma membrane (PM) is composed of sphingolipids, sterols, and glycerophospholipids, housing a myriad of proteins with pivotal roles in signalling, transport, cytoskeletal organisation, and more (Van Der Rest *et al*., 1995). Sterols, inherently hydrophobic, predominantly associate with the long-saturated acyl side chains of sphingolipids (Ahmed *et al*., 1997; Wattenberg & Silbert, 1983). The most renowned sterol in the animal kingdom is cholesterol, constituting 30-40 % of the mammalian PM (Pinkwart *et al*., 2019). Conversely, fungi such as *S. cerevisiae* have ergosterol, which is functionally analogous to cholesterol, comprising 12 mol % of the *S. cerevisiae* lipidome (Zinser *et al*., 1993; Ejsing *et al*., 2009). Plants exhibit a more intricate sterol composition, with more than 250 phytosterols identified (Cohn *et al*., 2010). Stigmasterol and sitosterol are the predominant constituents of plant phytosterols (Dufourc, 2008b). Sterols interact with lipids, modulating the fluidity and permeability of the PM (Luo *et al*., 2020).

The PM exhibits three distinct phases: the liquid-disordered phase, the gel phase, and the liquid-ordered phase. In the liquid-disordered phase, fluidity is high, and lipid packing is irregular, resulting in pronounced disorder and lateral mobility. The gel phase occurs when the temperature drops below the melting temperature, causing lipids to tightly pack together into a gel-like phase, limiting lateral lipid movement. The liquid-ordered phase, or sphingolipid-rich domain, forms when sterols are associated with PM sphingolipids. This causes acyl chains to pack more closely together compared to the liquid-disordered phase, all while retaining lateral mobility that the gel phase lacks (Quinn, 1985; Sprong *et al*., 2001; Lingwood & Simons, 2010; Johnston *et al*., 2020). This prevents gel phase formation at temperatures below the melting temperature (Quinn, 1985). Consequently, sterols, when present in high concentrations, augment PM rigidity and thickness (Nezil & Bloom, 1992; Sprong *et*

al., 2001). This effect arises from the sterols interacting with bilayer lipids, elongating the lipids relative to those without sterols (Nezil & Bloom, 1992). Sterols can form complexes with sphingolipids and phospholipids featuring saturated acyl chains, creating specialised membrane domains referred to as lipid rafts. These lipid rafts represent microdomains rich in sterols and sphingolipids, embedded within a sea of liquid disordered phases (Bagnat *et al*., 2000; Lingwood & Simons, 2010; Johnston *et al*., 2020). They play pivotal roles in signal transduction and the orchestration of molecular traffic across the membrane (Sheets *et al*., 1999; Waugh *et al*., 1999; Baumann *et al*., 2005; Li *et al*., 2018).

Sterols are not confined solely to the PM; other organelles possessing lipid bilayers, such as the endoplasmic reticulum (ER), also have sterols, though in lower quantities due to the necessity for increased membrane fluidity within this organelle (Sprong *et al*., 2001). Moreover, sterols influence the conformation of transmembrane proteins, thereby aiding their functionality, and participating in interactions with sterol transport proteins to regulate sterol production and distribution (Wong *et al*., 2019).

In yeast, investigations employing green fluorescent protein (GFP)-tagged PM proteins have uncovered evidence of enhanced PM compartmentalisation. For instance, yeast features MCC domains (membrane compartment of Can1), characterised by the patch-like distribution of proton-dependent permeases such as Can1, Fur1, and Tat2. In contrast, MCP domains (membrane compartments of Pma1) describe the distribution pattern of the ATPase Pma1. Importantly, these MCP domains are distinct from MCC domains (Merzendorfer & Heinisch, 2013).

3.1.1 Ergosterol biosynthesis in yeast

Wild-type (WT) *S. cerevisiae* produce ergosterol, which is equivalent in function to cholesterol in animals. The biosynthesis of ergosterol starts with isoprenoid biosynthesis, which has been outlined in detail in chapter 1.1.3 (Figure 12). Acetyl-CoA is converted to IPP and DMAPP in the cytoplasm, and then GPP synthase synthesises GPP from IPP and DMAPP. Another IPP is added to produce FPP. In the endoplasmic reticulum, two FPP molecules are condensed by squalene synthase (Erg9p) to produce the C30 molecule known as squalene (Dequin *et al*., 1988; Oulmouden & Karst, 1990; Fegueur *et al*., 1991; Jandrositz *et al*., 1991; Jennings *et al*., 1991; Tsay & Robinson, 1991; Corey *et al*., 1994; Moses *et al*., 2014; Kirby & Keasling, 2009; Feldmann, 2012).

Squalene is oxidised to 2,3-oxidosqualene by squalene epoxidase (Erg1p). This compound is then cyclised by lanosterol synthase (Erg7p) to produce lanosterol, which serves as the dedicated precursor for the synthesis of the essential molecule ergosterol. Then lanosterol 14-alpha-demethylase (Erg11p) demethylates C14 in lanosterol, resulting in the production of 4,4-dimethylcholesta-8,14,24-trienol, a process that requires haem. C14 sterol reductase (Erg24p) reduces the double C14-15 bond, leading to the formation of 4,4-dimethylzymosterol. Production of zymosterol utilises C-4 methyl sterol oxidase (Erg25p), C3 sterol dehydrogenase (Erg26p), and 3-keto sterol reductase (Erg27p) which collaboratively remove two methyl groups from 4,4-dimethylzymosterol. Additionally, two other proteins, Erg28p, which serves as a scaffold anchor facilitating protein-protein interactions between Erg26p and Erg27p, and Erg29p, which aids in regulating the activity of Erg25p, work together to produce zymosterol (Feldmann, 2012; Moretti-Almeida *et al*., 2013).

The final stage of the pathway involves the conversion of zymosterol to ergosterol in yeast or cholesterol in animals (Figure 13). While zymosterol can be incorporated into cellular membranes as is, it undergoes further modifications to produce fecosterol through the action of Erg6p (delta(24)-sterol C-methyltransferase) (Figure 14). Subsequently, fecosterol is transformed into episterol by Erg2p (C8 sterol isomerase), and finally into ergosterol through a series of desaturations and reductions catalysed

by Erg3p (C5 sterol desaturase), Erg5p (C22 sterol desaturase), and Erg4p (C24-28 sterol reductase) (Jordá & Puig, 2020).

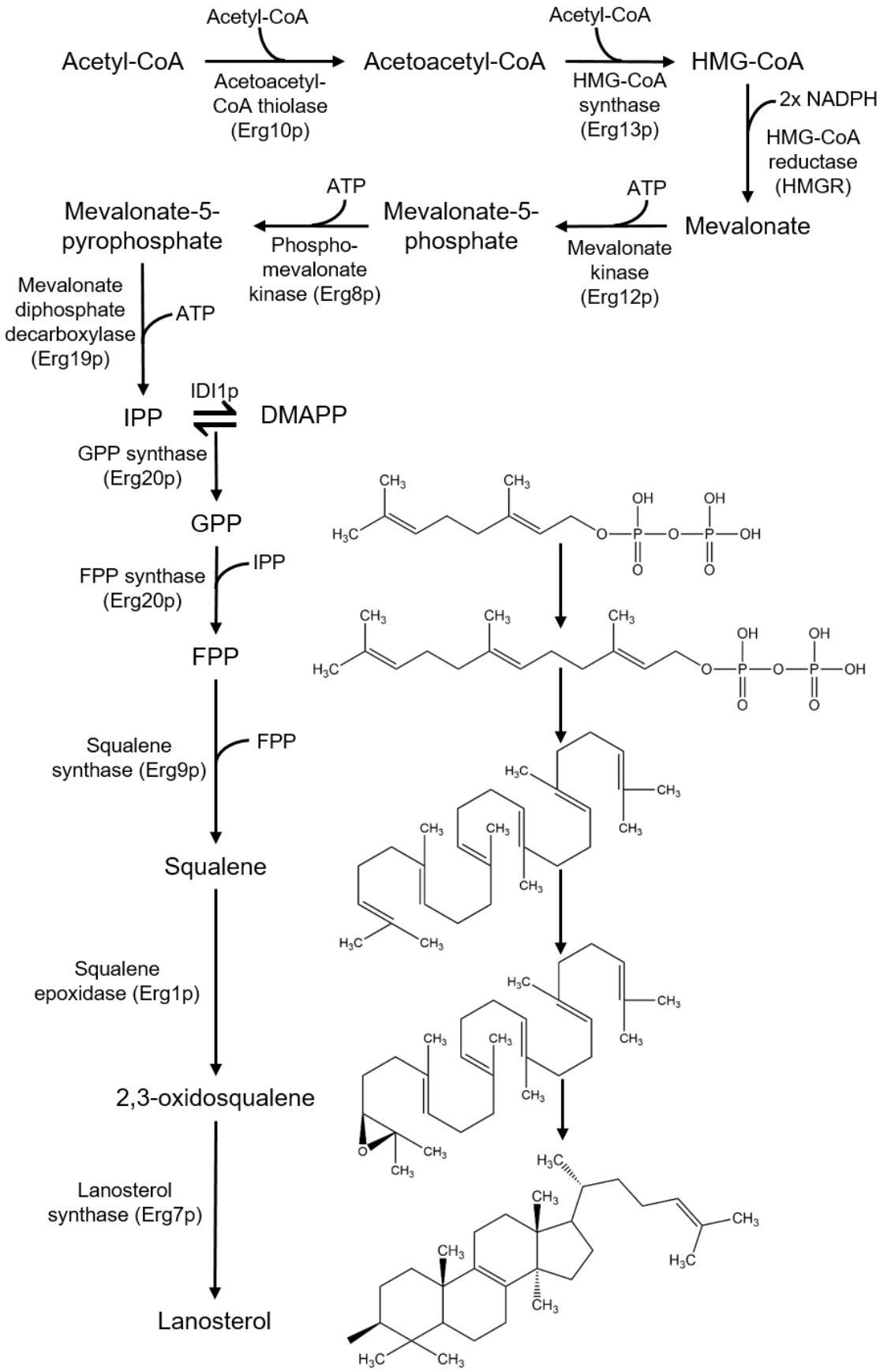

Figure 12: - Generation of lanosterol from acetyl-CoA. Full figure legend on next page.

Figure 12: - Generation of lanosterol from acetyl-Coenzyme A (acetyl-CoA). The mevalonate pathway converts acetyl-CoA to isopentenyl pyrophosphate (IPP), a 5-carbon molecule, via 3-hydroxy-3-methylglutaryl coenzyme A (HMG-CoA) and mevalonate. In ergosterol biosynthesis, mevalonate is used to produce IPP, which undergoes isomerisation to dimethylallyl pyrophosphate (DMAPP; 5C). Erg20p enzyme joins the two molecules, forming geranyl pyrophosphate (GPP; 10C), and then adds another IPP to generate farnesyl pyrophosphate (FPP; C15). Two FPP molecules combine to produce squalene (C30), which is subsequently epoxidised to form 2,3-oxidosqualene. Finally, Erg7p converts 2,3-oxidosqualene to lanosterol. The genes specific to *S. cerevisiae* are depicted in the figure.

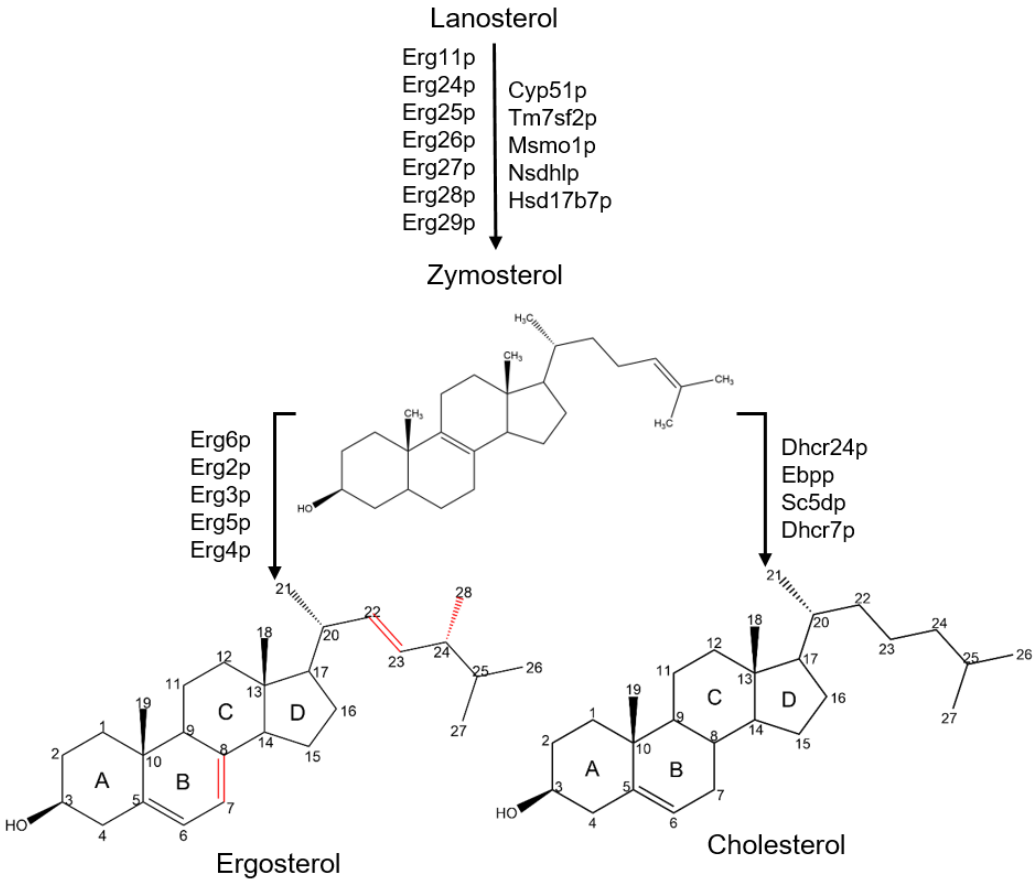

Figure 13: - Generation of ergosterol or cholesterol from lanosterol. The conversion of lanosterol to zymosterol is mediated by specific enzymes in yeast (presented on the left) and animals (presented on the right). In yeast, lanosterol 14-alpha-demethylase (Erg11p), C14 sterol reductase (Erg24p), C4 methyl sterol oxidase (Erg25p), C3 sterol dehydrogenase (Erg26p), 3-keto sterol reductase (Erg27p), endoplasmic reticulum membrane protein (Erg28p), and a protein involved in ergosterol biosynthesis (Erg29p) are involved. In animals, the corresponding enzymes are sterol 14-alpha-demethylase (Cyp51p), delta(14)-sterol reductase (Tm7sf2p), methylsterol monooxygenase 1 (Msmo1p), sterol-4alpha-carboxylate 3-dehydrogenase (Nsdhlp), and 17-beta-estradiol 17-dehydrogenase (Hsd17b7p). In animals, two biosynthetic pathways contribute to cholesterol production: the Bloch pathway and the Kandutsch-Russell pathway. These pathways differ in the order of cholesterol synthesis and the organs in which they are localised. Zymosterol is then converted to ergosterol in yeast through the action of delta(24)-sterol C-methyltransferase (Erg6p), C8 sterol isomerase (Erg2p), C5 sterol desaturase (Erg3p), C-22 sterol desaturase (Erg5p), and C24-28 sterol reductase (Erg4p).

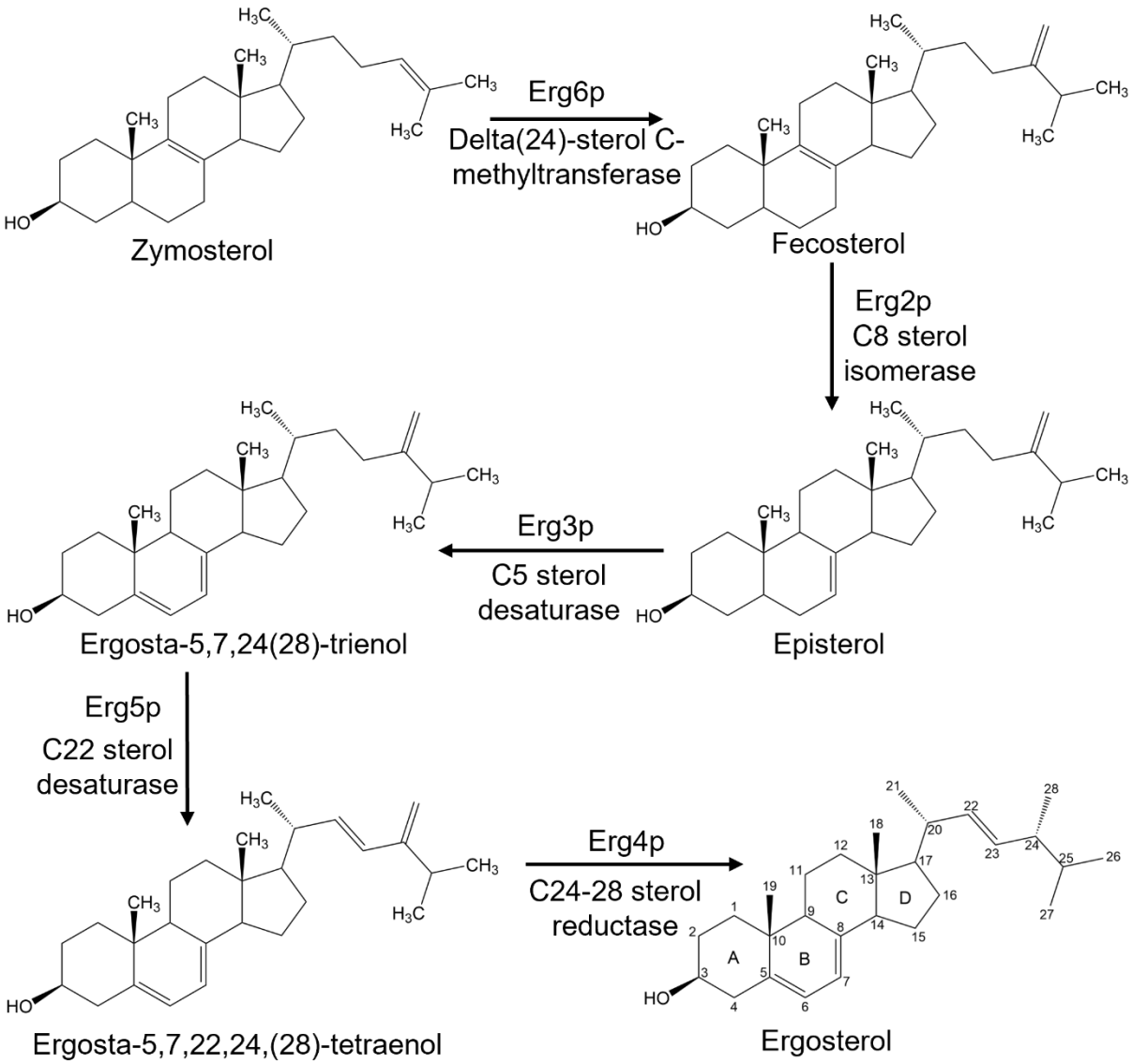

Figure 14: - Enzymatic pathway showing the production of ergosterol from zymosterol in *S. cerevisiae*. Erg6p uses S-adenosyl-L-methionine to donate a methyl group and thus S-adenosyl-L-homocysteine is produced. During the reaction of Erg3p and Erg5p, NADPH and oxygen are used to reduce episterol to ergosta-5,7,24(28)-trienol and ergosta-5,7,24(28)-trienol to ergosta-5,7,22,24(28)-tetraenol.

3.1.2 Cholesterol biosynthesis in animals

Cholesterol is produced by the same acetyl-CoA to mevalonate to lanosterol pathway as ergosterol (Figure 12). In animals, cholesterol is synthesised from lanosterol

through two interchangeable pathways known as the Bloch pathway and the Kandutsch-Russell pathway. The main distinction between these pathways lies in the saturation state of the side chain during the intermediates leading to cholesterol. In the Bloch pathway, zymosterol remains unsaturated at C24, whereas the Kandutsch-Russell pathway involves intermediates with side chain saturation. Both pathways encompass demethylation, isomerisation, and desaturation reactions to produce cholesterol (Cerqueira *et al*., 2016; Ershov *et al*., 2021). Finally, zymosterol is converted to cholesterol in animals by 24-dehydrocholesterol reductase (Dhcr24p), cholestenol delta-isomerase (Ebpp), sterol-C5-desaturase (Sc5dp), and 7-dehydrocholesterol reductase (Dhcr7p).

Ergosterol and cholesterol share very similar structures, with both molecules having a 30-carbon sterol structure comprising four rings and an aliphatic side chain (Figure 13). In ergosterol, there are double bonds located at positions C7-8 and C22-23, which are absent in cholesterol. Additionally, ergosterol contains a methyl group at C24 that is not present in cholesterol.

3.2 Sterol biosynthesis mutants

3.2.1 Viable strains

Glycosylated triterpenoids such as escin have been reported to interact with cholesterol (Augustin *et al*., 2011; Geisler *et al*., 2020; Sreij *et al*., 2019). Therefore, the hypothesis is that escin may inhibit yeast growth by interacting with ergosterol in the yeast PM (Zinser *et al*., 1993; Ejsing *et al*., 2009). Due to this we further hypothesise that yeast sterol biosynthesis mutants which accumulate sterols other than ergosterol, may show differing tolerances to escin. Therefore, we sought to compare sterol biosynthesis mutants alongside the WT to test this hypothesis.

There are five viable sterol biosynthesis single mutants, each with a single gene knockout in one of the following genes: *erg6, erg2, erg3, erg5, and erg4*. These genes have been replaced with a kanamycin resistance cassette (Giaever & Nislow, 2014). The *erg6Δ* mutant lacks delta(24)-sterol C-methyltransferase (Erg6p), which is responsible for methylating the C24 position of zymosterol to produce fecosterol in the WT strain (Figure 14). The *erg2Δ* mutant lacks C8 sterol isomerase (Erg2p), which catalyses the isomerisation of the C8-9 double bond to the C7-8 double bond. The *erg3Δ* mutant lacks C5 sterol desaturase, an enzyme involved in the formation of the second double bond in the B ring, specifically between positions C5-6, resulting in the formation of episterol in the WT strain. The *erg5Δ* mutant lacks C22 desaturase (Erg5p), a cytochrome P450 enzyme (CYP) responsible for the formation of the double bond between positions C22-23. The *erg4Δ* mutant, the last mutant in the series, lacks C24-28 sterol reductase (Erg4p), which is involved in the reduction of the double bond between positions C24 and C28. Loss of any of these five genes leads to viable mutants with different sterol compositions (Figure 15A). It is important to note that although the enzymes are depicted as acting sequentially, they can also act on other intermediates in the ergosterol biosynthesis pathway due to substrate promiscuity (Johnston *et al*., 2020). As a result, the membranes of the sterol biosynthesis mutants contain not just one sterol, but multiple sterols with slightly different configurations.

The *erg6Δ* mutant primarily produces four different sterols: zymosterol, cholesta-7,24-dienol, cholesta-5,7,24-trienol, and cholesta-5,7,22,24-tetraenol. The *erg2Δ* mutant produces three different sterols: fecosterol, ergosta-8-enol, and ergosta-5,8,22-trienol. The *erg3Δ* mutant also produces three sterols: episterol, ergosta-7,22,dienol, and ergosta-7-enol. The *erg5Δ* mutant produces two sterols: ergosta-5,7,24(28)-trienol and ergosta-5,7-dienol. Finally, the *erg4Δ* mutant produces ergosta-5,7,22,24(28)-tetraenol (Heese-Peck *et al*., 2002; Abe & Hiraki, 2009; Aguilar *et al*., 2010; Sun *et al*., 2013; Johnston *et al*., 2020). Ergosta-5,7,22,24(28)-tetraenol has the same structure as ergosterol, with an additional double bond between positions C24-28 (Figure 15B). The most predominant sterol in each mutant was investigated using Gas Chromatography-Mass Spectrometry (GC-MS) to further verify the mutants and check sterol compositions in different growth media.

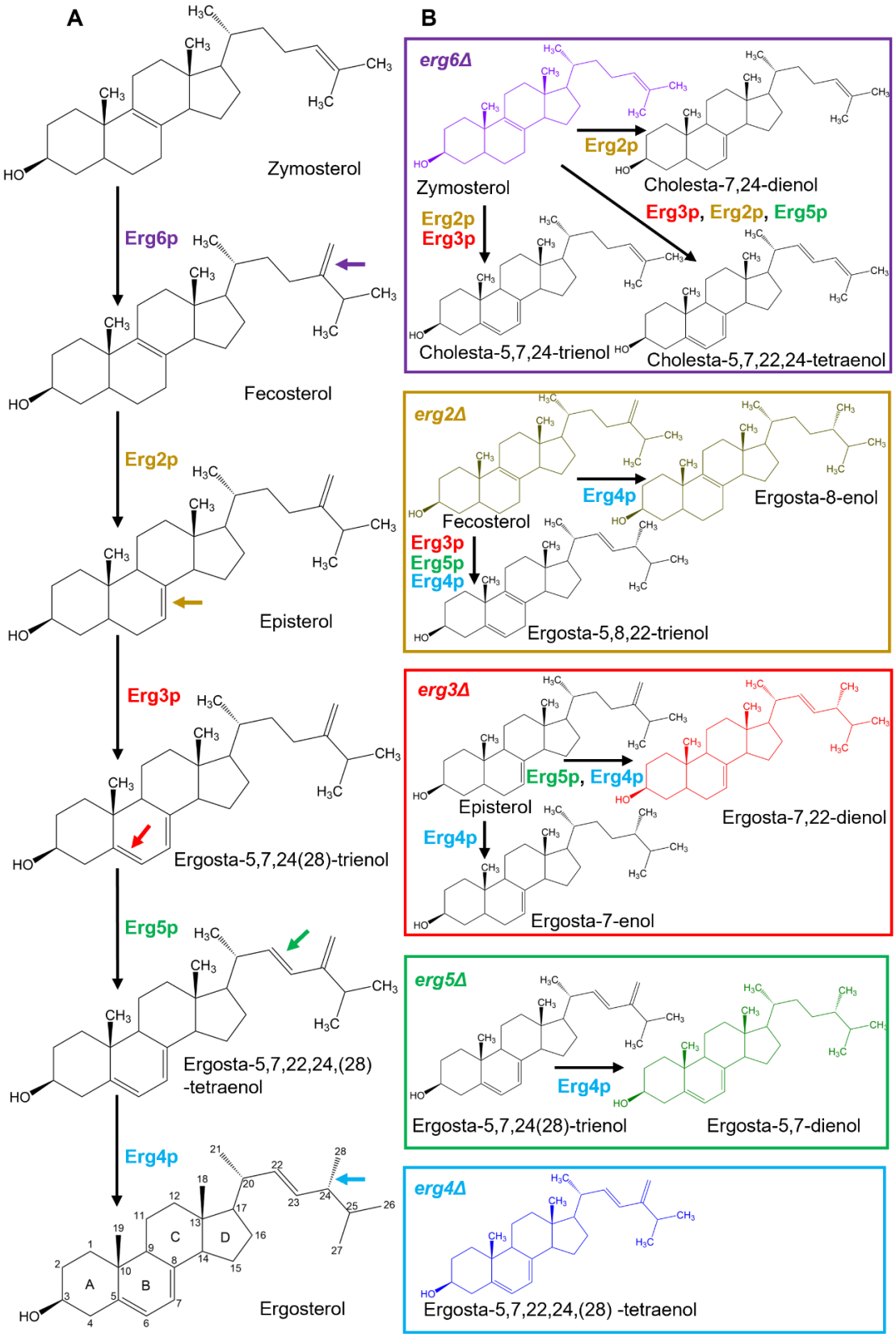

Figure 15: - Sterols in the sterol biosynthesis mutants. Full figure legend on next page.

Figure 15: - Sterols in the sterol biosynthesis mutants. A) Illustration of the pathway to ergosterol biosynthesis from zymosterol, with labelled enzymes. B) Sterols that are found in the sterol biosynthesis mutants, with the predominant sterol highlighted in colour. Sterol analysis was conducted using GC-MS. Adapted from (Johnston *et al*., 2020).

3.3 Confirming sterol composition of *S. cerevisiae* and sterol mutants with Gas Chromatography-Mass Spectrometry

3.3.1 Sterol composition of wild-type *Saccharomyces cerevisiae*

To confirm the sterol composition in the sterol biosynthesis mutants, sterols were extracted in hexane and ethyl acetate and subjected to GC-MS analysis. Previous studies have demonstrated that the sterol composition of these mutants is diverse, with multiple sterol intermediates present (Heese-Peck *et al*., 2002; Abe & Hiraki, 2009; Aguilar *et al*., 2010; Sun *et al*., 2013; Johnston *et al*., 2020). In this study, we focused on analysing the sterol content of the WT and sterol biosynthesis mutants after 24 hours of growth in rich media (YPD) and complete synthetic media (CSM). For the WT and *erg3Δ* mutant only, sterol content in low fluorescence media (LoFlo) was also verified. The inclusion of LoFlo media for the WT and *erg3Δ* mutant aimed to validate that the sterol composition was like that in other media, as it was required for subsequent experiments. Structures were determined using fragmentation patterns which have been previously published and compiled in Table 4.

Table 4: - Theoretical sterol fragmentation patterns of sterols. Under electron ionisation (EI) for various trimethylsilylated sterols present in the WT and sterol biosynthesis mutants.

Sterol	Molecular weight (Da)	Ions (m/z)	Fragmentation
Coprostanol	388	460	Parent ion $[M]^+$
		445	$[M -CH_3]^+$
		370	$[M -(CH_3)_3SiOH]^+$
		355	$[M -(CH_3)_3SiOH, -CH_3]^+$
Ergosterol	396	468	Parent ion $[M]^+$
		453	$[M -CH_3]^+$
		378	$[M -(CH_3)_3SiOH]^+$
		363	$[M -(CH_3)_3SiOH, -CH_3]^+$
Lanosterol	426	498	Parent ion $[M]^+$
		483	$[M -CH_3]^+$
		393	$[M -(CH_3)_3SiOH]^+$
		378	$[M -(CH_3)_3SiOH, -CH_3]^+$
Ergosta-5,7,22,24(28)-tetraenol	394	466	Parent ion $[M]^+$
		451	$[M -CH_3]^+$
		376	$[M -(CH_3)_3SiOH]^+$
		361	$[M -(CH_3)_3SiOH, -CH_3]^+$
Ergosta-5,7,24(28)-trienol	396	468	Parent ion $[M]^+$
		453	$[M -CH_3]^+$
		378	$[M -(CH_3)_3SiOH]^+$
		351	$[M -(CH_3)_3SiOH, -CH_3]^+$
Ergosta-5,7-dienol	398	470	Parent ion $[M]^+$
		455	$[M -CH_3]^+$
		480	$[M -(CH_3)_3SiOH]^+$
		365	$[M -(CH_3)_3SiOH, -CH_3]^+$
Episterol	398	470	Parent ion $[M]^+$
		455	$[M -CH_3]^+$
		480	$[M -(CH_3)_3SiOH]^+$
		365	$[M -(CH_3)_3SiOH, -CH_3]^+$

Table continued…

Sterol	Molecular weight (Da)	Ions (m/z)	Fragmentation
Ergosta-7,22-dienol	398	470	Parent ion $[M]^+$
		455	$[M -CH_3]^+$
		480	$[M -(CH_3)_3SiOH]^+$
		365	$[M -(CH_3)_3SiOH, -CH_3]^+$
Ergosta-7-enol	400	472	Parent ion $[M]^+$
		457	$[M -CH_3]^+$
		482	$[M -(CH_3)_3SiOH]^+$
		367	$[M -(CH_3)_3SiOH, -CH_3]^+$
Fecosterol	398	470	Parent ion $[M]^+$
		455	$[M -CH_3]^+$
		480	$[M -(CH_3)_3SiOH]^+$
		365	$[M -(CH_3)_3SiOH, -CH_3]^+$
Ergosta-8-enol	400	472	Parent ion $[M]^+$
		457	$[M -CH_3]^+$
		482	$[M -(CH_3)_3SiOH]^+$
		367	$[M -(CH_3)_3SiOH, -CH_3]^+$
Ergosta-5,8,22-trienol	398	470	Parent ion $[M]^+$
		455	$[M -CH_3]^+$
		480	$[M -(CH_3)_3SiOH]^+$
		365	$[M -(CH_3)_3SiOH, -CH_3]^+$
Zymosterol	384	456	Parent ion $[M]^+$
		441	$[M -CH_3]^+$
		366	$[M -(CH_3)_3SiOH]^+$
		351	$[M -(CH_3)_3SiOH, -CH_3]^+$
Cholesta-7,24-dienol	384	456	Parent ion $[M]^+$
		441	$[M -CH_3]^+$
		366	$[M -(CH_3)_3SiOH]^+$
		351	$[M -(CH_3)_3SiOH, -CH_3]^+$

Table continued…

Sterol	Molecular weight (Da)	Ions (m/z)	Fragmentation
Cholesta-5,7,24-trienol	382	454	Parent ion $[M]^+$
		439	$[M -CH_3]^+$
		364	$[M -(CH_3)_3SiOH]^+$
		349	$[M -(CH_3)_3SiOH, -CH_3]^+$
Cholesta-5,7,22,24-tetraenol	380	452	Parent ion $[M]^+$
		437	$[M -CH_3]^+$
		362	$[M -(CH_3)_3SiOH]^+$
		347	$[M -(CH_3)_3SiOH, -CH_3]^+$

In the WT strain, we observed slight differences in sterol content between YPD and CSM (Figure 16A). In YPD, ergosterol was the predominant sterol, comprising 66 % of the total sterols. Other sterols were also present and based on *m/z* ratios, previously reported relative abundances and retention times, these were predicted to be ergosta-5,7-dienol, and zymosterol (Nes *et al*., 2002; Bean *et al*., 2009; Guan *et al*., 2009; Jensen *et al*., 2015; Kaneshiro *et al*., 2015; (Weichert *et al*., 2016; Santivañez-Veliz *et al*., 2017; Voshall *et al*., 2021). Lanosterol, the precursor to ergosterol, accounted for 5 % of the sterols in YPD. Considering the conversion of lanosterol to ergosterol, it is expected that lanosterol content is low. Notably, 17 % of the sterols remained unidentified at the time of analysis. In CSM, the proportion of ergosterol decreased to 60 %, while the predicted ergosta-5,7-dienol and lanosterol contents increased to 19 % and 10 %, respectively (Figure 16B). This change is likely attributed to the slower growth of the WT in CSM compared to YPD, resulting in less conversion of lanosterol to ergosterol. The increased ergosta-5,7-dienol content could also be a consequence of the slowed growth, as it accumulates as the final intermediate in ergosterol synthesis. In LoFlo media, the ergosterol content (62 %) was slightly higher compared to that of the WT grown in YPD (Figure 16C). The elevated lanosterol content (increased from 7 % in YPD to 17 % in LoFlo) can be attributed to slower growth in LoFlo, leading to a build-up of precursors.

The determination of the sterols relied on the data presented in Table 4. Among these, ergosterol (Figure 17A) was identified as the peak at 12.837 minutes due to the

presence of the parent ion ($[M]^+$) with a mass-to-charge ratio (*m/z*) of 486. This *m/z* corresponds to the intact structure of ergosterol with the removal of one electron. The peak with a *m/z* of 378 corresponds to ergosterol with the removal of trimethylsilylate, while the 363 peak is ergosterol with neither trimethylsilylate nor a methyl group and the 337 peak is that of ergosterol without the A ring fragment (Kenny & Wetzel, 1995; Zhu *et al*., 2008; Feng *et al*., 2022). The other sterol positively identified in the WT was lanosterol (Figure 17B) at the peak at 14.564 minutes. The $[M]^+$ ion has a *m/z* value of 496. Two other ions were identifiable with 486 denoting lanosterol with the loss of a methyl group and 393 representing lanosterol with the loss of trimethylsilylate (Zhu *et al*., 2008; Hull *et al*., 2014; Feng *et al*., 2022). Subsequent figures (Figure 26) provide identification of zymosterol which is postulated to be present in the WT. The determination of the presence of zymosterol in the WT is based on the retention time.

3.3.2 Sterol composition of the sterol biosynthesis mutants

In the remaining mutants, ergosterol is absent and sterols were determined based on *m/z* ratios and relative abundances. In the *erg4Δ* mutant, only two sterols, ergosta-5,7,22,24(28)-tetraenol and lanosterol, were identified. When cultures were grown in YPD for 24 hours, the PM contained 93 % ergosta-5,7,22,24(28)-tetraenol and 7 % lanosterol (Figure 18A). However, in cultures grown in CSM for the same duration, the PM showed a lower percentage of ergosta-5,7,22,24(28)-tetraenol (73 %) and a higher percentage of lanosterol (27 %) compared to growth in YPD (Figure 18B). This indicates slower growth in CSM, as evidenced by the accumulation of lanosterol, the precursor, due to reduced production of ergosta-5,7,22,24(28)-tetraenol. It is worth noting that sterols can also be present in the cell interior, within the mitochondrial and endoplasmic reticulum membranes, but the fluidity of these membranes requires much less sterol than that of the PM. Therefore, throughout this thesis sterols are referred to as PM sterols only.

The only sterol present in the *erg4Δ* mutant other than lanosterol was ergosta-5,7,22,24(28)-tetraenol (Figure 19A) at peak 13.166 minutes. This was determined by the $[M]^+$ ion peak with an *m/z* value of 466. Two other ions were also present with 376 representing ergosta-5,7,22,24(28)-tetraenol with the removal of a

trimethylsilylate group and the 361 peak having neither trimethylsilylate nor a methyl group (Li Guan *et al*., 2009; Aguilar *et al*., 2010).

In the *erg5Δ* mutant, cultures grown in YPD for 24 hours exhibited three identifiable sterols in the PM, along with some unidentified sterols (Figure 20A). The most prevalent sterol in the *erg5Δ* mutant was ergosta-5,7-dienol at 79 %, followed by lanosterol at 10 %. Approximately 9 % of the sterols remained unidentified. When cultures were grown in CSM for 24 hours sterols present were ergosta-5,7-dienol at 54 % and its precursor lanosterol at 46 % (Figure 20B). The presumed slower growth in CSM was determined by a decrease in ergosta-5,7-dienol (Figure 21A) and an increase in lanosterol.

We were only able to identify ergosta-5,7-dienol (Figure 21A) in the *erg5Δ* mutant at peak 13.791 minutes. The $[M]^+$ ion was present, with a *m/z* value of 470, as well as *m/z* values for ergosta-5,7-dineol with the removal of either a methyl group (*m/z* 455), a trimethylsilylate group (*m/z* 380), or both (*m/z* 365). It has been previously reported that the *erg5Δ* mutant also has ergosta-5,7,24(28)-trienol in the PM (Guan *et al*., 2009; Sun *et al*., 2013; Johnston *et al*., 2020), but in this study, this sterol was not identified.

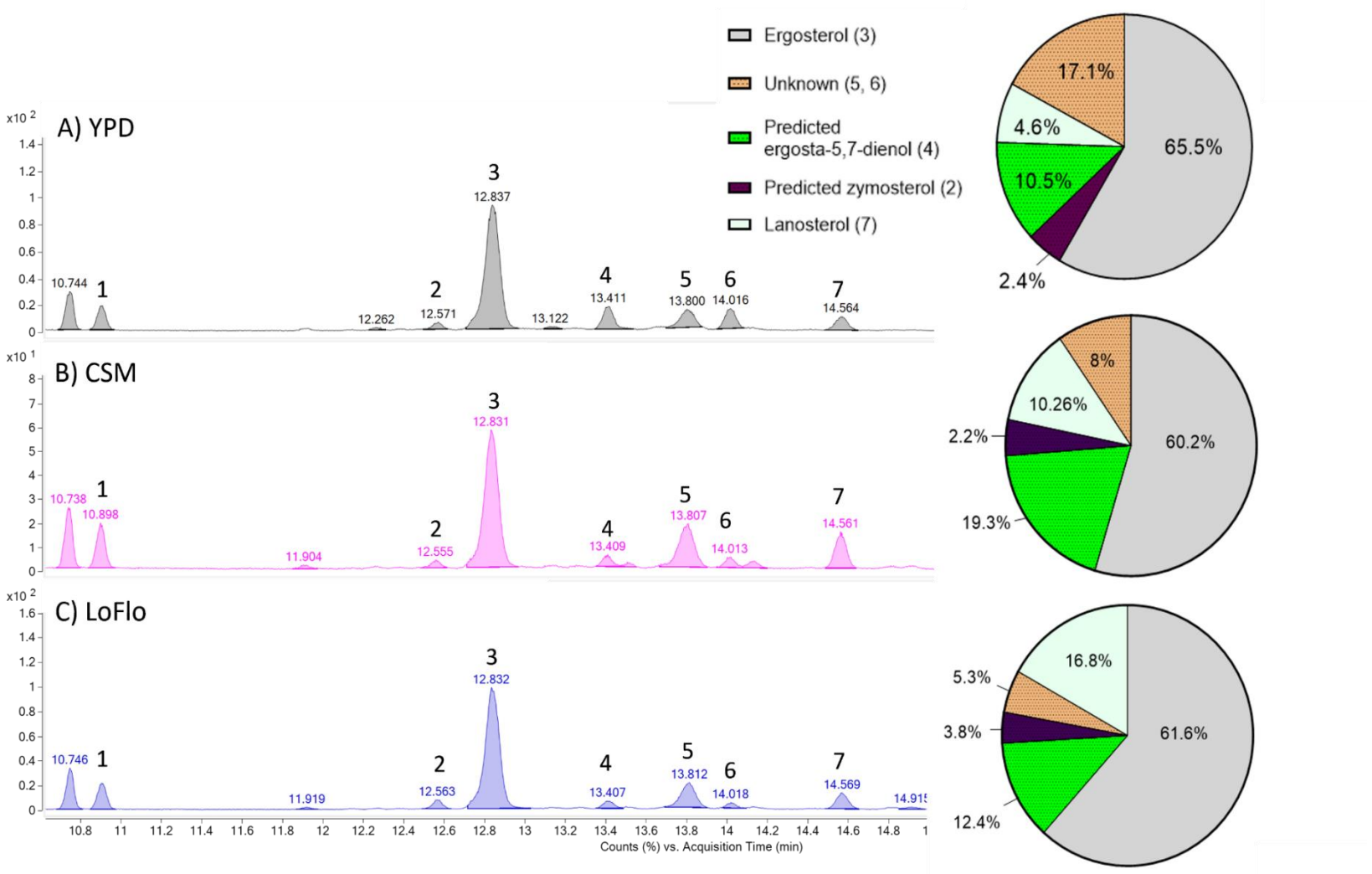

Figure 16: - Extracted ion chromatograms (EICs) showing peaks corresponding to sterols extracted from WT *S. cerevisiae*. See next page for full legend.

Figure 16: - Extracted ion Chromatograms (EICs) showing peaks corresponding to sterols extracted from WT *S. cerevisiae*. Yeast was cultured in either A) YPD, B) CSM or C) low fluorescence media for 24 hours. Peak annotation based on ion *m/z*, relative retention times and relative abundances from previous reports (Heese-Peck *et al*., 2002; Bean *et al*., 2009; Guan *et al*., 2009; Martel *et al*., 2010). (1) coprostanol, (2) predicted zymosterol, (3) ergosterol, (4) unknown, (5) predicted ergosta-5,7-dienol, (6) unknown, (7) lanosterol. Ergosterol and lanosterol were verified using reference standards. Average of triplicate values presented.

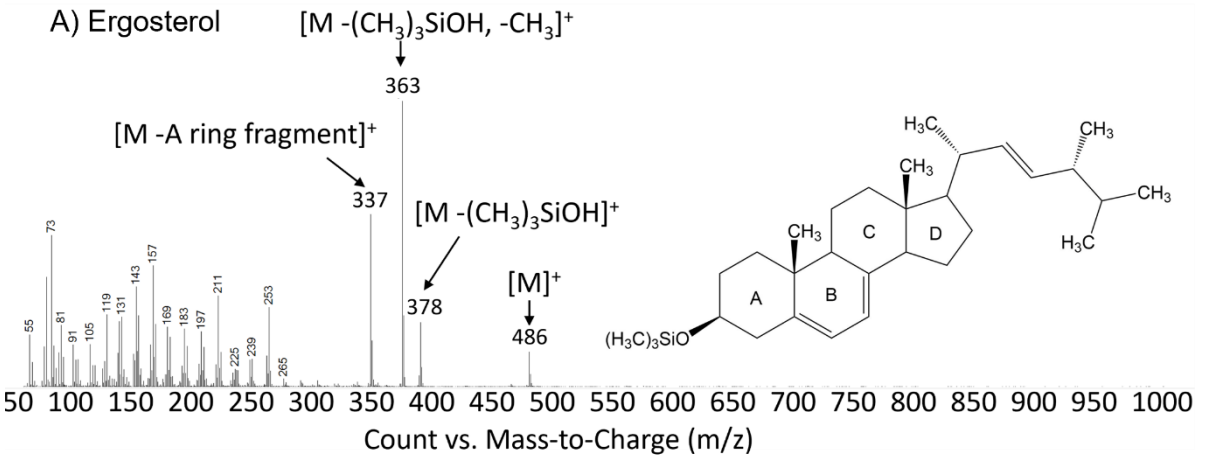

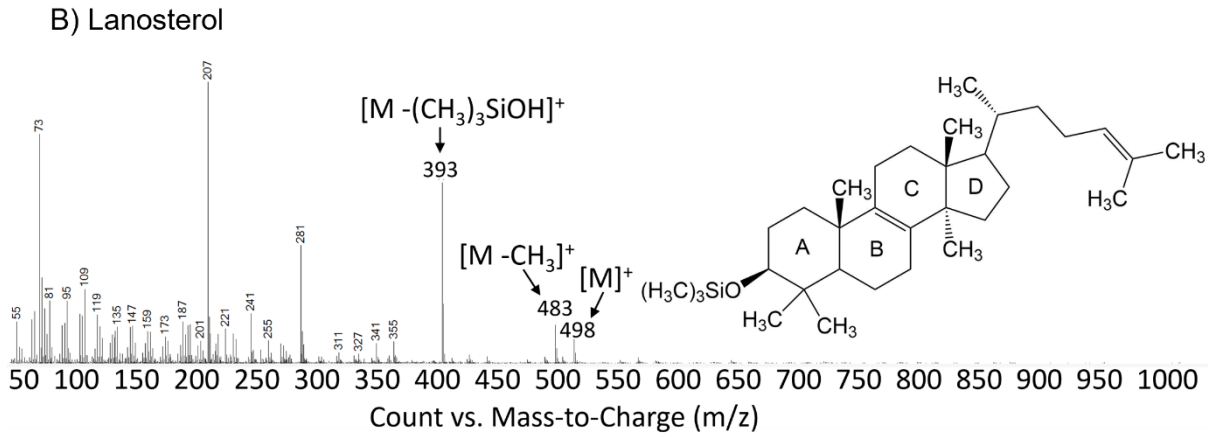

Figure 17: - Electron ion (EI) spectra of the WT sterols. A) ergosterol and B) lanosterol.

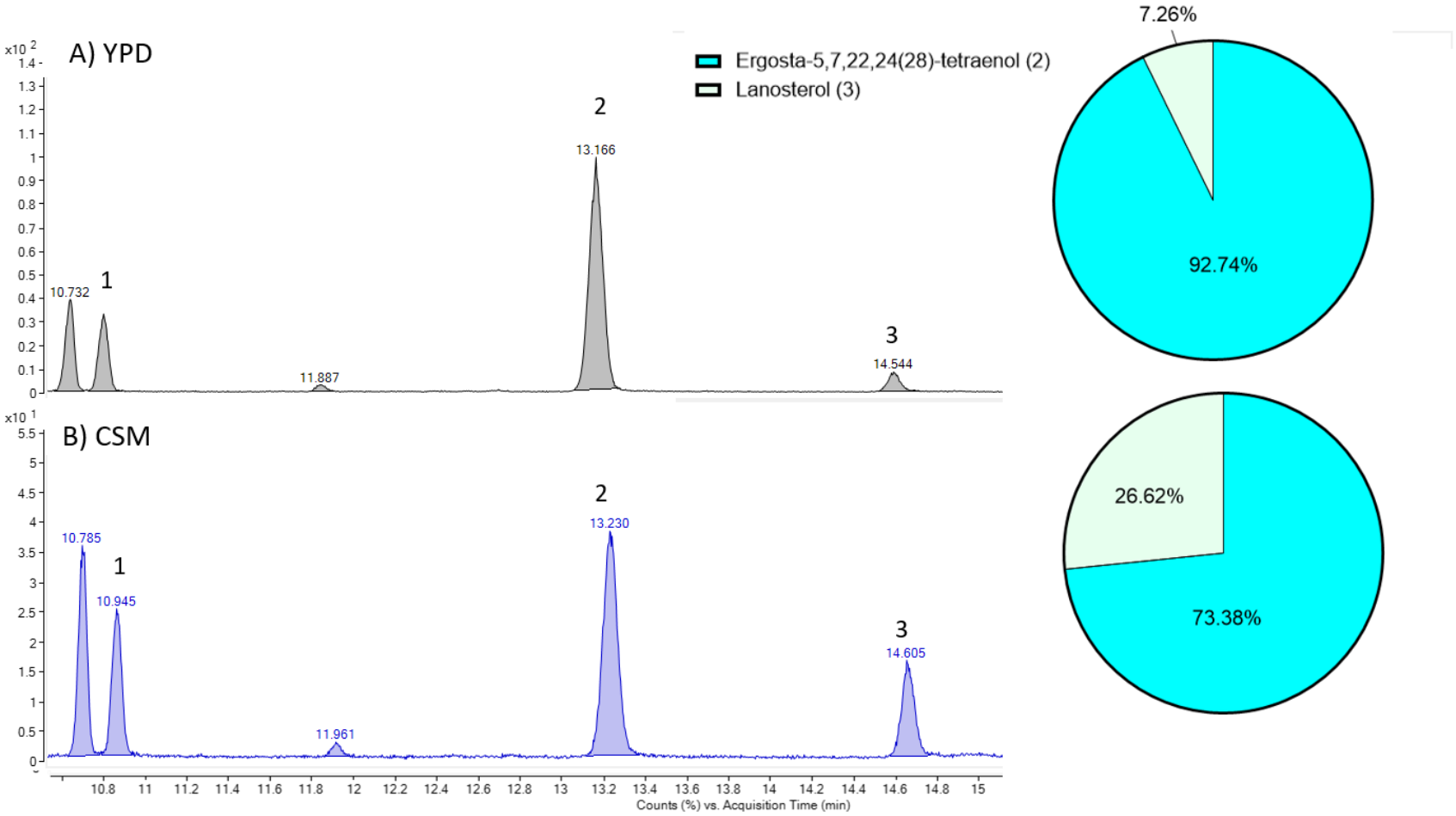

Figure 18: - Extracted ion chromatograms (EICs) showing peaks corresponding to sterols extracted from the *erg4Δ* mutant. Yeast cultured in either A) YPD or B) CSM media for 24 hours. Peak annotation based on ion m/z, relative retention times and relative abundances from previous reports (Heese-Peck *et al*., 2002). (1) coprostanol, (2) ergosta-5,7,22,24(28)-tetraenol, (3) lanosterol.

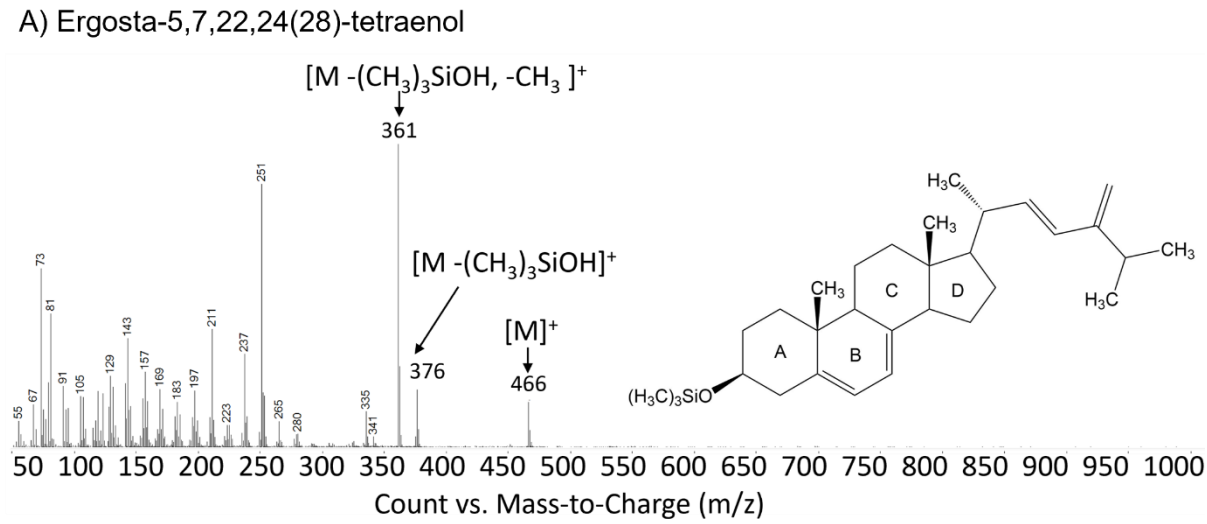

Figure 19: - Electron ion (EI) spectra of the sterols present in the *erg4Δ* mutant. A) ergosta-5,7,22,24(28)-tetraenol.

In the case of the *erg3Δ* mutant, we examined the sterols present after growth in YPD, CSM, or LoFlo media. In YPD-grown samples, ergosta-7,22-dienol dominated, accounting for up to 83 % of the sterol content (Figure 22A). The identifiable sterols were scarce, with episterol at 3 %, ergosta-7-enol at 2 %, and lanosterol at 0.3 %. The samples grown in YPD exhibited a high proportion of unknown sterols (12 %). However, in CSM, the content of ergosta-7,22-dienol halved to 42 %, while ergosta-7-enol significantly increased to 32 % (Figure 22B). Episterol content rose to 8 %, and lanosterol content increased to 6 %. The proportion of unknown sterols increased to 13 %. After 24 hours of growth in LoFlo media, the sterol composition of the *erg3Δ* mutant still favoured ergosta-7,22-dienol, comprising 49 % of the total sterols (Figure 22C). Ergosta-7-enol content decreased compared to CSM samples (17 % from 32 %), but it remained higher than that in the YPD samples (2 %). Episterol content was still higher in the LoFlo samples (12 %) compared to the YPD ones, while lanosterol remained at low levels (3 %). Unknown sterols were still present in large quantities (20 %).

The sterols present in the *erg3Δ* mutant were identified in peaks 12.586 minutes, 13.124 minutes and 14.129 minutes, corresponding to episterol (Figure 23A), ergosta-7,22-dienol (Figure 23B) and ergosta-7-enol (Figure 23C) respectively. Both

episterol and ergotsa-7,22-dienol have $[M]^+$ ions with a *m/z* value of 470 and similar fragmentation patterns, with a 455 (methyl group removal), 380 (trimethylsilylate removal) and 365 (methyl and trimethylsilylate removal) peak. Therefore, the identification of these sterols was determined by previously reported retention times, where episterol has been reported to have a quicker retention time than ergosta-7,22-dienol (Bean *et al*., 2009; Martel *et al*., 2010). These sterols were also differentiated based on composition reports, where ergosta-7,22-dienol has been reported to be present in the *erg3Δ* mutant at a higher concentration than that of episterol (Sanglard *et al*., 2003; Li Guan *et al*., 2009). Ergosta-7-enol was identified at the 14.129-minute peak with a $[M]^+$ ion at 472 and subsequent methyl removal with a *m/z* value of 457. Trimethylsilylate group removal was identified at peak 382 and both methyl group and trimethylsilylate group removal was identified at peak 367.

In the *erg2Δ* mutant, the most abundant sterols observed after 24 hours of growth in YPD were fecosterol and ergosta-8-enol, constituting 39 % and 29 % of the sterol content, respectively (Figure 24A). Additionally, a significant portion (29 %) of unknown sterols was found in the YPD-grown strain, while ergosta-5,8,22-trienol (Figure 25B), and lanosterol were present in small proportions (5 %, and 0.1 % respectively). Similarly, in CSM, fecosterol (Figure 25A) and ergosta-8-enol (Figure 25C) were present in comparable amounts (41 % and 35 % respectively), with reduced levels of unknown sterols (20 %) (Figure 24B). These results suggest that there are minimal differences in the sterol composition of the *erg2Δ* mutant grown in either YPD or CSM.

The sterols were determined in the *erg2Δ* mutant to be fecosterol (Figure 25A), ergosta-5,8,22-trienol (Figure 25B) and ergosta-8-enol (Figure 25C). Likewise, with episterol and ergosta-7,22-dienol, fecosterol and ergosta-5,8,22-trienol have similar fragmentation patterns. Both aforementioned sterols have a $[M]^+$ ion with a *m/z* value of 470, and subsequent fragmentation ions with *m/z* values of 455 (methyl group removal), 380 (trimethylsilylate removal) and 365 (methyl and trimethylsilylate removal). Therefore, identification was based on the retention times, where fecosterol has a slower retention time than ergosta-5,8,22-trienol (Jensen *et al*., 2015).

Ergosta-8-enol has a $[M]^+$ ion with a *m/z* value of 472 and removal of the methyl group, and trimethylsilylate group and both have *m/z* values of 457, 382 and 367 respectively.

Lastly, in the *erg6Δ* mutant, when cultures were grown in YPD for 24 hours, the predominant sterol in the PM was zymosterol at 55 % (Figure 26A). Another common sterol observed in the PM during YPD growth was cholesta-5,7,24-trienol at 29 %, followed by cholesta-5,7,22,24-tetraenol at 10 %. Small amounts of lanosterol and unknown sterols were detected at 3 % each. When cultures were grown in CSM for 24 hours, the proportions of zymosterol and cholesta-5,7,24-trienol remained relatively unchanged, with 57 % and 34 %, respectively (Figure 26B). However, cholesta-5,7,22,24-tetraenol exhibited a decrease in the PM of WT *S. cerevisiae* grown in CSM, comprising only 3 % compared to 10 % in YPD. Additionally, another intermediate, choelsta-7,24-dineol, was present in the CSM-grown cultures at 2 %. Similar to the YPD-grown cultures, small amounts of lanosterol and unknown sterols were found at 2 % each. These results suggest minimal differences in the sterol composition of the *erg6Δ* mutant when grown in YPD or CSM.

Present in the *erg6Δ* mutant, zymosterol (Figure 27A) and cholesta-7,24-dienol (Figure 27B) both have a $[M]^+$ ion with an *m/z* value of 456, therefore again these sterols were determined by their retention times and the concentration of the sterols in previous reports (Nes *et al*., 2002; Kaneshiro *et al*., 2015; Weichert *et al*., 2016). Cholesta-5,7,22,24-tetraenol (Figure 27C) has a $[M]^+$ ion with an *m/z* value of 452 and fragments at 362 (trimethylsilylate group removal) and 347 (trimethylsilylate and methyl group removal). Cholesta-5,7,24-trienol (Figure 27D) has a $[M]^+$ ion with an *m/z* value of 454 and subsequent *m/z* values of fragments of 364 (trimethylsilylate group removal) and 349 (trimethylsilylate and methyl group removal) (Zhu *et al*., 2008; Liu *et al*., 2011).

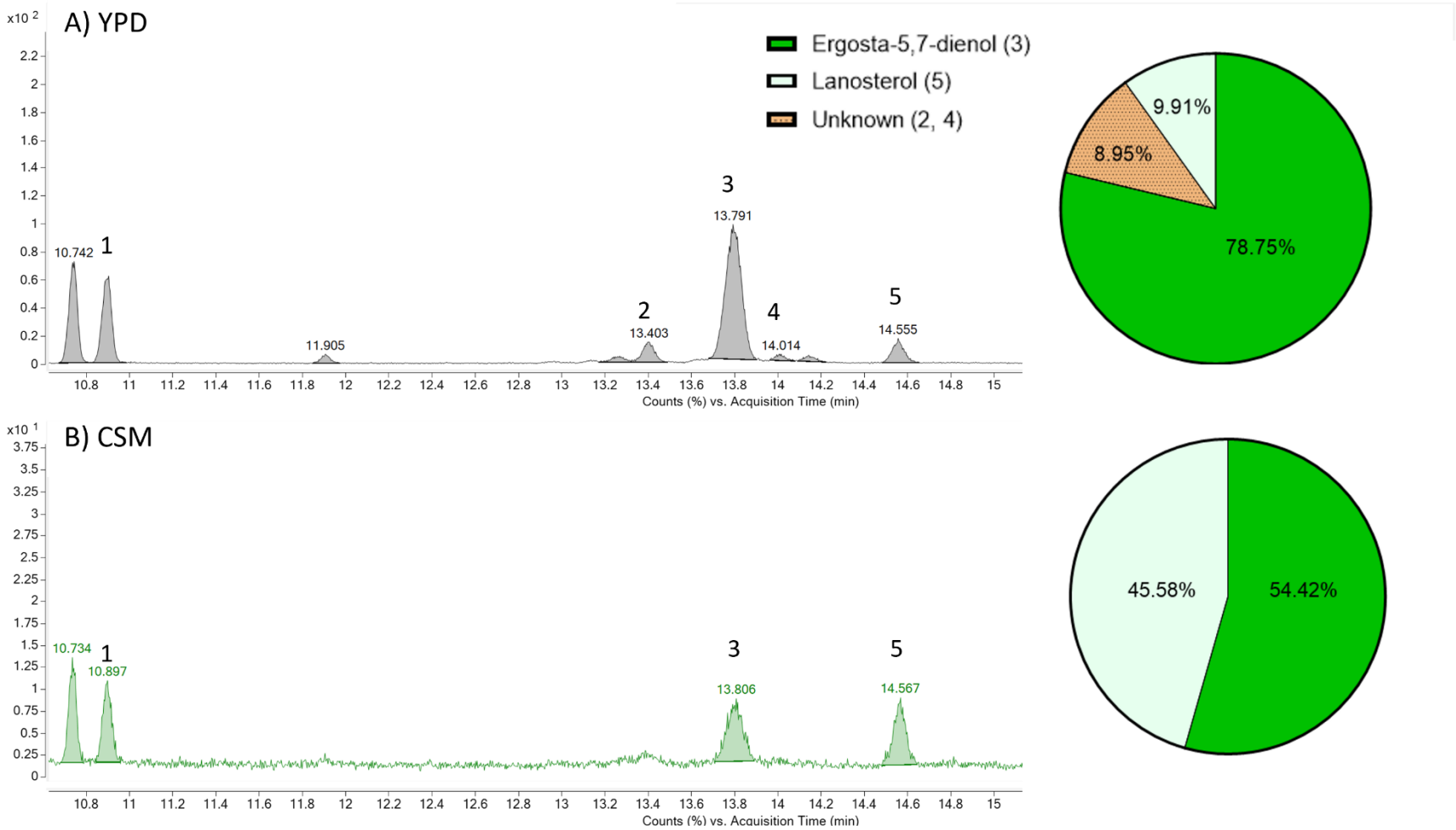

Figure 20: - Extracted ion chromatograms (EICs) showing peaks corresponding to sterols extracted from the *erg5Δ* mutant. Yeast cultured in either A) YPD or B) CSM media for 24 hours. Peak annotation based on ion m/z, relative retention times and relative abundances from previous reports (Voshall *et al*., 2021). (1) coprostanol, (2) unknown, (3) ergosta-5,7-dienol, (4) unknown, (5) lanosterol.

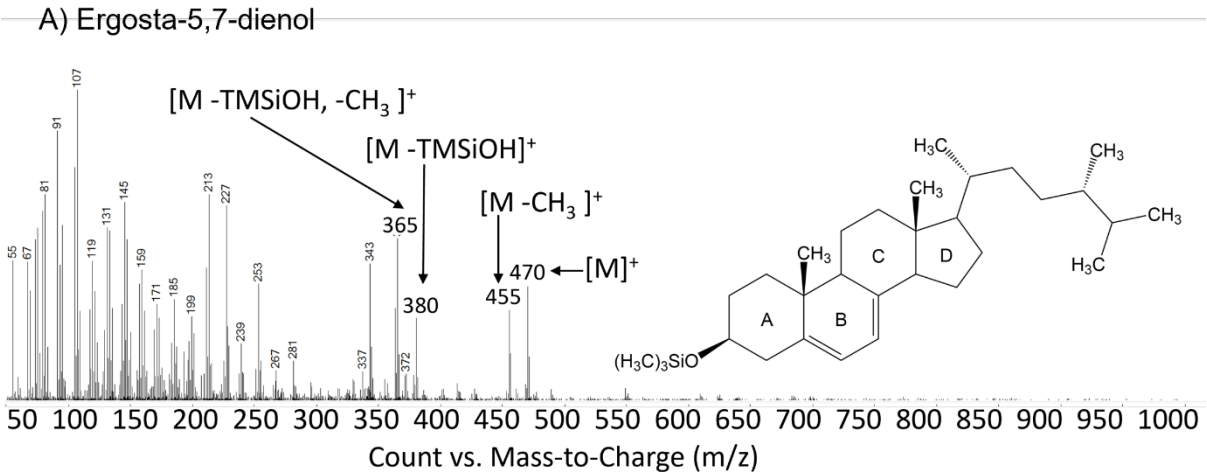

Figure 21: - Electron ion (EI) spectra of the sterols present in the *erg5Δ* mutant. A) ergosta-5,7-dienol.

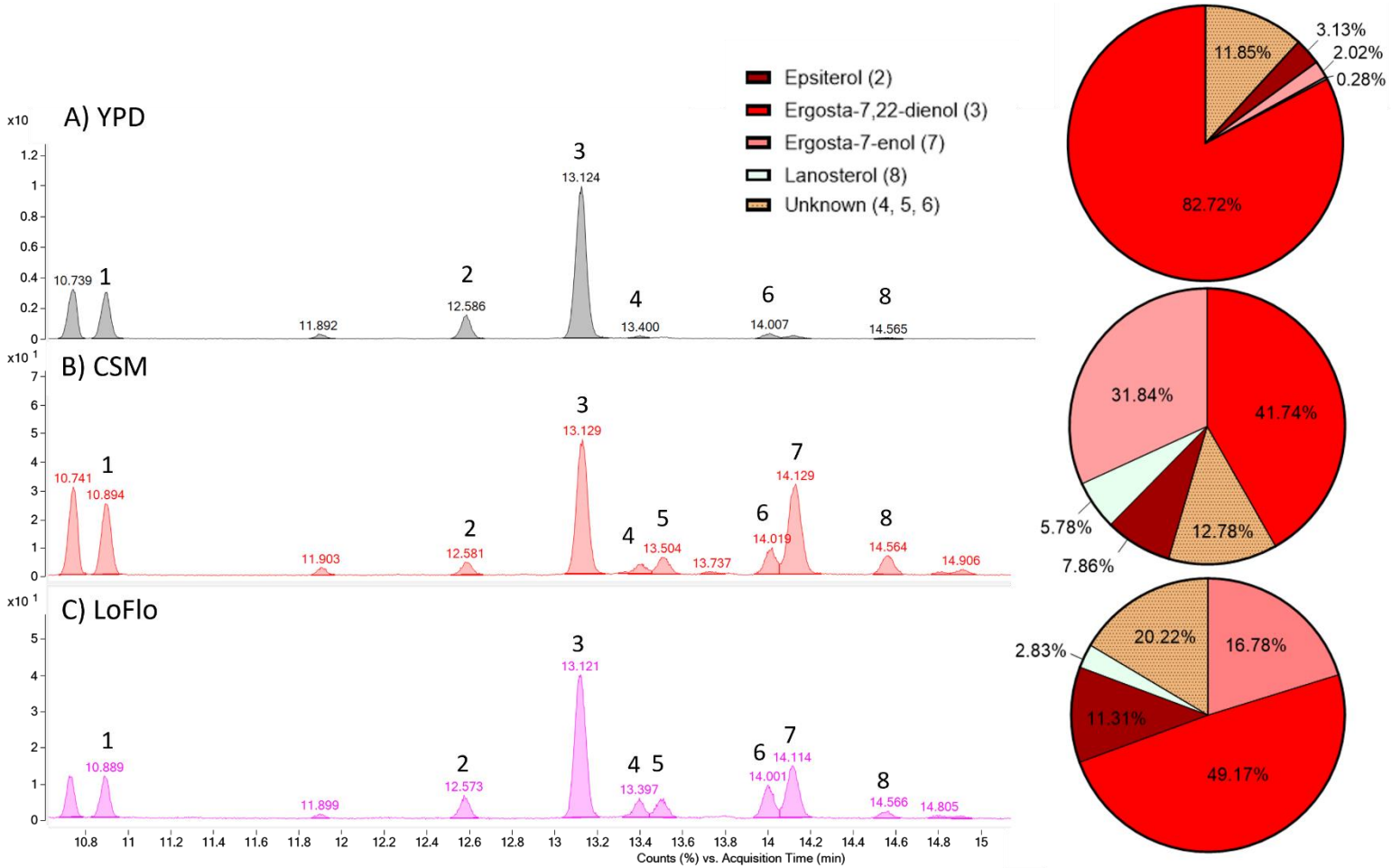

Figure 22: - Extracted ion chromatograms (EICs) showing peaks corresponding to sterols extracted from the *erg3Δ* mutant. Yeast cultured in either A) YPD or B) CSM media for 24 hours. Peak annotation based on ion m/z, relative retention times and relative abundances from previous reports (Bean *et al*., 2009; Martel *et al*., 2010). (1) coprostanol, (2) ergosta-7,22-dienol, (3) episterol, (4) unknown, (5) unknown, (6) unknown, (7) ergosta-7-enol, (8) lanosterol. Average of triplicate values presented.

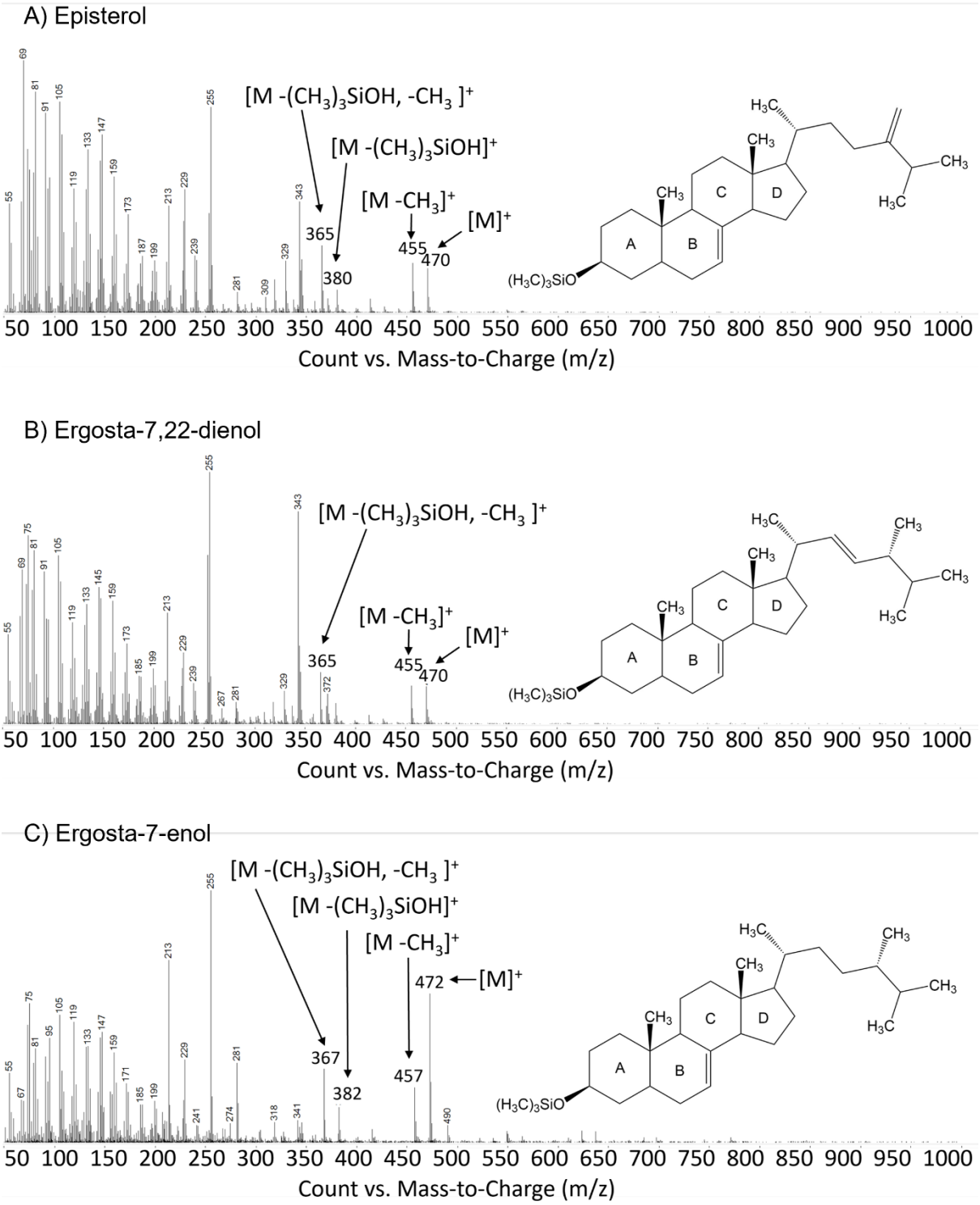

Figure 23: - Electron ion (EI) spectra of the sterols present in the *erg3Δ* mutant.

A) episterol, B) ergotsa-7,22-dienol and C) ergosta-7-enol.

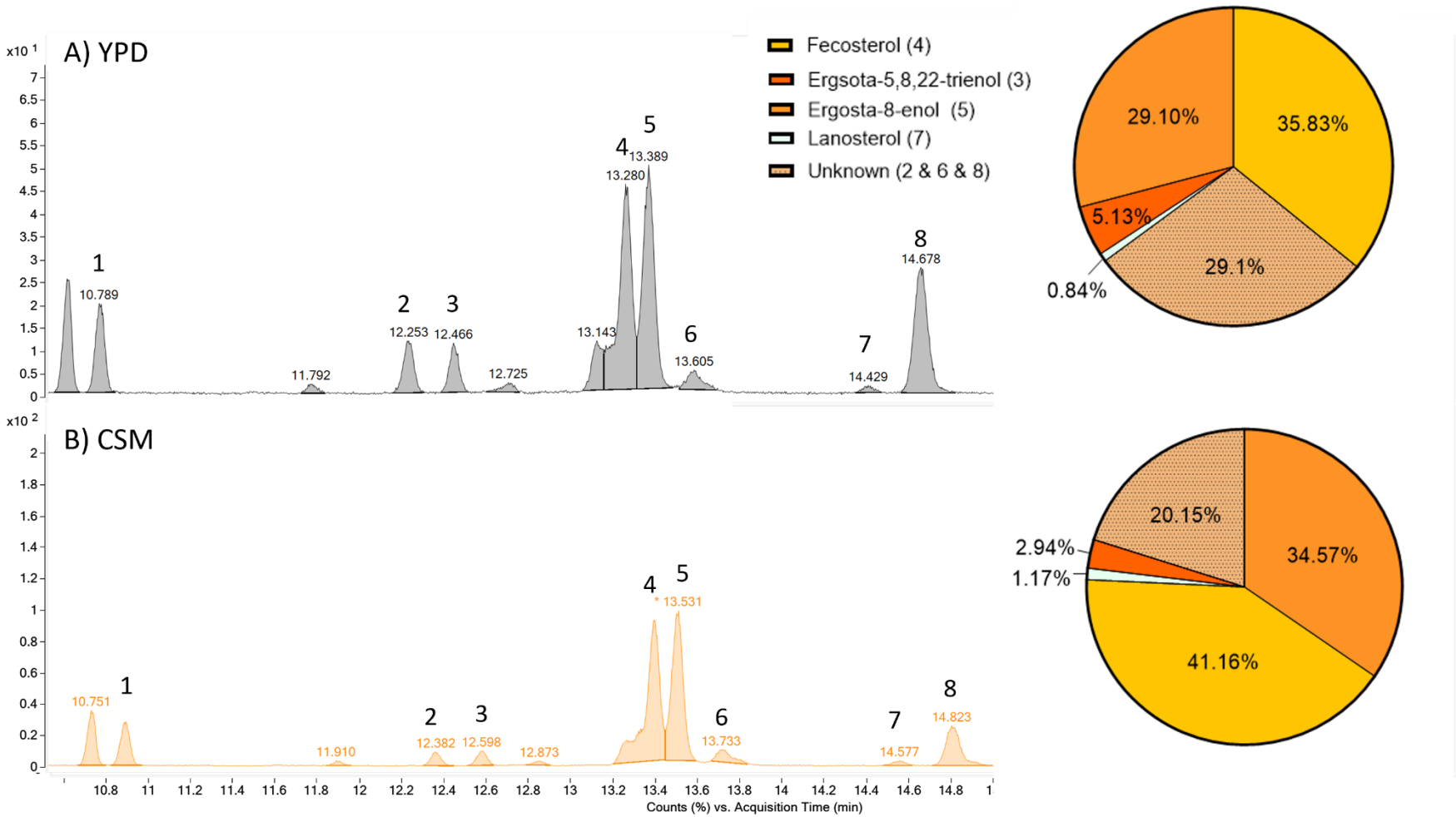

Figure 24: - Extracted ion chromatograms (EICs) showing peaks corresponding to sterols extracted from the *erg2Δ* mutant. Yeast cultured in either A) YPD or B) CSM media for 24 hours. Peak annotation based on ion m/z, relative retention times and relative abundances from previous reports (Jensen *et al*., 2015). (1) coprostanol, (2) unknown, (3) ergosta-5,8,22-trienol, (4) fecosterol, (5) ergosta-8-enol, (6) predicted ergosta-5,7-dienol, (7) lanosterol, (8) unknown.

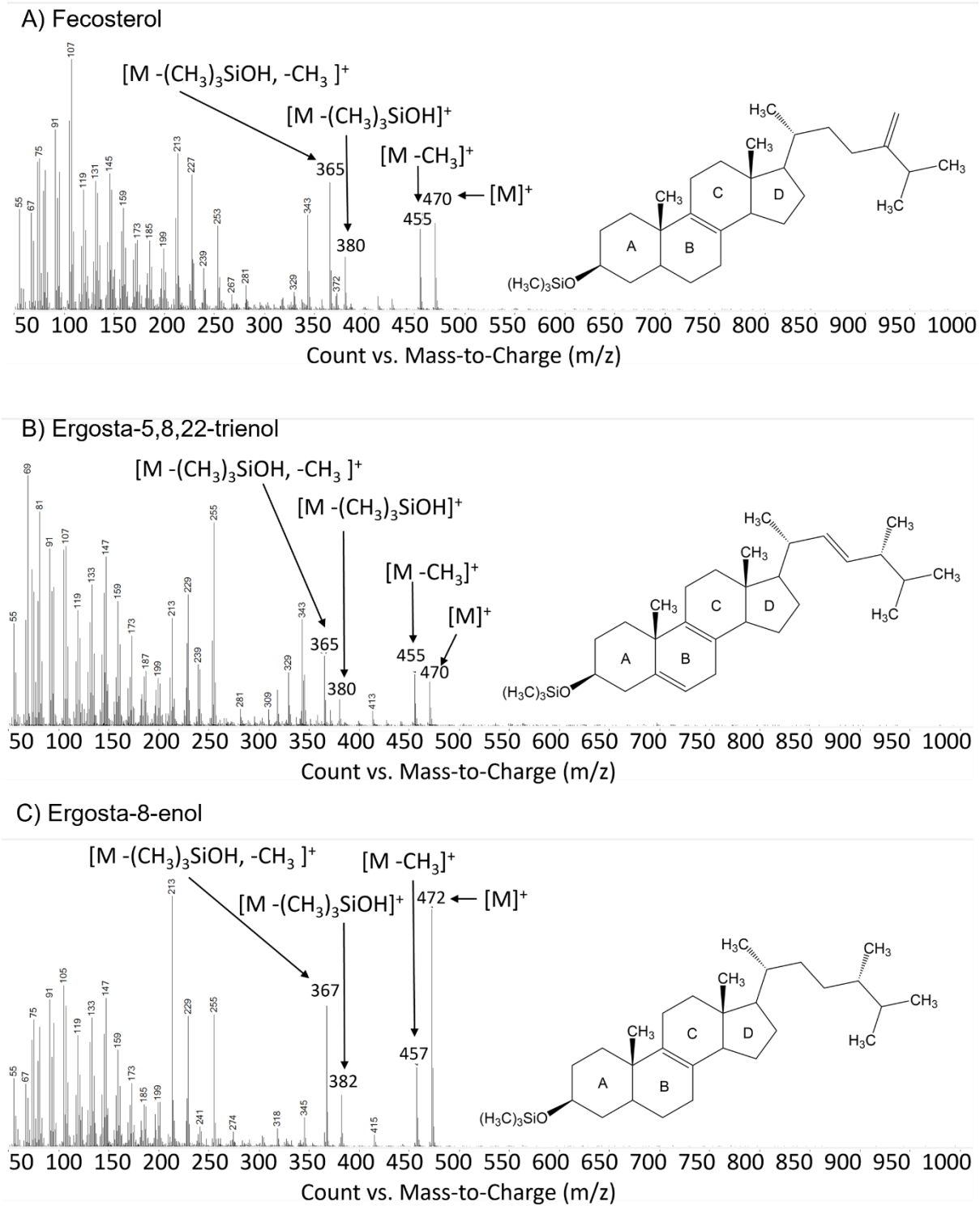

Figure 25: - Electron ion (EI) spectra of the sterols present in the *erg2Δ* mutant.

A) fecosterol, B) ergosta-5,8,22-trienol and C) ergosta-8-enol.

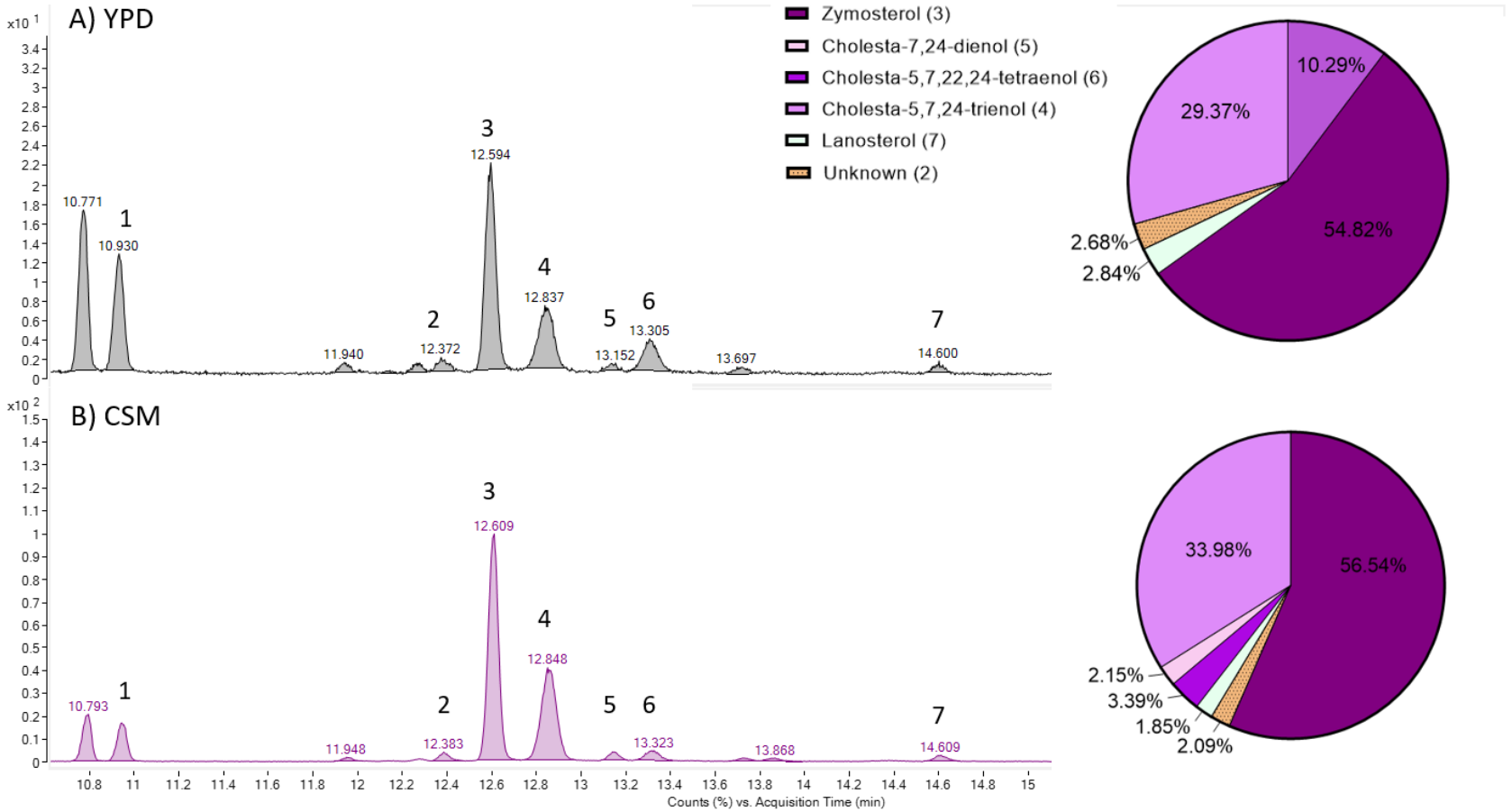

Figure 26: - Extracted ion chromatograms (EICs) showing peaks corresponding to sterols extracted from the *erg6Δ* mutant. Yeast cultured in either A) YPD or B) CSM media for 24 hours. Peak annotation based on ion m/z, relative retention times and relative abundances from previous reports (Nes *et al*., 2002; Kaneshiro *et al*., 2015; Weichert *et al*., 2016). (1) coprostanol, (2) unknown, (3) zymosterol, (4) cholesta-5,7,24-trienol, (5) cholesta-7,24-dienol, (6) cholesta-5,7,22,24-tetraenol, (7) lanosterol.

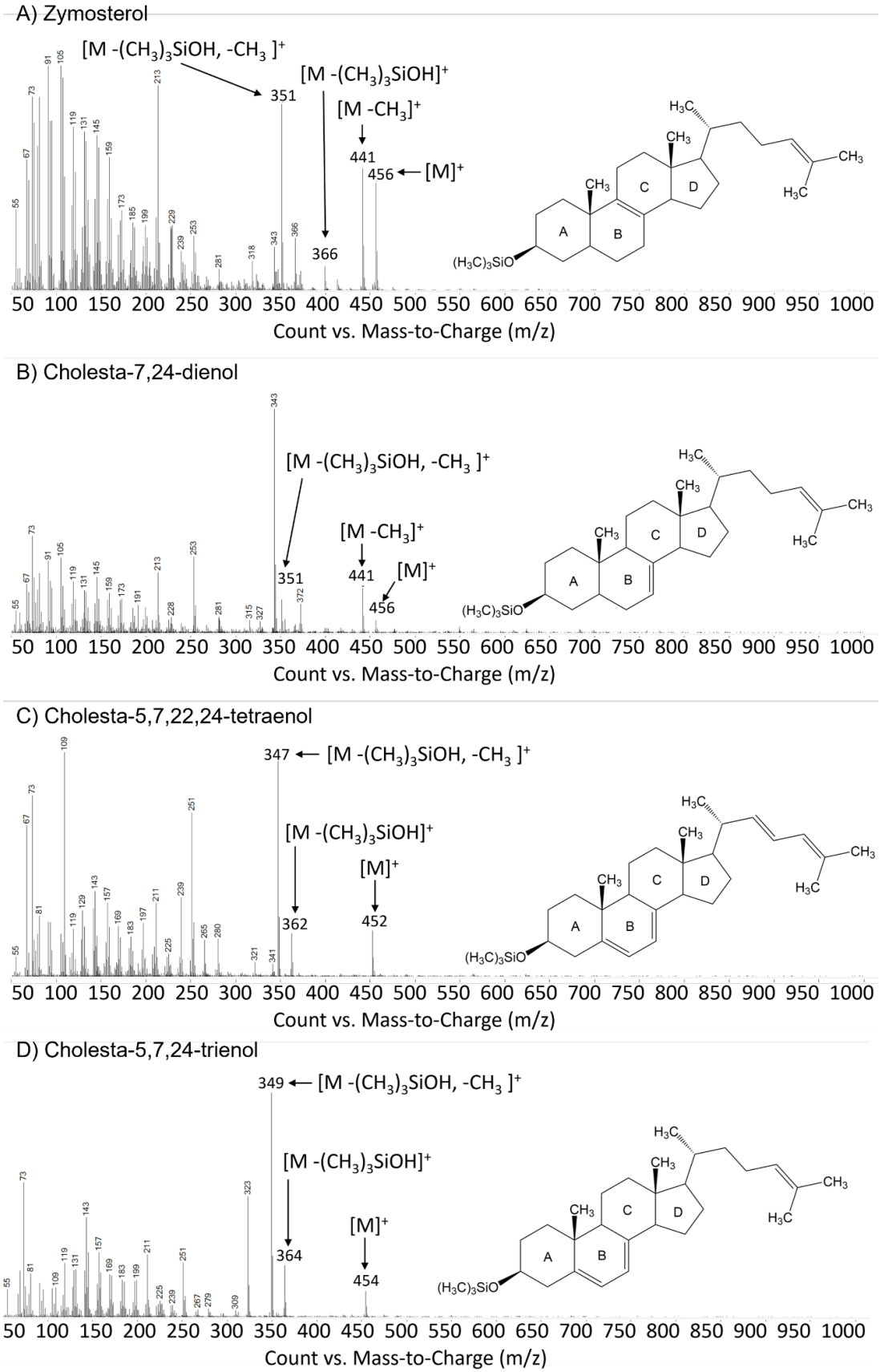

Figure 27: - Electron ion (EI) spectra of the sterols present in the *erg6Δ* mutant.

Full figure legend on next page.

Figure 27: - Electron ion (EI) spectra of the sterols present in the *erg6Δ* mutant. A) zymosterol, B) cholesta-7,24-dienol, C) cholesta-5,7,22,24-tetraenol and D) cholesta-5,7,24-trienol.

3.3 Discussion

The inclusion of LoFlo media in our experiments was due to subsequent experiments involving this medium, specifically in the context of the WT and *erg3Δ* mutant strain. Consequently, we wanted to confirm whether the sterol content in LoFlo media resembled that in the CSM. LoFlo media differs from CSM in the absence of riboflavin and folic acid, both of which are recognised for inducing background fluorescence in sensitive microscopy experiments (Sim *et al*., 2021; Tsyupka *et al*., 2021). Riboflavin, also known as vitamin B2, plays a crucial role in yeast growth as it serves as a precursor for flavin coenzymes, participating in cellular redox processes (Di Canito *et al*., 2023). Folic acid contributes to carbon metabolism, protein synthesis, and DNA production, but LoFlo media substitutes riboflavin and folic acid with essential vitamins and salts essential for yeast growth (Porzoor & Macreadie, 2015; Di Canito *et al*., 2023). We were able to determine that the sterol content of the cells grown in LoFlo media was different to that in CSM, but not different enough to hinder the following experiments.

Our analysis confirmed the absence of ergosterol in all sterol biosynthesis mutants, while in the WT strain, ergosterol emerged as the predominant sterol, accompanied by minor concentrations of zymosterol and lanosterol. These findings align with previous studies by Zinser *et al*., (1993) and Heese-Peck *et al*., (2002), although we did not detect episterol or fecosterol, as previously reported by Heese-Peck *et al*., (2002).

In the *erg4Δ* mutant, the most prominent sterol observed was ergosta-5,7,22,24(28)-tetraenol, consistent with (Aguilar *et al*., 2010). While no other

sterols were identified by us, reports indicate the presence of small amounts of ergosta-5,7,24(28)-trienol and ergosta-5,7-dienol (Aguilar *et al*., 2010).

The *erg5Δ* mutant predominantly exhibited ergosta-5,7-dienol, in agreement with Aguilar *et al*., (2010). Although we could not identify any other sterols in this mutant, even though it has been reported that there is ergosta-7,7,24(28)-trienol and small amounts of ergosta-5,7,22,24(28)-tetraenol in the *erg5Δ* mutant (Aguilar *et al*., 2010).

In the *erg3Δ* mutant, ergosta-7,22-dienol and episterol (in YPD) emerged as the dominant sterols, consistent with the findings of Heese-Peck *et al*., (2002) Hesse-Peck *et al*. (2002) also noted a majority of ergosta-7,22-dienol followed by episterol in YPD. In CSM, we observed a slight increase in episterol concentration, though significantly less than the rise in ergosta-7-enol concentration. However, we did not detect fecosterol or ergosta-8,22-dienol in these samples, which has been previously reported (Heese-Peck *et al*., 2002).

The *erg2Δ* mutant predominantly featured ergosta-8-enol and fecosterol, mirroring the findings of Heese-Peck *et al*., (2002), even with similar percentages. Heese-Peck *et al*., (2002) reported 33.2 % fecosterol and 35.4 % ergosta-8-enol in YPD, whereas our results indicated 35.8 % fecosterol and 29.1 % ergosta-8-enol. Additionally, we identified small amounts of ergosta-5,8,22-trienol, which were also noted in their study, but we did not detect zymosterol or ergosta-8,22-dienol.

The sterols predominantly observed in the *erg6Δ* mutant were zymosterol and cholesta-5,7,24-trienol, consistent with the findings of Heese-Peck *et al*., (2002), albeit at different ratios. While Heese-Peck *et al*., (2002) observed zymosterol at 39.4% and cholesta-5,7,24-trienol at 32.3% of the *S. cerevisiae* sterol content in YPD, our results showed 54.8% zymosterol and 29.3% cholesta-5,7,24-trienol in YPD.

In summary, our research provides a comprehensive and validated account of the predominant sterols found in the PM of WT *S. cerevisiae* as well as sterol biosynthesis mutants. We have established that the sterol composition remains relatively consistent between CSM and LoFlo media, with only minor variations in sterol concentrations. However, it is important to note that we observed more pronounced differences in sterol profiles when the strains were cultivated in the YPD medium. This discrepancy can likely be attributed to the favourable growth conditions that YPD offers to *S. cerevisiae* (Hahn-Hägerdal *et al*., 2005).

In conclusion, our findings not only contribute to a better understanding of the sterol landscape in *S. cerevisiae* but also underscore the importance of media selection in experimental design when studying sterol-related processes.

Chapter 4: - Escin and its effects on *Saccharomyces cerevisiae*

4.1 Escin

Escin is a complex mixture consisting of more than 20 glycosylated triterpenoid compounds (Yang *et al*., 1999; Savarino *et al*., 2023; Figure 28). Among these compounds, the most biologically active molecules are four escin isomers, namely escin 1a, escin 1b, isoescin 1a, and isoescin 1b (Wu *et al*., 2010). Of the mentioned escin isomers, two have an acetyl group at position C22 (R_2), along with either a tiglic acid group at position C21 (R_1) in the case of escin 1a, or an angelic acid group at position C21 (R_1) in the case of escin 1b. In contrast, the isoescins have the acetyl group at position C28 (R_3), and either a tiglic acid group at position C21 (R_1) in the case of isoescin 1a, or an angelic acid group at position C21 (R_1) in the case of isoescin 1b. In position C22 (R_2) the isoescins have a hydroxyl group rather than the acetyl group as seen in escin 1a and escin 1b. Of these four isomers, there is a hydroxyl at position C16 and a hydroxyl at position C23 (R_5). The sugar moiety positioned at C3 contains a glucuronic acid (GlcA) bound to two glucose (Glc) molecules (R_6).

Escin has an amphiphilic structure with both polar and non-polar regions. The glycosylated side chain at position C3 is hydrophilic and therefore polar, whereas the triterpenoid backbone is generally hydrophobic and therefore non-polar. However, there are additional polarities present in the triterpenoid backbone of escin, with all the modifications being on the underside of the molecule (positions C21, C22, C28, C16 and C23), this creates a slightly more polar side compared to the top half of the molecule (Wilkinson & Brown, 1999; Dargel *et al*., 2019; Geisler *et al*., 2020).

The natural yield of escin in horse chestnuts is extremely low, at 2-3 % dry cell weight (Singh, 2006). Consequently, it would be highly advantageous to produce escin in a microbial host, such as the yeast *S. cerevisiae* (baker's yeast). However, the biosynthetic enzymes required for escin biosynthesis in an exogenous host are currently unidentified.

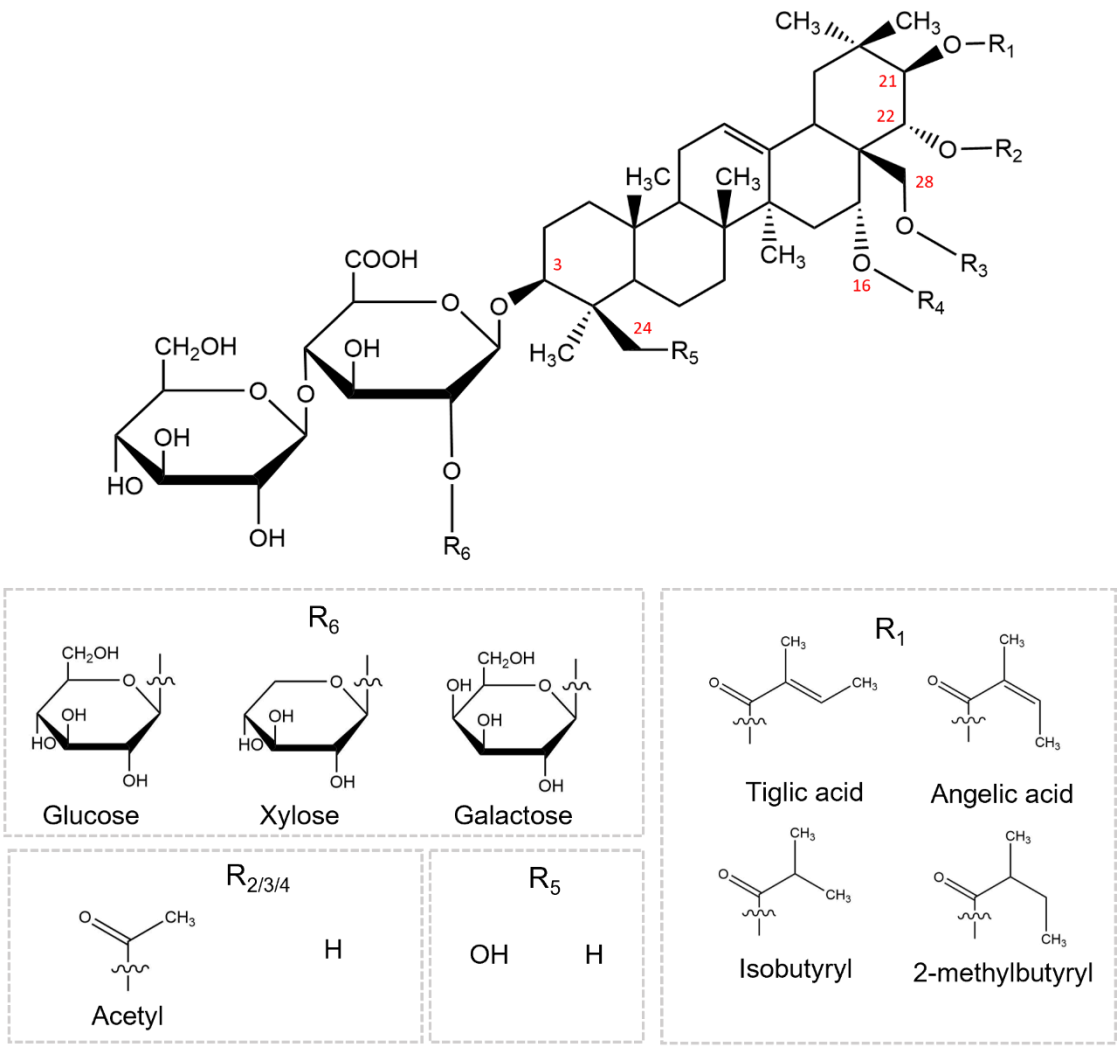

Figure 28: - The molecular structure of escin. The structure of escin contains hydrophobic and hydrophilic regions. The glycosylation containing glucuronic acid and glucose are hydrophilic (polar) whereas the triterpenoid backbone of escin is hydrophobic (non-polar). Figure adapted from Savarino *et al*., 2023.

Escin has been found to interact with cholesterol, leading to the formation of robust complexes that disrupt the permeability of the plasma membrane and inhibit cell

growth (Böttger & Melzig, 2013; Sreij *et al*., 2019, Figure 28) These complexes have several effects on the plasma membrane (PM). Firstly, they extract cholesterol from the PM into the supernatant, leading to a decrease in PM cholesterol content. Additionally, escin inhibits the uptake and integration of free cholesterol by occupying cholesterol sites within the membrane. Another proposed mechanism is that the escin-cholesterol complexes (in a ratio of 5:1), are significantly larger than cholesterol alone, resulting in the formation of pores in the membrane. This increases permeability in the membrane and allows small ions to pass through and impairs the structural integrity of the plasma membrane, rendering it more rigid (Böttger & Melzig, 2013; Sreij *et al*., 2019). Furthermore, it is hypothesised that escin treatment leads to an elevated uptake and liberation of cholesterol from the plasma membrane. Experimental evidence supports this hypothesis, as human urinary bladder epithelial carcinoma cells treated with escin exhibited a substantial reduction in membrane cholesterol compared to untreated cells (Böttger & Melzig, 2013). Based on these findings, we hypothesise that escin interacts with ergosterol, the sterol present in the yeast membrane, and this interaction is likely to inhibit the growth of *S. cerevisiae*.

The structural resemblances between ergosterol and cholesterol prompted us to hypothesise that they may exhibit similar interactions with escin. Therefore, the objectives of this chapter are twofold: (i) to confirm whether escin inhibits yeast growth and (ii) to determine the minimum inhibitory concentration of escin required to inhibit yeast growth.

4.1.1 Complete escin and its effect on S.cerevisiae growth

The impact of escin on the WT *S. cerevisiae* strain BY4741 remains uncertain. Therefore, the growth of the strain in the presence of escin was examined using microplate cultures. Initially, normal growth was assessed in both rich complex media (YPD) and standard defined media (CSM), with or without 1.25% methanol, as shown in Figure 29.

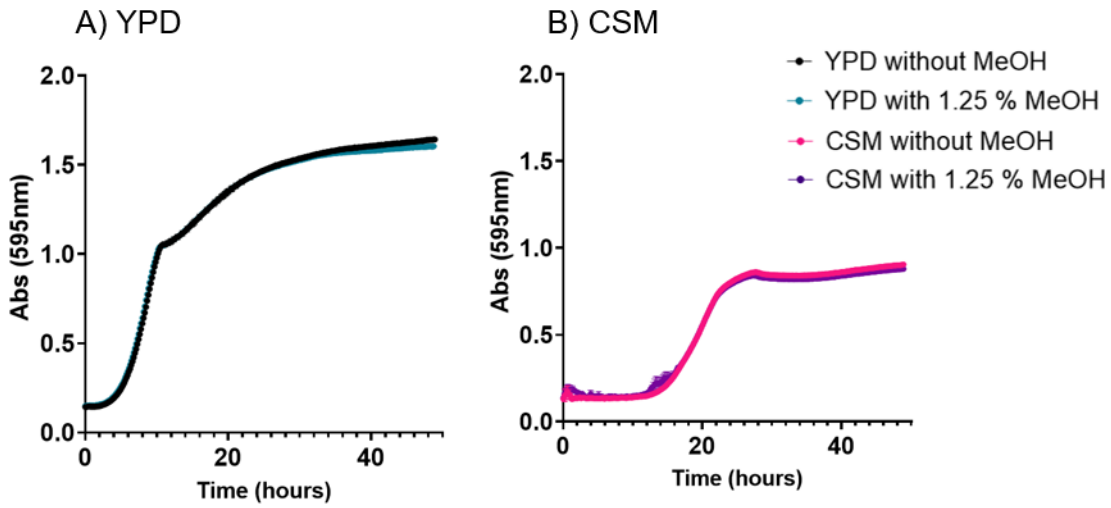

Figure 29: - Growth curves of WT *S. cerevisiae*. The average absorbance of triplicate measurements was plotted to depict the growth in A) YPD (rich media) or B) CSM (minimal defined media), with the presence of either 0 or 1.25 % methanol.

The inclusion of methanol ensured that any observed effects were attributed to escin rather than the methanol itself, as escin is dissolved in methanol. No significant change in the growth of *WT S. cerevisiae* was observed in the presence of 1.25 % methanol compared to growth without methanol. Consequently, the growth of the WT was monitored in the presence of 1.25 % methanol (0 $\mu g.mL^{-1}$ escin) or varying concentrations of escin up to 500 $\mu g.mL^{-1}$. It was observed that escin inhibited the growth of the WT. Hence, a minimum inhibitory concentration (MIC) assay, using growth as a readout, was performed. The MIC represents the lowest concentration of escin that prevents the growth of the WT *S. cerevisiae*, and it was determined to be 175 $\mu g.mL^{-1}$ after 24 hours of growth in YPD. The growth of the WT strain in the presence of escin was also examined in CSM. Surprisingly, the MIC after 24 hours of

growth differed from that observed in YPD (175 µg.mL^{-1}) and was determined to be 62.5 µg.mL^{-1} in CSM (Figure 30).

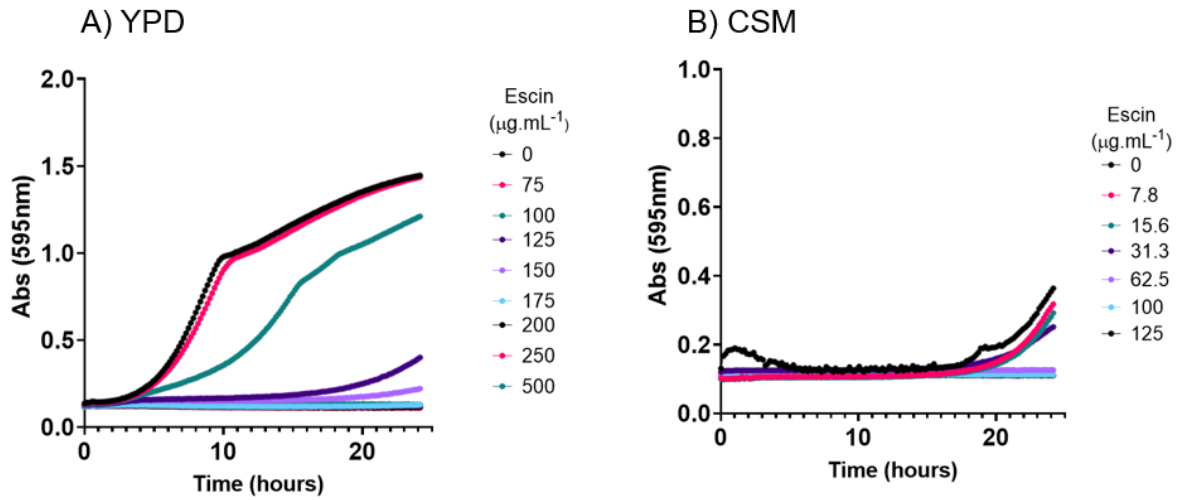

Figure 30: - Growth curves of WT *S. cerevisiae* with escin. The average absorbance of triplicate measurements was plotted to depict the growth in A) YPD (rich media) or B) CSM (minimal defined media), with the presence of up to 500 µg.mL^{-1} escin.

The cause of the difference in the MIC of the two different media is unknown, but it is speculated that the extra buffering capacity of the rich medium could potentially protect cells from the growth-inhibitory effects of escin, likewise, YPD has an increase in carbon source and availability of complex molecules compared to CSM. YPD, unlike CSM, has several undefined components which could also affect the direct interaction of escin with ergosterol, supporting a higher MIC of escin in YPD. The difference could also be caused by the naturally higher pH of YPD compared to CSM (~ 6.16 compared to ~ 4.19). It is known that the solubility of escin increases with pH, as the carboxylic acid on the hydrophilic aglycone is deprotonated above pH 4.7. Such deprotonation in YPD could increase the solubility of escin and perhaps render it in a form that is less toxic than intact escin (Hahn-Hägerdal *et al*., 2005; Dargel *et al.,* 2019; Geisler *et al*., 2020).

4.2 Effects of escin on *S. cerevisiae* sterol mutants' growth

In this chapter, our focus was to investigate the impact of escin on various ergosterol biosynthesis mutants to gain insights into the mechanism behind the inhibitory effect of escin. Our findings thus far demonstrate that escin exhibits toxicity to WT *S. cerevisiae* at concentrations exceeding 175 $\mu g.mL^{-1}$ when grown in YPD and above 62.5 $\mu g.mL^{-1}$ when grown in CSM. Based on the hypothesis that escin interacts with ergosterol to induce growth inhibition, we propose that *S. cerevisiae* ergosterol biosynthesis mutants, which possess altered sterols in their cell membranes, represent an ideal set of yeast strains for studying the specificity of sterols in mediating growth inhibition by escin.

To compare the response of these strains to escin, we conducted growth assays in microplates, exposing the strains to different concentrations of escin. Initially, the strains were grown in YPD, and an initial screen was performed using various concentrations of escin: 0 $\mu g.mL^{-1}$, 75 $\mu g.mL^{-1}$, 100 $\mu g.mL^{-1}$, 125 $\mu g.mL^{-1}$, 150 $\mu g.mL^{-1}$, 200 $\mu g.mL^{-1}$, 250 $\mu g.mL^{-1}$, or 500 $\mu g.mL^{-1}$, which were added to the medium just before growth, which was monitored for 24 hours. In the absence of escin, the sterol mutant strains exhibited poorer growth compared to the WT strain (Figure 31), with growth order ranging from WT > *erg6Δ* > *erg4Δ* > *erg2Δ* > *erg3Δ* > *erg5Δ*, indicating the best to least growth in 24 hours. In the presence of 175 $\mu g.mL^{-1}$ escin (the MIC), both the WT and all mutants, except the *erg3Δ* mutant, displayed no growth. Fig 4 illustrates the variation in growth among the mutants at different concentrations of escin. The *erg4Δ* and *erg5Δ* mutants failed to grow even at concentrations as low as 100 $\mu g.mL^{-1}$ escin, while the *erg6Δ* mutant did not grow at 125 $\mu g.mL^{-1}$. Surprisingly, the *erg3Δ* mutant demonstrated robust growth in the presence of escin, which was evident across all tested concentrations, up to 1 $mg.mL^{-1}$ (Figure 32).

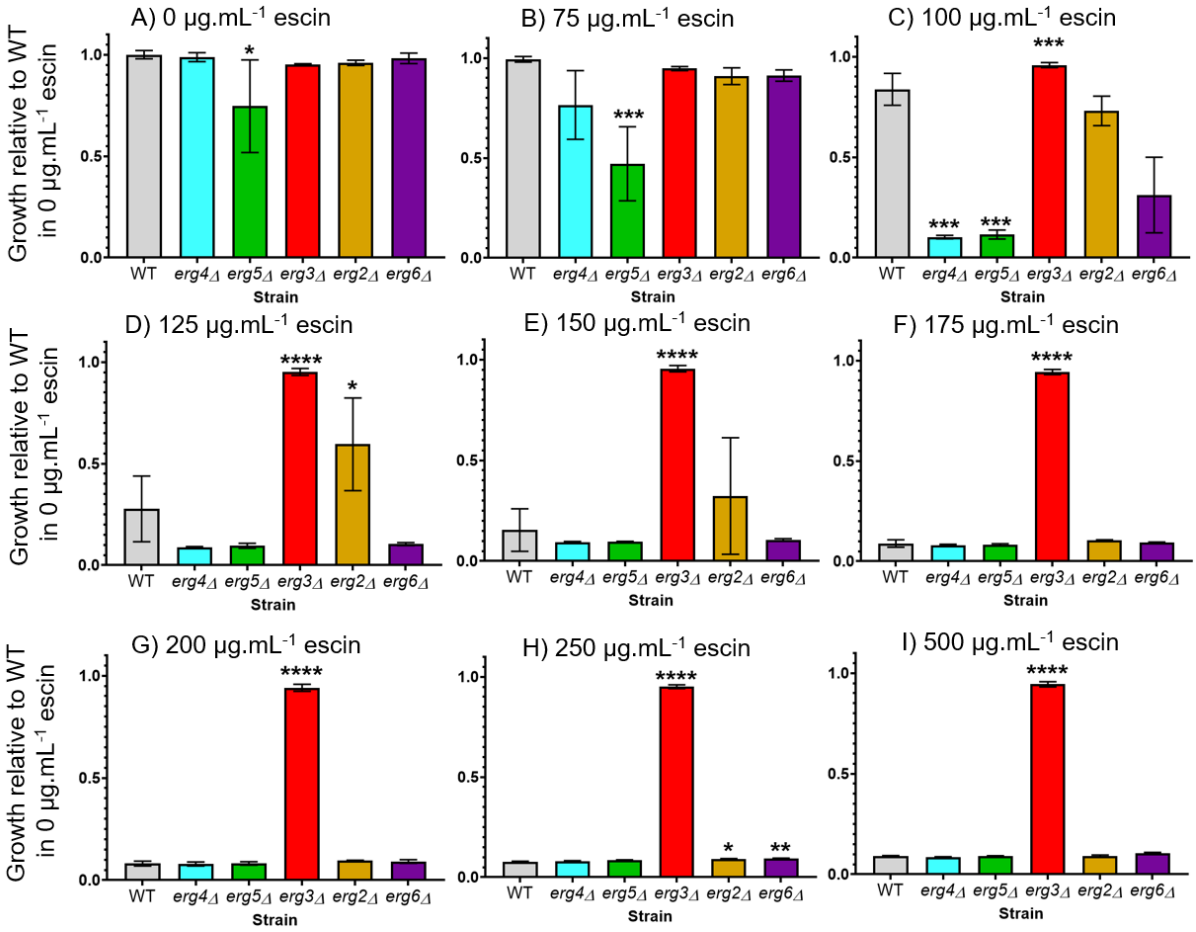

Figure 31: - Bar charts depicting the growth of ergosterol biosynthesis mutants relative to the WT strain after 24 hours in YPD at different concentrations of escin. The concentrations used were as follows: A) 0 µg.mL^{-1}, B) 75 µg.mL^{-1}, C) 100 µg.mL^{-1}, D) 125 µg.mL^{-1}, E) 150 µg.mL^{-1}, F) 175 µg.mL^{-1}, G) 200 µg.mL^{-1}, H) 250 µg.mL^{-1} or I) 500 µg.mL^{-1}. Statistical analysis was performed using a one-way ANOVA to compare each mutant with the WT strain at 0 µg.mL^{-1}. The sample size was n=3, and the p-values are indicated as follows: * = ≤ 0.05, ** = ≤ 0.01, *** = ≤ 0.001, **** = ≤ 0.0001.

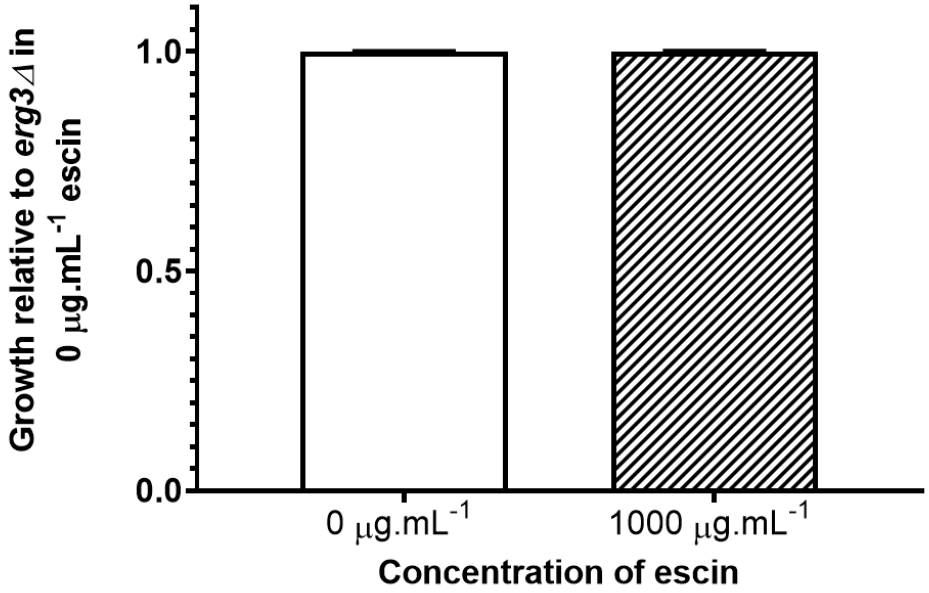

Figure 32: - Bar chart comparing the growth of the *erg3Δ* mutant at 0 μg.mL^{-1} escin and 1000 μg.mL^{-1} escin after 48 hours of growth in YPD. The sample size was n=3.

The *erg3Δ* mutant consistently exhibited tolerance to escin, which may be attributed to its distinct sterol composition compared to the WT and other mutants. Our previous findings highlighted that the primary sterol present in the *erg3Δ* mutant is ergosta-7,22-dienol (chapter 3). This sterol possesses a lone double bond between C7-8 in the B ring, whereas ergosterol contains an additional double bond between positions C5-6. The absence of this second double bond could be a contributing factor to the high tolerance of the *erg3Δ* mutant towards escin.

The growth of the WT and *erg3Δ* mutant in the presence of complete escin in CSM was determined. Considering the elevated tolerance of the *erg3Δ* mutant to complete escin, it was the sole mutant examined in this experiment. We examined the entire concentration range, spanning from 7.8 μg.mL^{-1} to 500 μg.mL^{-1} (Figure 33), and determined that the *erg3Δ* mutant maintained its tolerance to complete escin in CSM. Additionally, we confirmed that the MIC of escin for the WT was 62.5 μg.mL^{-1}.

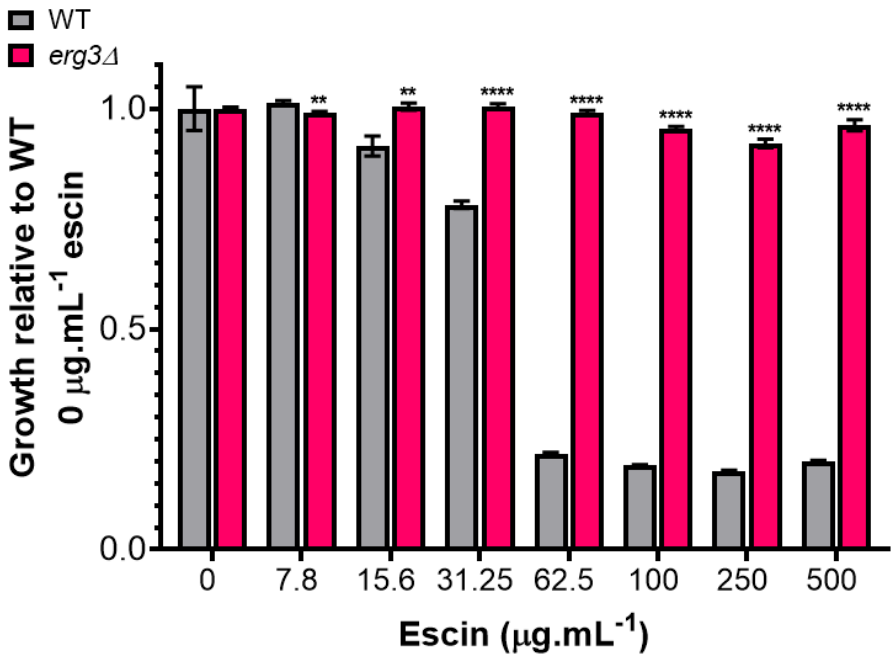

Figure 33: - Bar chart depicting the growth of the WT and *erg3Δ* mutant (relative to the WT at 0 µg.mL^{-1} escin) after 24 hours in CSM at different concentrations of escin. Statistical analysis was performed using multiple T-tests to compare the *erg3Δ* mutant with the WT strain at each concentration. The sample size was n=3, and the p-values are indicated as follows: * = ≤ 0.05, ** = ≤ 0.01, *** = ≤ 0.001, **** = ≤ 0.0001.

4.3 *S. cerevisiae* membrane permeability

We hypothesise that complete escin interacts with ergosterol, leading to the formation of pores in the membrane of WT *S. cerevisiae*. This hypothesis is based on the observed effect of complete escin on cholesterol, as discussed in Chapter 3.2.1. To further investigate this, we conducted a test to assess any changes in permeability in WT *S. cerevisiae* following escin treatment. Such changes would indicate that escin is indeed responsible for membrane disruption through pore formation. Therefore, we performed a membrane conductivity assay following the methodology described in (Simons *et al*., 2006).

Firstly, we tested the conductivity of the CSM and escin, which showed no difference (Figure 34A). Therefore, in this experiment, WT *S. cerevisiae* cultures were subjected to different treatments: a control treatment consisting of 0 $\mu g.mL^{-1}$ complete escin and 1.25 % methanol, 31.25 $\mu g.mL^{-1}$ complete escin, 61.5 $\mu g.mL^{-1}$ complete escin, or mechanical lysis. The cultures were monitored using a conductivity meter at three intervals over 24 hours. Mechanical lysis served as a positive control to assess complete membrane compromise. Electrolyte leakage, measured in µSiemens, reflects the presence of ions in the supernatant, indicating cell lysis or increased pore formation in the membrane of WT *S. cerevisiae*. However, no conclusive evidence of increased electrolyte leakage was observed upon the addition of complete escin (Figure 34).

Although there appears to be a slight increase in electrolyte leakage after escin treatment, a similar trend is also observed in the control condition (0 $\mu g.mL^{-1}$ complete escin, 1.25 % methanol). Consequently, this experiment did not yield consistent results with the previously published data, prompting the exploration of alternative approaches.

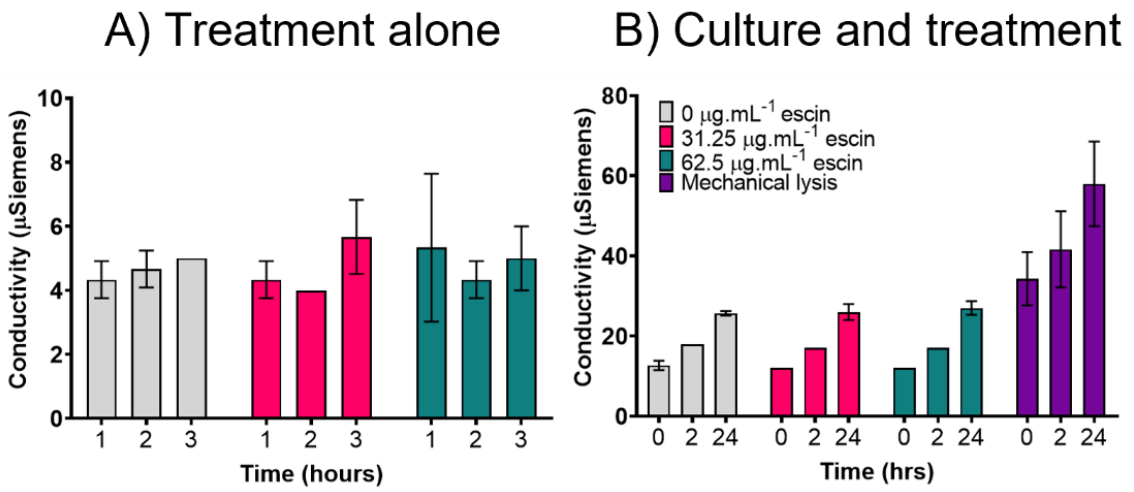

Figure 34: - Electrolyte leakage (measured as conductivity) of WT *S. cerevisiae* after treatment with 0 µg.mL^{-1}, 31.25 µg.mL^{-1}, 62.5 µg.mL^{-1} escin and mechanical lysis. A) Treatment conditions were tested alone to ensure that any differences seen were due to the electrolyte leakage from the cells and not the escin or methanol present. B) WT *S. cerevisiae* with varying amounts of escin. Measurements were taken at time 0, 2 hours and 24 hours after complete escin treatment or mechanical lysis. The sample size is n=3.

4.4 Escin and its interaction with exogenous ergosterol

4.4.1 Assessment of cell death caused by escin treatment using propidium iodide.

To determine whether escin acted on the yeast by inhibiting growth or causing cell death, we conducted a dye-based viability assay. In this assay, propidium iodide (PI) was used as an indicator for cell death. PI binds to chromosomal DNA, intercalating between the base pairs, with one dye molecule per 4 - 5 base pairs. This binding occurs only when cells are dead or when the plasma membrane is compromised. In live cells, PI is actively pumped out of the cell by transporters in the plasma membrane, thereby indicating cell viability and intact membrane integrity. The excitation/emission maximum (ex/em) of free PI in aqueous solution is 493/636 nm. However, once bound to base pairs, the fluorescence of PI enhances and the ex/em shifts to 535/617 nm (Crissman & Steinkamp, 1973; Davey & Hexley, 2011; Zhang *et al*., 2018). Consequently, fluorescent cells are considered dead or have compromised membranes, while non-fluorescent cells are considered alive.

However, it should be noted that the use of PI in yeast studies is not always straightforward. In the study by Davey & Hexley (2011), yeast cells subjected to stress, such as non-lethal temperatures or exposure to 30% ethanol, showed fluorescence when stained with PI. This fluorescence might conventionally be interpreted as cell death, but the study demonstrated that it could be attributed to a temporary increase in membrane permeability, allowing the uptake of PI. Hence, when referring to PI staining in this context, we are specifically indicating the compromise of the cell wall and not necessarily implying cell death, as absolute certainty cannot be achieved in such cases.

WT cells and the *erg3Δ* mutant were examined using PI staining in the absence and presence of escin in CSM. At 0 $\mu g.mL^{-1}$ escin, there was no significant difference in the percentage of stained and non-stained cells between the two strains, with

approximately 6 - 10% stained cells observed (Figure 35). Similarly, in the presence of 31.25 µg.mL^{-1} escin (a concentration below the MIC), the results remained quite comparable.

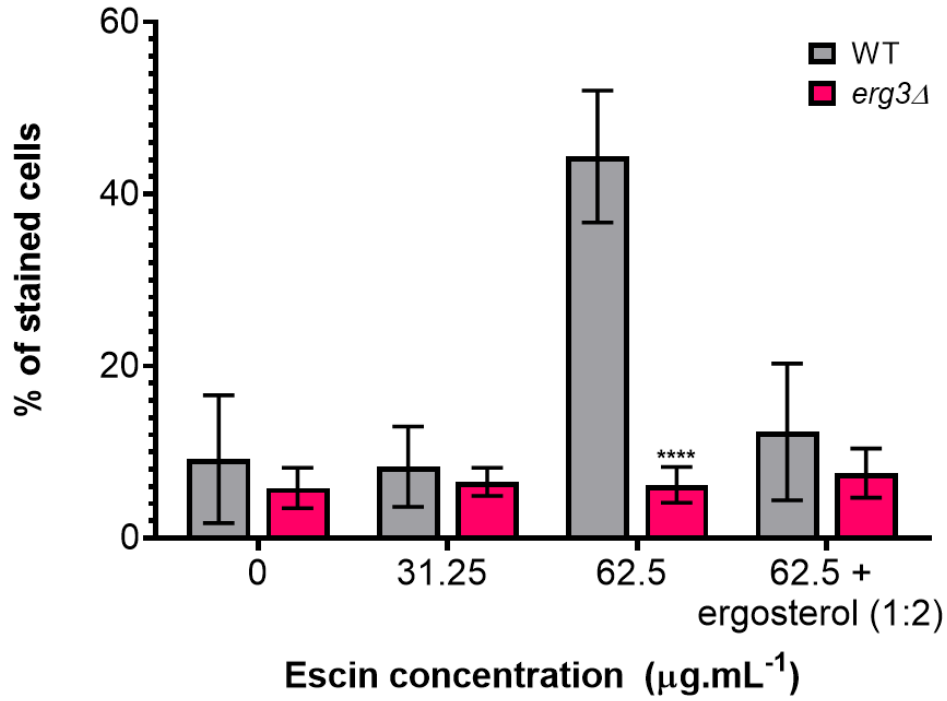

Figure 35: - Bar graph illustrating the percentage of stained WT *S. cerevisiae* cells following treatment with various concentrations of escin, along with supplementation with ergosterol. For statistical analysis, multiple t-tests were conducted to compare the WT in each treatment with the *erg3Δ* mutant. The sample size was n=16. The p-values are indicated as follows: * = ≤ 0.05, ** = ≤ 0.01, *** = ≤ 0.001, **** = ≤ 0.0001.

However, at 62.5 µg.mL^{-1} (the MIC of escin in CSM) a substantial increase in the percentage of stained cells was observed in the WT strain. The WT showed a 4.4-fold increase in stained cells (approximately 44 %), whereas the *erg3Δ* mutant did not display any significant difference. This increased fluorescence of cells suggests that 62.5 µg.mL^{-1} escin possibly induces cell death in the WT strain, or at the very least, compromises the plasma membrane (Figure 36; Figure 37). The disparity in stained cells between 62.5 µg.mL^{-1} escin and 31.25 µg.mL^{-1} is intriguing, as it implies that the latter concentration might be insufficient to affect the *S. cerevisiae* membrane significantly.

To further investigate the interaction between escin and ergosterol, we introduced exogenous ergosterol at a 1:2 molar ratio with escin. Interestingly, the staining decreased to levels comparable to the 0 $\mu g.mL^{-1}$ escin control (from 44 % to 10 %). This finding suggests that the externally supplied ergosterol competes with the endogenous ergosterol in the membrane for binding to escin (Figure 35). Moreover, it indicates that escin exhibits a greater affinity for binding to the exogenous ergosterol due to it being free in solution and not surrounded by the phospholipids of the PM. This observation provides compelling evidence for the interaction between ergosterol and escin.

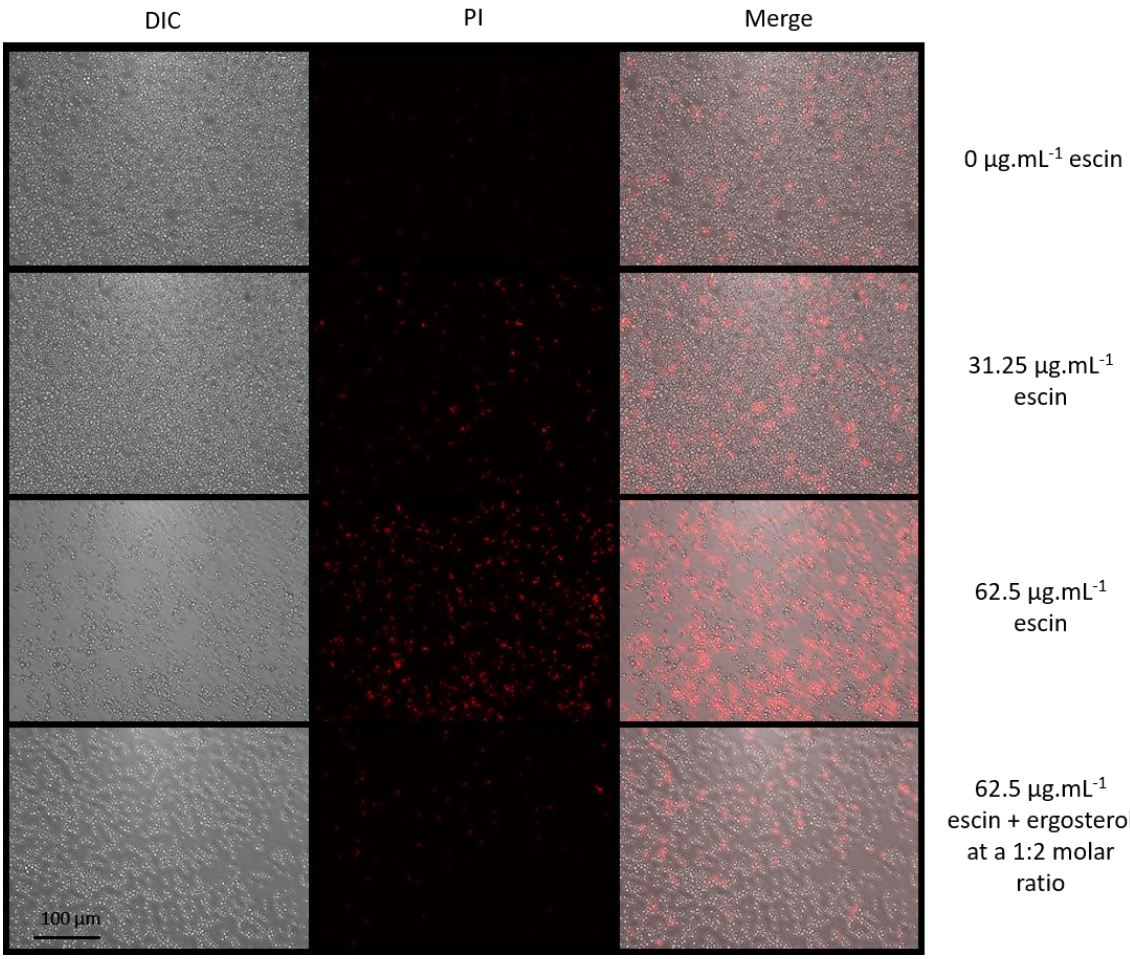

Figure 36: - Propidium iodide staining of WT *S. cerevisiae* in the presence of escin at concentrations of 0, 31.25, or 62.5 µg.mL^{-1}, with the addition of exogenous ergosterol at a 1:2 molar ratio in the final row. The first column exhibits the differential interference contrast (DIC) images of the cells, the second column presents the fluorescent images (where red fluorescence indicates cell death or a compromised plasma membrane), and the final column displays the merge of the two images.

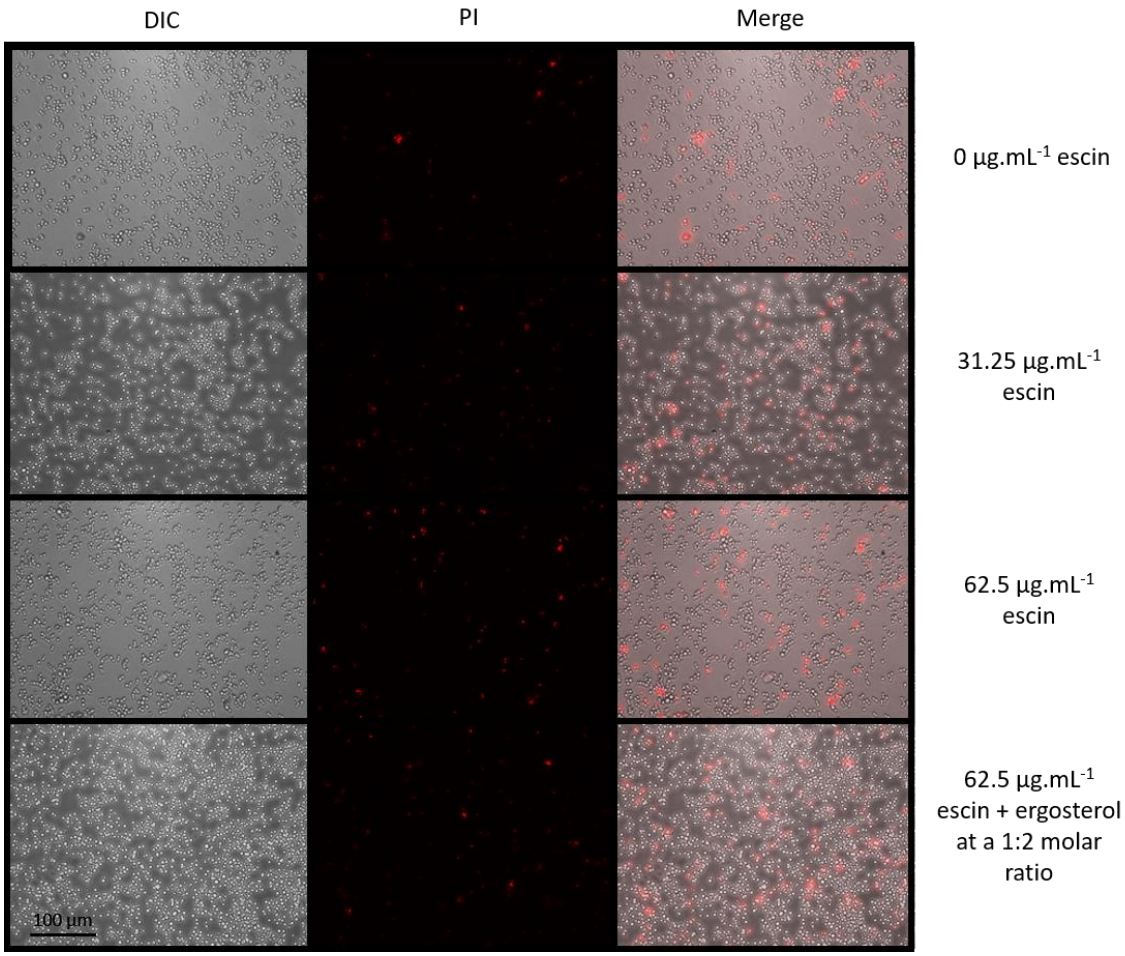

Figure 37: - Propidium iodide staining of the *erg3Δ* mutant in the presence of escin at concentrations of 0, 31.25, or 62.5 µg.mL^{-1}, with the addition of exogenous ergosterol at a 1:2 molar ratio in the final row. The first column exhibits the differential interference contrast (DIC) images of the cells, the second column presents the fluorescent images (where red fluorescence indicates cell death or a compromised plasma membrane), and the final column displays the merge of the two images.

4.4.2 Yeast growth in the presence of escin and exogenous ergosterol

To investigate the hypothesis that exogenous ergosterol mitigates the impact of escin on yeast cells, we assessed the toxicity of escin in the presence of exogenous ergosterol. It is already well established that *S. cerevisiae* does not uptake exogenous ergosterol under aerobic conditions (Lorenz *et al*., 1986), which gave us confidence that the addition of ergosterol would not alter the membrane composition of WT *S. cerevisiae*. Ergosterol was dissolved in methanol at 55 °C and combined with cells in a 1:1 or 1:2 molar ratio along with escin.

Firstly, we determined that the addition of exogenous ergosterol did not influence the growth of WT *S. cerevisiae* after 48 hours in CSM (Figure 38). Next, stoichiometric effects were taken into account, and parallel experiments were conducted as follows: (i) ergosterol and escin were premixed and incubated for one hour before being added to the yeast culture, and (ii) ergosterol and escin were separately added to the culture without premixing and incubation (Figure 39). Interestingly, it was observed that the timing of ergosterol addition (premixed or simultaneous) had no significant impact on the growth of the WT strain. Therefore, in subsequent experiments, both ergosterol and escin were added simultaneously to the culture.

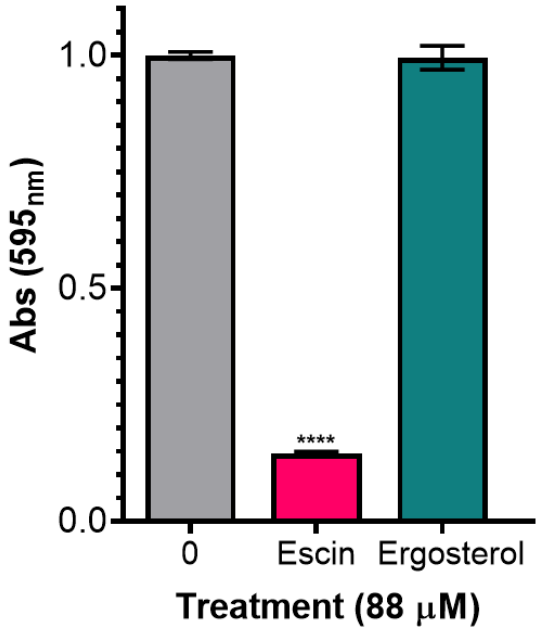

Figure 38: - Growth of WT *S. cerevisiae* in the presence of either 88 µM ergosterol (35 mg.mL^{-1}) or 88 µM escin (100 µg.mL^{-1}) in CSM after 48 hours. For statistical analysis, a one-way ANOVA was performed to compare each treatment with the 0 µM escin control. The sample size for each group was n=3. The p-values are indicated as follows: * = p ≤ 0.05, ** = p ≤ 0.01, *** = p ≤ 0.001, and **** = p ≤ 0.0001.

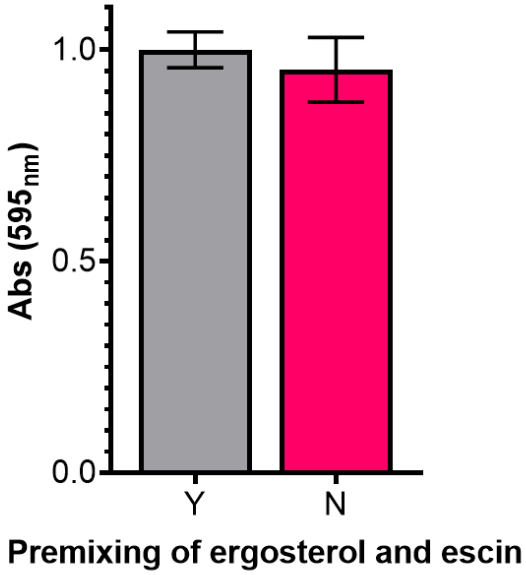

Figure 39: - WT *S. cerevisiae* grown in the presence of either 88 µM ergosterol (35 mg.mL^{-1}) or 88 µM escin (100 µg.mL^{-1}) in CSM after 48 hours. The compounds were either premixed for an hour or added to the culture simultaneously. The sample size was n = 3.

Next, we investigated the impact of the ratio of escin to ergosterol on yeast growth. Escin and ergosterol were combined at 1:1 or 1:2 molar ratios, and the effect on culture growth was monitored for 48 hours in microplates. A concentration of 62.5 µg.mL^{-1} of escin was used, and the cultures were grown in CSM. As expected, the WT strain exhibited no growth in the presence of escin, while growth remained unaffected in the presence of ergosterol (Figure 40). However, when both escin and ergosterol were present in the culture, the growth of the WT strain was restored. This restoration of growth was consistent across all tested ratios, with both ratios effectively restoring growth to levels equivalent to the 0 µg.mL^{-1} escin control. These findings suggest that the exogenous ergosterol acts as an inhibitor, dampening the toxicity of escin by competitively inhibiting its interaction with endogenous ergosterol in the plasma membrane.

To further support this observation, PI experiments were conducted to assess changes in fluorescent staining in the presence of exogenous ergosterol, presented in the previous section. The level of staining, and thus the number of dead cells or cells with

compromised cell walls, did not significantly differ from the 0 µg.mL^{-1} escin conditions. This result further strengthens the hypothesis that exogenous ergosterol mitigates the effect and reduces the toxicity of escin. To compare, the *erg3Δ* mutant was used, and no increase in fluorescence was observed at any tested concentrations with PI.

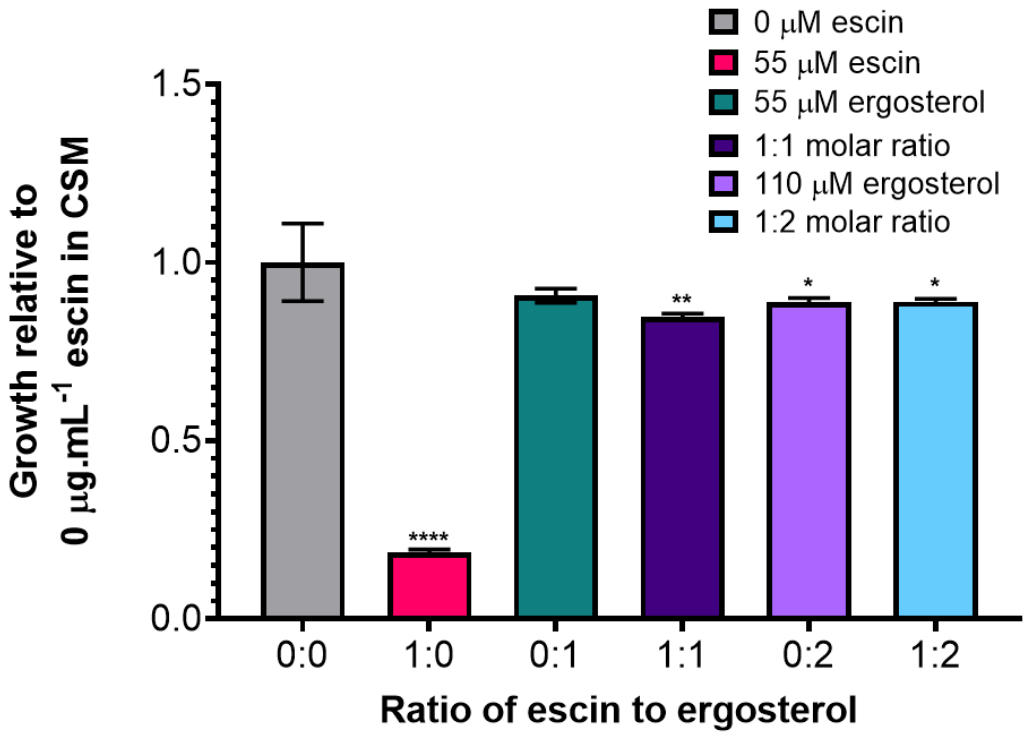

Figure 40: - Growth of WT *S. cerevisiae* in the presence of different molar ratios of escin and ergosterol after 48 hours, relative to the growth of the WT at 0 µM escin (0:0 represents the 0 µM escin control). Specifically, the ratios tested are as follows: 1:0 indicates 62.5 µg.mL^{-1} escin (55 µM); 0:1 corresponds to ergosterol alone at 21 mg.mL^{-1} (55 µM); 1:1 represents escin and ergosterol mixed at a 1:1 ratio; and 1:2 denotes escin and ergosterol mixed at a 1:2 ratio. For statistical analysis, a one-way ANOVA was conducted to compare each treatment with the 0 µM escin control. The sample size for each group was n=3. The p-values are indicated as follows: * = $p \leq 0.05$, ** = $p \leq 0.01$, *** = $p \leq 0.001$, and **** = $p \leq 0.0001$.

4.4.3 Yeast growth in the presence of escin and exogenous brassicasterol

Ideally, we would have repeated the above experiment using ergosta-7,22-dienol, the most prevalent sterol found in the *erg3Δ* mutant. Unfortunately, this sterol is not commercially available. Nevertheless, we have already demonstrated that escin interacts with ergosterol, leading to cell membrane compromise in the WT. Interestingly, in the *erg3Δ* mutant, there is no cell inhibition, suggesting that the sterols present in the *erg3Δ* mutant might not interact with escin as readily as ergosterol does.

To explore this further, we examined brassicasterol (Figure 41B), a phytosterol found in rapeseed and canola oils. Brassicasterol was chosen for testing because its structure closely resembles that of ergosterol (Figure 41A). with the only difference being the absence of one double bond in the B-ring at position C7-8. This characteristic of having only one double bond in the B ring is shared by all the sterols that accumulate in the *erg3Δ* mutant. Conversely, other ergosterol biosynthesis mutants accumulate sterols with at least one sterol containing two double bonds in the B ring (Johnston *et al*., 2020).

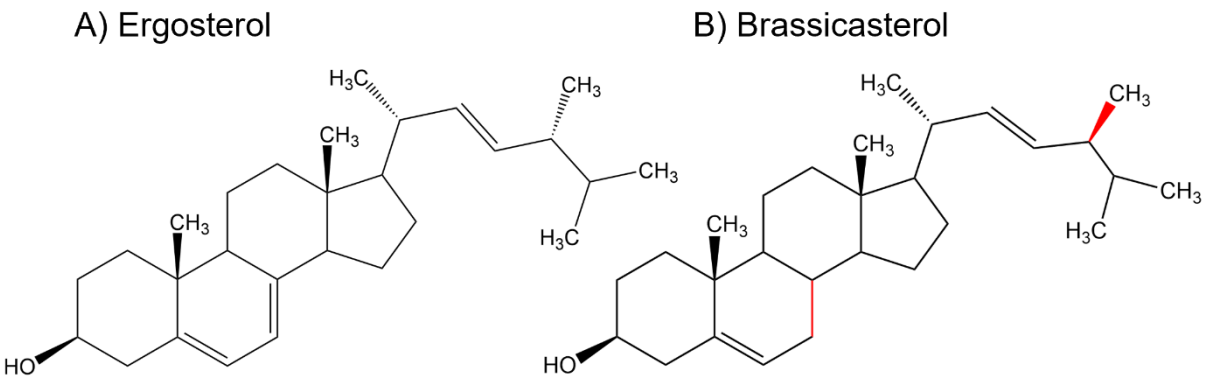

Figure 41: - Structural differences between ergosterol and brassicasterol. A) Ergosterol and B) brassicasterol. Different bonds are highlighted in red.

When escin was mixed with brassicasterol at a 1:1 molar ratio, the growth of yeast cells did not differ significantly from the treatment with 62.5 µg.mL^{-1} escin (Figure 42). However, at a 1:2 molar ratio of escin to brassicasterol, the yeast growth was slightly

better than that of the 0 µg.mL^{-1} escin treatment. These results provide additional support for the hypothesis that escin interacts directly with ergosterol, and to a lesser extent, with brassicasterol.

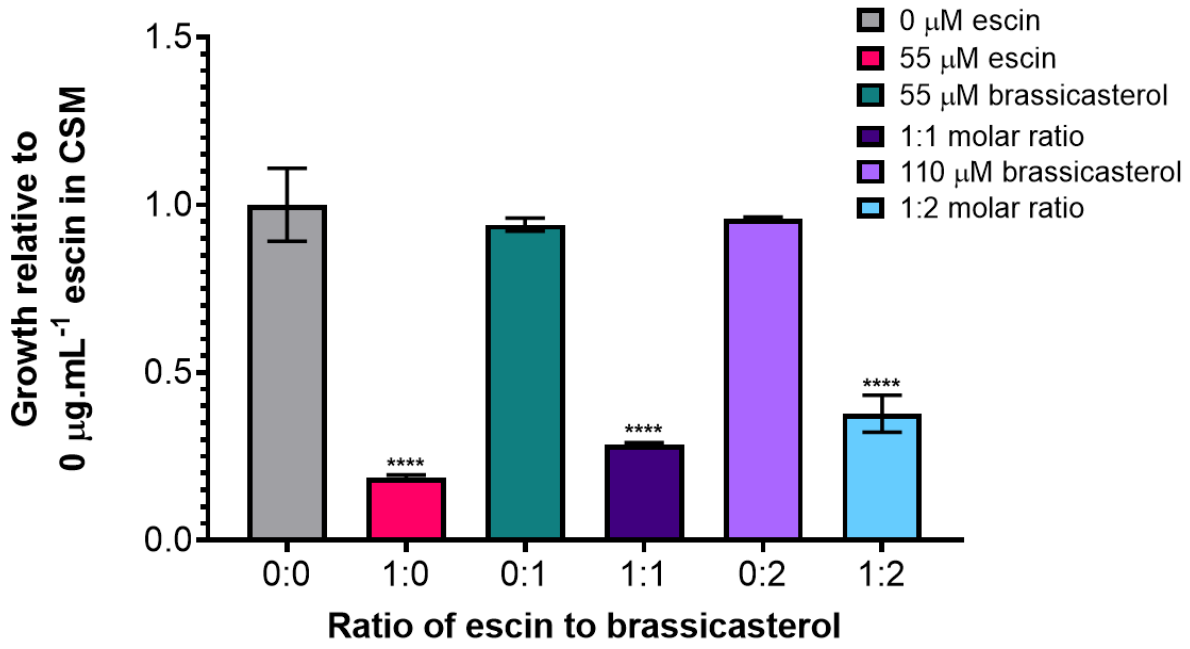

Figure 42: - Growth of WT *S. cerevisiae* in the presence of different molar ratios of escin and brassicasterol after 48 hours in CSM, relative to the growth of the WT at 0 µM escin. Specifically, the ratios tested are as follows: 1:0 indicates 62.5 µg.mL^{-1} escin (55 µM); 0:1 represents brassicasterol at 22 mg.mL^{-1} (55 µM); 1:1 represents escin and brassicasterol mixed at a 1:1 ratio; and 1:2 denotes escin and brassicasterol mixed at a 1:2 ratio. For statistical analysis, a one-way ANOVA was conducted to compare each treatment with the 0 µM escin control. The sample size was n=3. The p-values are indicated as follows: * = ≤ 0.05, ** = ≤ 0.01, *** = ≤ 0.001, **** = ≤ 0.0001

4.5 Determining the physical interaction of ergosterol and escin

4.5.1 Isothermal titration calorimetry

Isothermal titration calorimetry (ITC) is a commonly used physical technique to determine direct interactions between molecules, and we attempted to apply it to study the interaction between escin and ergosterol. Unlike methods relying on reporter signals like fluorescence, ITC measures the binding affinity (K_a) of a biomolecular reaction and provides a complete thermodynamic and kinetic profile, making it advantageous for avoiding false positives (Srivastava & Yadav, 2019; Johnson, 2021; Callies & Hernández Daranas, 2016). ITC is considered the "gold standard" label-free technique for protein-ligand characterisation (Johnson, 2021), although ergosterol and escin are not proteins, we aimed to gain insights into their possible binding affinity, similar to what was done in Welscher *et al*., 2008.

In our experiment, we attempted to dissolve ergosterol in 2:1 phosphate-buffered saline (PBS): ethanol and escin in DMSO (5 mM). However, it became evident that this procedure to dissolve ergosterol in 2:1 PBS: ethanol was not compatible with our experimental conditions due to insolubility.

Unfortunately, despite three attempts, we were unable to obtain any conclusive results from the ITC data due to a significant mismatch in the similarity of the two buffers used in the cells. As a result, the heat generated during each titration likely stemmed from the difference in buffers between the syringe and cell solution, rather than from the binding of escin and ergosterol. This discrepancy is likely attributed to the high solvent content required to dissolve escin, which is unavoidable.

Considering the challenges posed by the solvent content of escin solutions, it was determined that continuing the experiment without using lipid unilamellar vesicles (LUVs), as described in Welscher *et al*., 2008, was not a feasible approach. As such,

we were unable to obtain meaningful insights into the binding affinity of escin and ergosterol using ITC under our experimental conditions.

The ITC instrument comprises two cells made of a highly thermally conducting material: one cell for injecting the molecules of interest, and another filled with reference buffer (Figure 43). Tiny volumes of the ligand are injected into the sample cell, where they are mixed with a paddle, and the resulting temperature change caused by binding is measured (Johnson, 2021).

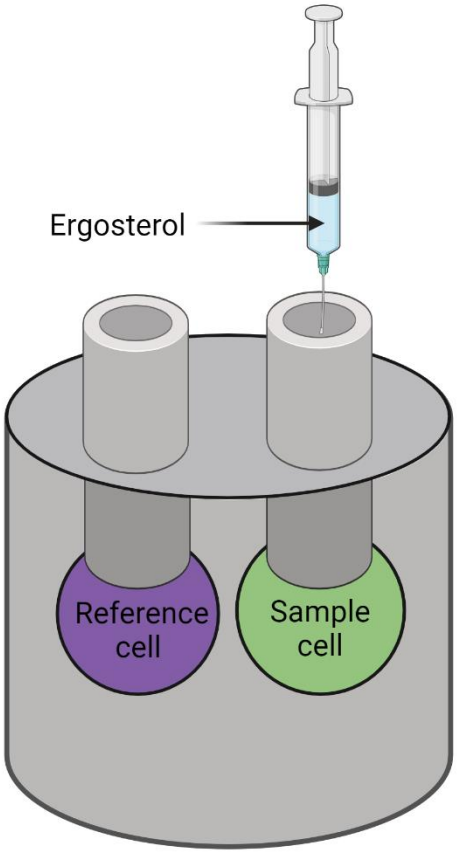

Figure 43: - Simplified schematic of ITC. A syringe is filled with ergosterol and injected into the sample cell. The heat difference is compared to the reference cell and the binding affinity (K_a) is calculated. Figure created in Biorender.com.

4.5.2 Confocal microscopy to determine interaction *in vivo*

The data presented thus far strongly supports the hypothesis of an interaction between escin and ergosterol. As a result, we sought to investigate the impact of escin on the dynamics and organisation of the plasma membrane.

The plasma membrane (PM) of *S. cerevisiae* is approximately 7.5 nm thick and consists of a lipid bilayer that houses enzymes involved in signal transduction, cell wall synthesis, and transport, as well as serving as cytoskeletal anchors. Notably, the PM features occasional invaginations or furrows known as eisosomes, which protrude into the cytoplasm (Strádalová *et al*., 2009; Feldmann, 2012; Douglas & Konopka, 2014). Key components of the PM include sterols and phospholipids, and their structure and functionality undergo frequent changes depending on various conditions and stages of growth (Feldmann, 2012).

Sterols play a vital role in maintaining optimal PM dynamics for essential biological functions (Dufourc, 2008). They are crucial for the formation of liquid-ordered membrane states, commonly known as lipid rafts, which are specialised microdomains within the membrane responsible for regulating signal transduction, cellular sorting, and more. Sterols are also essential for maintaining the fluidity of the plasma membrane, especially under environmental stressors (Dufourc, 2008; Feldmann, 2012).

Moreover, the PM exhibits lateral organisation into microdomains, such as the MCC domains (membrane compartment of Can1), which contain colocalised family tetraspanner proteins Can1p, Sur7p, and Nce102p (Douglas & Konopka, 2014). Eisosomes are closely associated with MCC domains, forming around the upper edge of the furrows (Strádalová *et al*., 2009). These eisosomes and MCC domains are rich in ergosterol, and the size and distribution of these structures are known to be disrupted in ergosterol biosynthesis mutants (Grossmann *et al*., 2008; Spira *et al*., 2012).

To understand the dynamics and organisation of the *S. cerevisiae* membrane following the addition of escin, we utilised a strain expressing two plasma membrane proteins tagged with fluorescent markers: sur7-mRFP and nce102-GFP, both under the control of their native promoters. Sur7p serves as a marker for MCC domains, exhibiting stable localisation at these domains even after various treatments (Grossmann *et al*., 2008; Douglas & Konopka, 2014). On the other hand, Nce102p primarily localises at MCC domains and eisosomes. However, under conditions of increased membrane tension, such as alkaline stress, Nce102p is distributed across the plasma membrane due to the flattening of eisosomes when the cell volume increases (Appadurai *et al*., 2020; Figure 44).

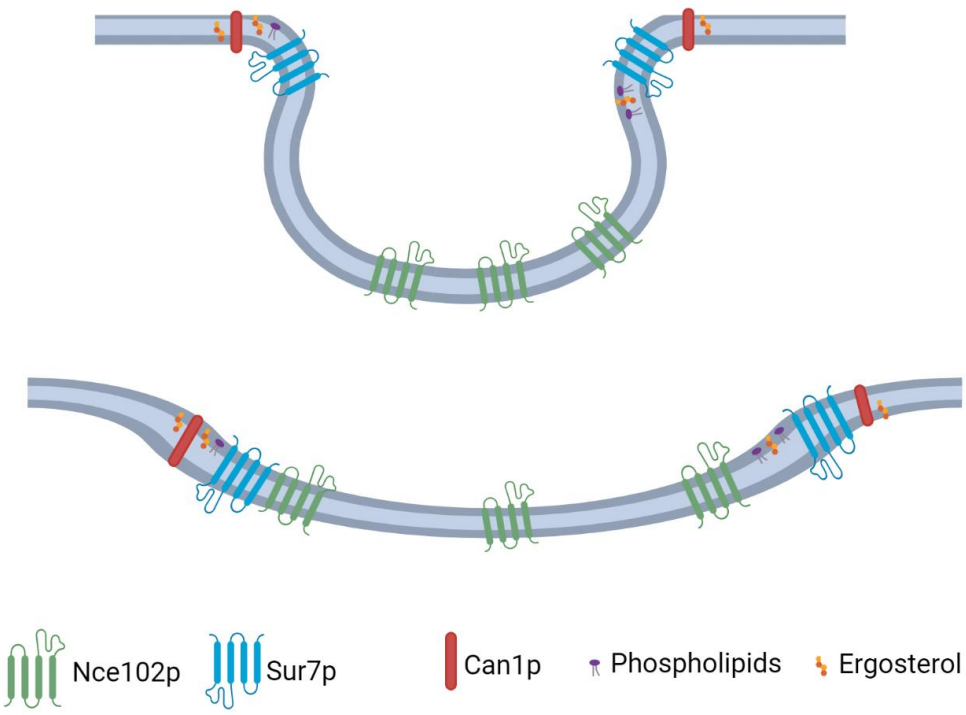

Figure 44: - Schematic illustrating the *S. cerevisiae* eisosome. Can1p is associated with MCC domains and regions of high ergosterol content. Within the eisosome complex, both Nce102p and Sur7p are present, with Sur7p in closer proximity to Can1p. Under conditions of membrane stress, the tension of the eisosome increases, causing Nce102p to spread out across the membrane. This figure was created using Biorender.com.

To ensure that this strain responds to escin similarly to the WT, we conducted a growth analysis in the presence of escin in CSM for 24 hours (Figure 45). The results confirmed that the growth of the sur7-mRFP; nce102-GFP *S. cerevisiae* strain was comparable to the WT strain, with the MIC of escin determined to be 62.5 µg.mL^{-1}.

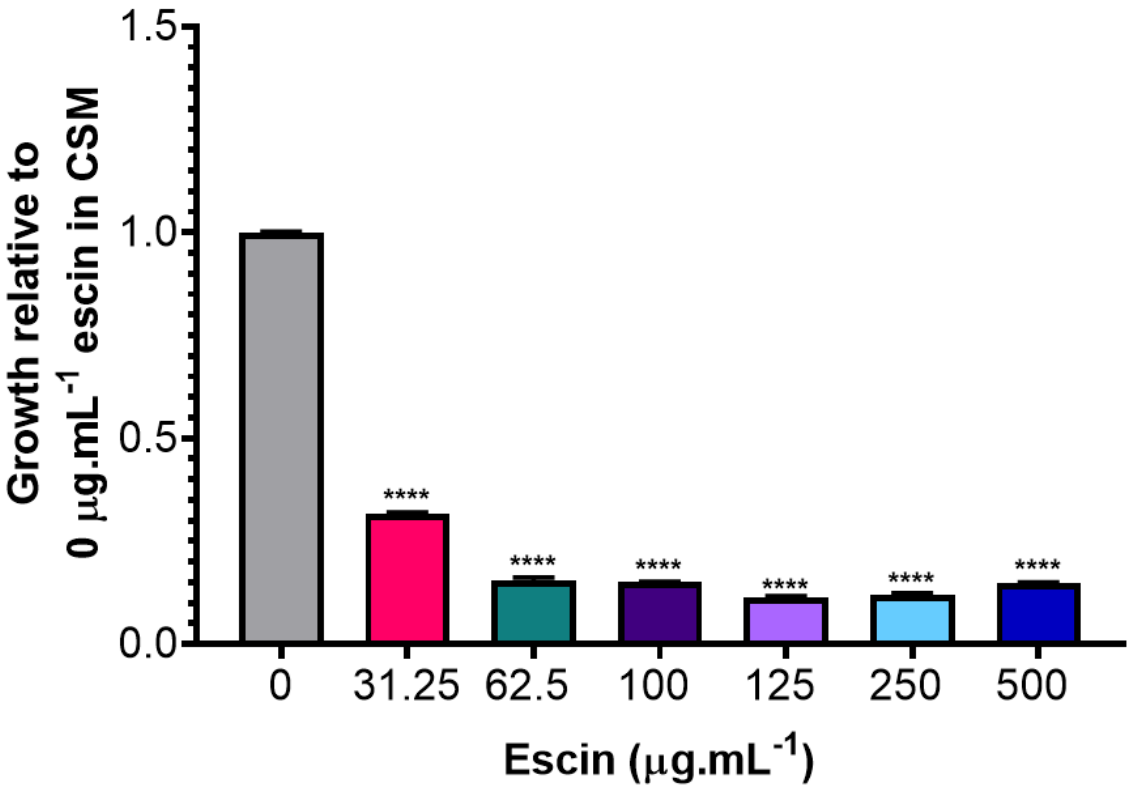

Figure 45: - Growth of the *sur7*-mRFP; *nce102*-GFP *S. cerevisiae* strain in the presence of escin after 24 hours of growth in CSM relative to the 0 µg.mL^{-1} escin control. For statistical analysis, a one-way ANOVA was conducted to compare each treatment with the 0 µM escin control. The sample size was n=3. The p-values are indicated as follows: * = ≤ 0.05, ** = ≤ 0.01, *** = ≤ 0.001, **** = ≤ 0.0001

This study aimed to investigate potential changes in the size and distribution of MCC domains, as well as the overall size of yeast cells after treatment with escin. The hypothesis was that escin, through its interaction with ergosterol, creates pores in the membrane, leading to observable differences in the size and distribution of these domains rich in ergosterol.

To visualise the yeast cells, they were immobilised on slides and observed using confocal microscopy. Concanavalin A was used for immobilisation, as it binds to glycans on the yeast cell wall, effectively securing them in place without causing any damage to the yeast cell (Caloca *et al*., 2022). The treatment conditions included 0, 31.25, and 62.5 $\mu g.mL^{-1}$ escin, as well as 400 $\mu g.mL^{-1}$ geneticin (G418) for 1 hour. G418 is an aminoglycoside known to block polypeptide synthesis, serving as a control to discern changes in the plasma membrane during cell death, rather than specifically due to escin treatment (Johnston *et al*., 2023). Additionally, a positive control of 50 mM Tris-HCl pH 8 was included, as it has been previously shown to disrupt the osmotic pressure and increase membrane tension of the yeast PM, resulting in the dissipation of MCC domains into the membrane, leading to a more disordered membrane (Appadurai *et al*., 2020).

Each cell was compared to itself, and analysis was conducted using IMARIS software, which measured the volume of MCC domains (μm^3), the number of MCC domains, and cell area (μm^2) (Figure 46). Throughout the experiment, it was evident that the MCC domains per cell (normalised to cell area), cell area, and volume of individual clusters did not exhibit significant changes under the various treatments with the positive control, escin, or G418.

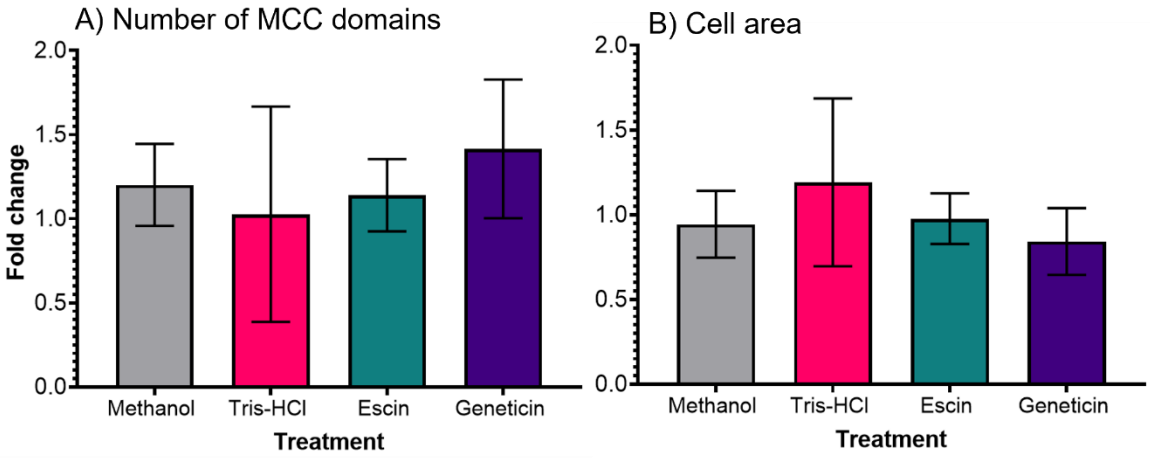

Figure 46: - Bar charts displaying the fold change of MCC domains and cell area under different treatment conditions. A) MCC domain fold change under the following treatments: control 0 $\mu g.mL^{-1}$ escin (MeOH 1.25 %), 50 mM Tris-HCl (pH 8), 31.25 $\mu g.mL^{-1}$ escin and 400 $\mu g.mL^{-1}$ geneticin. B) Cell area fold change under the same treatments mentioned above. The sample size for each treatment condition was n=9.

Cell area (μm^2) did not change after any of the treatments and neither did the number of MCC domains in each cell or volume of the clusters (Figure 46), even in the positive control treatment. Using the IMARIS software allowed us to annotate the volume of the clusters and the number of them but did not allow analysis of the differences in fluorescence levels between the clusters. Therefore, a different mode of analysis was used, with help from Dr David Kelly, facility manager of the COIL facility where the experiment was conducted. In the new analysis, fluorescence intensity around the membrane from a slice of the image around the midsection was measured, peaks of high intensity indicate MCC domains and the lack of peak is the background fluorescence/plasma membrane (Figure 47). It was reasoned that if the membrane is undergoing stress, either due to escin pulling ergosterol from the membrane or escin incorporating itself in the membrane, then the intensity of the SUR7-RFP and NCE102-GFP would change. This is due to the proteins leaking into the membrane and away from MCC domains (as would be seen in Figure 44) during membrane stress.

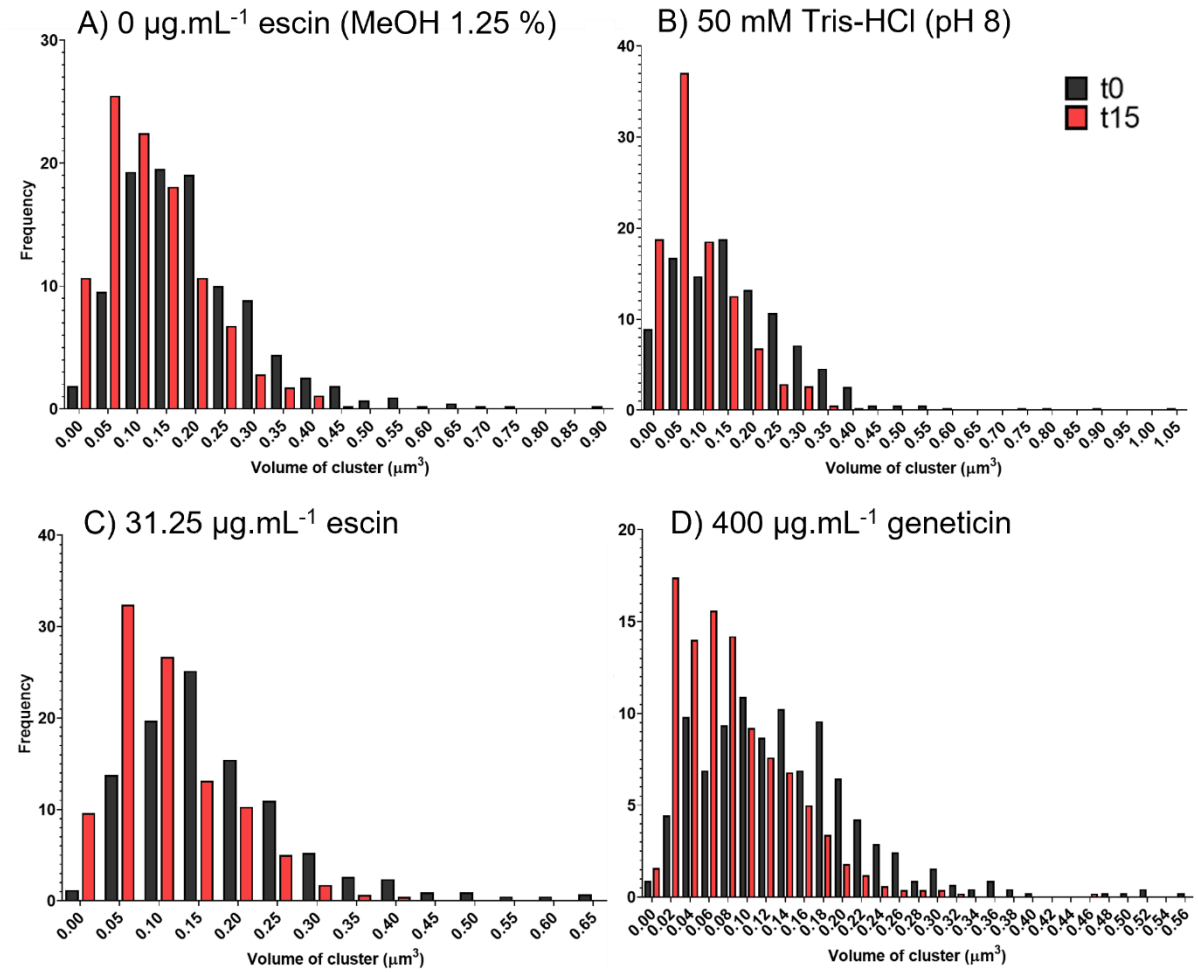

Figure 47: - The frequency distribution of membrane cluster volume before and after 15 mins of treatment. A) 0 µg.mL^{-1} escin (1.25% methanol) treatment; n=421. B) 50 mM Tris-HCl pH 8 treatment; n=394. C) 31.25 µg.mL^{-1} escin treatment; n=430. D) 400 µg.mL^{-1} geneticin treatment; n=449.

In all conditions, where we measured the same cell before and after treatment, there was no difference in the change of intensity of the MCC domains. In the negative control (Figure 48) we saw both results we expected and results that were not expected. The expected result resembles what is observed in Figure 48C, where there is no difference in the intensity of the MCC domains before and after methanol treatment. However, in Figure 48F there are some cells which display a difference after 15 minutes of treatment. This occurred in all the conditions tested. This was apparent in all treatments tested, in the positive control (Figure 49) escin treatment (Figure 50) and G418 (Figure 51).

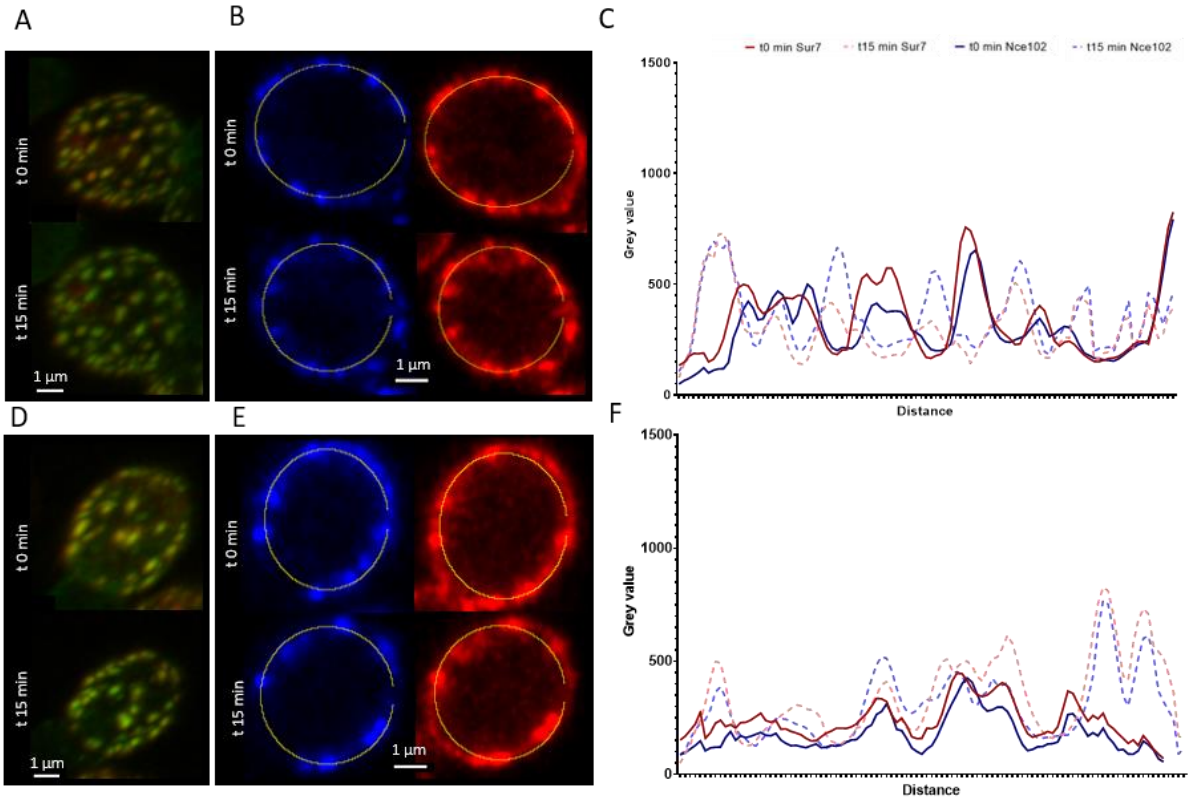

Figure 48: - Confocal microscopy images and histogram data representing MCC domain intensity of two individual cells before and after treatment with methanol (1.25%). A) and D). Three-dimensional images of the Sur7-mRFP Nce102-GFP strain were captured using confocal microscopy before and after treatment with methanol (1.25%) on two different cells. Co-localisation of the proteins is represented in yellow. B) and E) Two-dimensional images of two different cells of the Sur7-mRFP (red) Nce102-GFP (blue) strain before and after treatment with methanol (1.25%). A line was drawn around the perimeter of the cells and intensity was measured. Clusters of high intensity are shown in C and F as histograms. C) Demonstrates what was expected of the negative control. After 15 minutes of methanol treatment, the intensity of the peaks and background intensity of the membrane is the same, as demonstrated by the dotted line. However, as seen in F) mapping the cell present in D, a different result is shown, where it shows a clear difference between the two-time points. n = 22.

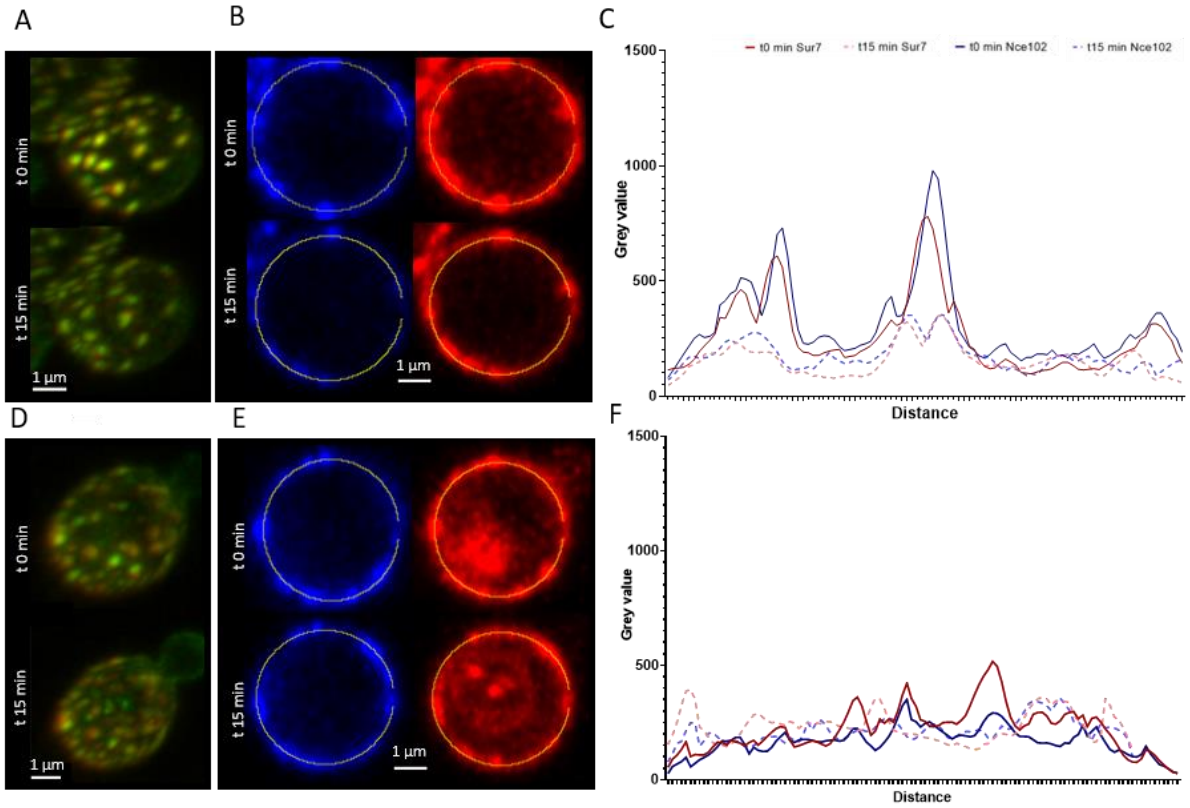

Figure 49: - Confocal microscopy images and histogram data representing MCC domain intensity of two individual cells before and after treatment with Tris-HCl pH8. A) and D) Three-dimensional images of the Sur7-mRFP Nce102-GFP strain captured using confocal microscopy before Tris-HCl pH8 exposure on two different cells. Co-localisation of the proteins is represented in yellow. B) and E) Two-dimensional images of two different cells of the Sur7-mRFP (red) Nce102-GFP (blue) strain before and after 15 minutes of Tris-HCl pH8 exposure. A line was drawn around the perimeter of the cells and intensity was measured. Clusters of high intensity are shown in C and F as histograms. C) Demonstrates what was expected of Tris-HCl pH8 treatment as a positive control for a change in membrane dynamics. After 15 minutes, the intensity of the peaks and background intensity of the membrane decreases, as demonstrated by the dotted line. However, as seen in F) mapping the cell present in D, a different result is shown, where there is no correlation with treatment and intensity of the MCC domains. n = 18.

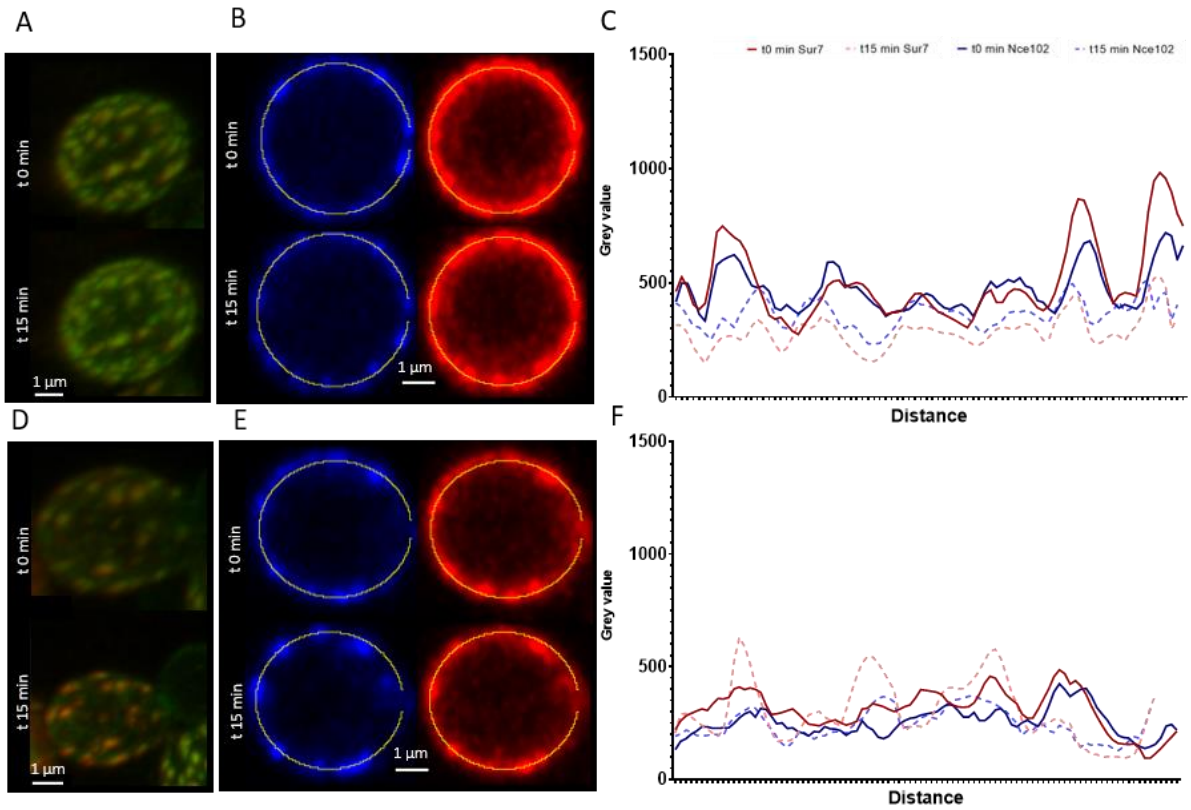

Figure 50: - Confocal microscopy images and histogram data representing MCC domain intensity of two individual cells before and after treatment with 31.25 µg.mL^{-1} escin. A) and D) Three-dimensional images of the Sur7-mRFP Nce102-GFP strain captured using confocal microscopy before 31.25 µg.mL^{-1} escin exposure on two different cells. Co-localisation of the proteins is represented in yellow. B) and E) Two-dimensional images of two different cells of the Sur7-mRFP (red) Nce102-GFP (blue) strain before and after 15 minutes of 31.25 µg.mL^{-1} escin exposure. A line was drawn around the perimeter of the cells and intensity was measured. Clusters of high intensity are shown in C and F as histograms. C) demonstrates what was expected of 31.25 µg.mL^{-1} escin treatment. After 15 minutes, the intensity of the peaks and background intensity of the membrane decreases, as demonstrated by the dotted line. However, as seen in F) mapping the cell present in D, a different result is shown, where there is no correlation with treatment and intensity of the MCC domains. n = 29.

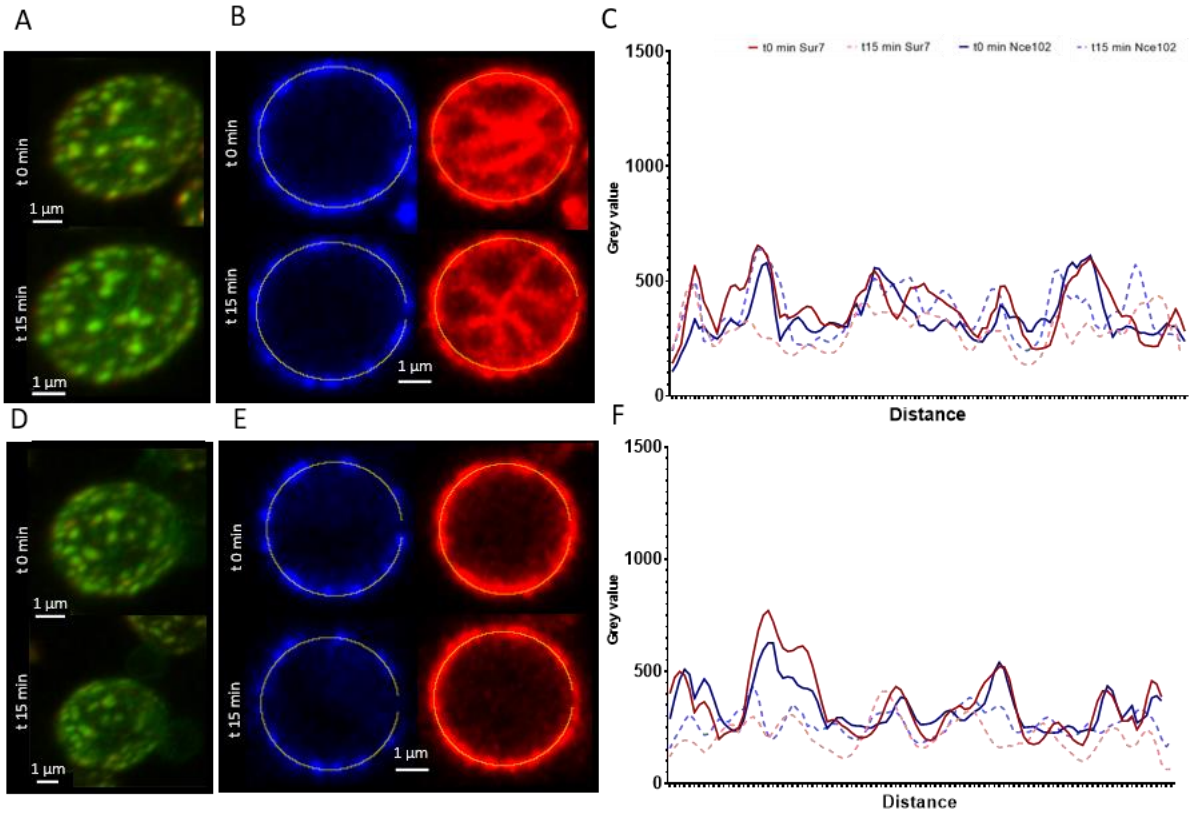

Figure 51: - Confocal microscopy images and histogram data representing MCC domain intensity of two individual cells before and after treatment with 400 µg.mL^{-1} geneticin. A and D) Three-dimensional images of the Sur7-mRFP Nce102-GFP strain captured using confocal microscopy before 400 µg.mL^{-1} geneticin exposure on two different cells. Co-localisation of the proteins is represented in yellow. B and E) Two-dimensional images of two different cells of the Sur7-mRFP (red) Nce102-GFP (blue) strain before and after 15 minutes of 400 µg.mL^{-1} geneticin exposure. A line was drawn around the perimeter of the cells and intensity was measured. Clusters of high intensity are shown in C and F as histograms. C) demonstrates what was expected of 400 µg.mL^{-1} geneticin treatment. After 15 minutes, the intensity of the peaks and background intensity of the membrane is the same, as demonstrated by the dotted line. However, as seen in F) mapping the cell present in D, a different result is shown, where it shows what is expected of Tris-HCl pH8 and escin 31.25 µg.mL^{-1} treatment. n = 24.

4.6 Differential gene expression after escin treatment

Transcriptomic analysis was conducted by Dr Emily Johnston which allowed for the identification of stress indicator genes in response to 100 μg.mL^{-1} escin. The data revealed differential gene expression of *LAM4*, *ARE2*, and *UPC2* in wild-type (WT) yeast, but not in the ***erg3Δ*** mutant (Johnston *et al*., 2023). These genes are primarily involved in sterol biosynthesis. Lam4p, a membrane-anchored lipid binding protein, acts as a sterol binding protein localised at the contact sites between the endoplasmic reticulum (ER) and the plasma membrane (PM), where sterols are synthesised and located. Lam4p belongs to a family of six *LAM* proteins, all of which possess steroidogenic acute regulatory protein-related lipid transfer domains (Jentsch *et al*., 2018), facilitating sterol binding. These proteins are believed to be involved in intracellular sterol transfer between membranes, and deletion of these genes has been shown to increase the sterol content in the PM (Sokolov *et al*., 2020). Are2p, a sterol-acetyl transferase, is an ER enzyme responsible for sterol esterification (Polakowski *et al*., 1999; Zweytick *et al*., 2000). *ARE2* is a paralogous gene that arose from a whole-genome duplication event involving ARE1. Are2p is the primary enzyme involved in the formation of most cellular ergosteryl esters derived from ergosterol. These sterol esters are translocated to lipid particles and combined with triacylglycerides to form lipid droplets, which serve as storage sites for sterols. Excessive ergosterol accumulation triggers the transport of sterols out of the cell (Liu *et al*., 2019c; Jordá & Puig, 2020). Upc2p, a sterol regulatory element binding protein, functions as a zinc cluster transcription factor (TF) that influences ergosterol biosynthesis when ergosterol levels are depleted. In the presence of ergosterol, it binds to Upc2p, covering the nuclear localisation signal (NLS) and keeping the TF in the cytoplasm (Marie *et al*., 2008). However, in the absence of ergosterol, the NLS of Upc2p is exposed, allowing it to translocate to the nucleus and induce the transcription of most ergosterol biosynthesis and sterol uptake genes (Yang *et al*., 2015b; Jordá & Puig, 2020).

We also investigated *ERG11*, an enzyme known as lanosterol 14-alpha-demethylase (Erg11p), which plays a role in the demethylation process of lanosterol. Lanosterol is a precursor to ergosterol, and Erg11p is among the genes responsible for ergosterol

biosynthesis, which is regulated by Upc2p (Vik & Rine, 2001). Our selection of *ERG11* for analysis was based on its activation by Upc2p and the observed upregulation in both the ***erg3Δ*** and ***erg6Δ*** mutants under control conditions (Johnston *et al*., 2023). Previous studies have highlighted the significance of *ERG11*, along with *ERG3* and *NCP1*, as important targets for Upc2p (Woods & Höfken, 2016). However, since our analysis focused on an ***erg3Δ*** mutant, which was not a viable target, and our transcriptomics data did not indicate any differential expression in *NPC1*, we did not pursue further investigation with those genes. This enabled us to determine whether any upregulation in Upc2p resulted in increased activation of the *ERG11*. Reverse transcription-quantitative real-time polymerase chain reaction (RT-qPCR) was performed to verify the transcriptome data with the mutants available to us in replicate.

We conducted a transcriptomic analysis to examine gene expression levels, specifically focusing on the expression of *LAM4* and *ARE2* genes in both the WT strain and the ***erg3Δ*** and ***erg6Δ*** mutant strains. The baseline expression of *LAM4* showed no significant difference between the WT and ***erg3Δ*** mutant strain, which is consistent with the RT-qPCR data (Figure 52). However, in the ***erg6Δ*** mutant data, we observed a small but significant increase (1.4-fold) in *LAM4* expression compared to the WT. Additionally, we noticed a slight increase in *LAM4* expression in the ***erg2Δ*** mutant (1.5-fold) and a more substantial increase in the ***erg5Δ*** mutant (3.9-fold; Figure 52A). Similarly, we observed a 1.5-fold increase in the baseline expression of *ARE2* in the ***erg2Δ*** mutant. This could be attributed to the presence of ***erg2Δ-specific*** sterols, particularly ergosta-8-enol, which might serve as a potential regulatory signal for *ARE2*. Previous studies have demonstrated that ergosterol intermediates can modulate the gene expression of *ARE2* and a decrease in ergosterol content has been shown to upregulate *ARE2* expression as well (Jensen-Pergakes ***et al***., 2001).

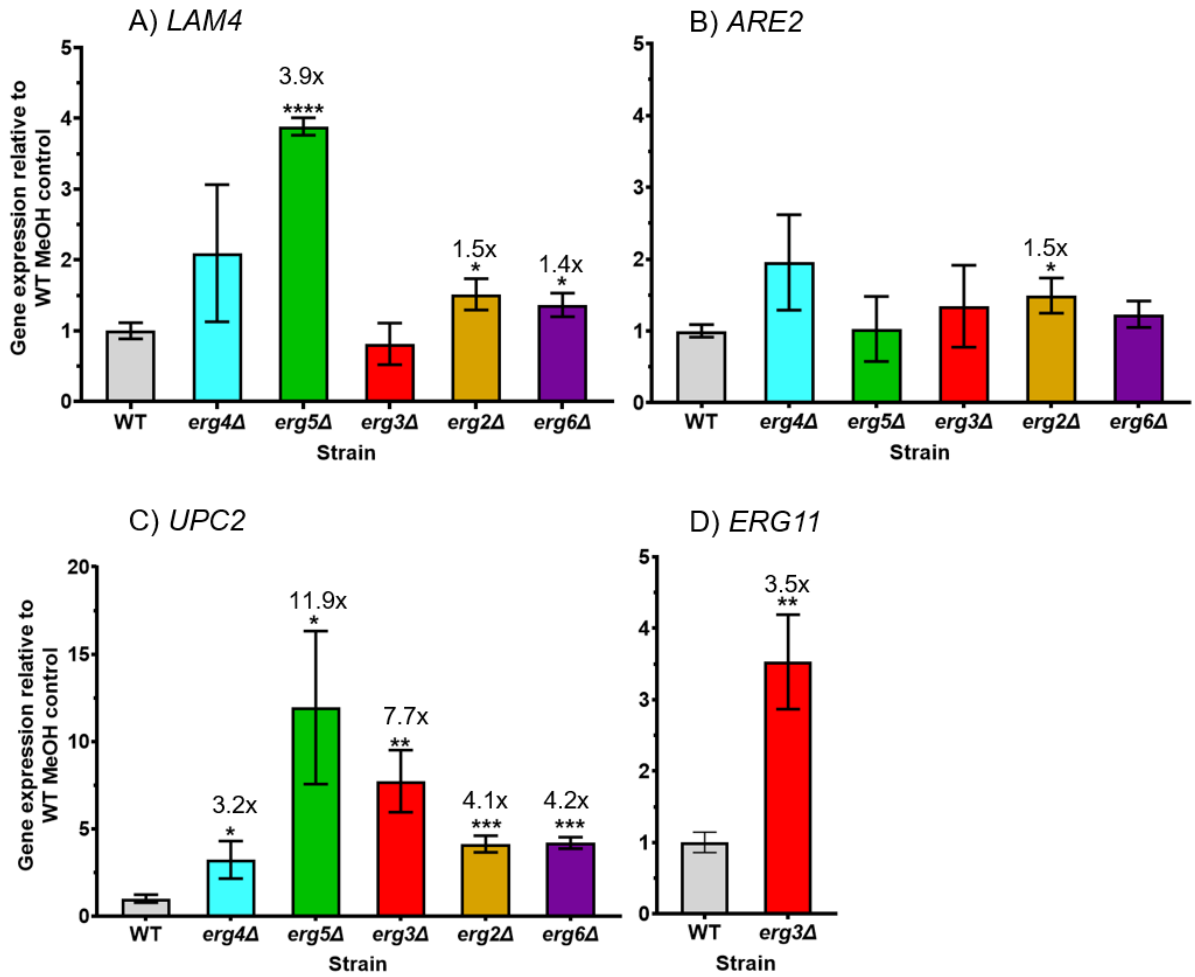

Figure 52: - Analysis of the gene expression in methanol controls (1.25 %) only for four genes of interest. Comparisons were made between the WT and individual strains only. The following genes were investigated A) *LAM4*, B) *ARE2*, C) *UPC2* and D) *ERG11*. For statistical analysis, multiple t-tests were conducted to compare each strain with the WT. The sample size was n=3. The p-values are indicated as follows: * = ≤ 0.05, ** = ≤ 0.01, *** = ≤ 0.001, **** = ≤ 0.0001.

In the transcriptome analysis (Johnston *et al*., 2023), an elevated expression of *UPC2* was observed in the *erg3Δ* and *erg6Δ* mutants. This finding aligns well with our data, as we confirmed increased *UPC2* expression in the *erg2Δ*, *erg4Δ*, and *erg5Δ* mutants (Figure 52C). Specifically, we noted a 4.1-fold increase in *UPC2* expression in the *erg2Δ* mutant compared to the WT, a 7.7-fold increase in the *erg3Δ* mutant, a 3.2-fold increase in the *erg4Δ* mutant, an 11.9-fold increase in the *erg5Δ* mutant, and a 4.2-fold increase in the *erg6Δ* mutant. These observations may be due to the absence of ergosterol in the mutants. Consequently, more Upc2p is produced to compensate for

the lack of ergosterol, thereby activating the biosynthesis genes responsible for ergosterol production. The correlation between the RT-qPCR data and the transcriptomics data is also evident for *ERG11*, where the ***erg3Δ*** mutant exhibited a 3.5-fold increase in baseline expression compared to the WT (Figure 52D). This relationship can be explained by the influence of the transcription factor Upc2p on *ERG11*, as the increase in Upc2p levels (Figure 52C) promotes the activation of ergosterol biosynthesis genes, including *ERG11*, in the absence of ergosterol in all the mutants. We only investigated *ERG11* expression in the WT and ***erg3Δ*** strains due to limitations in plate setup.

Treatment with 100 $\mu g.mL^{-1}$ of escin resulted in a slight increase in *LAM4* expression in the WT, but not in any of the other mutants. Although this increase was not statistically significant in this experiment, it corresponds with the findings from the transcriptomic study. The transcriptomics study indicated a general upregulation of *ARE2* expression, which is also consistent with the RT-qPCR results (Figure 53B). The WT and ***erg3Δ*** mutant exhibited expression levels similar to those observed in the transcriptomic data, although they did not reach statistical significance. Notably, we observed a general increase in *ARE2* expression in the WT, while significant increases were observed in the ***erg2Δ*** and ***erg6Δ*** mutants, with a 2.3 and 2.4-fold increase respectively. It is important to note that the previous study did not report this trend for the ***erg6Δ*** mutant, and the ***erg2Δ*** mutant was not included in their analysis. The ***erg4Δ*** mutant exhibited a non-significant increase in *ARE2* expression following exposure to escin, while no difference in *ARE2* expression was observed in the ***erg5Δ*** mutant after escin exposure.

In the presence of escin, there were slight, non-significant increases in the expression of *LAM4* and *ARE2* in the WT. This can be attributed to the role of Lam4p as a sterol transfer protein. When the sterol concentration is lower, the demand for Lam4p decreases accordingly. If escin removes ergosterol from the plasma membrane (PM), Lam4p becomes redundant, and there is no need for additional expression. Similarly, the presence of escin affects Are2p, which is responsible for esterifying excess ergosterol for storage or transport out of the cell. If escin reduces the content of ergosterol, it is reasonable to assume that *ARE2* would not be induced since there is insufficient ergosterol rather than an excess. However, previous findings have shown

increased *ARE2* expression under conditions of ergosterol depletion (Jensen-Pergakes *et al*., 2001).

Furthermore, the transcriptomic data indicated an upregulation in the expression of *UPC2* in the presence of escin, both in the WT and the ***erg6Δ*** mutant. This finding aligns with the RT-qPCR study, where a statistically significant 2.1-fold increase in *UPC2* expression was observed in the WT treated with escin. The same trend was observed in the ***erg2Δ*** and ***erg6Δ*** mutants, with fold increases of 2 and 1.4, respectively. There was no change in *UPC2* expression in the ***erg3Δ*** or ***erg5Δ*** mutants, while the ***erg4Δ*** mutant displayed a small, non-significant increase in expression. The observed increase in *UPC2* expression (Figure 53C) following the addition of escin in the WT suggests a hypothesis that escin leads to a depletion of ergosterol in the PM. This hypothesis is supported by the fact that Upc2p is activated in response to ergosterol deficiency and subsequently binds to ergosterol biosynthesis genes in the nucleus. Therefore, we can infer that escin is responsible for removing the excess ergosterol, thereby triggering the need for replacement ergosterol.

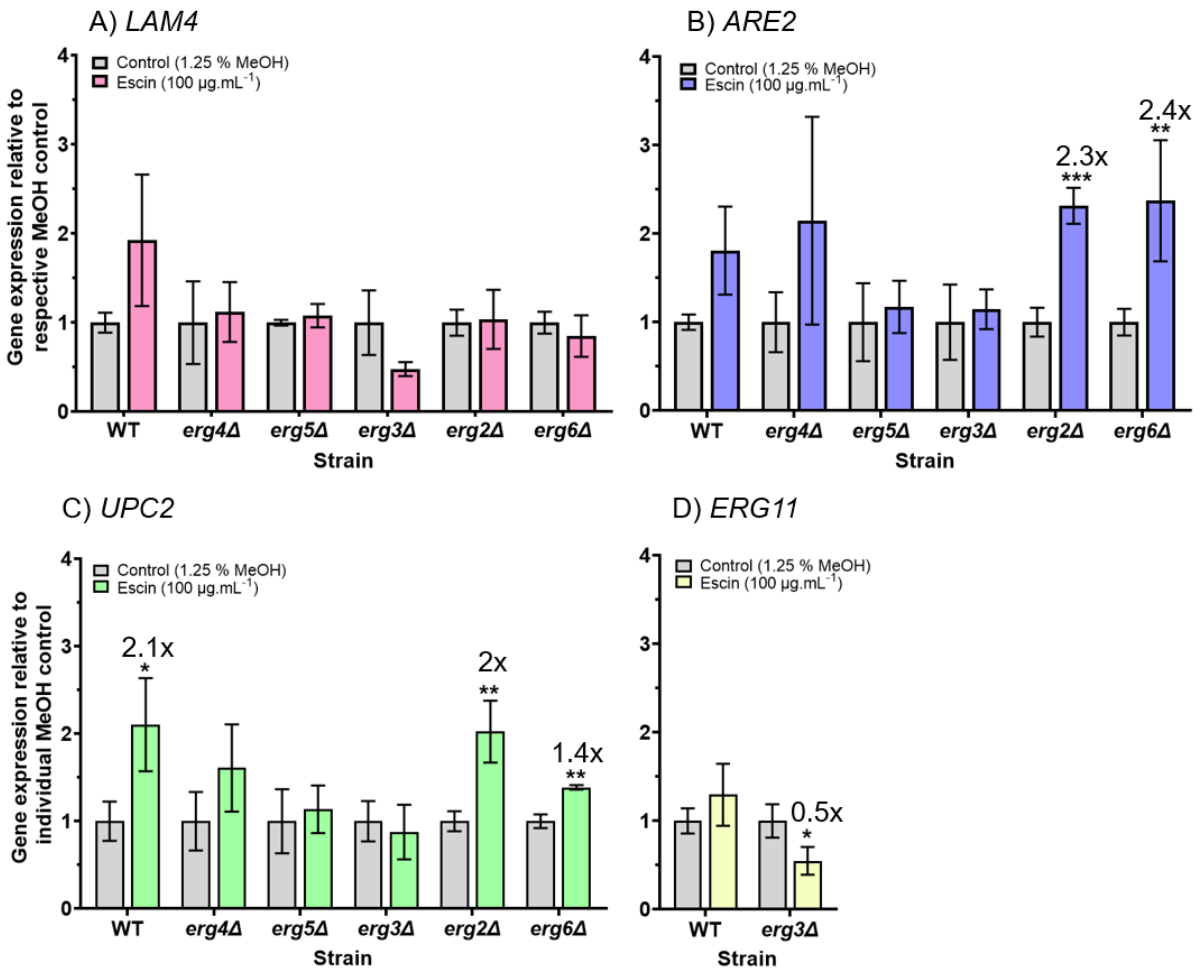

Figure 53: - Analysis of the gene expression relative to the methanol controls for four genes of interest in the presence or absence of escin (100 µg.mL^{-1}). Expression levels were normalised to the mean of the individual methanol controls. The following genes were investigated A) *LAM4*, B) *ARE2*, C) *UPC2* and D) *ERG11*.The expression levels of these genes were compared between the methanol control and exposure to escin (100 µg.mL^{-1}). For statistical analysis, multiple t-tests were conducted to compare each treatment with its respective methanol control. The sample size was n=3. The p-values are indicated as follows: * = ≤ 0.05, ** = ≤ 0.01, *** = ≤ 0.001, **** = ≤ 0.0001.

The significant increase in the expression of *ARE2* and *UPC2* in the presence of escin within the *erg2Δ* and *erg6Δ* mutants suggests that the sterols present in these mutants

also play a role. This influence can potentially be attributed to the specific structures of the prominent sterols in these mutants. Erg6p and Erg2p are sequential enzymes in the ergosterol biosynthesis pathway, responsible for converting zymosterol to fecosterol and then to episterol (refer to Figure 3.4). Consequently, the sterols produced by these knockout mutants exhibit striking similarities. The *erg6Δ* mutant predominantly produces zymosterol, while the *erg2Δ* mutant predominantly produces ergosta-8-enol (Figure 54) These mutant sterols share a common characteristic of having a double bond in the main sterol backbone between positions C8-9. Their differences lie in the branch chain extending from position C17, with zymosterol possessing a double bond between position C24-25 and ergosta-8-enol lacking double bonds in the branching chain.

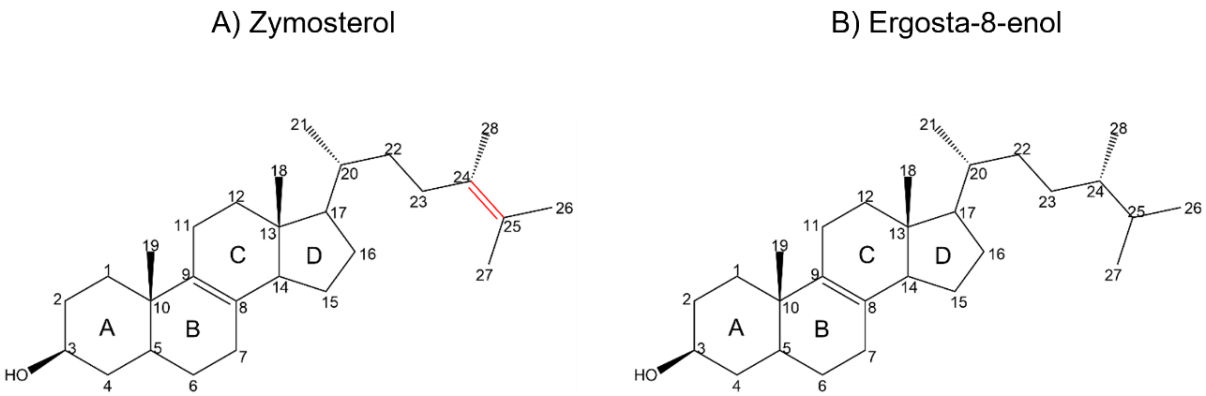

Figure 54: - Structures of the predominant sterols found in the *erg6Δ* and *erg2Δ* mutants. A) zymosterol and B) ergosta-8-enol. The red bond shows the difference between the two sterols.

Given the structural similarities between these sterols, particularly the presence of the C8-9 double bond (which is absent in other mutant sterols), it is plausible to hypothesise that these specific sterols may interact with both *ARE2* and *UPC2* in a manner more akin to ergosterol. When sterol depletion occurs, UPC2 may be activated similarly to transcriptional responses triggered by ergosterol depletion. Therefore, in the absence of escin, it appears that both zymosterol and ergosta-8-enol possess inhibitory capabilities similar to those of ergosterol. The observed increase in *ARE2* expression in the presence of escin in the *erg2Δ* and *erg6Δ* mutants may be attributed to the baseline increase in *ARE2* expression already present in these strains under

normal conditions. When escin is introduced, it induces cellular stress, leading to further expression of *ARE2*. This could be explained by the interaction between the sterol intermediates and the activation of *ARE2*. Consequently, the depletion of these sterols caused by escin could potentially enhance the activation of *ARE2* expression.

Lastly, we investigated *ERG11* expression in only the WT and ***erg3Δ*** strains due to limitations in plate setup (Figure 53D). While the transcriptomic data showed no increase in *ERG11* expression in the WT in the presence of escin, we observed a significant 0.5-fold decrease in expression in the ***erg3Δ*** mutant when exposed to escin. This finding is particularly interesting because, under control conditions, the ***erg3Δ*** mutant exhibits a higher expression of *ERG11* compared to the WT strain (3.5-fold). However, when escin is introduced, the expression of *ERG11* in the ***erg3Δ*** mutant decreases dramatically. This suggests that escin may specifically repress *ERG11* in the ***erg3Δ*** mutant, or the unique sterols present in the ***erg3Δ*** mutant are capable of binding to Upc2p in the presence of escin, thereby suppressing the activation of *ERG11*.

Based on our RT-qPCR experiment, we can conclude that *LAM4* is not a reliable indicator of stress response in the presence of escin, as we did not observe any significant differential gene expression in any of the strains. On the other hand, *ARE2*, *UPC2* and potentially *ERG11* serve as better indicators of this stress response.

4.7 Discussion

In this comprehensive study, we delved into the intricate interactions between the natural compound escin and yeast cells, particularly *Saccharomyces cerevisiae*. Our investigation spanned various aspects, from cellular morphology to gene expression, highlighting the multifaceted effects of escin on yeast physiology.

The primary focus was on understanding how escin interacts with ergosterol, the cholesterol equivalent in the yeast cell membrane. In the initial experiments, conducted with WT *S. cerevisiae*, we confirmed the toxic impact of escin on yeast cells. The addition of exogenous ergosterol, however, demonstrated a restorative effect, returning growth and reducing toxicity. The stoichiometry of escin to ergosterol played a role, with both 1:1 and 1:2 molar ratios effectively restoring growth. This indicated that exogenous ergosterol acts as an inhibitor, competing with endogenous ergosterol and dampening the toxic effects of escin.

Furthermore, we explored the impact of escin on yeast cells in the presence of brassicasterol, a sterol found in rapeseed and canola oils. The results, which were similar to the results with ergosterol, provided additional support for the hypothesis that escin has a specific interaction with ergosterol. However, this interaction was less pronounced with brassicasterol, further emphasising the specificity of escin on yeast membranes.

To gain insights into the dynamics and organisation of the plasma membrane, we used a strain expressing fluorescently tagged proteins (sur7-mRFP and nce102-GFP) which are associated with membrane microdomains. Confocal microscopy revealed that escin did not induce significant changes in the size and distribution of membrane compartments, which suggested that despite its impact on growth and ergosterol, escin might not disrupt the overall organisation of specific membrane domains. As well as this, our attempts to use ITC to directly measure the interaction between escin and ergosterol faced challenges due to the solubility of escin and ergosterol. Despite these

limitations, ITC remains a powerful technique for studying molecular interactions, and future studies may benefit from alternative experimental conditions or techniques.

The transcriptomic analysis provided a deep dive into the molecular responses triggered by escin exposure. Key sterol biosynthesis genes, *LAM4, ARE2*, and *UPC2*, exhibited differential expression. While Lam4p appeared less responsive, Are2p and Upc2p emerged as good indicators of stress response to escin. Particularly, the specific genetic background and sterol composition of yeast strains played a significant role in shaping the observed responses, introducing a layer of complexity to the impact of escin on gene expression.

The influence of escin on yeast cells appears to be complicated. Escin interacts specifically with ergosterol, altering membrane dynamics and triggering stress responses at the molecular level. The differential gene expression patterns highlight the dynamic interplay between escin, sterol composition, and cellular stress pathways. In conclusion, this study provides a comprehensive understanding of how escin affects yeast cells. From the cellular to the molecular level, these findings contribute insights into the specificity and complexity of escin and the impact it has on *S. cerevisiae*. This knowledge lays the groundwork for further investigations, which could lead to the development of targeted strategies for using or avoiding the cytotoxic effects of escin in different biological contexts.

Chapter 5: - Structure-activity relationship of the escin isomers on *S. cerevisiae* growth and inhibition

Due to the interesting relationship of escin with the *erg3Δ* mutant, it was decided to investigate the bioactive isomers of escin to determine the structure-activity relationship of the isomers.

5.1 Escin isomers

As previously mentioned in Chapter 4, complete escin is a mixture of many glycosylated triterpenoids. The biologically active compounds, escin 1a, escin 1b, isoescin 1a and isoescin 1 (Figure 55) were further investigated to identify whether there were differences in the toxicity to *S. cerevisiae* and ergosterol biosynthesis mutants. We received characterised fractions of escin from Unilever, containing escin 1a, escin 1b, isoescin 1a and isoescin 1b with a purity of 80 %.

The effect of the escin isomers on *S. cerevisiae* growth has not been studied. Therefore, we conducted growth assays on WT *S. cerevisiae* using the same methodology as described in Chapter 4 where we identified the MIC of complete escin. It was found that the MIC of escin on WT and mutant *S. cerevisiae* was 175 $\mu g.mL^{-1}$ in YPD and 62.5 $\mu g.mL^{-1}$ in CSM.

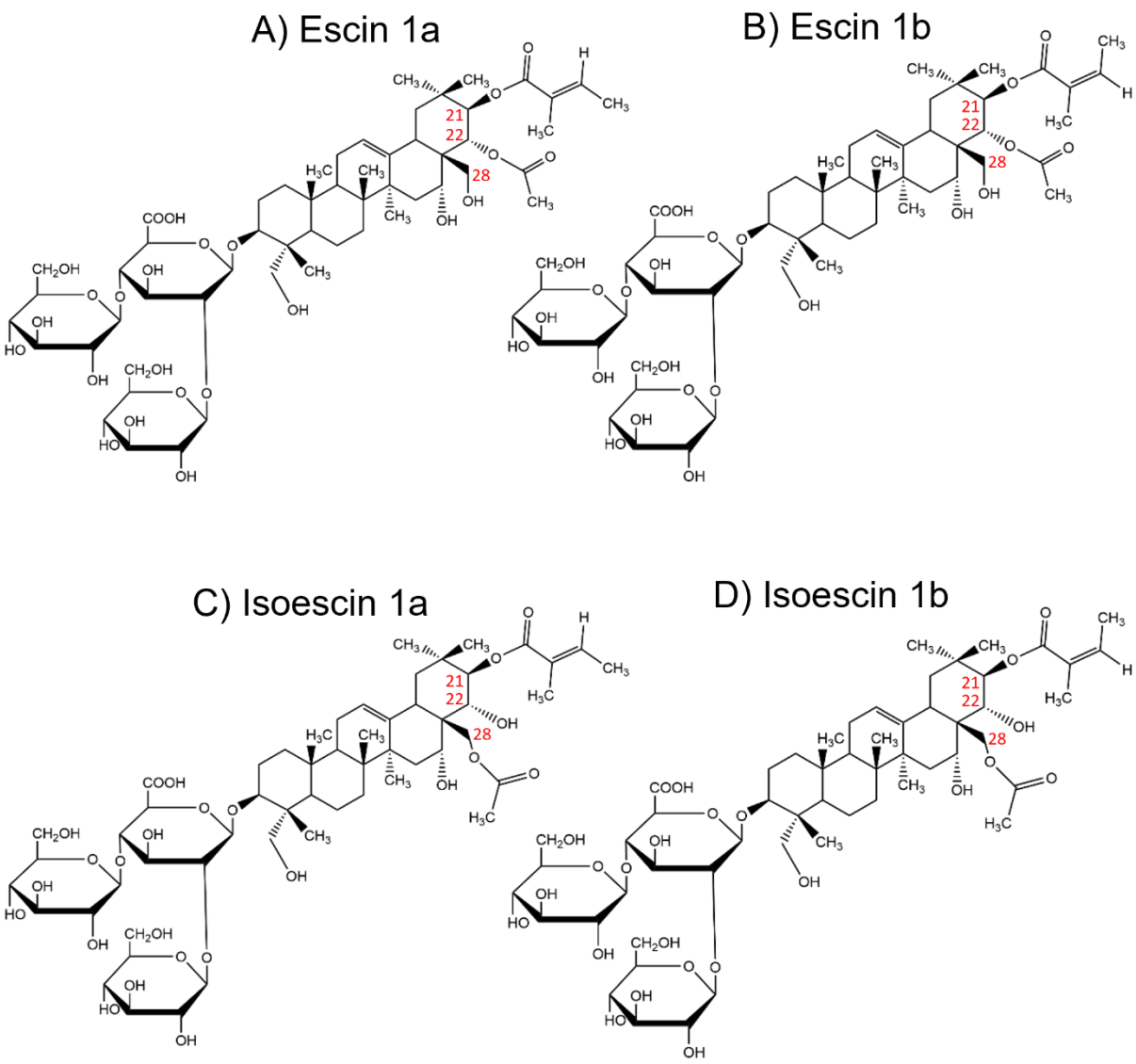

Figure 55: - The most bioactive escin isomers. A) escin 1a, B) escin 1b, C) isoescin 1a, D) isoescin 1b. Escin 1a and escin 1b have an acetyl group at position C22, and a hydroxyl at position (B). Isoescin 1a and isoescin 1b have a hydroxyl group at position C22, an acetyl at position C28 and an acid at C21. The acid group is either tiglic acid (C) or an angelic acid (D). C28 and an acid at C21. The acid group is either tiglic acid (A) or an angelic acid.

5.1.1 Effects of escin isomers on growth of *S. cerevisiae* and ergosterol biosynthesis mutants grown in YPD

In the case of WT *S. cerevisiae*, complete escin inhibited growth completely after 24 hours (Figure 56A). However, when only escin 1a was present, we observed growth at the concentration of 125 $\mu g.mL^{-1}$ but not at higher concentrations. In contrast, escin 1b alone showed a similar inhibitory effect as complete escin, with no growth observed at any of the tested concentrations. This suggests that escin 1b has a stronger impact on WT *S. cerevisiae* compared to escin 1a, as the growth pattern in escin 1b mirrors that of complete escin. The fact that escin 1a does not show an inhibitory effect at 125 $\mu g.mL^{-1}$ indicates that the WT is more tolerant to this isomer than to escin 1b. In contrast, there was no significant change in the growth of the WT at any of the tested concentrations in the presence of isoescin 1a or isoescin 1b, indicating that these two isomers alone do not have inhibitory properties against the WT strain.

Due to the differences seen in escin 1a and escin 1b, we decided to mix them both at a 1:1 ratio to attempt a restoration of full toxicity known percentages of escin 1a to escin 1b in horse chestnuts naturally, which is roughly 1:1 (Savarino *et al*., 2023). When we mixed escin 1a and escin 1b in a 1:1 ratio, we observed some growth at 125 $\mu g.mL^{-1}$ and no growth at higher concentrations. We can conclude that escin 1b contributes to the toxicity of complete escin more than escin 1a. These findings suggest that complete escin contains a higher proportion of escin 1b than escin 1a since the growth at 125 $\mu g.mL^{-1}$ is more indicative of the growth pattern in the presence of escin 1a, which does not correlate with the current literature. Savrarino *et al*., 2023 observed that escin 1a and escin 1b are present in horse chestnuts at a percentage of 21.7 and 18.4 % respectively and therefore, there must be other isomers present in complete escin that is affecting the viability of the cells.

These findings indicate that the structural characteristics of the escin isomers are associated with their inhibitory effects. Both escin 1a and escin 1b have an acetyl group at position C22, which is absent in the isoescins. Additionally, the angelic acid at position C21, present in escin 1b, exhibits greater biological activity compared to

the tiglic acid found in escin 1a. Therefore, the positioning of the acid and acetyl groups are responsible for the inhibitory effect of these compounds on WT *S. cerevisiae*. Considering the stronger inhibitory effect of escin 1b, we can hypothesise that the position of the angelic acid plays a role in this inhibition. It is plausible that the proximity of the acid and acetyl groups in space allows for interactions between them, thereby resulting in enhanced inhibition. In escin 1b the region between the C21 angelic acid and C22 acetyl group is a bit more open than that in escin 1a, due to the conformation of the tiglic acid group. This more open conformation may be the reason for the increased inhibitory effect, as there is more room for interactions with ergosterol. In contrast with the isoescins, the acetyl group is found on position C28, which is even further away than the C21 acid group in space. The difference in stereochemistry may play a role too, as in the isoescins C21 acid and C28 acetyl project from the plane in the same direction, which is not the case for the C21 acid and C22 acetyl in escin 1a and 1b (Figure 55). Therefore, the distance between the acid group at C21 and the acetyl at either C22/C28 plays a role in the inhibitory effect of the different escin isomers.

To further consolidate these findings, we investigated the impact of escin 1a, escin 1b, isoescin 1a, isoescin 1b, and a mixture of escin 1a and 1b on ergosterol biosynthesis mutants. Beginning with the *erg4Δ* mutant which exhibited no growth when exposed to complete escin at concentrations of 125, 250, or 500 $\mu g.mL^{-1}$ (Figure 56B). This lack of growth was also observed in the presence of escin 1a and escin 1b. Furthermore, there was no noticeable change in the growth of the *erg4Δ* mutant when isoescin 1a was present. However, in the presence of isoescin 1b, we observed growth inhibition at the concentration of 500 $\mu g.mL^{-1}$ and a decrease in growth at the concentration of 250 $\mu g.mL^{-1}$. This observation is intriguing since the isoescins were previously shown to be non-inhibitory to WT yeast. However, our results indicate that isoescin 1b does exhibit inhibitory effects on the *erg4Δ* mutant at high concentrations. When escin 1a and 1b were combined, no growth was observed in the *erg4Δ* mutant.

The *erg5Δ* mutant displayed a very similar growth pattern to the *erg4Δ* mutant. No growth was observed in the presence of complete escin, escin 1a, and escin 1b (Figure 56C). In the isoescin 1a condition, the growth of the *erg5Δ* mutant was comparable to

that of the WT. However, in the isoescin 1b condition, growth was observed except at the concentration of 500 µg.mL^{-1}. Similarly, when the mixture of escin 1a and escin 1b was tested, no growth of the *erg5Δ* mutant was observed at any of the tested concentrations.

The *erg3Δ* mutant showed no inhibition in any of the concentrations tested and this did not change in the presence of the different isomers (Figure 56D).

In the *erg2Δ* mutant, we observed growth inhibition at concentrations of 250 µg.mL^{-1} and above in the presence of complete escin. However, there was reduced growth, 32.4 % of that of the *erg2Δ* mutant at 0 µg.mL^{-1} escin, at the concentration of 125 µg.mL^{-1} (Figure 56E). This suggests that the *erg2Δ* mutant may exhibit slightly higher tolerance to complete escin compared to the WT. In the presence of escin 1a, we observed growth like the no escin control (1.25 % methanol) at 125 µg.mL^{-1}, reduced growth at 250 µg.mL^{-1} compared to the WT (30 % of that of the WT at 0 µg.mL^{-1} escin), and no growth at 500 µg.mL^{-1}. For escin 1b, we observed some growth at 125 µg.mL^{-1} but not at higher concentrations. These results further support the hypothesis that escin 1b has stronger inhibitory effects than escin 1a, as the *erg2Δ* mutant was still able to grow to some extent in the presence of 250 µg.mL^{-1} escin 1a. When examining the isoescins, we observed that the *erg2Δ* mutant displayed reduced growth compared to the WT, although it still exhibited growth. This suggests that the isoescins are relatively harmless to the yeast, and the decreased growth in the *erg2Δ* mutant could be attributed to the mutant strain's overall reduced tolerance and slower growth characteristics. In the case of the 1:1 mixture of escin 1a and 1b, we observed growth at 125 µg.mL^{-1} but not at higher concentrations, which aligns with the similar results observed in the WT under the same conditions (Figure 56A).

This heightened tolerance in the *erg2Δ* mutant could be attributed to the structural similarities in the membrane sterol composition between the *erg2Δ* and *erg3Δ* mutants. The structures of ergosta-8-enol and fecosterol (the most common sterols in the *erg2Δ* mutant) and ergosta-7,22-dienol (the most prevalent sterol in the *erg3Δ*

mutant) are similar in the sense that they both have only one double bond in the B ring. Although they are in different positions, the presence of only one double bond appears to play a crucial role. The absence of two double bonds in the B ring could potentially impede the ability of escin to interact with the sterol, leading to the increased tolerance observed in the *erg3Δ* mutant.

The *erg6Δ* mutant did not exhibit any growth at any of the tested concentrations in the presence of escin 1a and escin 1b. Only a minor decrease in growth was observed in the presence of isoescin 1a at concentrations of 250 and 500 $\mu g.mL^{-1}$. However, growth inhibition was evident when isoescin 1b was present at a concentration of 500 $\mu g.mL^{-1}$. Similar to the *erg5Δ* mutant, the growth of the *erg6Δ* mutant was completely inhibited when a mixture of escin 1a and 1b was introduced to the culture (Figure 56F).

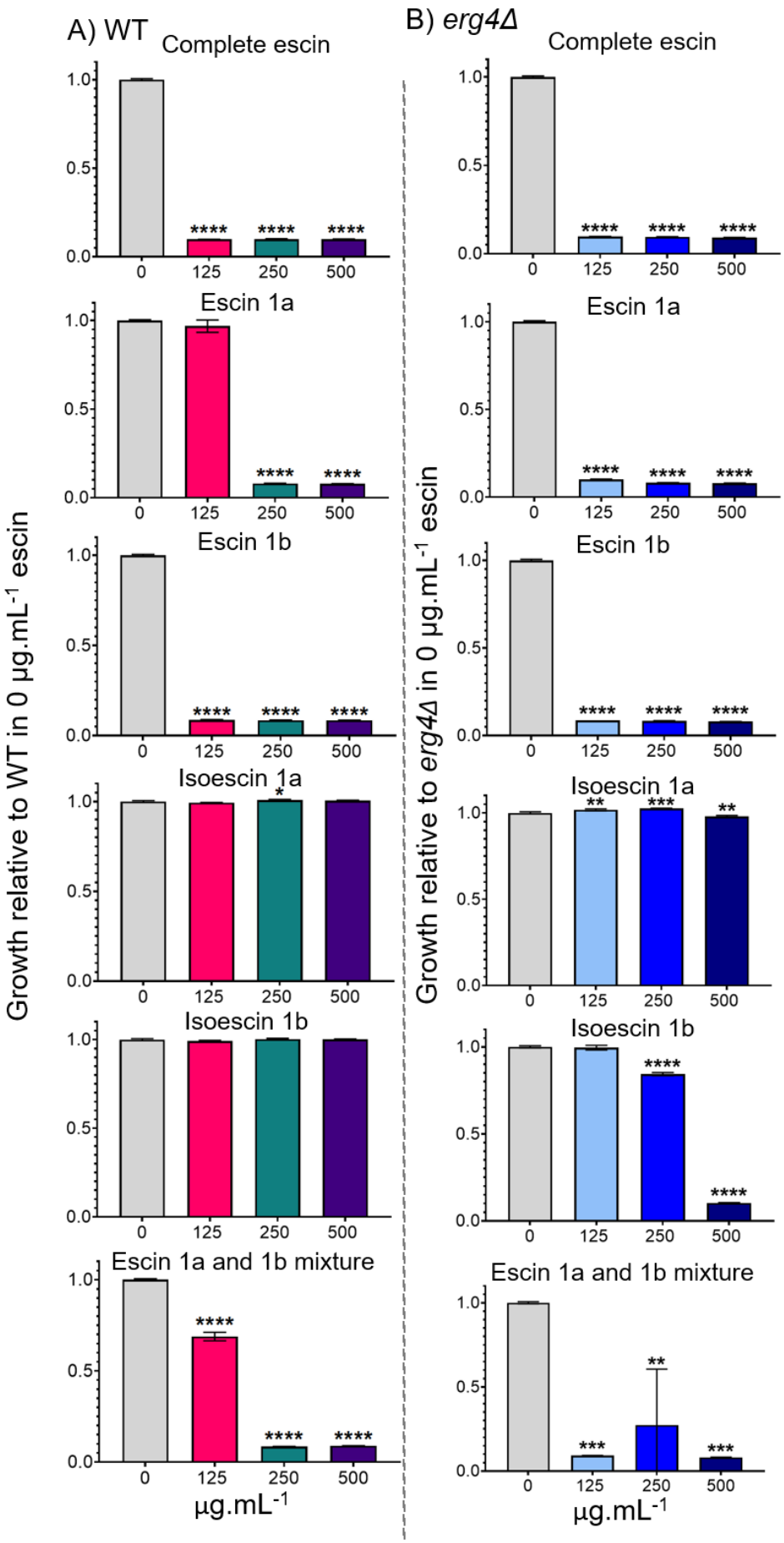

Figure continued…

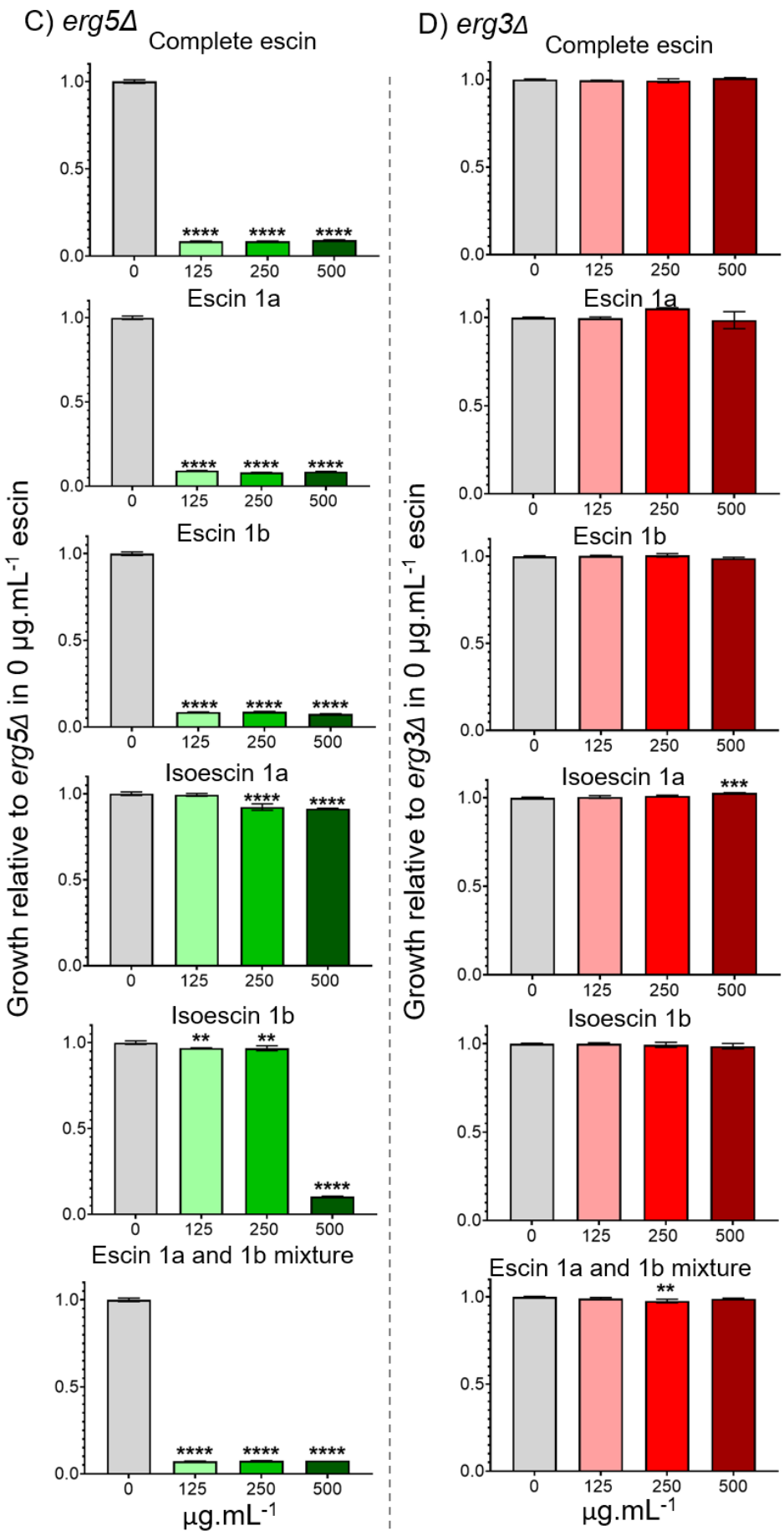

Figure continued...

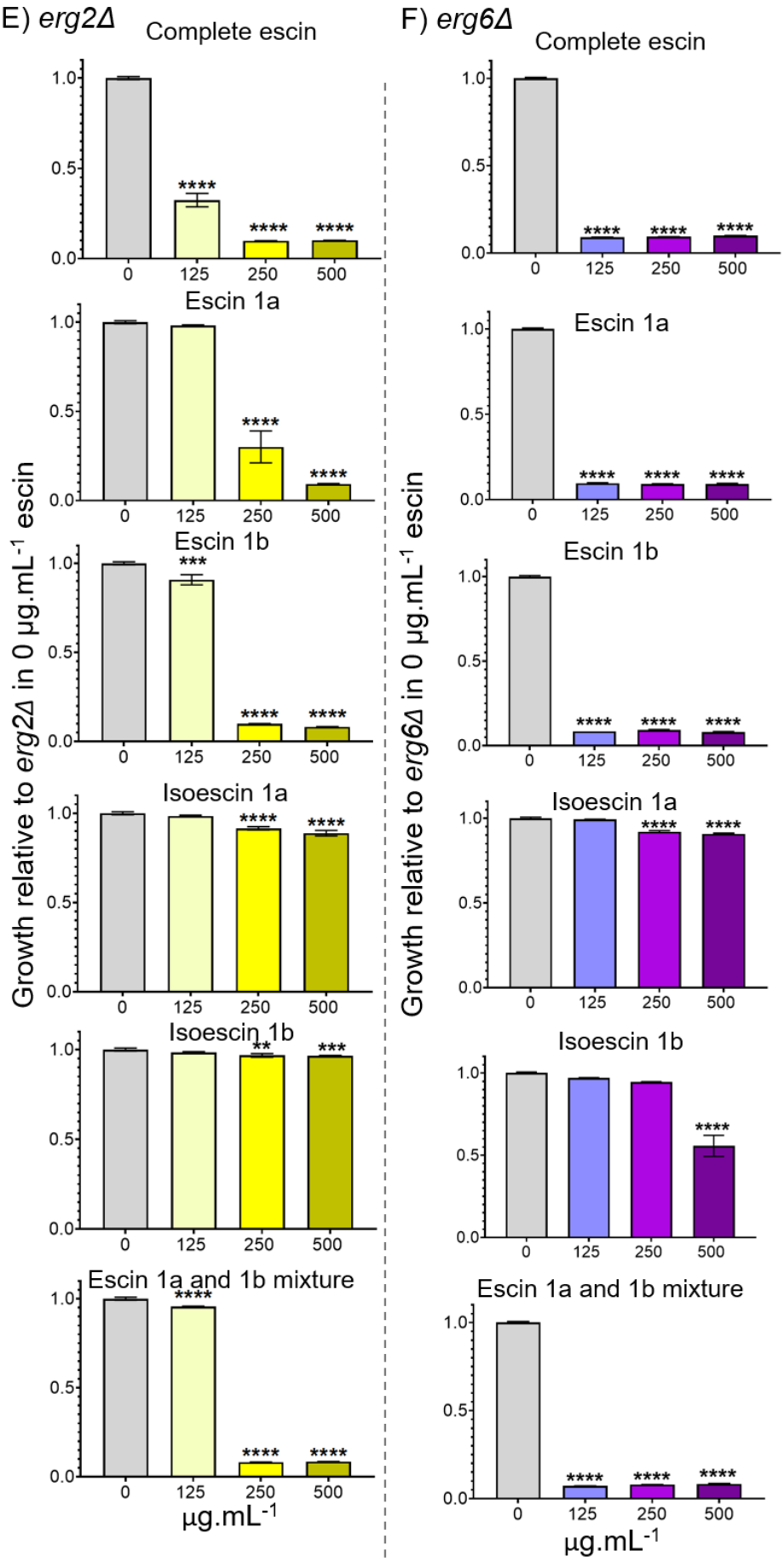

End of figure.

Figure 56: - Bar charts illustrating the growth of *S. cerevisiae* relative to 0 µg.mL^{-1} escin in YPD after 24 hours of growth. A) Growth of WT in the presence of 125, 250, and 500 µg.mL^{-1} complete escin, escin 1a, escin 1b, isoescin 1a, isoescin 1b, and a mixture of escin 1a and 1b at a 1:1 ratio. B) Growth of the *erg4Δ* mutant in the presence of 125, 250, and 500 µg.mL^{-1} complete escin, escin 1a, escin 1b, isoescin 1a, isoescin 1b, and a mixture of escin 1a and 1b at a 1:1 ratio. C) Growth of the *erg5Δ* mutant in the presence of 125, 250, and 500 µg.mL^{-1} complete escin, escin 1a, escin 1b, isoescin 1a, isoescin 1b, and a mixture of escin 1a and 1b at a 1:1 ratio. D) Growth of the *erg3Δ* mutant in the presence of 125, 250, and 500 µg.mL^{-1} complete escin, escin 1a, escin 1b, isoescin 1a, isoescin 1b, and a mixture of escin 1a and 1b at a 1:1 ratio. E) Growth of the *erg2Δ* mutant in the presence of 125, 250, and 500 µg.mL^{-1} complete escin, escin 1a, escin 1b, isoescin 1a, isoescin 1b, and a mixture of escin 1a and 1b at a 1:1 ratio. F) Growth of the *erg6Δ* mutant in the presence of 125, 250, and 500 µg.mL^{-1} complete escin, escin 1a, escin 1b, isoescin 1a, isoescin 1b, and a mixture of escin 1a and 1b at a 1:1 ratio. Relative averages compared to the 0 µg.mL^{-1} control, and standard deviation were plotted. Statistical analysis was performed using a one-way ANOVA to compare each treatment to the 0 µg.mL^{-1} escin sample. The sample size is n=3, and p-values are indicated as follows: * ≤ 0.05, ** ≤ 0.01, *** ≤ 0.001, **** ≤ 0.0001.

5.1.2 Effects of escin isomers on the growth of *S. cerevisiae* and ergosterol biosynthesis mutants grown in CSM

When cultivated in CSM at concentrations of 31.25, 62.5, and 125 ug.mL^{-1} for each treatment, we observed outcomes like those grown in YPD. The concentrations used in CSM were lower due to the MIC of *S. cerevisiae* in the presence of escin being 62.5 ug.mL^{-1}, whereas it was 175 ug.mL^{-1} in YPD.

In the case of the WT, it is evident that complete escin slightly inhibits growth at 31.25 µg.mL^{-1} (78.6 % of that of the WT at 0 µg.mL^{-1}) and fully inhibits growth at 62.5 µg.mL^{-1} and higher (Figure 57A). Escin 1b has a more pronounced inhibitory effect on the WT compared to escin 1a, particularly at the 62.5 µg.mL^{-1} concentration. However, there was no difference in growth when treated with isoescin 1a and 1b, compared to the control with 0 µg.mL^{-1} of escin. When escin 1a and escin 1b are combined in a 1:1 ratio, we observe a growth pattern similar to the escin 1b treatment, further indicating that escin 1b is more toxic than escin 1a. The absence of a consistent inhibition pattern with either escin 1a or 1b in comparison to complete escin suggests that other isomers present in complete escin might play a role in the inhibition, particularly in WT cultures grown in CSM.

These findings provide additional support for the hypothesis that complete escin is more toxic to *S. cerevisiae* in CSM than in YPD. Moreover, the structural differences of escin 1a, escin 1b, isoescin 1a, and isoescin 1b, and their effects on toxicity are evident here as well, with escin 1b showing more growth inhibition at 62.5 µg.mL^{-1} compared to escin 1a. Likewise, the *S. cerevisiae* grown in the presence of isoescin 1a and isoescin 1b in CSM shows comparable growth to the control with 0 µg.mL^{-1} of escin, similar to the YPD-grown cultures.

For the *erg4Δ* mutant, there was no growth observed in the presence of complete escin, across all concentrations tested in CSM (Figure 57B). This finding provides further evidence that the *erg4Δ* mutant is less tolerant to complete escin compared to

the WT strain. When exposed to escin 1a, growth was comparable to the 0 $\mu g.mL^{-1}$ escin control at 31.25 $\mu g.mL^{-1}$, but growth was inhibited at higher concentrations. A similar pattern was observed for cultures treated with escin 1b. In the case of isoescin 1a, there was no significant difference in growth, whereas isoescin 1b led to inhibited growth at 125 $\mu g.mL^{-1}$. These results parallel those observed with the *erg4Δ* mutant grown in YPD and treated with isoescin 1b, where isoescin 1a had no inhibitory effect, while isoescin 1b did.

This provides additional evidence that the configuration of escin 1b and isoescin 1b has a stronger inhibitory effect on the yeast compared to escin 1a and isoescin 1a, suggesting that the angelic conformation of the acid at C21 plays a more significant role in inhibition than the tiglic acid at C21 found in escin 1a and isoescin 1a. When escin 1a and escin 1b were combined, growth inhibition was observed at all tested concentrations. The inhibition observed in the mixture of escin 1a and escin 1b indicates a synergistic effect, where the two components work together. This is evident from the fact that when treated with escin 1a and escin 1b individually, the *erg4Δ* mutant's growth is comparable to the WT strain. However, when both components are mixed at a 1:1 ratio, growth inhibition occurs. This suggests that the presence of both escin 1a and 1b may interact in a way that increases the affinity towards ergosterol, thereby causing heightened growth inhibition.

In the *erg5Δ* mutant, complete growth inhibition was observed when exposed to both complete escin and escin 1b at all three tested concentrations (Figure 57C). However, there was reduced growth at 31.25 $\mu g.mL^{-1}$ of escin 1a (60 % of that of the *erg5Δ* mutant with 0 $\mu g.mL^{-1}$ of escin), reaffirming that escin 1a is less inhibitory compared to escin 1b. When treated with isoescin 1a, the growth was comparable to the 0 $\mu g.mL^{-1}$ escin control, whereas isoescin 1b led to inhibition at 125 $\mu g.mL^{-1}$. Upon mixing escin 1a and escin 1b, reduced growth was observed at the 31.25 $\mu g.mL^{-1}$ concentration, and no growth was evident at the higher concentrations. The observed reduction in growth resembles that of the escin 1a sample, this is likely to be due to the lower concentration of escin 1b in the media, which explains the lack of complete inhibition.

In the *erg3Δ* mutant, there was no significant difference in growth in the presence of any of the treatments (Figure 57D). Although there was a slight reduction in growth at the 125 μg.mL^{-1} concentration for all treatments, none of them led to complete growth inhibition. This slight reduction in growth might be attributed to the very high escin concentration in CSM, keeping in mind that the MIC of complete escin on *S. cerevisiae* in CSM is 62.5 μg.mL^{-1}. While it may be possible to grow the *erg3Δ* mutant in 1 mg.mL^{-1} complete escin in YPD, this is not the case in CSM without experiencing some minor growth reductions.

In the *erg2Δ* mutant, we observed inhibited growth in the presence of complete escin at all tested concentrations (Figure 57E). When exposed to escin 1a, growth was observed even at the MIC (62.5 μg.mL^{-1}), but not at the higher concentration of 125 μg.mL^{-1}. In the presence of escin 1b, there was growth at the lowest concentration but not at higher concentrations. However, growth inhibition was evident in the *erg2Δ* mutant when treated with 125 μg,mL^{-1} of complete escin, escin 1a, and escin 1b. When escin 1a and escin 1b were combined, a growth pattern like the escin 1b culture was observed, with reduced growth at 31.25 μg.mL^{-1} and significantly reduced growth at 62.5 and 125 μg.mL^{-1}.

In the *erg6Δ* mutant, minimal growth was observed in the presence of 31.25 μg.mL^{-1} of complete escin, and complete growth inhibition occurred in the 62.5 and 125 μg.mL^{-1} samples (Figure 57F). However, in the presence of escin 1a and 1b, similar results were obtained. Some growth was observed at the 31.25 μg.mL^{-1} concentration, with growth inhibition at higher concentrations. When exposed to isoescin 1a and isoescin 1b, there was no inhibition of growth in the *erg6Δ* mutant, but there was some reduced growth at 125 μg.mL^{-1} of isoescin 1b. Upon mixing escin 1a and 1b, almost complete inhibition was observed at all concentrations tested, with slight growth (31 % of that of the *erg6Δ* mutant with 0 μg.mL^{-1} of escin) remaining at 31.25 μg.mL^{-1}.

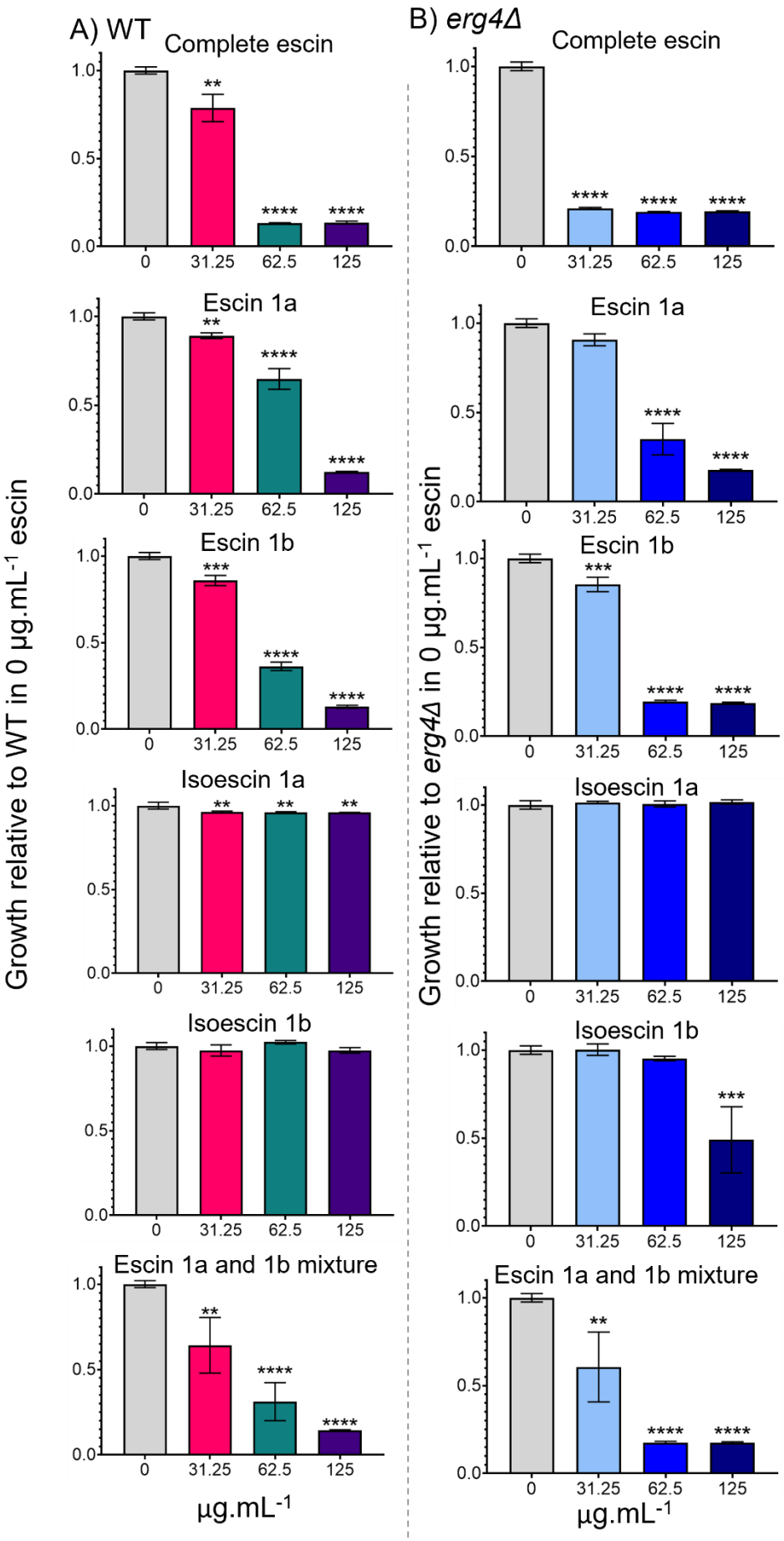

Figure continued…

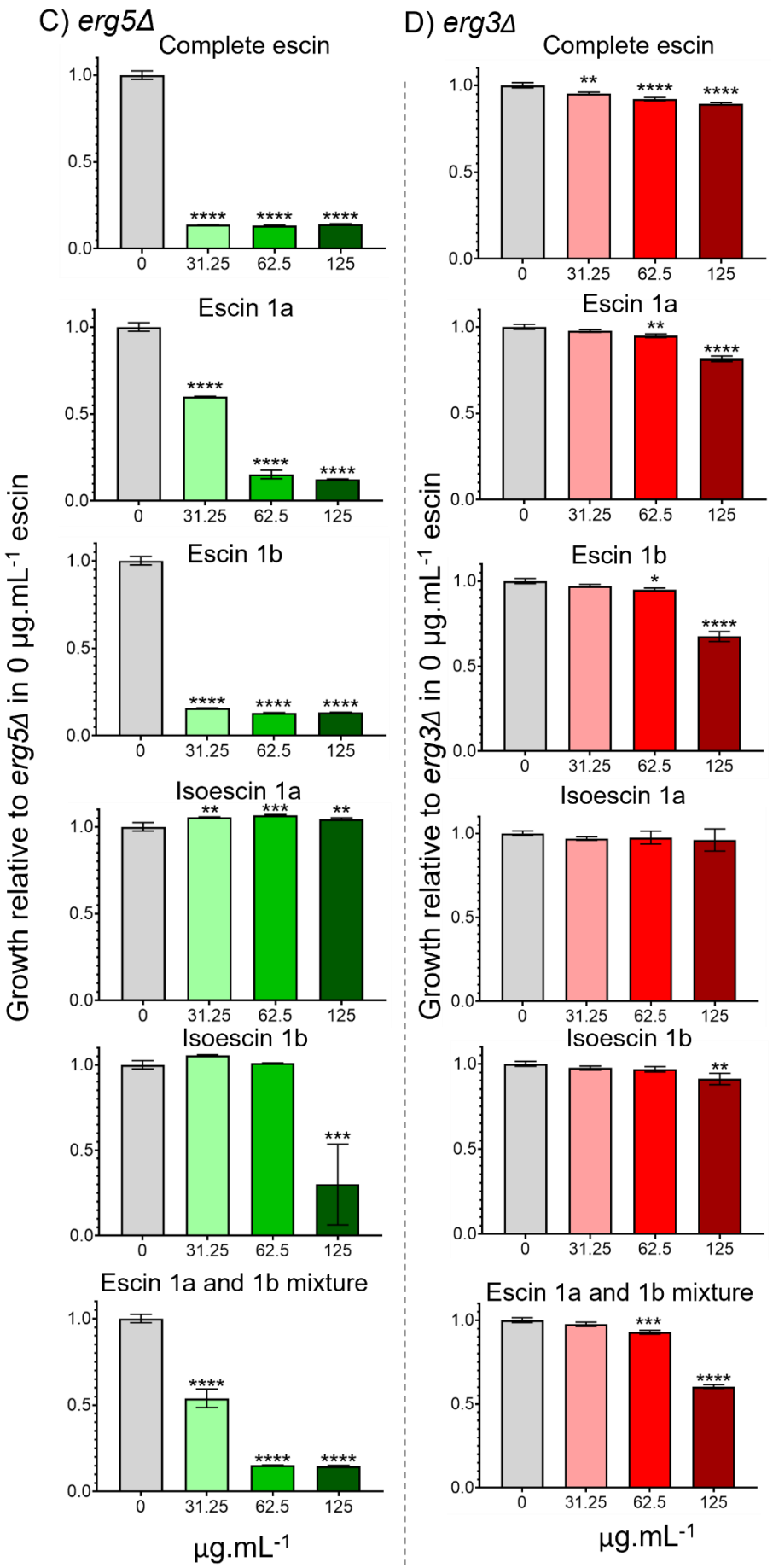

Figure continued...

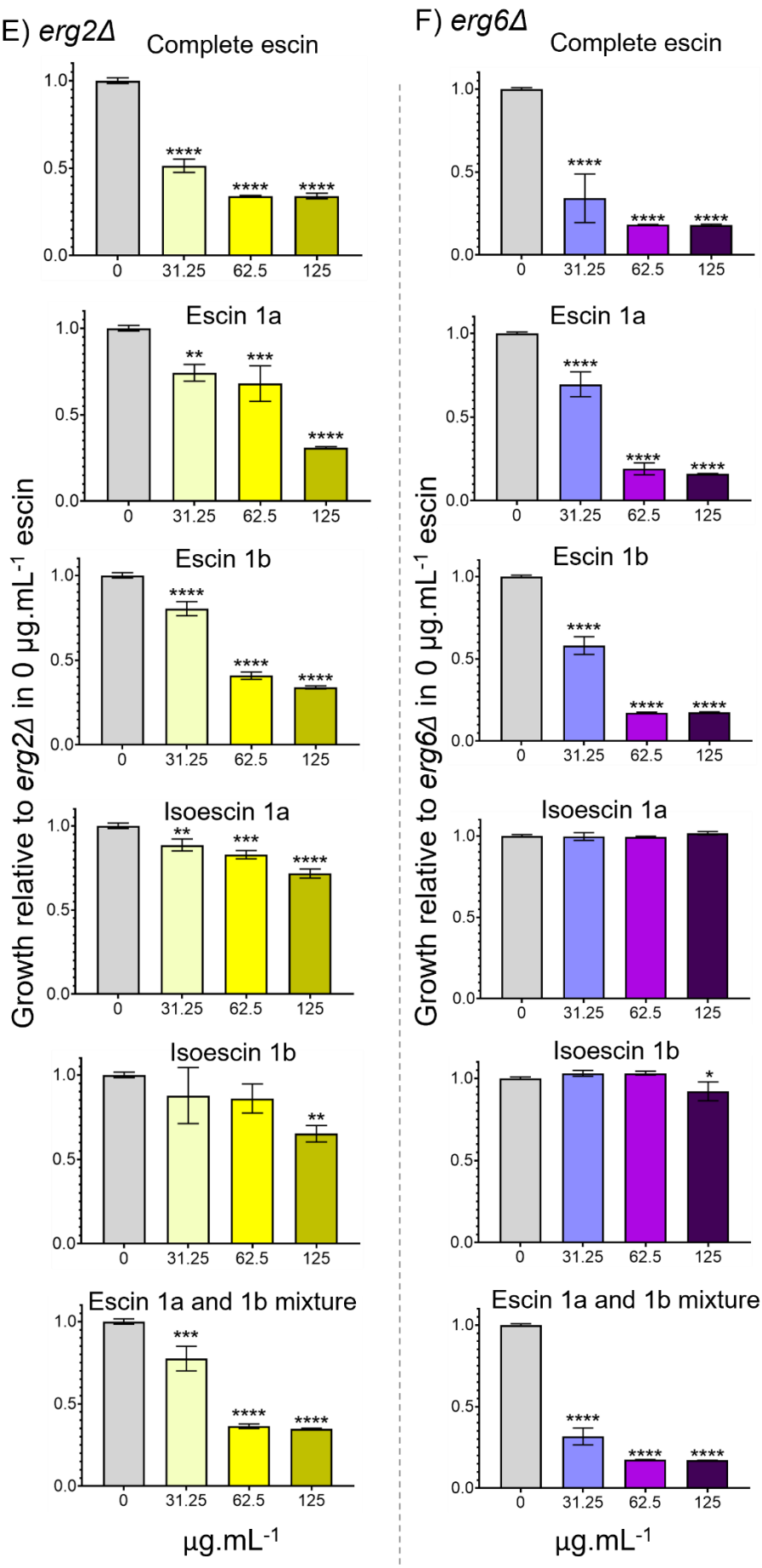

End of figure.

Figure 57: - Bar charts illustrating the growth of *S. cerevisiae* relative to 0 µg.mL^{-1} escin in CSM after 24 hours of growth. A) Growth of WT in the presence of 125, 250, and 500 µg.mL^{-1} complete escin, escin 1a, escin 1b, isoescin 1a, isoescin 1b, and a mixture of escin 1a and 1b at a 1:1 ratio. B) Growth of the *erg4Δ* mutant in the presence of 125, 250, and 500 µg.mL^{-1} complete escin, escin 1a, escin 1b, isoescin 1a, isoescin 1b, and a mixture of escin 1a and 1b at a 1:1 ratio. C) Growth of the *erg5Δ* mutant in the presence of 125, 250, and 500 µg.mL^{-1} complete escin, escin 1a, escin 1b, isoescin 1a, isoescin 1b, and a mixture of escin 1a and 1b at a 1:1 ratio. D) Growth of the *erg3Δ* mutant in the presence of 125, 250, and 500 µg.mL^{-1} complete escin, escin 1a, escin 1b, isoescin 1a, isoescin 1b, and a mixture of escin 1a and 1b at a 1:1 ratio. E) Growth of the *erg2Δ* mutant in the presence of 125, 250, and 500 µg.mL^{-1} complete escin, escin 1a, escin 1b, isoescin 1a, isoescin 1b, and a mixture of escin 1a and 1b at a 1:1 ratio. F) Growth of the *erg6Δ* mutant in the presence of 125, 250, and 500 µg.mL^{-1} complete escin, escin 1a, escin 1b, isoescin 1a, isoescin 1b, and a mixture of escin 1a and 1b at a 1:1 ratio. Relative averages compared to the 0 µg.mL^{-1} control, and standard deviation were plotted. Statistical analysis was performed using a one-way ANOVA to compare each treatment to the 0 µg.mL^{-1} escin sample. The sample size is n=3, and p-values are indicated as follows: * ≤ 0.05, ** ≤ 0.01, *** ≤ 0.001, **** ≤ 0.0001.

In conclusion, the findings from this study provide valuable insights into the toxicity and inhibitory effects of the escin isomers on WT and ergosterol biosynthesis mutant *S. cerevisiae*. The main conclusions drawn from the results are as follows: a) the isoescins exhibit significantly lower toxicity towards *S. cerevisiae* compared to the escins, b) escin 1b demonstrates a more pronounced inhibitory effect on the WT and the majority of ergosterol biosynthesis mutants growth than escin 1a, c) complete escin contains a higher concentration of escin 1b and escin 1a compared to isoescin 1a and isoesicn 1b, d) isoescin 1b is the more toxic than isoescin 1a. The greater inhibitory effect of escin 1b and isoescin 1b compared to escin 1a and isoescin 1a suggests that the structural differences, specifically the presence of the angelic acid group at position C21, play a crucial role in this function. The hypothesis is that escin 1b and isoescin 1b have a stronger interaction between the angelic acid group at position C21 and ergosterol, potentially contributing to the removal of ergosterol from

the membrane and thus inducing cell death. Esicn 1a and isoescin 1a have the tiglic acid conformation at position C21 and this is less inhibitory to the yeast. Additionally, the acetyl group at position C22, as seen in escin 1b and escin 1a, may further enhance the interaction between escin and ergosterol, intensifying its impact on membrane integrity.

The sterol composition of the ergosterol biosynthesis mutants plays a significant role in determining their tolerance to escin. The presence or absence of specific double bonds in the B ring of the sterols appears to be crucial. For instance, the *erg3Δ* mutant is unique in having only one double bond in the B ring, which is not found in the sterols produced by the other ergosterol biosynthesis mutants. The other mutants have at least one sterol that contains a second double bond in the B ring. In the case of the *erg2Δ* mutant, it possesses one double bond in the two most prominent sterols it produces, which might explain its slightly increased tolerance to escin compared to the WT strain.

These findings deepen our understanding of the structure-activity relationships of the escin isomers, shedding light on their mode of action and potential implications for further research and development of related compounds.

5.2 Differential gene expression in the presence of escin 1b and isoescin 1a

Likewise, to the experiment conducted in chapter 4.5, It was decided to focus on our panel of stress response genes (*LAM4*, *ARE2*, *UPC2* and *ERG11;* described in chapter 4.5) and investigate the impact of escin 1b and isoescin 1a on the gene expression in WT *S. cerevisiae* and the ergosterol biosynthesis mutants. In the previous chapter, we discussed the difference in toxicity between the escin isomers towards WT *S. cerevisiae*, which implies potential dissimilarities in gene expression when exposed to different isomers. For this analysis, we specifically chose escin 1b and isoescin 1a due to their contrasting structural configurations (Figure 58). Escin 1b has an angelic acid group at C21 and an acetyl group at C22, while isoescin 1a features a tiglic acid group at C21, a hydroxyl group at C22, and an acetyl group at C28.

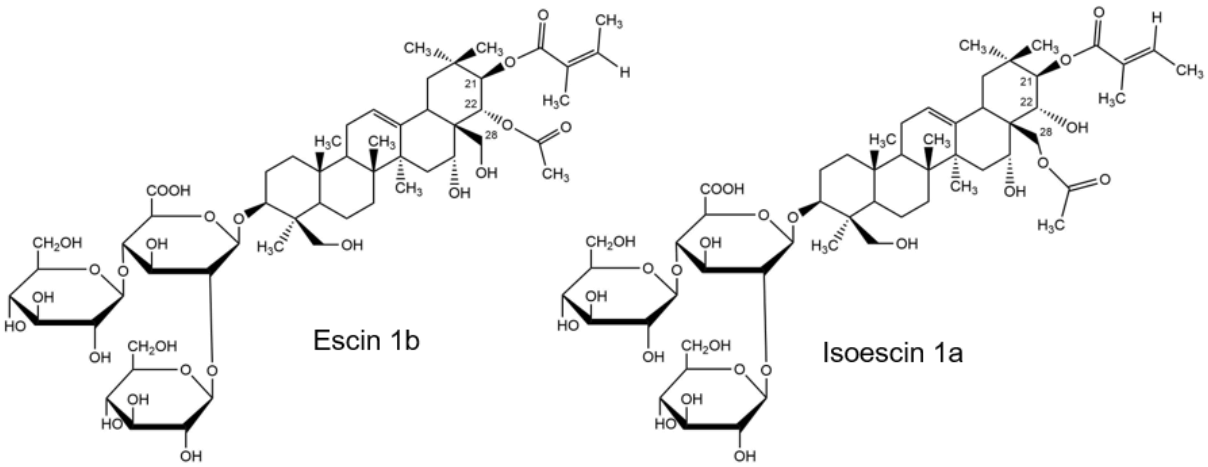

Figure 58: - Structural comparison of escin 1b and isoescin 1a.

In both the WT (Figure 59A) and the *erg5Δ* mutant (Figure 59E), the presence of escin 1b (100 µg.mL^{-1}) resulted in a decrease in *LAM4* expression, resulting in a 0.6-fold and 0.7-fold decrease. On the other hand, no significant difference was observed in *LAM4* expression when isoescin 1a was present compared to the control in the WT or the mutants.

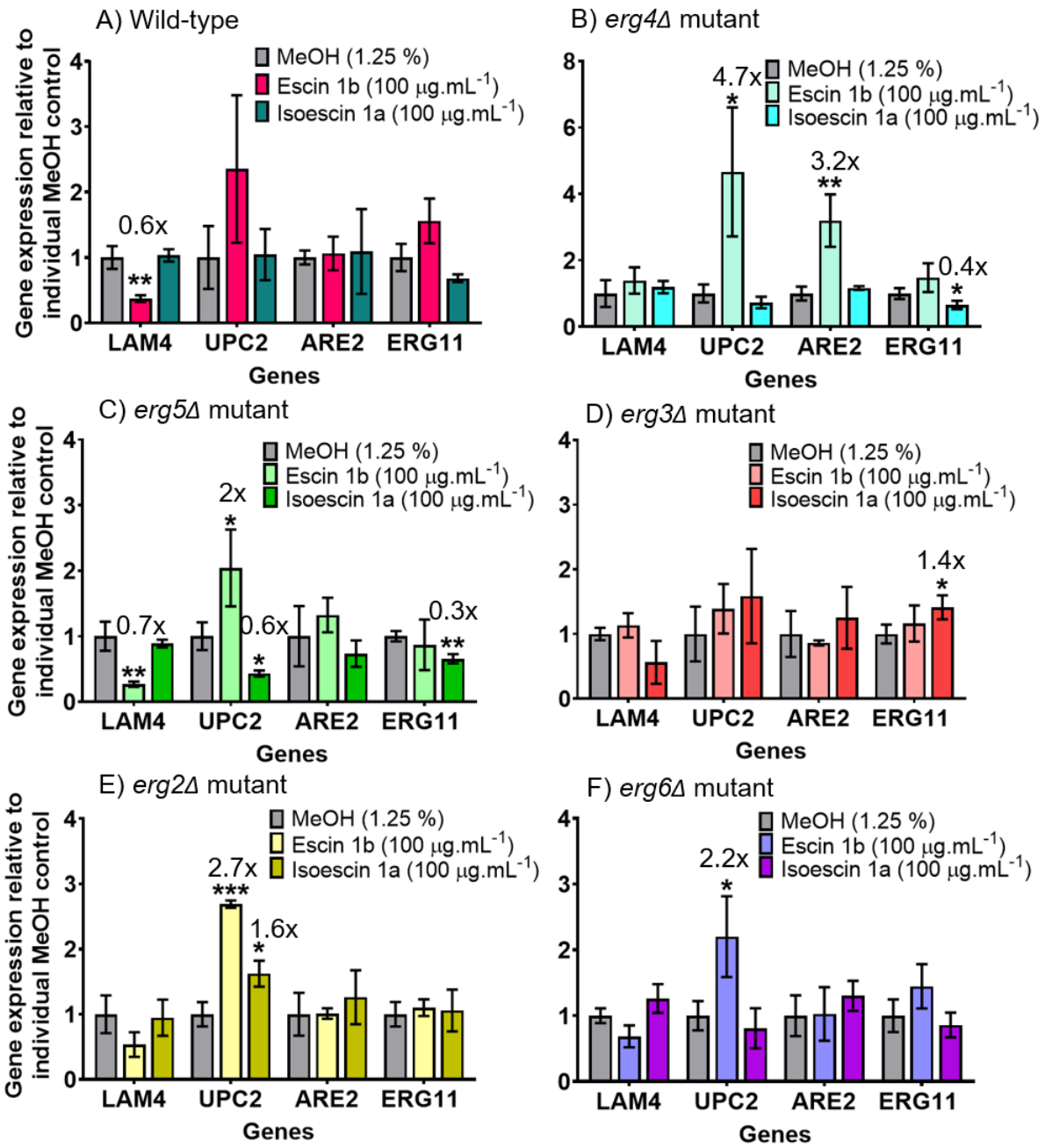

Figure 59: - Analysis of the gene expression relative to the methanol controls for four genes of interest in the presence or absence of escin 1b (100 µg.mL^{-1}) or isoescin 1a (100 µg.mL^{-1}). Expression levels were normalised to the mean of the individual methanol controls. The following strains were investigated A) WT, B) *erg4Δ*, C) *erg5Δ*, D) *erg3Δ*, E) *erg2Δ* and F) *erg6Δ*. The expression levels of these genes were compared between the methanol control and exposure to escin 1b or isoescin 1a (100 µg.mL^{-1}). For statistical analysis, multiple t-tests were conducted to compare each treatment with its respective methanol control. The sample size was n=3. The p-values are indicated as follows: * = ≤ 0.05, ** = ≤ 0.01, *** = ≤ 0.001, **** = ≤ 0.0001.

The specific reduction in *LAM4* expression observed in the presence of escin 1b, but not with complete escin, suggests that in the WT, ergosterol depletion prevents its binding to Lam4p (refer to chapter 4.5 for protein functions). This finding supports the hypothesis that escin, particularly escin 1b, effectively removes ergosterol from the PM. Furthermore, the absence of differential *LAM4* expression in the presence of isoescin 1a further suggests that escin 1b plays a more active role in ergosterol removal from the PM. In the *erg5Δ* mutant, the primary sterol produced is ergosta-5,7-dienol which has a highly similar structure to ergosterol (Figure 60), *LAM4* expression also decreased in the presence of escin 1b. These sterols share a common cyclic backbone with two double bonds in the B ring, specifically between positions C5-6 and C7-8. However, ergosterol has an additional double bond between C22-23, which is absent in ergosta-5,7-dienol. Hence, the decrease in *LAM4* expression in the presence of escin 1b in the *erg5Δ* mutant may be attributed to the removal of ergosta-5,7-dienol from the PM, similar to the hypothesised removal of ergosterol in the WT strain. The depletion of these sterols subsequently reduces the requirement for Lam4p, leading to decreased transcription of the *LAM4* gene.

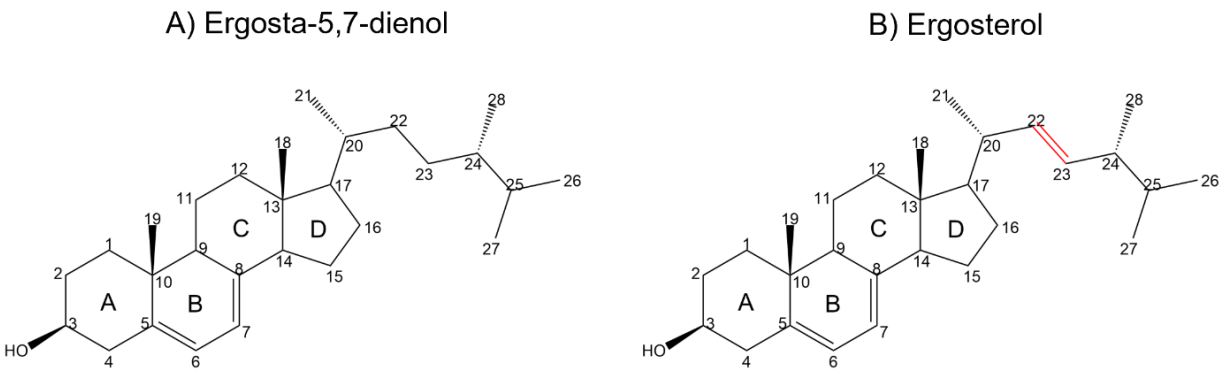

Figure 60: - Structures of the predominant sterols found in the *erg5Δ* mutant and WT. A) ergosta-5,7-dienol and B) ergosterol. The red bond shows the difference between the two sterols

Significant differences in *UPC2* expression were observed, particularly in the *erg2Δ*, *erg4Δ*, *erg5Δ* and *erg6Δ* mutants (Figure 59B, D, 3 and F). Escin 1b caused a 2.7-fold

increase in expression in the *erg2Δ* mutant, a 4.7-fold increase in the *erg4Δ* mutant, a 2-fold increase in the *erg5Δ* mutant and a 2.2-fold increase in the *erg6Δ* mutant. On the other hand, isoescin 1a led to a 1.6-fold increase in the *erg2Δ* mutant but a 0.6-fold decrease in the *erg5Δ* mutant.

The significant increase in *UPC2* expression observed in all the mutants, except the *erg3Δ* mutant, along with the non-significant increase in the WT strain, demonstrates the effectiveness of this gene as a stress indicator. It is not surprising to find that the expression of *UPC2* remains unchanged in the presence of escin 1b in the *erg3Δ* mutant, as this mutant has been shown to tolerate high concentrations of complete escin. However, noticeable changes in *UPC2* expression are observed in the other mutants. These findings suggest the possibility of synergistic effects among the escin isomers present in complete escin. Escin 1b induces a reduction in sterol levels in the mutants, indicating that the presence of other isomers is necessary to achieve this sterol decrease in the WT strain. This observation is further supported by the data on isoescin 1a, where an increase in *UPC2* expression is observed in the *erg2Δ* mutant, despite the assumption that this isomer is less toxic than escin 1b. In this case, it is plausible that isoescin 1a can bind to the predominant sterol (ergosta-8-enol) in the *erg2Δ* mutant and remove it from the PM, preventing its potential interaction with Upc2p. Conversely, the decrease in *UPC2* expression in the *erg5Δ* mutant further suggests for the synergistic effect of the escin isomers. In this scenario, isoescin 1a fails to reduce the sterol content in the membrane, thereby failing to activate Upc2p and resulting in decreased expression of *UPC2*.

In the case of *ARE2*, no expression differences were observed in the presence of isoescin for any of the strains. However, escin 1b resulted in a 3.2-fold increase in expression in the *erg4Δ* mutant (Figure 59D). *ERG11* expression exhibited changes in the presence of isoescin 1b in the *erg3Δ*, *erg4Δ*, and *erg5Δ* mutants (Figure 59C, D and E). Notably, a 1.4-fold increase was observed in the *erg3Δ* mutant, whereas the *erg4Δ* and *erg5Δ* mutants displayed 0.4-fold and 0.3-fold decreases, respectively.

The observation that *ERG11* expression only changed upon the addition of isoescin 1a is intriguing. Interestingly, the *erg3Δ*, *erg4Δ*, and *erg5Δ* sterol mutants exhibit distinct responses to complete escin in terms of growth (refer to Figure 4.4). Notably,

the *erg3Δ* mutant demonstrates tolerance to complete escin up to 1 $mg.mL^{-1}$, a significantly higher concentration compared to the other two mutants. The unique characteristic of the *erg3Δ* mutant sterols is the presence of a single double bond in the B ring of the sterol backbone between positions C7-8, which is absent in the other mutants. This suggests that perhaps only the isoescins can interact with these specific sterols, thereby explaining the observed activation of *ERG11* expression. This could also shed light on why the *erg3Δ* mutant exhibits higher tolerance to complete escin, as it is possible that only the isoescins (the less toxic isomers) can interact with the *erg3Δ* mutant sterols, rendering them more resistant to the effects of complete escin. The decreases in *ERG11* expression in the *erg4Δ* and *erg5Δ* mutants are likely due to the similarities in their sterols. Erg4p and Erg5p are sequential enzymes in the ergosterol biosynthesis pathway (refer to figure 3.4), resulting in the main sterols having only a difference of two double bonds. Ergosta-5,7-dienol (the predominant sterol in the *erg5Δ* mutant) lacks double bonds in the branching chain, while ergosta-5,7,22,24(28)-tetraenol (the sterol present in the *erg4Δ* mutant) has two double bonds, one between positions C22-23 and another between positions C24-28 (Figure 61). The decrease in *ERG11* expression could be attributed to these sterols binding to Upc2p and subsequently repressing its activity, given that they share the closest structural backbone as ergosterol. In the presence of isoescin 1b, there is reduced pressure on the cell to produce more sterols (considering that isoescin 1a is less toxic than escin 1b and is believed not to extract sterols from the membrane). Consequently, the expression of *ERG11* is decreased.

In conclusion, our findings highlight the critical role of specific groups located at the C21 and C22 positions of escin in exerting inhibitory effects on *S. cerevisiae* and ergosterol biosynthesis mutant strains. The presence of the angelic acid group at position C21 in escin 1b appears to contribute to its heightened toxicity compared to escin 1a and isoescins. The positioning of the acetyl group is also pivotal for the toxicity of complete escin, as isoescins exhibit significantly fewer inhibitory effects on WT *S. cerevisiae* compared to escins.

A) Ergosta-5,7-dienol

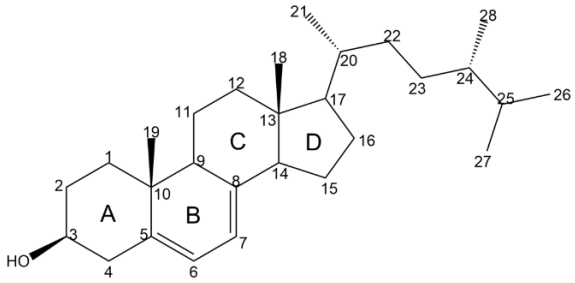

B) Ergosta-5,7,22,24(28)-tetraenol

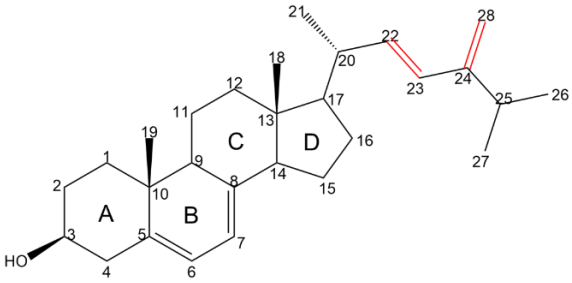

Figure 61: - Structures of the predominant sterols found in the *erg5Δ* and *erg4Δ* mutants. A) ergosta-5,7-dienol and B) ergosta-5,7,22,24(28)-tetraenol. The red bond shows the difference between the two sterols.

Moreover, we observed a synergistic effect between the escin isomers when mixed at a 1:1 ratio, the pattern of inhibition differed from that of complete escin. This suggests that the presence of other escin isomers may inhibit or mitigate the toxicity of escin 1b and escin 1a. This is further supported by the gene expression changes observed, particularly in the expression patterns of *LAM4*. However, simple modifications such as hydroxylation at C21 and C22 do not seem to play a significant role in complete escin toxicity.

Furthermore, our results indicate that the sterol content of the ergosterol biosynthesis mutants influences the toxicity of complete escin. The sterols found in the *erg3Δ* mutant (episterol, ergosta-7-enol, and ergosta-7,22-dienol; refer to chapter 3.3) remain unaffected by the escin isomers. These sterols possess a single double bond in the B ring, specifically between positions C7-8 (Figure 62). This isolated double bond alone does not exist in other sterols produced by either WT *S. cerevisiae* or ergosterol biosynthesis mutants. Hence, the position of this double bond appears to be crucial for escin binding. When this double bond is present alone, escin cannot interact with the sterol, thereby failing to inhibit growth. However, when this double bond is accompanied by other double bonds in the B ring, escin can interact and

induce inhibition. These findings show the structural and functional factors of complete escin toxicity and provide insight for further investigations and potential applications.

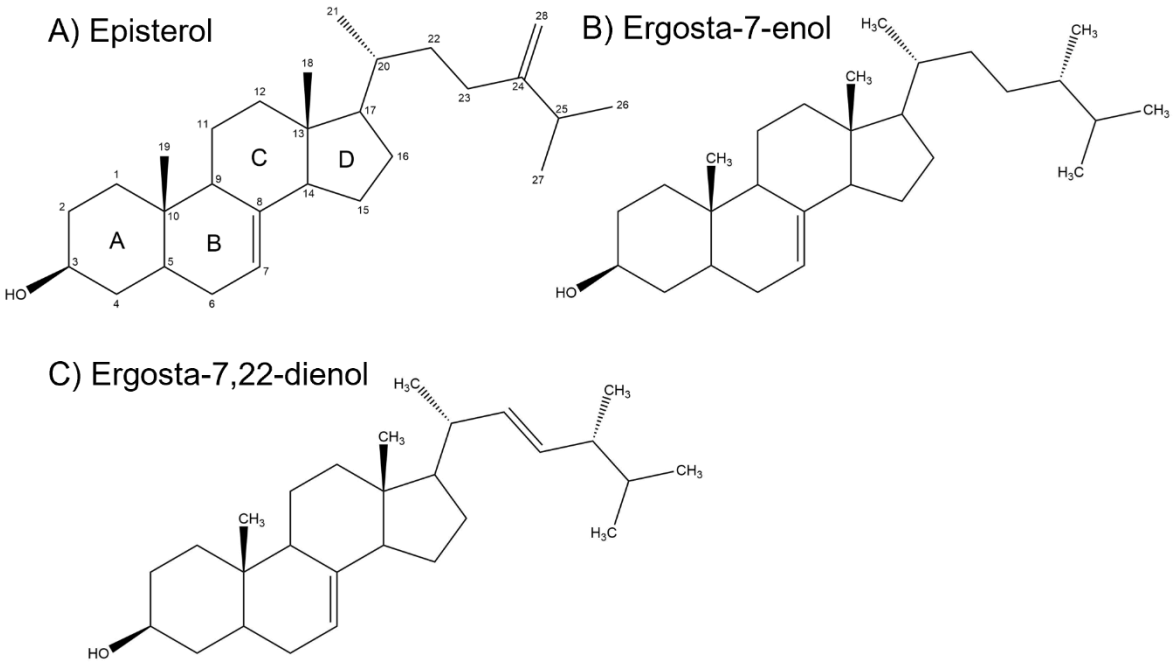

Figure 62: - Structures of the *erg3Δ* mutant sterols. A) episterol, B) ergosta-7-enol, and C) ergosta-7,22-dienol.

5.3 Investigation into the C21 and C22 groups and the impact on structure-activity relationship

To further explore the significance of the C21 and C22 groups in the escin isomers and their associated toxicity, our investigation extended to commercially available triterpenoids with similar structures (Figure 63). Limited options exist for compounds that closely resemble the general structure of escin from the precursor β-amyrin, with soyasapogenol B, soyasapogenol A, and protoescigenin being the only candidates commercially available. These compounds exhibit minor structural variations, with soyasapogenol B featuring a hydroxyl group at position C22, soyasapogenol A having an additional hydroxyl group at position C21, and protoescigenin sharing the same structural framework as escin but lacking the specific acetyl/acid groups at positions C21 and C22 as well as the glycosylation at position C3 (Figure 64). Motivated by this, we chose these triterpenoids to investigate the individual inhibitory effects of the C21 and C22 modifications, determining whether they act independently as hydroxyl groups or not. For the scope of this study, we intended to maintain consistent compound concentrations as previously tested in CSM. CSM was the chosen media as the MIC of escin for *S. cerevisiae* is lower than that in YPD. These compounds are only available in small quantities and there is little knowledge of the solubility in methanol, it was deemed the lower concentrations would be the most reasonable to test. We used the same concentrations as tested in the other CSM experiments 62.5, 100 and 250 $\mu g.mL^{-1}$ (which are equivalent to 55, 88, and 220 µM respectively).

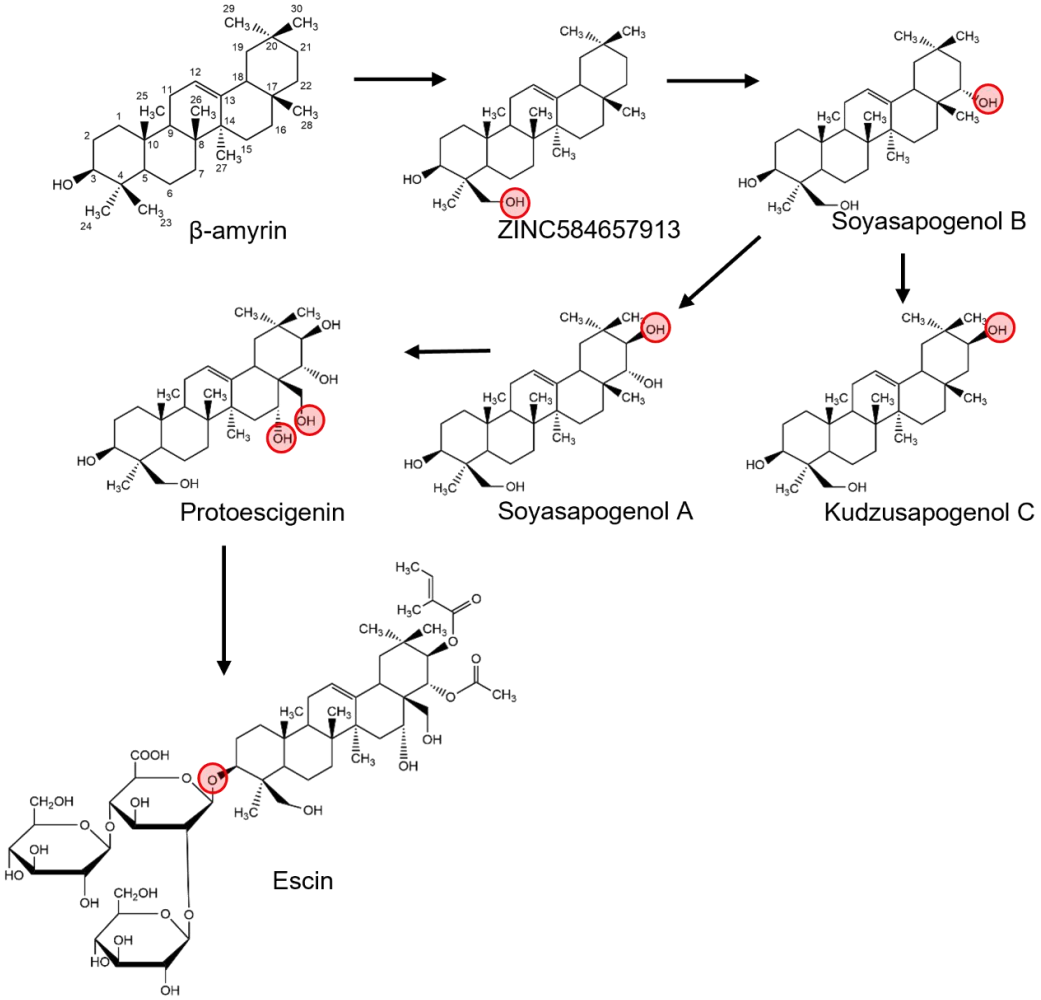

Figure 63: - Sequence of structures depicting the transformation from β-amyrin to escin. Each structure exhibits only one or two distinct differences from the preceding one. It is important to note that these structures are not presented in sequential order and are not synthesised by the same species. The purpose of this representation is solely to emphasise the singular differences in the structures, which are circled in red.

The presence of soyasapogenol A, soyasapogenol B, and protoescigenin did not impact the growth of WT *S. cerevisiae,* as observed in the growth curves (Figure 64) In fact, their growth was comparable to or even better than that of the WT at concentrations up to 250 µg.mL^{-1}. Particularly, the presence of soyasapogenol A resulted in slight increases in the growth of the WT (Figure 64D). These findings indicate that the specific conformation of the acid and acetyl groups at positions C21 and C22 in escin 1a and escin 1b are crucial for its toxicity, while the general hydroxylation of these carbons does not contribute significantly to its toxic properties.

Glycosylation is recognised in the field for enhancing triterpenoid solubility, potentially rendering them more toxic to cells (Simons *et al*., 2006). This effect can be attributed to the facilitated entry of glycosylated triterpenoids into the cell membrane, which may lead to the removal of ergosterol from the membrane and is therefore also essential in the toxicity of escin.

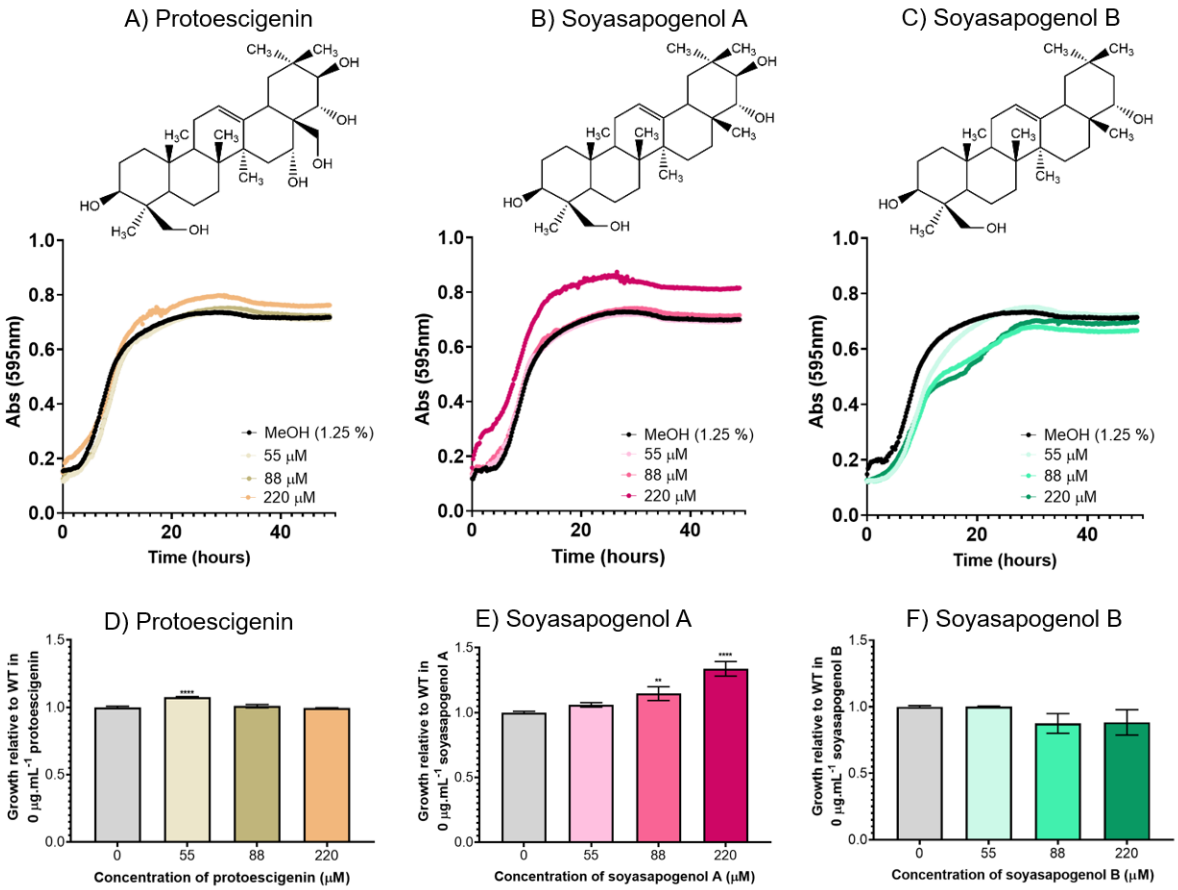

Figure 64: - Growth curves and bar charts illustrating the growth of the WT in the presence of different escin like compounds in CSM after 48 hours of growth. Structure and growth curve of the WT in the presence of 55, 88, and 220 µM A) protoescigenin, B) soyasapogenol A, and C) soyasapogenol B. The sample size was n=3 and averages have been plotted. Bar chart of the WT relative to the methanol control in the presence of 55, 88, and 220 µM D) protoescigenin, E) soyasapogenol A, F) soyasapogenol B. Statistical analysis was performed using multiple t-tests to compare each treatment to the methanol control sample. The sample size n=3, and p-values are indicated as follows: * ≤ 0.05, ** ≤ 0.01, *** ≤ 0.001, **** ≤ 0.0001.

5.4 Discussion

This chapter provides an exploration of the toxicity and inhibitory effects of escin isomers on both WT *Saccharomyces cerevisiae* and various ergosterol biosynthesis mutants. The study delves into the structural variations among escin isomers, specifically escin 1a, escin 1b, isoescin 1a, and isoescin 1b, and their impact on growth and gene expression. The findings elucidate the intricate relationship between the chemical structure of escin isomers and their biological activity.

The investigation starts by evaluating the growth inhibition patterns of escin isomers on WT *S. cerevisiae* and ergosterol biosynthesis mutants. The study reveals differential responses, with escin 1b demonstrating stronger inhibitory effects on both WT and mutants compared to escin 1a and isoescins. This observation is possibly attributed to the presence of an angelic acid group at position C21 in escin 1b, suggesting its crucial role in the toxicity mechanism. The acetyl group at C22 is also highlighted as significant, indicating its contribution to the interaction with ergosterol and subsequent growth inhibition.

The synergistic effect observed when combining escin 1a and escin 1b in a 1:1 ratio provides intriguing insights. The unique growth patterns, distinct from those of complete escin, suggest potential interactions or counteracting effects between different isomers. This phenomenon is further supported by the observation that the mixture of escin 1a and 1b displays growth patterns like that of escin 1b alone, emphasising the dominance of escin 1b in toxicity.

We also investigated ergosterol biosynthesis mutants, revealing distinct growth patterns and responses to escin isomers. Most notably, the *erg3Δ* mutant demonstrates higher tolerance to complete escin, which is attributed to the unique sterol composition characterised by a single double bond in the B ring. This isolated double bond appears to hinder the interaction with escin, leading to increased

tolerance. Additionally, the *erg2Δ* mutant's structural similarities with *erg3Δ* contribute to its slightly higher tolerance compared to the WT strain.

To further understand the molecular mechanisms behind escin toxicity, the study explored the impact of escin 1b and isoescin 1a on the expression of stress response genes (*LAM4, ARE2, UPC2*, and *ERG11*). The findings shed light on the differential gene expression patterns, linking them to specific isomers. Escin 1b induces a reduction in *LAM4* expression, suggesting its active role in removing ergosterol from the plasma membrane. *UPC2* expression changes across various mutants indicate the effectiveness of *UPC2* as a stress indicator. The unique response of the *erg3Δ* mutant supports the hypothesis that isoescins may interact specifically with its sterols, leading to decreased toxicity.

In this chapter, we have highlighted examples of how structure plays a role in toxicity. The presence of the angelic acid group at C21 in escin 1b is shown as a key factor in its heightened toxicity, with potential interactions with ergosterol contributing to membrane disruption and cell death. The acetyl group at C22 is recognised for its role in enhancing the interaction with ergosterol, intensifying the impact on membrane integrity. The study concludes that simple modifications, such as hydroxylation at C21 and C22, do not significantly affect the toxicity of complete escin.

In conclusion, this chapter provides a thorough analysis of the complex relationship between escin isomers and *S. cerevisiae*, uncovering crucial structural determinants of toxicity. The combination of growth assays and gene expression analyses deepens our understanding of the underlying mechanisms, offering valuable insights for future studies and potential applications in various fields.

Chapter 6: - Production of escin-like glycosylated triterpenoids in *S. cerevisiae.*

6.1 JEscin

6.1.1 JEscin production

To assess the impact on the production of triterpenoids in strains containing the *erg3Δ* mutant, we aimed to synthesise a compound closely resembling escin, which we henceforth refer to as JEscin. We decided to try and produce this rather than escin as the biosynthesis steps for escin production have not yet been identified. JEscin lacks the acetylations present at the C21 and C22 positions found in escin and instead features hydroxylations and carboxylations (Figure 65).

Our initial approach involved utilising strain TME90 (provided by Dr Tessa Moses), an *S. cerevisiae* strain proficient in the production of the triterpenoid erythrodiol (Figure 65A). TME90 was genetically engineered, as detailed in Chapter 1.4.2, to incorporate additional mevalonate pathway genes, including tHMG1, ERG9, and mERG1(K311R), which increase the pool of precursors for triterpenoid biosynthesis (Dale *et al*., 2020). Furthermore, TME90 features the integration of specific genes, namely AaBAS, CYP716A75, and ATR2, into its genome. AaBAS is a β-amyrin synthase from *Artemisia annua*, catalysing the cyclisation of 2,3-oxidosqualene to β-amyrin with high efficiency (Dale *et al*., 2020b)). MlCYP716A75 from *Maesa lanceolata* is a P450 cytochrome monooxygenase responsible for hydroxylating the C28 position of β-amyrin (Moses *et al*., 2015; Dale *et al*., 2020), while ATR2 functions as an NADPH cytochrome P450 reductase, supplying electrons for the CYP-mediated hydroxylation reaction.

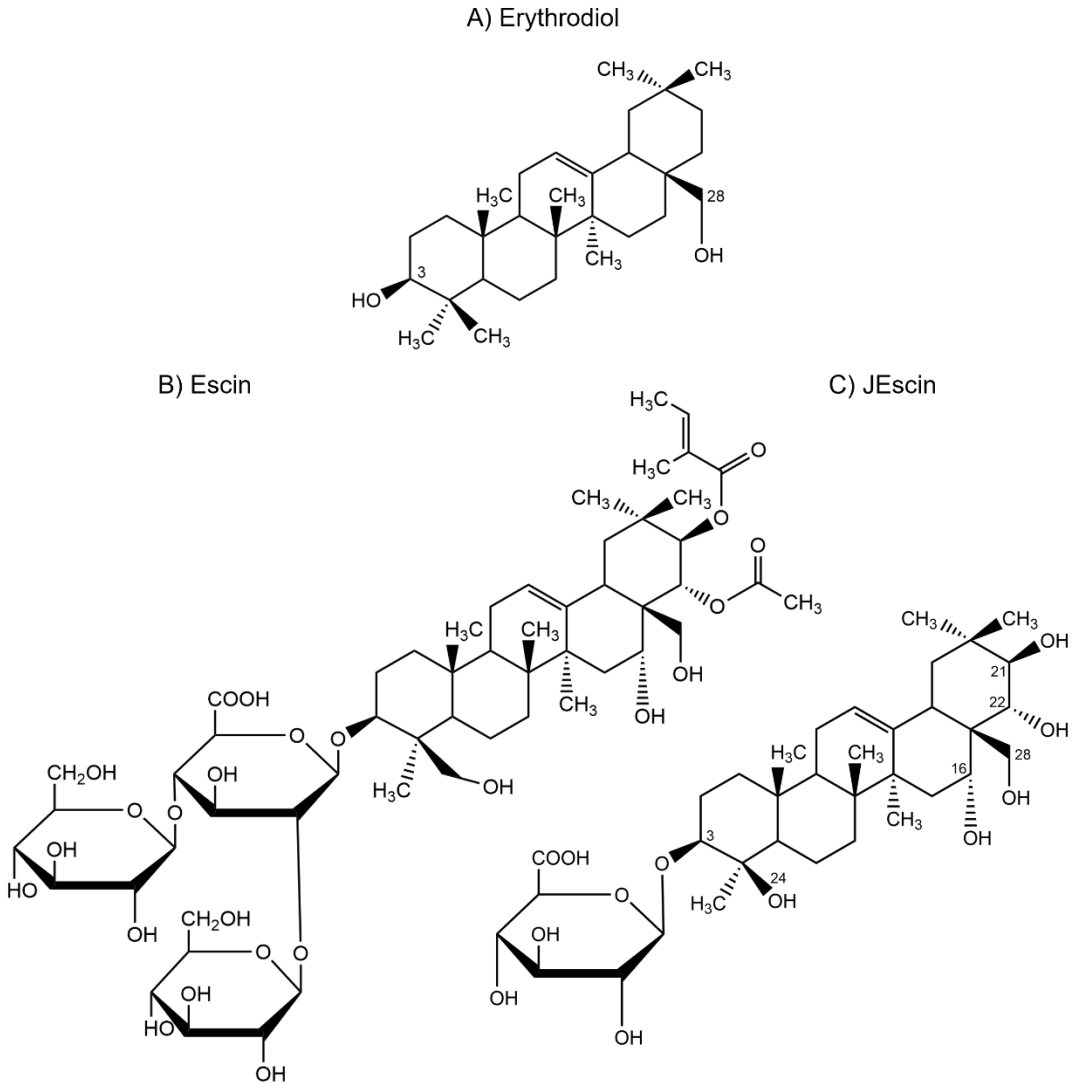

Figure 65: - The structures of erythrodiol, escin, and JEscin exhibit distinct features. A) Erythrodiol showcases hydroxylations at positions C3 and 28. B) Escin displays modifications at positions C21, C22, C28, and C16. Additionally, glycosylations are present at the C3 positions of the backbone. C) JEscin contains a C3 glucuronic acid moiety and hydroxylations at positions C21, 22, 16, 24, and 28. Despite the structural differences, the pentacyclic backbone remains consistent across all compounds. JEscin can theoretically be synthesised by modifying erythrodiol through the involvement of cytochrome P450 monooxygenases (CYPs) and UDP glycosyltransferases (UGTs).

Given the substantial structural differences between erythrodiol and JEscin (Figure 65A; Figure 65C), additional cytochrome P450 enzymes (CYPs) were deemed

necessary for the modification of C16, C21, C22, and C24 positions in erythrodiol. Additionally, uridine diphosphate glycosyltransferases (UGTs) were required to glycosylate the C3 region. Consequently, we introduced BfCYP716Y1 (for C16 hydroxylation), MtCYP72A61v2 (for C22 hydroxylation), PvCYP939E (for C24 hydroxylation), GmCYP72A69 (for C21 hydroxylation), HsUGT1A3 (for C3 glycosylation), and AtUGD1 (for C3 glucose to glucuronic acid conversion). As the genes necessary for escin production were not fully identified, these genes were sourced from various organisms, including *Bupleurum falcatum*, *Medicago trunculata*, *Phaseolus vulgaris*, *Glycine max*, *Homo sapiens*, and *Arabidopsis thaliana* (Oka & Jigami, 2006; Lu *et al*., 2009; Seki *et al*., 2011; Fukushima *et al*., 2013; Moses *et al*., 2014; Moses *et al*., 2014c; Gao *et al*., 2016; Yano *et al*., 2017; He *et al*., 2019).

Plasmids for the transient and chromosomal integration of the genes were constructed using the MoClo-YTK method (Lee *et al*., 2015), and these genes were codon-optimised by Dr Matt Dale. The genes were assembled into transcriptional units comprising promoters, genes, and terminators, all driven by galactose-inducible promoters. This design allowed for a clear separation between the growth and production phases. Initially, strains were cultured in glucose-containing media, and once they reached the desired growth stage, the media was transitioned to galactose-containing media, facilitating the transcription and translation of the introduced genes. This is especially important as we do not know if or how strongly JEscin will inhibit the growth of the strains.

For transient expression of the JEscin transcriptional units, plasmids (Table 5) were introduced either in sets of three, with two full plasmids harbouring all six transcriptional units, or individually, enabling the evaluation of enzyme productivity. The backbone plasmids employed featured HIS3 and LEU2 genes, enabling plasmid selection upon transformation into TME90 via media lacking histidine or leucine. Additionally, the backbone plasmids were of high copy number, ensuring the production of lots of protein. It is worth noting that the UGT/UGD genes were not successfully expressed in the strain, leading to the creation of strains designated as

JTE01, JTE02, JTE03, JTE04, and JTE05 (refer to Chapter 2 for complete genome details). These strains possessed distinct combinations of the introduced CYPs.

In the case of chromosomal integration plasmids, we consolidated the six transcriptional units into two specialised plasmids designed for integration into specific chromosomal loci, namely the HO and 308a loci. The HO locus encodes an endonuclease responsible for interconverting the mating-type locus (Ivanov *et al*., 1994; Voth *et al*., 2001), a function redundant in yeast strains not intended for mating. Moreover, the HO locus plays no essential role in yeast growth, and mutations within this locus are commonplace in laboratory strains (Bagnaz *et al*., 1997; Voth *et al*., 2001). The 308a region, situated on chromosome III and adjacent to an autonomously replicating sequence (ARS), was another integration site selected. ARS regions are known for containing origins of replication, enabling self-replication, but the 308a region itself is non-essential for growth, has demonstrated efficient expression of integrated heterologous genes, demonstrates good rates for successful integration and exceptional expression of transgenes (Yamane *et al*., 1998; Flagfeldt *et al*., 2009 Apel *et al*., 2017).

The plasmids designed for chromosomal integration shared a structural similarity with transient plasmids, featuring homology arms specific to the HO or 308a loci. TME90 was transformed with the plasmids alongside a single guide RNA (sgRNA) and Cas9 protein. This combination facilitated site-directed cleavage at the targeted integration site via sgRNA recognition of the specific DNA strand within that region. Following identification, the Cas9 protein introduced a double-strand cut at the site. Subsequently, the homology arms present on the introduced plasmids used homologous recombination with the cleaved DNA strands, thereby effecting repair of the cut while simultaneously integrating the new transcriptional units into the chromosome. In practice, we succeeded in integrating GmCYP72A69 (responsible for C21 hydroxylation), HsUGT1A3 (catalysing C3 glycosylation), and AtUGD1 (mediating C3 glucose to glucuronic acid conversion) solely in the 308a region of the TME90 strain. This was confirmed with colony PCR (cPCR).

This comprehensive approach allowed the investigation of the potential for enhanced escin tolerance in the *erg3Δ* mutant by synthesising JEscin in *S. cerevisiae* using a set of carefully selected genes.

Table 5: - Descriptions of the plasmids produced in this study.

Plasmid	Genes	Relevant characteristics	Strain
Transient 1	*BfCYP716Y1*	High copy number, HIS3. C16 hydroxylation	JTE01
Transient 2	*BfCYP716Y1, MtCYP72A61v2*	High copy number, HIS3. C16 and C22 hydroxylation	JTE02
Transient 3	*BfCYP716Y1, PvCYP939E*	High copy number, HIS3. C16 and C24 hydroxylation	JTE03
Transient 4	*BfCYP716Y1, MtCYP72A61v, PvCYP939E*	High copy number, HIS3. C16, C22 and C24 hydroxylation	JTE04 JTE05 (with transient 5)
Transient 5	*GmCYP72A69*	High copy number, LEU2. C21 hydroxylation	JTE05 (with transient 4)
pJT017	*BfCYP716Y1, MtCYP72A61v, PvCYP939E*	HO homology C16, C22 and C24 hydroxylation	X
pJT019	*GmCYP72A69, HsUGT1A3, AtUGD1*	308a homology C21 hydroxylation C3 glucuronic acid	JTE09, JTE11

6.1.2 Expression of the genes required for JEscin biosynthesis

The extract from strains JTE01, JTE02, JTE03, JTE04, and JTE05 underwent GC-MS analysis, after being cultured for two weeks, to elucidate the compounds generated and validate the functionality of the introduced CYPs. The TME90 strain served as the background, having chromosomal integration of genes responsible for erythrodiol production, while additional CYPs were expressed on plasmids into the other yeast strains. Specifically, JTE01 was equipped with a CYP catalysing C16 hydroxylation. JTE02 featured both the CYP for C16 hydroxylation and another responsible for C22 hydroxylation. JTE03 harboured the CYP for C16 hydroxylation in addition to a C24 hydroxylation CYP. JTE04 encompassed all the CYPs mentioned thus far, while JTE05 included all of them along with a C21 hydroxylation enzyme (Table 6).

Table 6: - Strains used in this study, the genes introduced, the modifications present and the theoretical compound produced.

Strain	Genes introduced	Modification	Theoretical compound produced
TME90	*tHMG1, ERG9, mERG1(K311R), AaBAS, CYP716A75, ATR2*	Overproduction of mevalonate; C28 hydroxylation	Erythrodiol
JTE01	*TME90; BfCYP716Y1*	C28 and C16 hydroxylations	C16-hydroxy-erythrodiol
JTE02	*TME90; BfCYP716Y1, MtCYP72A61v2*	C28, C16, C22 hydroxylations	16, 22-dihydroxy-erythrodiol
JTE03	*TME90; BfCYP716Y1, PvCYP939E*	C28, C16, C24 hydroxylations	16, 24-dihydroxy-erythrodiol
JTE04	*TME90; BfCYP716Y1, MtCYP72A61v2, PvCYP939E*	C28, C16, C22, C24 hydroxylations	16, 22, 24-trihydroxy-erythrodiol
JTE05	*TME90; BfCYP716Y1, MtCYP72A61v2, PvCYP939E, GmCYP72A69*	C28, C16, C22, C24, C21 hydroxylations	16, 21, 22, 24-tetrahydroxy-erythrodiol

The strains were cultivated in a galactose-containing medium to induce the CYPs for two weeks, with the addition of methyl-β-cyclodextrin (MβCD). MβCD is a

toroidal-shaped sugar molecule featuring a slightly hydrophobic interior and a slightly hydrophilic exterior, and so possesses the unique ability to encapsulate and solubilise hydrophobic triterpenoids. This facilitates their sequestration into the growth medium by mitigating the toxic burden of the product and reduces the loss of volatile products (Moses *et al*., 2014), resulting in the presence of triterpenoids both in the cell pellet and the supernatant. After growth, hexane and ethyl-acetate solvent extraction procedures were performed on both the cell pellet and supernatant, followed by GC-MS analysis.

For identifying compounds in this chapter, we relied on the theoretical triterpenoid fragmentation patterns outlined in (Table 7). Our analysis allowed us to confidently confirm the presence of erythrodiol, oleanolic aldehyde, oleanolic acid, β-amyrin, and ergosterol. Modified hydroxylated forms of erythrodiol, β-amyrin, and oleanolic aldehyde were determined based on theoretical values for the unmodified compounds and differences in retention time.

.

Table 7: - Theoretical fragmentation patterns of triterpenoids from electron ionisation.

Triterpenoid	Molecular weight (Da)	Ions (m/z)	Fragmentation
β-amyrin	426	498	Parent ion $[M]^+$
		483	$[M -CH_3]^+$
		408	$[M -(CH_3)_3SiOH]^+$
		393	$[M -(CH_3)_3SiOH, -CH_3]^+$
		218	C*DE rings of $[M]^+$
		203	C*DE rings of $[M -CH_3]^+$
		189	C*DE rings of $[M -CH_3, -CH_2]^+$ CH_3 from C28 and CH_2 from C17
Erythrodiol	442	586	Parent ion $[M]^+$
		571	$[M -CH_3]^+$
		496	$[M -(CH_3)_3SiOH]^+$
		481	$[M -(CH_3)_3SiOH, -CH_3]^+$
		406	$[M -2(CH_3)_3SiOH]^+$
		391	$[M -2(CH_3)_3SiOH, -CH_3]^+$
		306	C*DE rings of $[M]^+$
		216	C*DE rings of $[M -(CH_3)_3SiOH]^+$
		203	C*DE rings of $[M -(CH_3)_3SiOCH_2]^+$
		189	C*DE rings of $[M -(CH_3)_3SiOCH_2, -CH_2]^+$ CH_2 from C17
		188	C*DE rings of $[M -(CH_3)_3SiOCH_2, -CH_3]^+$
Oleanolic aldehyde	440	512	Parent ion $[M]^+$
		497	$[M -CH_3]^+$
		232	C*DE rings of $[M]^+$
		203	C*DE rings of $[M -CHO]^+$
		189	C*DE rings of $[M -CHO, -CH_2]^+$ CH_2 from C17
Oleanolic acid	456	600	Parent ion $[M]^+$
		585	$[M -CH_3]^+$
		482	$[M -(CH_3)_3SiOOH]^+$
		320	C*DE rings of $[M]^+$
		203	C*DE rings of $[M -(CH_3)_3SiOO]^+$
		202	C*DE rings of $[M -(CH_3)_3SiOOH]^+$
		189	C*DE rings of $[M -(CH_3)_3SiOOH, -CH_2]^+$ CH_2 from C17

We observed notable differences in the triterpenoids produced by the strains. Additionally, we noted more variety of triterpenoids in the supernatant compared to the pellet, attributable to MβCD's role in extracting triterpenoids from the cells and releasing them into the growth medium.

In the TME90 pellet (Figure 66), our analysis revealed the presence of ergosterol, erythrodiol, and, upon specific $[M]^+$ extraction, oleanolic aldehyde. Ergosterol and erythrodiol were consistently present in the pellets of all strains. However, in the JTE02 strain, we were able to detect β-amyrin, while in JTE05, 16-hydroxy-erythrodiol was identified inside the cell. In the supernatants (Figure 67), our analysis unveiled a more extensive array of triterpenoids, including oleanolic aldehyde, 16-hydroxy-erythrodiol, 16-hydroxy-β-amyrin, and 22-hydroxy-β-amyrin. These identifications were based on the following justifications

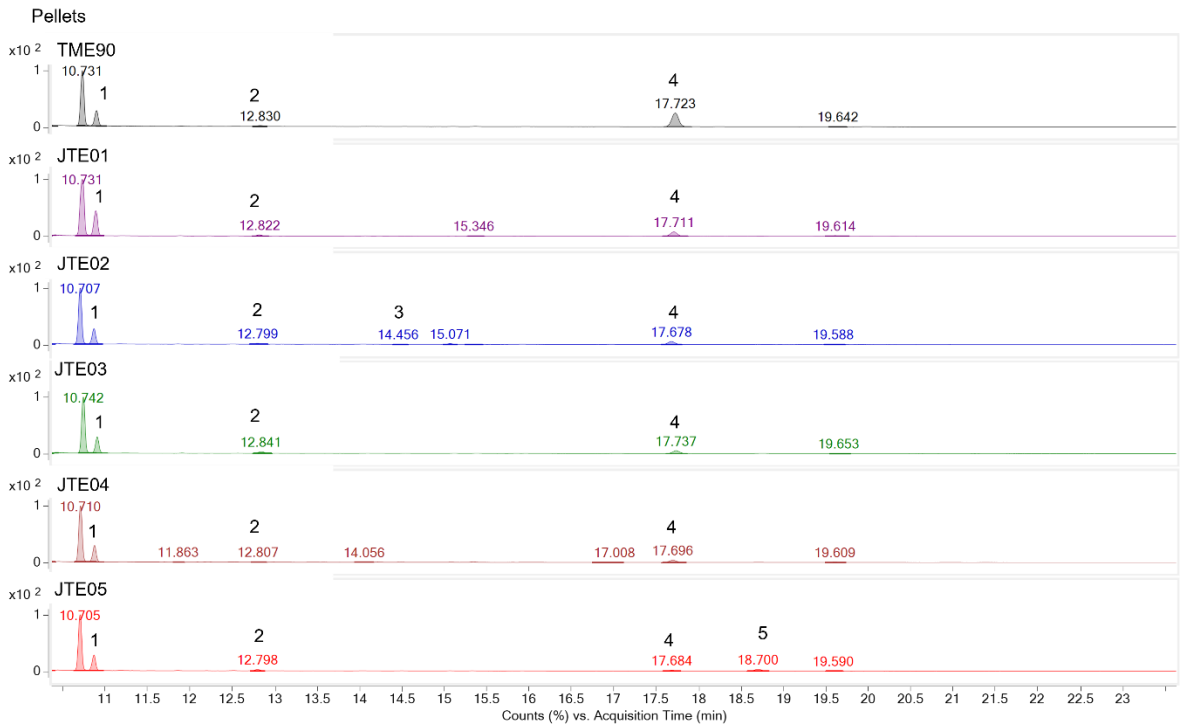

Figure 66: - Total ion chromatograms (TICs) of the triterpenoids and sterols extracted from the pellet of the strains. 1, coprostanol; 2, ergosterol; 3, β-amyrin; 4, erythrodiol; 5, 16-hydroxy-erythrodiol.

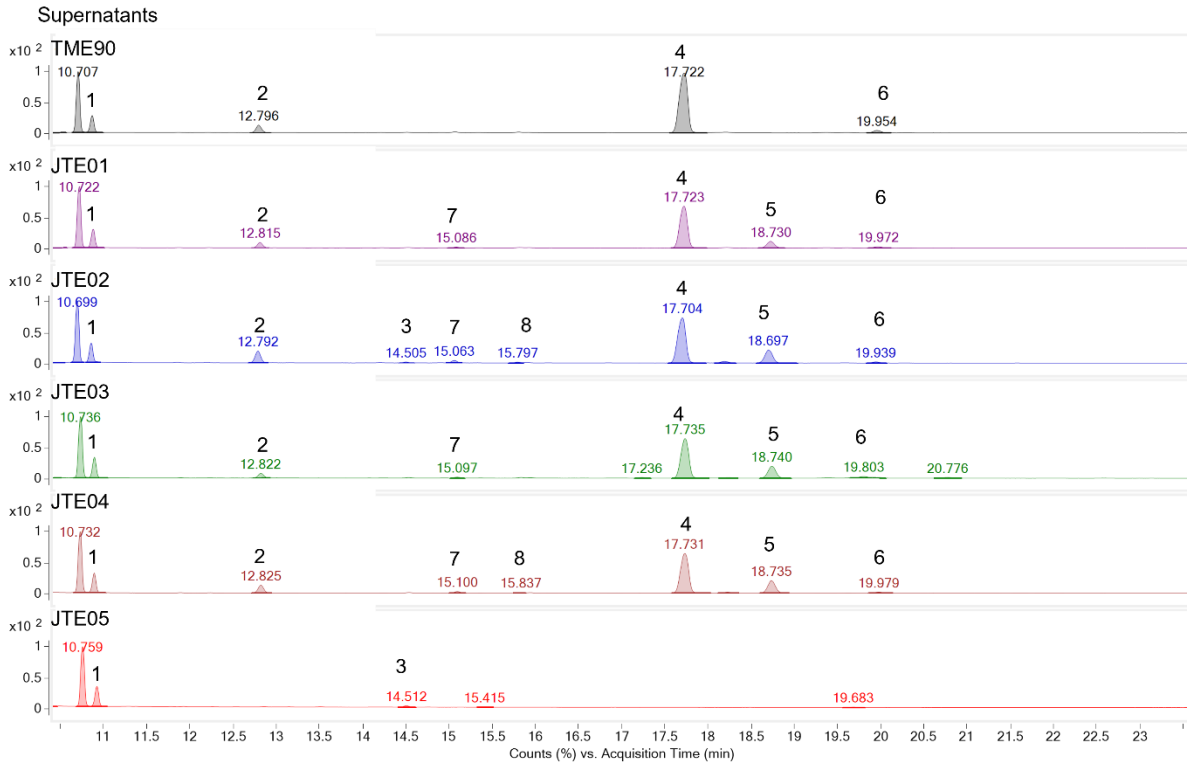

Figure 67: - Total ion chromatograms (TICs) of the triterpenoids and sterols extracted from the supernatant of the strains. 1, coprostanol; 2, ergosterol; 3, β-amyrin; 4, erythrodiol; 5, 16-hydroxy-erythrodiol; 6, oleanolic aldehyde; 7, 16-hydroxy-β-amyrin; 8, 22-hydroxy-β-amyrin.

In the TME90 strain, our analysis revealed the presence of several triterpenoids, including ergosterol, β-amyrin, erythrodiol, oleanolic acid, and oleanolic aldehyde. The identification of oleanolic aldehyde and oleanolic acid demonstrates the multifunctional nature of the CYP enzyme, as it can modify the C28 position of erythrodiol to produce oleanolic aldehyde, and further transform it into oleanolic acid (as discussed in Chapter 1 regarding multifunctional CYPs).

We previously discussed the identification of ergosterol (chapter 3), and its recognition

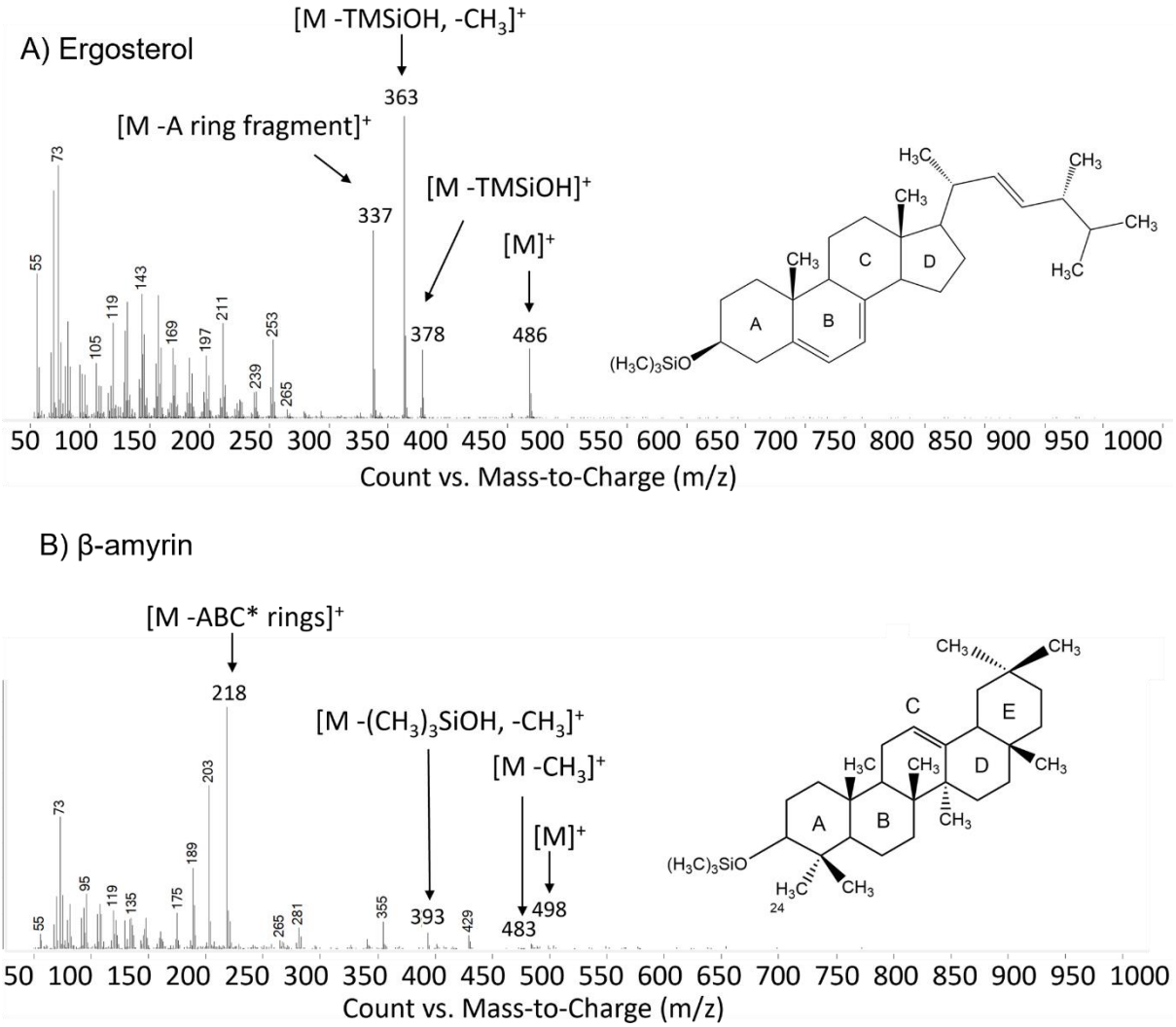

Figure 68: - Spectra of ergosterol and β-amyrin. A) Ergosterol is identifiable by the parent ion $[M]^+$ with an *m/z* value of 486, and other fragments at *m/z* values of 378, 363 and 337. B) β-amyrin is identified by the $[M]^+$ ion peak at *m/z* value of 496, and other notable peaks with values of 481, 391, and 216.

was straightforward (Figure 68A). The identification of β-amyrin was achieved by observing its $[M]^+$ ion with an *m/z* value of 496 (Table 7) and locating the corresponding peak at 14.5 minutes in the chromatogram (Figure 66; Figure 67; Figure 68B).

Erythrodiol was speculated at 17.7 minutes based on its fragmentation pattern and retention time (Figure 69A). Although we could not confirm its $[M]^+$ ion, we observed ions at 496 (representing the removal of a trimethylsilyate group), 481, 391, and 216. These ions correspond to the $[M]^+$ ion with the removal of a trimethylsilylate and methyl

group (-$(CH_3)_3SiOH$, -CH_3), two trimethylsilylate groups and a methyl group (-2$(CH_3)_3SiOH$, -CH_3), or the removal of the ABC* rings alongside a trimethylsilylate group (- ABC*, -$(CH_3)_3SiOH$), respectively. Additional unannotated ions in the spectra, indicative of erythrodiol, had *m/z* values of 406, 203, and 188.

Oleanolic aldehyde was speculated as the peak at 19.9 minutes, primarily due to the presence of the 203 and 190 fragments (Figure 69C). The 203 peak represents the C*DE rings, which have lost the ABC* rings as well as the aldehyde group (M -ABC* ring, -CHO), while the 190 peak corresponds to the same configuration but with the additional loss of the C17 carbon and two hydrogen molecules (-ABC* rings, -CHO, -CH_2). Oleanolic acid, known to elute after oleanolic aldehyde (Moses *et al*., 2014), was also detected in the analysis (Figure 69B).

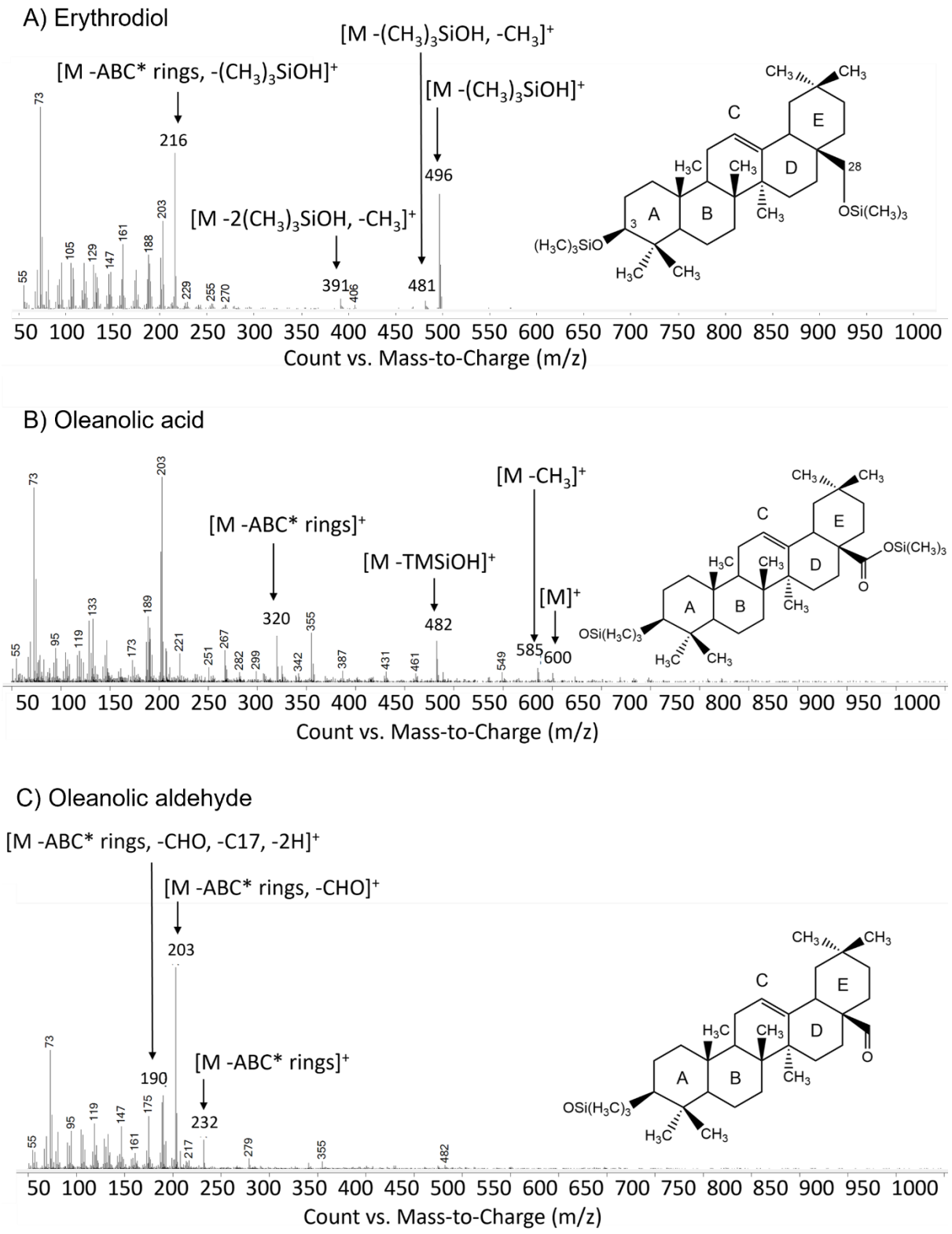

Figure 69: - Spectra of erythrodiol, oleanolic acid and oleanolic aldehyde. Full figure legend on next page.

Figure 69: - Spectra of erythrodiol, oleanolic acid and oleanolic aldehyde. A) Erythrodiol is identifiable by the presence of the ions with a 496 *m/z* value which indicates the parent ion $[M]^+$ with the loss of a trimethylsilylate group. Other notable fragments are the *m/z* values of 481, 391, and 216. B) Oleanolic acid is identifiable by the parent ion $[M]^+$ with an *m/z* value of 600, and other fragments at *m/z* values of 585, 482, and 320. C) Oleanolic aldehyde was identified via an extracted ion chromatogram (EIC), where the ion extracted was the $[M]^+$ with a *m/z* value of 512.

In the case of JTE01, we observed a peak at 18.7 minutes, which we hypothesise to be 16-hydroxy-erythrodiol based on its fragmentation patterns. The presence of an ion at 481 *m/z* suggests the $[M]^+$ ion with the loss of two trimethylsilylate groups and a methyl group. This fragmentation pattern closely resembles that of erythrodiol, leading us to believe it is a modified version of erythrodiol. Since JTE01 contains a C16 CYP, we can conclude that this peak represents 16-hydroxy-erythrodiol (Figure 70). The observed peaks align with what we would expect for erythrodiol, considering that the parent ion of 16-hydroxy-erythrodiol would have an *m/z* value of 674. Thus, the ions present in the spectra are indicative of the stepwise removal of trimethylsilylate groups. Another supporting factor that this is 16-hydroxy-erythrodiol is its presence in all the strains except TME90. The common factor among these strains, but not in TME90, is the inclusion of the C16 BfCYP716Y1.This observation leads us to infer that the C16 BfCYP716Y1 is efficient and functional in these strains.

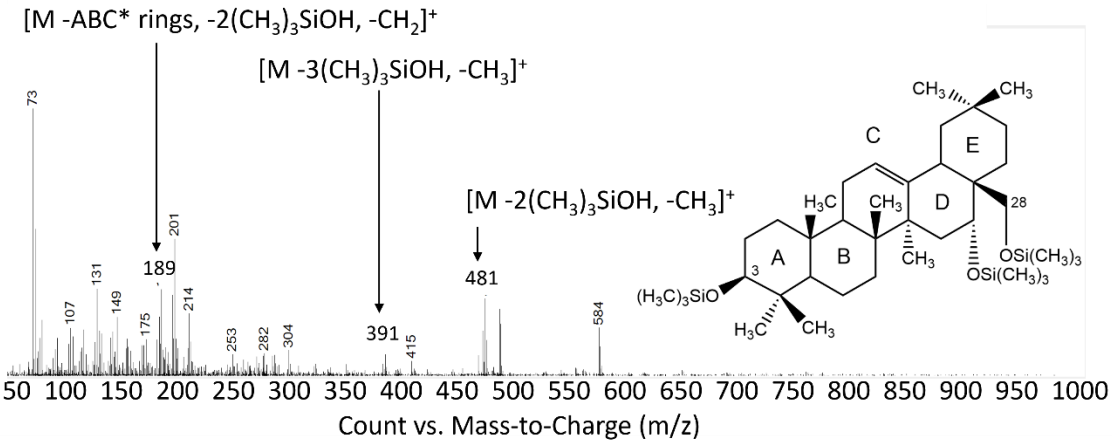

Figure 70: - Mass spectrum of 16-hydroxy-erythrodiol.

Similarly, 16-hydroxy-β-amyrin was suspected to be the peak at 15 minutes (Figure 71). This compound was present in all strains except TME90, and again, shared CYP among these strains was the C16 BfCYP716Y1. The spectra of 16-hydroxy-β-amyrin closely resemble those of β-amyrin, with the additional removal of a trimethylsilylate group from the C16 modification. Additionally, it is known that hydroxy-β-amyrin elutes after β-amyrin but before erythrodiol, and so this result is consistent with the elution order described in previous studies (Moses *et al*., 2014).

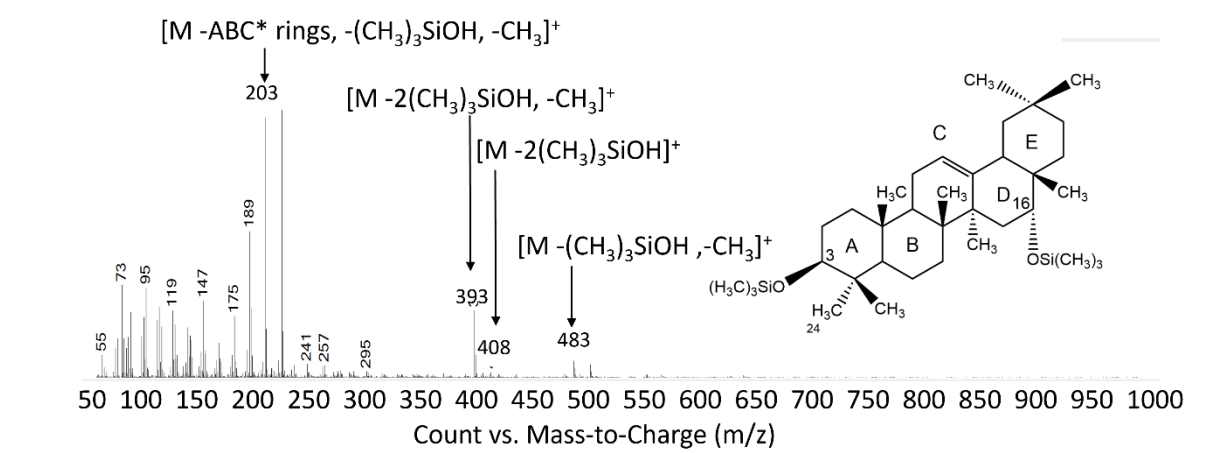

Figure 71: - Mass spectrum of 16-hydroxy-β-amyrin.

In the case of JTE02, we successfully identified the previously noted peaks and additionally detected the presence of 22-hydroxy-β-amyrin (Figure 72). This identification was based on the observed fragmentation patterns which have been previously described. Since this peak was observed in JTE02 and not JTE01, we can confirm that it is likely the C22 modified version and not the C16 modified β-amyrin. Furthermore, this compound was also found in JTE04. Considering that both JTE02 and JTE04 share the C22 MtCYP72A61v2, it is reasonable to infer that this modification is consistent between them.

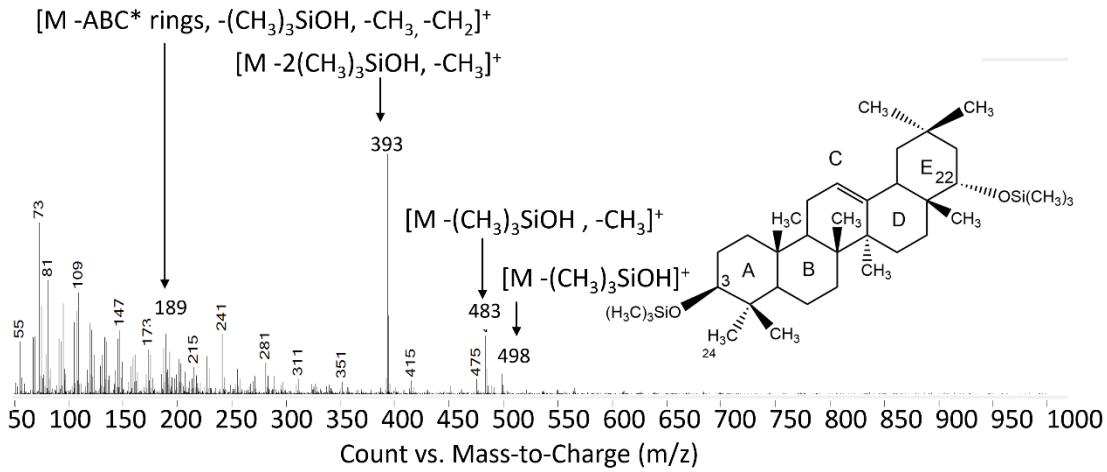

Figure 72: - Mass spectrum of 22-hydroxy-β-amyrin.

Conversely, JTE03 did not exhibit any presence of 22-hydroxy-β-amyrin, suggesting that the combination of the three CYPs (MlCYP716A75, BfCYP716Y1, PvCYP939E) might not work effectively together. However, the presence of 16-hydroxy-erythrodiol and 16-hydroxy-β-amyrin in JTE03 indicates that the C16 CYP remains functional. Nevertheless, there were no other distinct triterpenoids identified in this strain.

In JTE04, we exclusively identified compounds that had been previously identified in the strains, including β-amyrin, erythrodiol, 16-hydroxy-erythrodiol, oleanolic aldehyde, 16-hydroxy-β-amyrin, and 22-hydroxy-β-amyrin. The presence of these compounds provides insights into the relative effectiveness of different CYPs. For instance, the consistent presence of the C16 modification in all strains suggests that this CYP can efficiently modify both β-amyrin and erythrodiol. Similarly, the presence of 22-hydroxy-β-amyrin indicates that the C22 CYP can modify β-amyrin, although possibly not erythrodiol or modified erythrodiol. Notably, the C24 CYP appears to be less effective at modifying compounds, as it was not detected at all. It is worth noting that this pattern might have been evident in the JTE05 strain as well, but this strain did not exhibit robust growth compared to the others, and therefore, drawing conclusions from it is challenging due to insufficient evidence. These results justified the decision to proceed with the chromosomal integration of genes to determine if this approach would yield better gene expression. All the strains and the triterpenoids produced are shown in Table 8.

Table 8: - The triterpenoids produced and predominant sterol in each transiently expressing strain.

Strain	Sterol	Triterpenoids annotated
TME90	Ergosterol	β-amyrin, erythrodiol, oleanolic aldehyde, oleanolic acid
JTE01	Ergosterol	β-amyrin, erythrodiol, oleanolic aldehyde, oleanolic acid, 16-hydroxy-β-amyrin, 16-hydroxy-erythrodiol
JTE02	Ergosterol	β-amyrin, erythrodiol, oleanolic aldehyde, oleanolic acid, 16-hydroxy-β-amyrin, 16-hydroxy-erythrodiol
JTE03	Ergosterol	β-amyrin, erythrodiol, oleanolic aldehyde, oleanolic acid, 16-hydroxy-β-amyrin, 16-hydroxy-erythrodiol
JTE04	Ergosterol	β-amyrin, erythrodiol, oleanolic aldehyde, oleanolic acid, 16-hydroxy-β-amyrin, 16-hydroxy-erythrodiol
JTE05	Ergosterol	β-amyrin

6.1.3 Analysis of chromosomal integration of JEscin genes with GC-MS

Due to not being able to integrate all six JEscin transcriptional units, the anticipated compound produced by the chromosomal integration strains is glycosylated 21-hydroxy-erythrodiol (Figure 73). The potential toxicity of this compound towards *S. cerevisiae* remains uncertain. Previous engineering efforts have enabled yeast to produce erythrodiol, and it is known to exhibit low toxicity at the concentrations typically generated (Dale *et al*., 2020). However, the glycosylated form may exhibit increased toxicity due to the generally higher toxicity associated with glycosylated triterpenoids compared to their aglycone counterparts (Crombie *et al*., 1984).

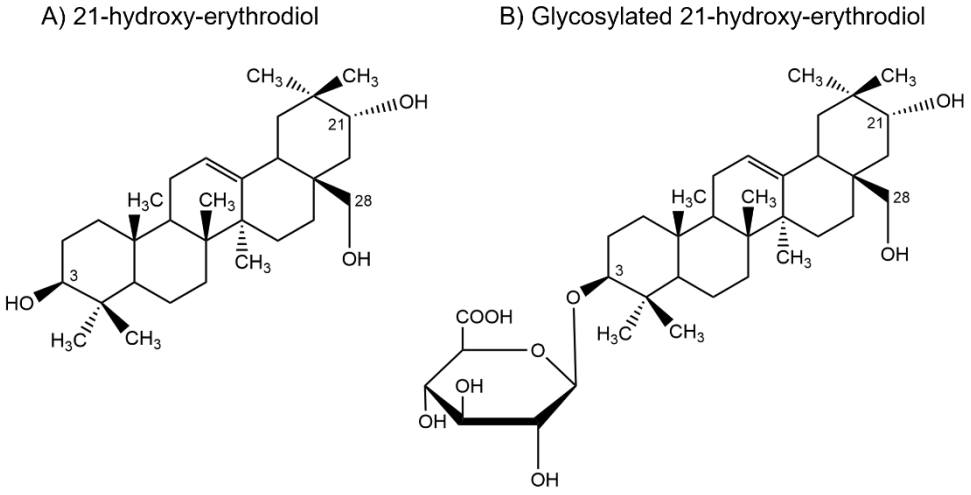

Figure 73: - The structure of 21-hydroxy-erythrodiol and its glycosylated derivative. Glycosylated 21-hydroxy-erythrodiol is the hypothetical product produced by JTE09 and JTE11 which can be in the form of either A) 21-hydroxy-erythrodiol aglycone or B) glycosylated 21-hydroxy-erythrodiol which has a glucuronic acid moiety at the C3 position.

The strain produced for this study is JTE09, which has a TME90 background with chromosomally integrated GmCYP72A69 (responsible for C21 hydroxylation), HsUGT1A3 (catalysing C3 glycosylation), and AtUGD1 (mediating C3 glucose to glucuronic acid conversion) in the 308a region of the chromosome. Therefore, the only

differences between these two strains are the potential addition of C21 hydroxylation and hopefully the addition of a glucuronic acid at the C3 position.

Both the pellet and supernatant underwent solvent extraction for GC- and LC-MS analysis to confirm the localisation of triterpenoids or glycosylated triterpenoids within the cells, ensuring they were not exported into the supernatant. This confirmation was successfully achieved using GC-MS (Figure 74A). A comparison of the chromatograms between the TME90 pellet and supernatant demonstrated that the supernatant (Figure 74B). contained significantly fewer detectable sterols and triterpenoids than the pellets. While this difference was less pronounced in the case of JTE09 due to lower sterol and triterpenoid production, comparing the normalised peak areas still revealed reduced detectable levels in the supernatant (Figure 75). In this context, the minimal triterpenoid presence in the supernatant resulted from our omission of MβCD. Across all strains, 99 % of the total erythrodiol content was localised in the pellet, with only 1 % detected in the supernatant.

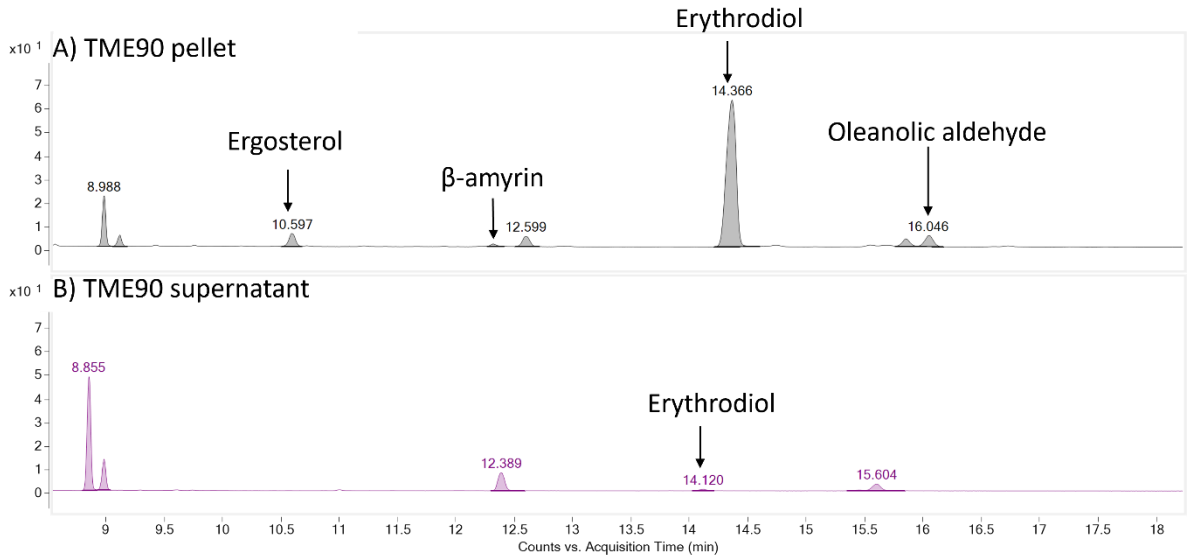

Figure 74: - Chromatograms of the sterols and triterpenoids present in the TME90 pellet and supernatant. A) The TME90 contained ergosterol, β-amyrin, oleanolic acid and oleanolic aldehyde, whereas in B) the TME90 supernatant, there was no detectable ergosterol or oleanolic aldehyde, detectable levels of β-amyrin and oleanolic acid. Peaks at 8.9 minutes are the internal standard coprostanol. The unannotated at peaks could not be identified as triterpenes at this time.

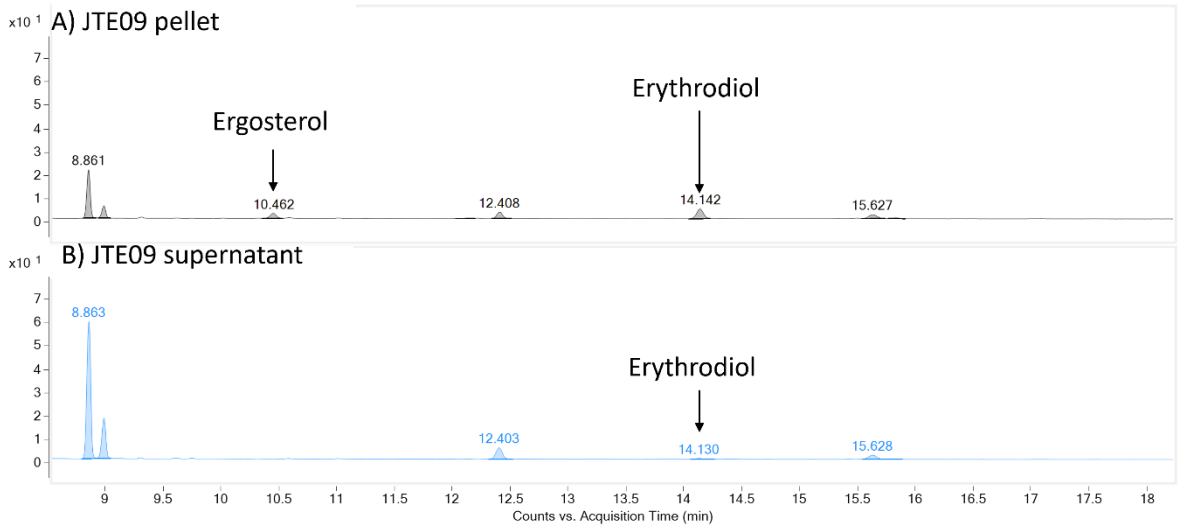

Figure 75: - Chromatograms of the sterols and triterpenoids present in the JTE09 pellet and supernatant. A) The JTE09 contained ergosterol, β -amyrin and oleanolic acid, whereas in B) the JTE09 supernatant, there was no detectable ergosterol, but detectable amounts of β-amyrin and oleanolic acid. Peaks at 8.9 minutes are the internal standard coprostanol.

The extracts from JTE09 alongside TME90, underwent both GC- and LC-MS analyses. This allowed us to assess the modifications resulting from GmCYP72A69 and determine whether glycosylation had occurred at the C3 position. Upon comparing TME90 to JTE09, no differences were observed in the composition of the compounds produced, as evident in the overlay image. The chromatogram (Figure 76) revealed the presence of expected compounds such as ergosterol and erythrodiol. Additionally, oleanolic acid and oleanolic aldehyde were extracted. However, there was no evidence of 21-hydroxy-erythrodiol.

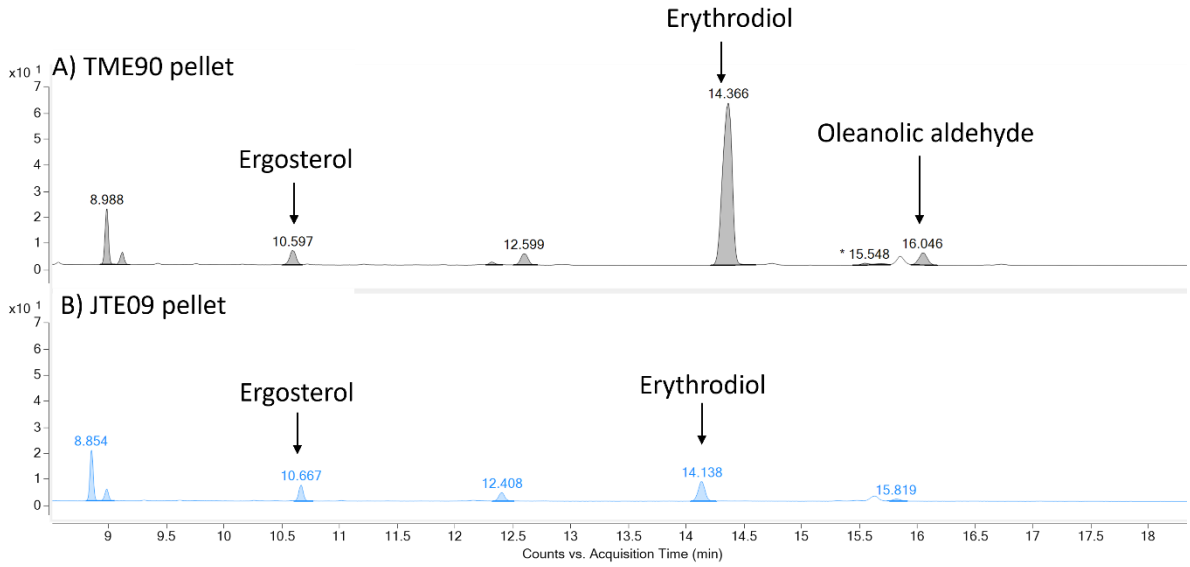

Figure 76: - Chromatograms of the compounds produced in TME90 and JTE09. A) The TME90 pellet had ergosterol, erythrodiol, oleanolic acid and oleanolic aldehyde present. In the B) JTE09 pellet only ergosterol and erythrodiol was identified. Peaks at 8.9 minutes are the internal standard coprostanol.

Ergosterol was confidently identified based on the previously discussed fragmentation patterns outlined in Chapter 3. The identification of β-amyrin was facilitated by its $[M]^+$ ion with an *m/z* value of 498. This was identified in the same way as discussed previously. Furthermore, we successfully identified erythrodiol, oleanolic aldehyde, and oleanolic acid. Oleanolic aldehyde and oleanolic acid are produced due to the multifunctional nature of CYPs. The MlCYP716A75 used to produce erythrodiol can further oxidise the hydroxyl group at the C28 position to yield oleanolic aldehyde and subsequently oleanolic acid. This suggests that in our strains, MlCYP716A75 could convert some of the erythrodiol to oleanolic aldehyde and then to oleanolic acid. To identify these compounds, we conducted an Extracted Ion Chromatogram (EIC) using their respective $[M]^+$ ions. Erythrodiol possesses a $[M]^+$ *m/z* value of 586, and although this specific ion was not evident in the spectra, most other fragments associated with erythrodiol were detected. Oleanolic acid, on the other hand, has an $[M]^+$ *m/z* value of 600, while oleanolic aldehyde features an $[M]^+$ *m/z* value of 512. These were, therefore, identified as the peaks detected at 15.6 minutes for oleanolic acid and 15.8 minutes for oleanolic aldehyde.

The peak appearing at 14.1 minutes was identified as erythrodiol based on the observed fragmentation pattern. As previously mentioned, the $[M]^+$ ion was not explicitly identified; however, the presence of ions at 496, signifying the removal of a trimethylsilylate group, was evident. Additional ions in the spectra with *m/z* values of 406, 203, and 188 also corroborated the identification of erythrodiol.

The identification of the minor peak at 15.3 minutes as oleanolic acid was supported by the presence of ions at 585 and 482, representing the removal of a methyl group ($-CH_3$) and a trimethylsilylate group with a carboxyl group ($-(CH_3)_3SiOOH$), respectively. Furthermore, peaks at *m/z* 320 and 203 in the spectra indicated the presence of the C*DE rings of the pentacyclic triterpenoid backbone, which had undergone Retro-Diels-Alder fragmentation originating from the ABC* rings. The 320 peak denoted the C*DE rings, while the 203 peak represented the C*DE rings with the removal of trimethylsilylate and carboxyl group ($- (CH_3)_3SiOO$). Oleanolic aldehyde was confidently identified as the peak at 15.8 minutes due to the presence of the 203 fragment and the 190 fragment. A description of all the triterpenoids produced in each strain is shown in Table 9.

Table 9: - The triterpenoids produced and predominant sterol in each chromosomally integrated strain.

Strain	Sterol	Triterpenoids annotated
TME90	Ergosterol	β-amyrin, erythrodiol, oleanolic aldehyde, oleanolic acid
JTE06	Ergosta-7,22-dienol	β-amyrin, erythrodiol, oleanolic aldehyde, oleanolic acid
JTE09	Ergosterol	β-amyrin, erythrodiol, oleanolic aldehyde, oleanolic acid
JTE11	Ergosta-7,22-dienol	β-amyrin, erythrodiol, oleanolic aldehyde, oleanolic acid

6.1.4 LC-MS analysis of chromosomal integration of JEscin genes

The LC-MS analysis of both TME90 and JTE09 provided further evidence that neither the glycosylated form of 21-hydroxy-erythrodiol nor glycosylated erythrodiol were synthesised. This result was in line with our expectations, as we had previously failed to detect any 21-hydroxy-erythrodiol in JTE09.

To ensure accurate quantification in the LC-MS analysis, we used echinocystic acid-3-*O*-glucoside as an internal standard. This compound has a molecular weight of 634 Da, facilitating its identification in the LC-MS by searching for the specific ion with an *m/z* value of 633. As depicted in the chromatograms at 4.2 minutes (Figure 77), the presence of the internal standard is evident. However, it's worth noting that glycosylated 21-hydroxylated erythrodiol also possesses a molecular weight of 634 Da. Consequently, identifying the product of interest becomes challenging, as it may be concealed by the internal standard, if they have very similar retention times.

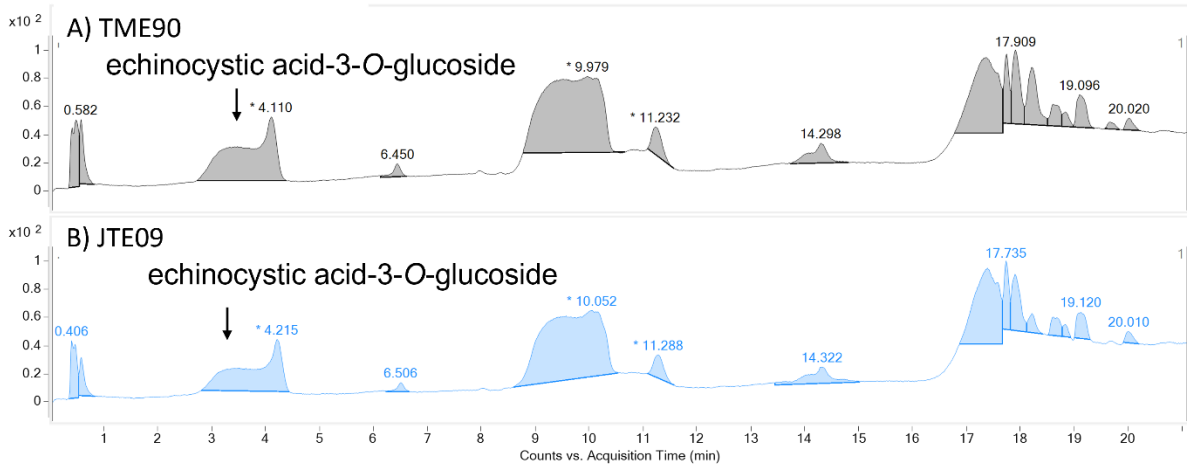

Figure 77: - Chromatograms from the internal standard echinocystic acid-3-*O*-glucoside of TME90 and JTE09. A) The TME90 pellet which contains the genes needed for erythrodiol only production. B) The JTE09 pellet which contains the genes needed for glycosylated 21-hydroxy-erythrodiol production. Due to the similarities in the spectra, we can conclude that there is no presence of glycosylates 21-hydroxy-erythrodiol.

To distinguish between the internal standard and our target product, we conducted an EIC analysis to search for the specific ion. The ion of interest was only observed at the 4.2-minute mark, indicating that if glycosylated 21-hydroxy-erythrodiol were produced, it would likely exhibit a distinct retention time. To further validate that our product of interest was not being masked by the internal standard, we compared the areas under the peaks. This analysis revealed no significant difference in the peak areas between TME90 and JTE09. As a result, we can confidently conclude that no glycosylated 21-hydroxy-erythrodiol was generated in the course of this experiment.

6.2 Introduction of the *erg3* knockout in 16-hydroxy-erythrodiol producing strain

Considering the *erg3Δ* sterol mutant's demonstrated increased tolerance to exogenous escin, as discussed in chapters 4 and 5, we decided to introduce the *erg3Δ* mutation into both TME90 and JTE09 strains. The objective was to assess whether this genetic alteration would lead to an increase in 16-hydroxy-erythrodiol production or enhanced cell viability. While these strains generated the same compounds previously identified in Section 5.1.3, the sterol composition was in line with that of the *erg3Δ* sterol mutant. We focused on investigating potential differences in the quantity of the produced compounds, irrespective of their nature.

Using GC-MS, we successfully confirmed the functionality of the *erg3Δ* mutant and determined that strains JTE06 and JTE11 did possess a non-functional *erg3Δ* gene. This was introduced by introducing an early stop codon in the *ERG3* gene. Furthermore, our analysis revealed that the primary sterol present in TME90 and JTE09 was ergosterol, whereas in JTE06 and JTE11, it was ergosta7,22-dienol (Figure 78). This finding aligns with the data presented in Chapter 3 that indicated the *erg3Δ* sterol mutant predominantly contains ergosta-7,22-dienol (Figure 79).

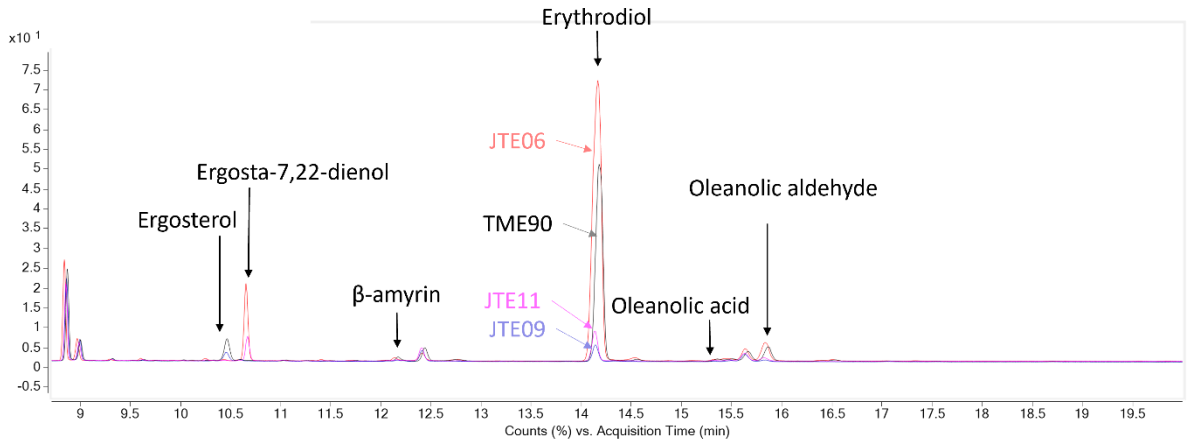

Figure 78: - An overlay of GC-MS chromatograms showing the accumulation of oleanolic acid and oleanolic aldehyde produced in strains. TME90 expressing mevalonate biosynthesis genes as well as AaBAS, CYP716A75 and ATR2, which produce β-amyrin, and hydroxylate it at the C28 position. JTE06 expressing everything present in TME90 but with an *erg3Δ* mutation, JTE09 expressing everything TME90 has as well as HsUGT1A3, AtUGD1 and GmCYP72A69, which glycosylate the C3 region of b-amyrin, modify it to a glucuronic acid and insert a hydroxylation at position C21. JTE11 expresses everything JTE09 has but includes the *erg3Δ* mutation like JTE06. JTE06 and JTE11 produce ergsota-7,22-dienol instead of ergosterol in their plasma membranes.

Erythrodiol was consistently identified as the most abundant compound produced in all strains, comprising approximately 65 %, 80 %, 62 %, and 62 % of the total extract on average in TME90, JTE06, JTE09, and JTE11, respectively. Nevertheless, the normalised peak area revealed variations in the amount of erythrodiol produced by the different strains. TME90 and JTE06, both of which primarily produced erythrodiol, yielded considerably higher amounts compared to JTE09 and JTE11, which aimed to produce glycosylated 21-hydroxy-erythrodiol. The marked disparity in the normalised peak areas between these two groups of strains is evident (Figure 80; Figure 81) Several factors could contribute to this observed difference. Firstly, the additional burden placed on JTE09, which contains three extra heterologous genes to transcribe and translate, might account for its reduced erythrodiol production. However, it is also possible that the production of 21-hydroxy-erythrodiol, utilising erythrodiol as a precursor, impacted the overall erythrodiol levels. Notably, we did not detect any

evidence of 21-hydroxy-erythrodiol in the GC-MS spectra. Consequently, we can reasonably conclude that the C21 GmCYP72A69 was unable to modify either β-amyrin or erythrodiol under the conditions tested in this study.

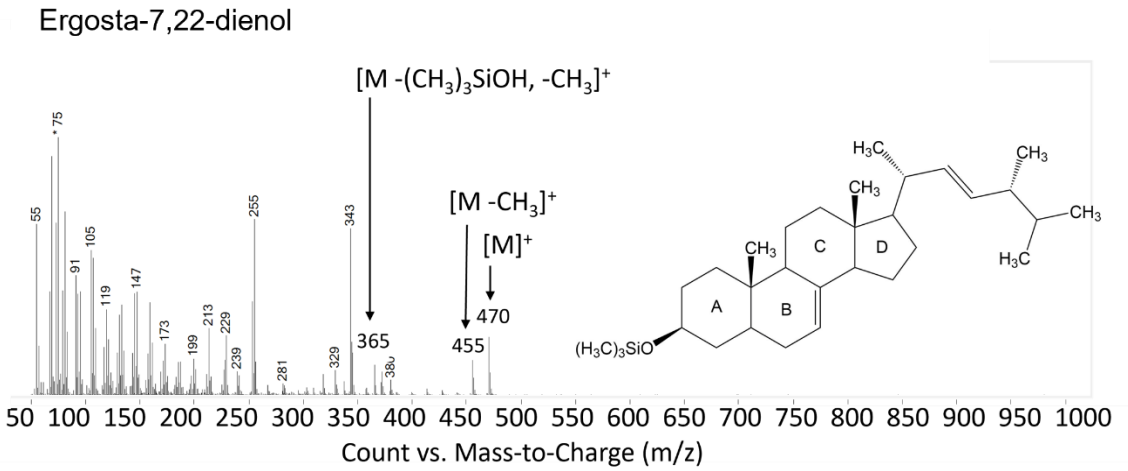

Figure 79: - Mass spectrum of ergosta-7,22-dienol found in the JTE06 and JTE11 strains.

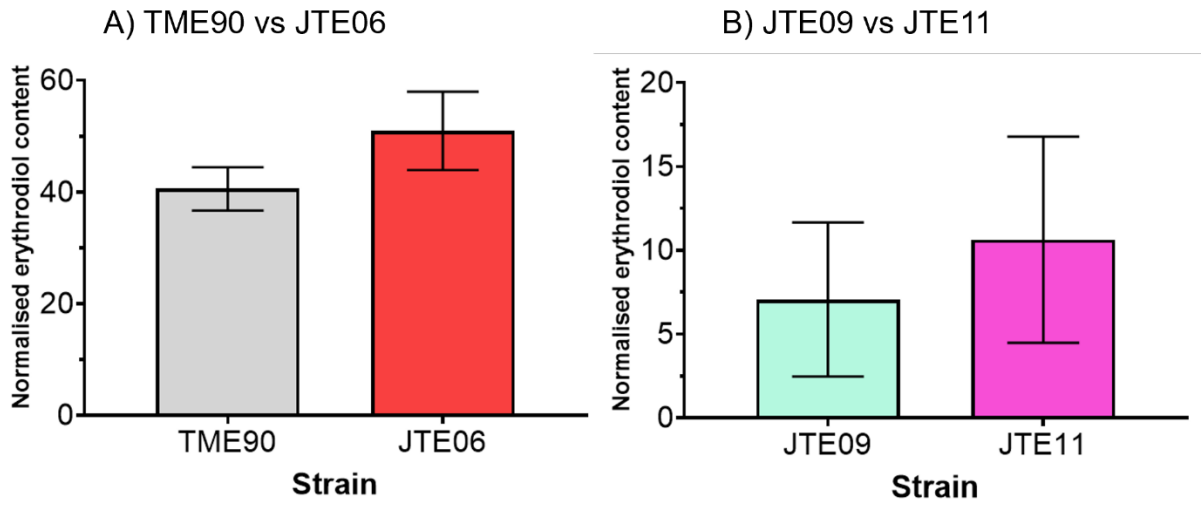

Figure 80: - Charts showing the normalised erythrodiol content in the strains TME90, JTE06, JTE09 and JTE11. A) Compares TME90 and JTE06 which are erythrodiol producing strains with the same genome except from the presence of an *erg3Δ* mutation in JTE06. B) Compares JTE09 and JTE11 which are JEscin producing strains with the same genome except from the presence of an *erg3Δ* mutation in JTE11. Normalised averages compared to the internal standard coprostanol, and standard deviation were plotted. Statistical analysis was performed using a t-test to compare the strains. The sample size is n=3, and p-values are indicated as follows: * ≤ 0.05, ** ≤ 0.01, *** ≤ 0.001, **** ≤ 0.0001.

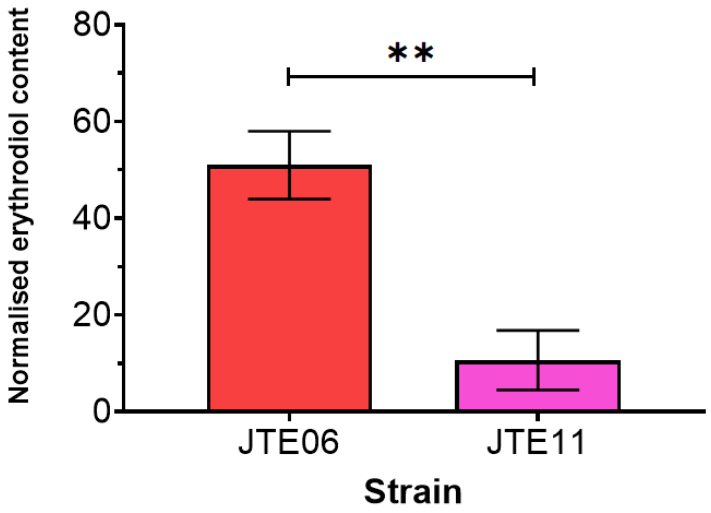

Figure 81: - Charts showing the normalised erythrodiol content in the strains JTE06 and JTE11. Normalised averages compared to the internal standard coprostanol, and standard deviation were plotted. Statistical analysis was performed using a t-test to compare the strains. The sample size is n=3, and p-values are indicated as follows: * ≤ 0.05, ** ≤ 0.01, *** ≤ 0.001, **** ≤ 0.0001.

Based on our observations, we propose that the *erg3Δ* mutation does not lead to an increase in the quantity of produced triterpenoids, particularly regarding erythrodiol. Analysis of the chromatograms, specifically the area under the peaks, reveals no significant difference in the production of oleanolic acid and oleanolic aldehyde among the *erg3Δ* mutants (JTE06 and JTE11) in comparison to TME90 or JTE09 (Figure 82).

Regarding oleanolic acid, there was no noticeable variance in the amount produced. Conversely, concerning oleanolic aldehyde, the *erg3Δ* mutation itself did not alter the production quantity, but the introduction of chromosomally integrated JEscin genes did. Notably, JTE09 and JTE11 exhibited significantly lower levels of oleanolic aldehyde in the extract compared to TME90 and JTE06 (Figure 82B). This suggests that the challenge of expressing three additional heterologous genes imposed a burden on the cells, impeding their ability to produce oleanolic aldehyde.

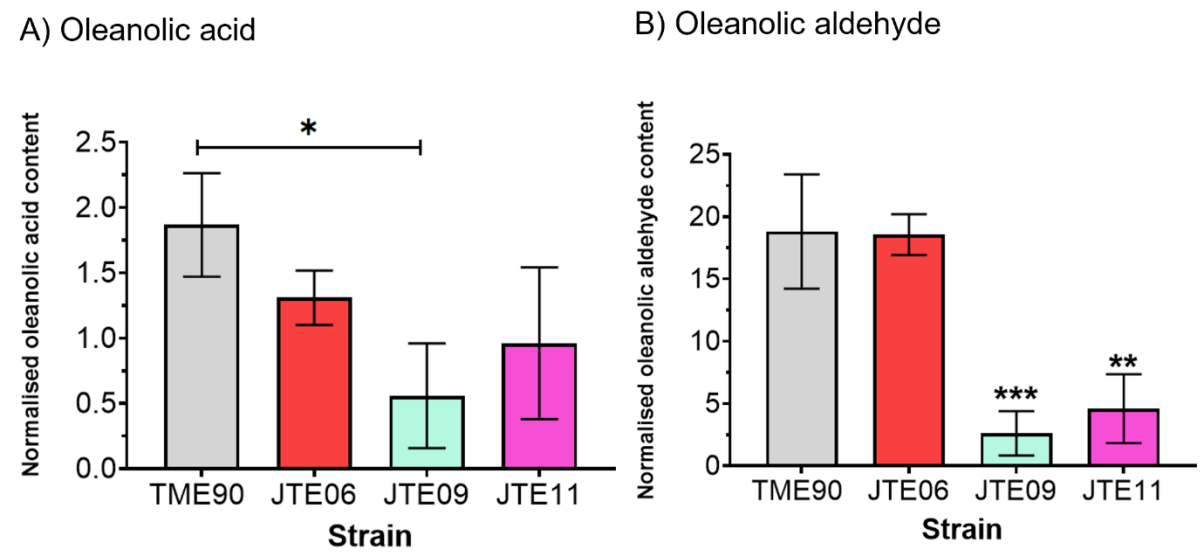

Figure 82: - Charts showing the normalised oleanolic acid or oleanolic aldehyde content in the strains TME90, JTE06, JTE09 and JTE11. A) Compares all the strains and the amount of oleanolic acid produced. B) Compares all the stains and the amount of oleanolic aldehyde produced. Normalised averages compared to the internal standard coprostanol, and standard deviation were plotted. The statistical analysis in B) show a *** or ** p-value compared to both the TME90 and JTE06 strain. Statistical analysis was performed using a t-test to compare the strains. The sample size is n=3, and p-values are indicated as follows: * ≤ 0.05, ** ≤ 0.01, *** ≤ 0.001, **** ≤ 0.0001.

6.2.1 LC-MS analysis of *erg3Δ* mutant JEscin producing strains

Like the previous section (5.1.4), there was no significant difference in the peak area of the internal standard, echinocystic acid-3-*O*-glucoside, between the JTE06 and JTE11 strains (Figure 83). This once more supports our conclusion that this compound was not produced in the current experiment.

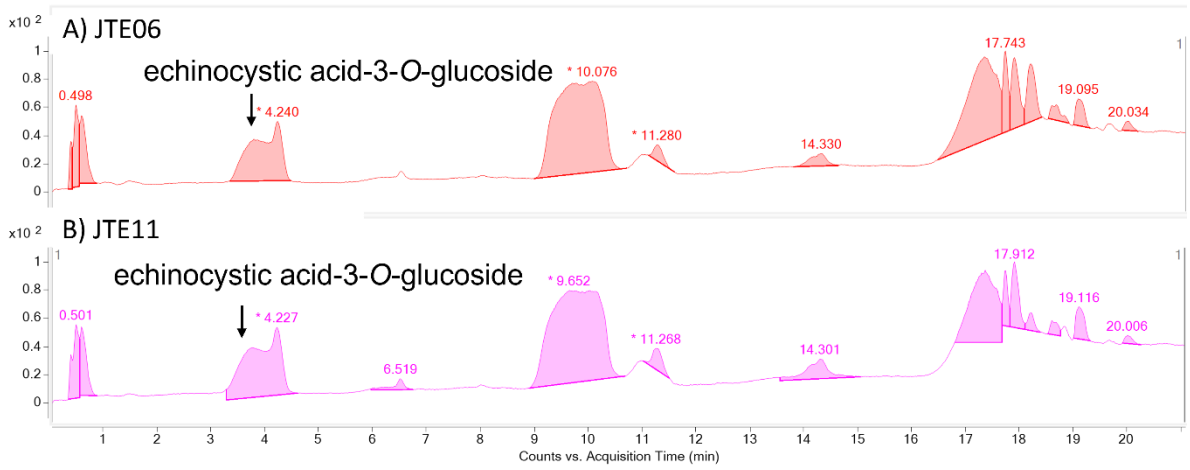

Figure 83: - Chromatograms from the internal standard echinocystic acid-3-O-glucoside of JTE06 and JTE11. A) The JTE06 pellet which contains the genes needed for erythrodiol only production and has an *erg3Δ* mutation. B) The JTE11 pellet which contains the genes needed for glycosylated 21-hydroxy-erythrodiol production and has an *erg3Δ* mutation. Due to the similarities in the spectra, we can conclude that there is no presence of glycosylates 21-hydroxy-erythrodiol.

6.3 Discussion

This chapter aimed to synthesise a glycosylated triterpenoid analogous to escin, but this was unsuccessful. By manipulating the yeast biosynthetic pathways and introducing various heterologous genes, we aimed to explore the production of JEscin and its impact on yeast physiology. Our results provide valuable insights into the genetic modifications necessary for achieving this goal and offer implications for future research in the field of triterpenoid biosynthesis. The motivation behind this was to refine the production of glycosylated triterpenoids with specific modifications tailored for precise applications. One such application is the use of glycosylated triterpenoids as surfactants. Creating a compound like escin but with reduced toxicity to *S. cerevisiae* could be advantageous in an industrial context.

Our inability to produce JEscin may be attributed to the specific CYPs employed in our study. It is worth noting that certain CYPs identified in this research have not been previously described to interact with erythrodiol; instead, they are known to primarily target β-amyrin, which constitutes only a small fraction of the final product, as it is consumed in the biosynthesis of erythrodiol. For instance, the literature has documented that BfCYP716Y1 functions as a catalyst for both β-amyrin and α-amyrin (Moses *et al*., 2015). Our findings confirm this, as we detected the presence of 16-hydroxy-β-amyrin. However, the existing literature does not specify its activity on erythrodiol. Nonetheless, our experiments confirmed that BfCYP716Y1 can use erythrodiol as a substrate.

Conversely, MtCYP72A61v2 has been reported to use 24-hydroxy-β-amyrin as its substrate (Fukishima *et al*., 2013; Seki *et al*., 2011), which explains why we did not observe any C22-hydroxylated products in JTE02, where only C28 and C16 hydroxy CYPs were present alongside it. Similarly, PvCYP939E has been documented to solely target β-amyrin as its substrate (Moses *et al*., 2014c), rendering the combinatorial synthesis of 16-22-dihydroxy-β-amyrin or 16-22-dihydroxy-erythrodiol an unexpected outcome. Moreover, the substrate of GmCYP72A69 is soyasapogenol B (Yano *et al*., 2017), which may explain why we did not observe C21 hydroxylation

on erythrodiol, as its structural dissimilarity compared to soyasapogenol B could hamper the enzymatic conversion (Figure 84).

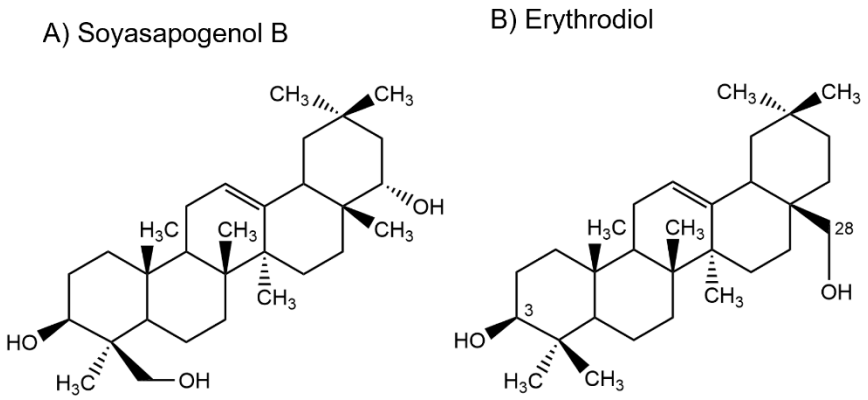

Figure 84: - Structures of soyasapogenol B and erythrodiol. A) Soyasapogenol B has modifications at the C24 and C22 positions, whereas B) erythrodiol has modification at the C28 position only. The differences in their structure is a likely reason why the GmCYP72A69 was not able to use erythrodiol as a substrate.

Another plausible reason for the failure to produce JEscin could be the insufficient expression of the integrated genes within the yeast genome. It remains unclear whether these genes were adequately expressed under the galactose promoter in the presence of galactose. To address this concern, two potential approaches can be employed for verification. The first method involves a Western blot assay, which requires the tagging of the protein with a marker recognised by a specific antibody. Subsequently, all proteins in the sample are separated via electrophoresis, and the protein of interest can be detected using the corresponding antibody (Mahmood & Yang, 2012). Alternatively, protein expression can be analysed via RT-qPCR, a method previously used in Chapters 4 and 5 of this thesis. Using RT-qPCR would provide valuable insights into the transcription and translation of the genes in question, explaining whether they are actively participating in the biosynthetic process.

Due to the possibility that JEscin might not be made due to its potential toxicity, the *erg3Δ* mutant was explored as a potential solution. However, it was observed that this mutant did not exhibit the same growth as the WT *S. cerevisiae*. Our investigation into the *erg3Δ* mutant was twofold: to understand its mechanism of action and to explore the possibility of modifying it to alleviate its interaction with ergosterol.

One of the primary objectives of this study was to introduce the necessary genetic modifications to enable the production of JEscin. To achieve this, we integrated a set of heterologous genes, including CYPs and UGTs, into *S. cerevisiae* strains capable of producing erythrodiol. Although we successfully integrated one set of the target genes, the expected production of glycosylated 21-hydroxy-erythrodiol was not observed. This outcome suggests that the introduced genes may not have functioned as anticipated or that the glycosylation process at the C3 position was not efficient under the conditions tested.

The low-level production of the hydroxylated forms of the compounds could be due to suboptimal folding of the CYPs or the incorrect localisation of the CYPs within the cell. Alternatively, there could also be mis-localisation of the precursors, limiting CYP activity (Moses *et al*., 2014). These factors may have collectively contributed to the observed results.

We have also successfully confirmed the efficacy of MβCD in transporting triterpenoids out of the cell and into the growth media. This ability alleviates the burden on yeast cells from toxic heterologous compounds, a factor that has been shown to enhance production levels (Moses *et al*., 2014).

Comparative analysis of the engineered strains provided insights into the impact of specific genetic modifications on triterpenoid production. Erythrodiol was identified as the most abundant compound across all strains, with substantial variation in its production levels. Strains with glycosylation modifications (JTE09 and JTE11) exhibited decreased erythrodiol production compared to those without glycosylation engineering (TME90 and JTE06). This discrepancy may be attributed to the additional metabolic burden imposed by the expression of three extra heterologous genes involved in glycosylation. It is also possible that the glycosylation of erythrodiol and subsequent production of 21-hydroxy-erythrodiol did not occur efficiently under the conditions employed.

The introduction of the *erg3Δ* mutation, known to cause increased tolerance to exogenous escin, aimed to assess its potential to enhance triterpenoid production or

cell viability. Our results demonstrated that the *erg3Δ* mutation did not significantly impact the overall triterpenoid production levels, particularly concerning erythrodiol.

This chapter provides insight into the challenges associated with engineering yeast to produce structurally complex triterpenoids like JEscin. The lack of glycosylated 21-hydroxy-erythrodiol production suggests that further optimisation of the glycosylation process and metabolic engineering may be necessary. Additionally, the observed metabolic burden associated with production highlights the need for strategies to enhance enzyme efficiency.

This chapter shows the challenges in engineering yeast to produce complex triterpenoids like JEscin. The absence of glycosylated 21-hydroxy-erythrodiol production emphasises the need for further optimisation of glycosylation processes and metabolic engineering. The metabolic burden associated with production underscores the importance of strategies to enhance enzyme efficiency. Future research avenues should explore alternative glycosylation enzymes, optimise growth conditions, and use synthetic biology tools for efficient JEscin production, keeping in mind potential toxicity for both industrial and therapeutic applications. This work lays the foundation for customised bio-surfactant production and sets the stage for future projects in this domain.

Chapter 7: - Conclusions and future work

7.1 Project Overview

This work aimed to engineer *S. cerevisiae* for enhanced glycosylated triterpenoid production. Leveraging the yeast's inherent ability to produce 2,3-oxidosqualene, a key precursor in triterpenoid biosynthesis, we aimed to introduce heterologous pathways to transform 2,3-oxidosqualene into triterpenoids. This intricate process involves the cyclisation of 2,3-oxidosqualene into triterpenes by oxidosqualene cyclases, followed by oxidation through cytochrome P450 monooxygenases to yield triterpenoids. Subsequently, these triterpenoids undergo glycosylation by UDP-glucosyltransferases to form glycosylated triterpenoids, also known as saponins (Thimmappa *et al*., 2014).

We conducted a series of investigations and experiments to advance our understanding of this complex process. Chapter 3 delved into characterising the sterol composition of sterol biosynthesis mutants under different growth conditions, providing insights into how yeast adapts its sterol profiles. Our findings underscored the significance of media selection, revealing substantial variations in sterol profiles when strains were cultivated in a YPD medium, emphasising the role of growth conditions in sterol-related processes (Hahn-Hägerdal *et al*., 2005).

Chapter 4 explored the toxicity of escin, an industrially relevant glycosylated triterpenoid derived from conker seeds to, *S. cerevisiae*. We established that escin exhibited toxicity towards the yeast, with the minimal inhibitory concentration (MIC) varying in different growth media. In rich media (YPD), the MIC was determined to be 175 $\mu g.mL^{-1}$, while in minimal media (CSM), it was 62.5 $\mu g.mL^{-1}$.

Furthermore, in Chapter 5, we investigated the interaction between escin and yeast membranes. Our research revealed that the structural isomers of escin, particularly those with angelic acid at position C21, exhibited greater inhibitory effects on yeast compared to their tiglic acid counterparts at the same position. Additionally, the presence of an acetyl group at C22 played a pivotal role in the toxicity of escin, as observed in escin 1a and 1b. These findings show the specific structural determinants influencing the toxicity of escin, potentially through its interaction with ergosterol within the yeast cell membrane.

Chapter 6 was dedicated to genetically engineering yeast strains to produce triterpenoids, specifically glycosylated triterpenoids, and introducing the *erg3Δ* mutation to discern differences in these strains. Our investigation, conducted through GC- and LC-MS analysis, revealed that while the *erg3Δ* mutation was effective in altering sterol composition, it did not lead to an increase in triterpenoid production in the strains under scrutiny.

Whilst investigating the genetic modifications essential for glycosylated triterpenoid biosynthesis in yeast, qPCR was shown to be a crucial tool in unravelling the intricate transcriptional landscape. Across the chapters, qPCR data provided insights into the expression patterns of heterologous genes integrated into *S. cerevisiae* strains. Chapter 4 used qPCR to probe the impact of escin on the transcription of crucial genes, revealing responses that underscored the complex regulatory network governing yeast response to glycosylated triterpenoids. Chapter 5 extended this exploration, employing qPCR to decipher the transcriptional changes induced by different structural isomers of escin, shedding light on the specific gene expression signatures induced by these variants. This approach enriched our understanding of the regulatory dynamics influencing triterpenoid biosynthesis and also laid the foundation for future investigations into optimising gene expression for enhanced glycosylated triterpenoid production in yeast.

7.2 Future work

Building upon the research conducted in this project, there are several promising avenues for future investigations aimed at advancing the production and application of glycosylated triterpenoids in yeast. One such avenue is the exploration of alternative glycosylation enzymes capable of glycosylating the C3 position of erythrodiol and other triterpenoids within a laboratory setting. The optimisation of this glycosylation process holds the potential to diversify the range of glycosylated triterpenoids that can be synthesised, each with unique properties and applications.

Furthermore, conducting a comprehensive toxicity assessment of glycosylated triterpenoids is essential. While this study has addressed the toxicity of escin, a broader evaluation of the toxicity of various glycosylated triterpenoids is warranted. This assessment should encompass their impact on microbial hosts, such as *S. cerevisiae*, including effects on cell growth, membrane integrity, and overall cellular physiology. Insights gained from such research can inform the development of more resilient yeast strains capable of withstanding the challenges posed by glycosylated triterpenoids.

The investigation and engineering of yeast tolerance to escin and other glycosylated triterpenoids represent another promising research direction. Given the influence of yeast sterol composition on their susceptibility to escin, there is an opportunity to explore engineering strategies that enhance yeast tolerance. These strategies may involve modifying sterols without compromising yeast growth, thereby enhancing their resistance to glycosylated triterpenoids.

Additionally, the potential use of alternative yeast hosts should be considered. Yeast species like *Y. lipolytica*, could serve as improved platforms for glycosylated triterpenoid production. These alternative hosts may offer advantages in terms of mitigating the toxic effects of glycosylated triterpenoids, potentially by sequestering them in lipid bodies, as has been observed with terpenes (Matthäus *et al*., 2014; Gao

et al., 2017; Zhang *et al*., 2020). Further exploration is needed to ascertain whether *Y. lipolytica* and similar yeast hosts can effectively manage glycosylated triterpenoids.

In conclusion, the future of glycosylated triterpenoid research in yeast holds considerable promise, with opportunities for innovation and advancement in various aspects of production, toxicity assessment, yeast tolerance enhancement, and the exploration of alternative yeast hosts. These endeavours are poised to contribute to the broader field of metabolic engineering and the utilisation of glycosylated triterpenoids across diverse industries and applications.

7.3 Closing comments

In this thesis, the *erg3Δ* sterol biosynthesis mutant was widely described and investigated due to its differing sterol content compared to WT *S. cerevisiae*. The difference in membrane sterol composition allowed for the increased tolerance to escin and gave insight into the mechanisms of action of escin on the yeast cell membrane. However, the introduction of an *erg3Δ* mutation in erythrodiol and other triterpenoid-producing strains did not increase the amount of triterpenoid produced.

In conclusion, this thesis represents a significant step in understanding the intricacies of glycosylated triterpenoid biosynthesis in yeast. While challenges persist, the research contributes valuable insights into genetic modifications, metabolic pathways, and cellular responses. The pursuit of triterpenoid biosynthesis in *S. cerevisiae* holds promise for diverse applications, contributing to the broader field of metabolic engineering and natural product synthesis. Future endeavours can build upon these findings, promoting innovation and advancements in glycosylated triterpenoid research.

Acknowledgements

First and foremost, I would like to express my deepest gratitude to my supervisor, Professor Susan Rosser, for granting me the opportunity to pursue this PhD in her lab. Her words of encouragement and unwavering support throughout these four years have been invaluable. Thank you for taking a chance on me, giving this weirdo from a council estate the chance of a lifetime. I would also like to extend my heartfelt thanks to my second supervisor, Dr Tessa Moses, for keeping me focused and grounded. Your guidance and reassurance have been instrumental in helping me reach the finish line. A very special thank you goes to Dr Emily Johnston, who has been an exceptional mentor in the lab, patiently answering my endless stream of questions and taking the time to read and give feedback on this thesis. I am also grateful to my industrial supervisor, Sarah Hosking, for her valuable advice and provision of samples.

To my examiners, Professor Anne Osbourn and Dr Joanna Sadler, thank you for taking the time to read my thesis, give constructive feedback and for the discussion during the viva.

Thank you to my funders, The Industrial Biotechnology Innovation Centre (IBioIC) as without, this PhD would not have happened. Thanks to Dr Ian Archer, Dr Mary Doherty, Dr Kirsty Robb and Stephen Gordon and all the staff that have come and gone throughout the years for your hard work.

To the Rosser Lab, I cannot begin to express my appreciation. Throughout these four years, you have been an incredible source of support, never making me feel inadequate or unworthy. Thank you for always combatting my imposter syndrome. I want to give a special mention to my fellow PhD candidates, Ben and James. It has been a challenging journey, but we made it through together! Your presence has provided the stability I needed, both as lab mates and friends. I would also like to thank

Alex for being the glue that binds us all, constantly bringing laughter into our lives and fostering a friendship that goes beyond mere colleagues.

I extend my thanks to my committee chair, Dr Karl Burgess, his lab group, and the EdinOmics team, whose thought-provoking questions have pushed me to think beyond my limits and for their support with GC- and LC-MS. A special thanks to Georgie for being a voice of reason throughout this journey. I would also like to thank Dr Dave Kelly and Dr Toni McHugh for their help with confocal microscopy and imaging. As well as this, many thanks to all those who provided samples and strains, in particular Dr Jan Milinsky who supplied the *S. cerevisiae* sur7m-RFP nce102-GFP strains.

To my close friends Charlie, Lannie, Sophie, Aleesa, Bing, Kei, Nas and Robbie. I cannot thank you enough for being there for me during the toughest times and for believing in me when I didn’t believe in myself.

Thank you, Mum, Dad, Liam, Jack and Ciaran for never pressuring me in any direction and for allowing me to pursue my dreams. Your love and support have been beyond measure, and our daily chats have always brought a smile to my face. Thanks for giving me your brains Mum! Lastly, Graeme, I struggle to find the words to express how much you have guided me in the right direction, nurtured my confidence, and supported me throughout this journey. I could not have completed this without your love, patience and support. Thank you.

Appendix A

Copy of “Yeast lacking the ergosterol biosynthesis gene *ERG3* are tolerant to the anti-inflammatory triterpenoid saponin escin” by Emily Johnston, Jess Tallis, Edward Cunningham-Oakes, Tessa Moses, Simon J. Moore, Sarah Hosking and Susan J. Rosser. Published in August 2023 in Scientific Reports.

scientific reports

Check for updates

OPEN

Yeast lacking the sterol C-5 desaturase Erg3 are tolerant to the anti-inflammatory triterpenoid saponin escin

Emily J. Johnston[1✉], Jess Tallis[1], Edward Cunningham-Oakes[2], Tessa Moses[3], Simon J. Moore[4], Sarah Hosking[5] & Susan J. Rosser[1✉]

Escin is a mixture of over 30 glycosylated triterpenoid (saponin) structures, extracted from the dried fruit of horse chestnuts. Escin is currently used as an anti-inflammatory, and has potential applications in the treatment of arthritis and cancer. Engineered yeast would enable production of specific bioactive components of escin at industrial scale, however many saponins have been shown to be toxic to yeast. Here we report that a *Saccharomyces cerevisiae* strain specifically lacking the sterol C-5 desaturase gene *ERG3*, exhibits striking enhanced tolerance to escin treatment. Transcriptome analyses, as well as pre-mixing of escin with sterols, support the hypothesis that escin interacts directly with ergosterol, but not as strongly with the altered sterols present in *erg3Δ*. A diverse range of saponins are of commercial interest, and this research highlights the value of screening lipidome mutants to identify appropriate hosts for engineering the industrial production of saponins.

Saponins (glycosylated triterpenoids) are amongst the most numerous and diverse groups of plant natural products, with huge potential in many industries[1,2]. In addition to pharmaceutical applications as vaccine adjuvants[3] and anti-inflammatories[4], saponins also have potential in therapeutics against arthritis, obesity, cancer and Alzheimer's disease[5–7]. Some saponins have also been used as foam stabilisers and emulsifiers in cosmetics and soaps[8]. Many saponin compounds have haemolytic properties, and in nature saponins are generally considered to function as plant defence compounds, although few studies have investigated the degree and mechanism of antifungal activity[9–16]. This is of relevance towards understanding the biological role of saponins in plants, and towards the engineering of yeast as factories for saponin production. Whilst saponin extraction from plants is seasonal and of limited yield, yeast can easily be engineered to express plant genes, and there is established infrastructure for large-scale rapid yeast culture and product extraction. In contrast to bacteria, yeast have endoplasmic reticulum (ER) which support the activity of ER-localised cytochrome P450 enzymes that are involved in saponin biosynthesis. Production in engineered yeast also enables targeted saponin structures to be produced and extracted at high purity, in contrast to the mixtures of saponins which are extracted from plants.

Escin (also termed Aescin) is a mixture of over 30 saponin structures extracted from fruit of the horse chestnut tree *Aesculus hippocastanum* L. Approximately 60% of escin is β-escin (Fig. 1a), comprising a protoaescigenin triterpenoid backbone, esterified at the C-22 position with acetic acid, and at the C-21 position with angelic or tiglic acid[17]. Escin has potent anti-inflammatory properties, and is used in the treatment of chronic venous insufficiency, postoperative oedema and haemorrhoids[4,18,19]. Escin also has promise in the treatment of arthritis[20,21] and cancer; escin interferes with tumour cell cycles, induces cancer cell apoptosis, inhibits cell migration, and increases the impact of chemotherapy drugs[22]. Whilst horse chestnut provides a seasonal supply of a mixture of saponins, engineered yeast could potentially enable year-round industrial-scale manufacture of specific active components of this potent therapeutic, however escin has previously been shown to have antifungal activity[23,24].

[1]Centre for Engineering Biology, University of Edinburgh, Edinburgh EH9 3BD, UK. [2]Department of Infection Biology and Microbiomes, Institute of Infection, Veterinary and Ecological Sciences, University of Liverpool, Liverpool L69 7ZB, UK. [3]EdinOmics, RRID:SCR_021838, University of Edinburgh, Max Born Crescent, Edinburgh EH9 3BF, UK. [4]Genetic Science Division, Thermo Fisher Scientific, 7 Kingsland Grange, Warrington, Cheshire WA1 4SR, UK. [5]Unilever R&D Port Sunlight, Quarry Road East, Bebington, Wirral CH63 3JW, UK. ✉email: emily.johnston@ed.ac.uk; susan.rosser@ed.ac.uk

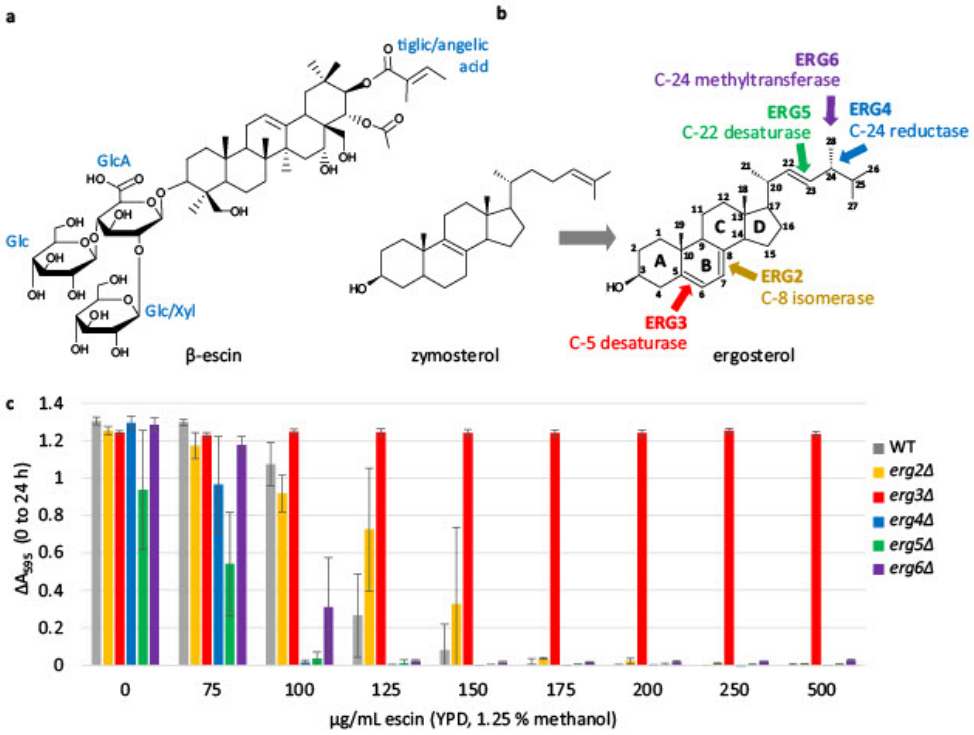

Figure 1. (**a**) Structure of β-escin, which comprises approximately 60% of saponins in escin[17]. The protoaescigenin backbone is esterified at C-22 with acetic acid and at C-21 with either angelic or tiglic acid (tiglic acid shown). Glucuronic acid (GlcA) is conjugated at C-3. Two glucose (Glc) sugars are attached to the glucuronic acid, one of which can be substituted with xylose (Xyl). (**b**) Activity of enzymes involved in the latter stages of ergosterol biosynthesis, from the precursor zymosterol. The reactions are depicted in Fig. S1. (**c**) Growth in microplate cultures indicated by ΔA_{595} (0–24 h). Three biological replicates ± standard deviation (SD).

Many saponins, including escin, have been reported to interact with the mammalian sterol cholesterol[9,17,25]. We hypothesised that escin may inhibit fungal growth via interaction with ergosterol, which comprises 12 mol% of the *S. cerevisiae* lipidome, and is the predominant sterol at the yeast plasma membrane[26,27]. In support of this, it has recently been shown that supplementation of *Leptosphaeria maculans* culture with ergosterol alleviates growth inhibition mediated by escin treatment[24]. We further hypothesised that yeast strains accumulating sterols other than ergosterol, may exhibit enhanced escin tolerance. Here we report that a *S. cerevisiae* strain lacking the sterol C-5 desaturase Erg3, exhibits striking enhanced tolerance to high concentrations of escin, supporting our hypotheses. Therefore, an engineered strain lacking Erg3 would enable microbial production of escin saponins.

Results

Yeast lacking the C-5 sterol desaturase Erg3 exhibit striking enhanced tolerance to escin. We hypothesised that if escin toxicity is mediated by direct interaction with ergosterol, then ergosterol biosynthesis mutants may differ in escin tolerance. Sterols are considered to have a key role in maintaining homeostasis of plasma membrane dynamics[28], however yeast strains lacking enzymes which catalyse the final five steps in ergosterol biosynthesis (Erg2, Erg3, Erg4, Erg5 or Erg6; Figs. 1b and S1) are viable. Due to the substrate promiscuity of the latter enzymes in ergosterol biosynthesis, these deletion mutants accumulate a mixture of sterol structures, which differ from ergosterol in the number and position of double bonds in the sterol B-ring, and the sterol side chain[29]. We used microplate cultures of the wild type strain BY4741 (WT) and mutants from the Yeast Deletion Collection[30], to assess growth of the ergosterol biosynthesis mutants in complex rich medium (YPD) in the presence and absence of escin (Fig. 1c). Sterol extraction and analysis by Gas Chromatography–Mass Spectrometry verified that ergosterol did not accumulate in the mutant strains (Figs. S2 and S3). The Minimum Inhibitory Concentration (MIC) of escin for the WT strain in YPD medium was 150 μg/mL. Similar MICs were observed

for the *erg2Δ*, *erg4Δ*, *erg5Δ* and *erg6Δ* strains, however growth of the *erg3Δ* strain was uninhibited up to the highest concentration tested (1000 µg/mL; Fig. S4).

Transcriptome analysis. In order to further explore the impact of escin on WT cells, and the mechanism of escin tolerance in *erg3Δ*, we analysed the transcriptomes of WT, *erg3Δ* and *erg6Δ* cells, treated with 0 or 100 µg/mL escin in YPD for 1 h, in shake flask cultures. The *erg6Δ* strain was included in this experiment as this strain shares many similar phenotypes with *erg3Δ*[29], but does not have enhanced escin tolerance (MIC 150 µg/mL; Fig. 1c). Within the scope of this experiment, we also analysed the transcriptomes of *erg3Δ* and *erg6Δ* cells which were treated with 75 µg/mL escin for 1 h.

K means clustering of the 2000 genes with the most variable expression levels is shown in Fig. S5, with full details of gene set enrichment analysis included in the Supplementary Information (SI). Cluster B genes (n = 82) are in general expressed at a higher level in *erg3Δ* and *erg6Δ* compared to WT under all conditions and, as anticipated, this cluster is enriched in genes relating to sterol biosynthesis, sterol transport, siderophore transport, and regulation of transcription by glucose. Cluster A genes (n = 821) are downregulated in WT and *erg6Δ* in response to escin treatment. This cluster is enriched in genes relating to ribosome biogenesis and RNA processing. Cluster C (n = 897) and D (n = 200) genes are in general upregulated in WT and *erg6Δ* in response to escin treatment, with cluster D genes upregulated to a greater extent than cluster C. Cluster D is enriched in genes relating to trehalose, mannose, fructose and glutamate metabolism, as well as glycolysis and cell wall organisation. Cluster D is also enriched in genes associated with responses to osmotic, oxidative, temperature and starvation stress. Cluster C is enriched in genes relating to late nucleophagy, lipid catabolism, sulphur assimilation, the tricarboxylic acid cycle and gluconeogenesis.

Differentially Expressed Genes (DEGs) with ≥ 2-fold differential expression between conditions of interest (Fig. 2) are discussed in more detail below, with full gene set enrichment details in SI.

Impact of *ERG3* and *ERG6* deletion on the yeast transcriptome. Comparing the transcriptomes of strains under control conditions reveals interesting differences between the mutant strains and WT. Deletion of *ERG6* results in a greater number of DEGs (n = 162) than *ERG3* deletion (n = 106). In both mutants, upregulated DEGs are enriched in genes relating to sterol biosynthesis and transport, including the sterol sensor and transcriptional activator *UPC2* (Fig. S6). In contrast, only a very small number of genes involved in sphingolipid and phospholipid supply are upregulated (*YSR3*, *RSB1*, *FAA2* and *ELO2* in both strains, and additionally *SUR1* in *erg6Δ*; Fig. S7), although large changes in sphingolipid composition have been reported for sterol biosynthesis mutants[31].

Anaerobic response cell wall mannoprotein genes are also highly upregulated in both strains (Fig. S8). Several steps of ergosterol biosynthesis require oxygen and iron as cofactors, and there is complex crosstalk between the regulatory responses to ergosterol, oxygen and iron[32–35]. A number of iron starvation response genes[36] are upregulated in *erg6Δ* (*FIT2*, *FIT3*, *ARN2*, *SIT1*, *TIS11*), but not *erg3Δ*, relative to WT (Fig. 3a). It has recently been reported that the iron-sensing transcription factor Aft1, which usually shuttles between the cytoplasm and nucleus, accumulates in the vacuoles of ergosterol-diminished *upc2Δ* cells[37]. Our data suggests that this signalling pathway may be impacted to differing extents in *erg6Δ* and *erg3Δ*.

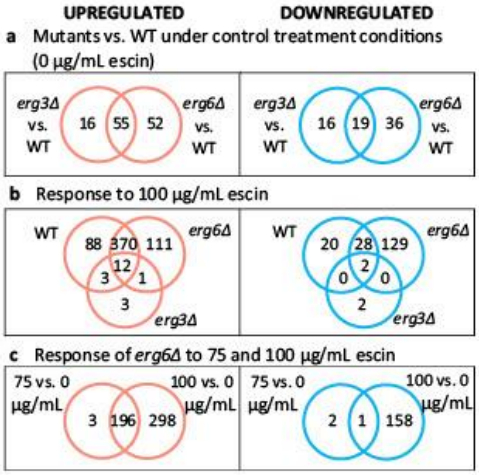

Figure 2. Venn diagrams for Differentially Expressed Genes (DEGs). DEGs have ≥ 2-fold differential expression, and a False Discovery Rate (FDR) ≤ 0.1.

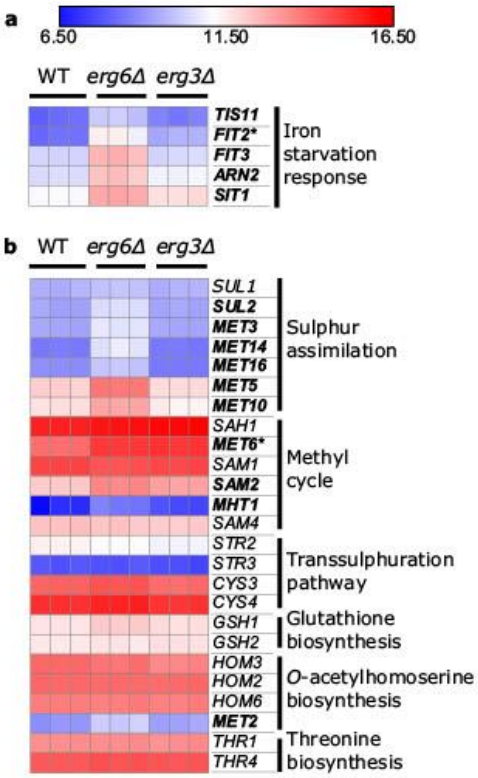

Figure 3. The *erg6*Δ strain exhibits elevated expression of sulphur assimilation genes and iron starvation response genes. Expression of genes relating to (**a**), iron homeostasis and (**b**), the methionine biosynthesis pathway, under control conditions, units log2(CPM + 4). Bold; gene upregulated ≥ 2-fold in *erg6*Δ versus WT. Asterisk; gene upregulated ≥ 2-fold in *erg3*Δ versus WT (FDR ≤ 0.1).

Methionine metabolism genes are also upregulated in *erg6*Δ, but not *erg3*Δ (Fig. 3b). Specifically, the upregulated genes are associated with the sulphur assimilation pathway (*SUL2*, *MET3*, *MET14*, *MET16*, *MET5*, *MET10*), and the methyl cycle (*MET6*, *SAM2*, *MHT1*) which generates S-adenosylmethionine (SAM) (Fig. S9). The Erg6 enzyme uses the methyl donor SAM to methylate zymosterol[38], and an Erg6-deficient strain has previously been found to accumulate SAM, which was attributed to reduced SAM consumption[39].

Both strains downregulate a number of genes involved in mating (Fig. 4). These are mainly genes which are involved in conjugation between mating schmoo tips (*FUS1*, *AGA1*, *AGA2*, *FIG1*, *SHC1*), and notably reduced mating efficiency has previously been described for ergosterol biosynthesis mutants[40,41].

Both strains also express *NCE102* at a lower level than WT (42% of WT level in *erg3*Δ, and 40% of WT level in *erg6*Δ). Although primarily localised at plasma membrane eisosomes, Nce102 has recently been reported to have a role in vacuole fusion[42], and vacuoles are highly fragmented in many ergosterol biosynthesis mutant strains, including *erg3*Δ, although not *erg6*Δ[43–45].

It is notable that several DEGs between the mutants and WT are of unknown function; 20 and 29 upregulated DEGs, and 10 and 13 downregulated DEGs, in *erg3*Δ and *erg6*Δ respectively.

Transcriptome responses to escin treatment. In response to 100 µg/mL escin, the WT and *erg6*Δ strains upregulate 473 and 494 genes, respectively (Fig. 2b). These DEGs are enriched in genes which are also associated with responses to desiccation, osmotic stress, oxidative stress, temperature, chemical treatment and changes in nutrient levels (SI). Treatment of *erg6*Δ cells with 75 µg/mL escin resulted in upregulation of 199 genes (Fig. 2c). These 199 DEGs are enriched in genes which are associated with responses to oxidative stress, chemical stress and starvation (SI).

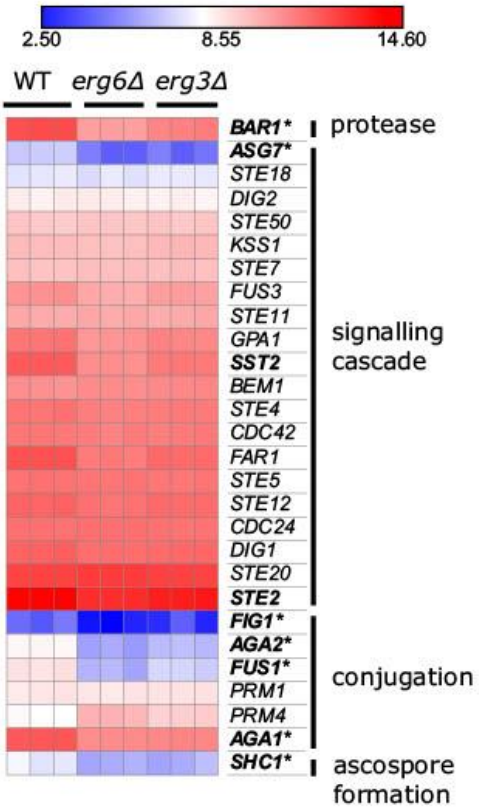

Figure 4. The *erg3*Δ and *erg6*Δ strains exhibit reduced expression of mating genes. Expression of genes relating to mating, units log2(CPM + 4). Bold; downregulated ≥ 2-fold in the comparison *erg6*Δ 0 µg/mL escin versus WT 0 µg/mL escin. Asterisk; downregulated ≥ 2-fold in the comparisons *erg3*Δ 0 µg/mL escin versus WT 0 µg/mL escin (FDR ≤ 0.1).

The impact of escin treatment on central carbon metabolism genes is shown in Fig. S10. In response to 100 µg/mL escin, both WT and *erg6*Δ strongly upregulate genes relating to the biosynthesis of trehalose, glycogen and glycerol. The glucose polymer glycogen is considered to primarily function as a storage carbohydrate, which has little impact on the internal osmotic pressure of the cell[46,47]. The disaccharide trehalose is considered to have a key role in protecting the structure of lipid membranes and proteins, by displacing water from lipid bilayers and protein surfaces, and preventing aggregation of denatured proteins which would prevent their subsequent refolding[47]. Glycerol acts as a key osmolyte during hyperosmotic stress, and forms the backbone of phospholipids and storage lipid triacylglycerols[48]. The upregulation of trehalose, glycogen and glycerol biosynthesis is part of a general response to environmental change[47–49]. Additionally, both WT and *erg6*Δ strains upregulate genes encoding proteins of the Glucose Induced degradation Deficient (GID) complex, which negatively regulates gluconeogenesis, in favour of glycolysis, by initiating polyubiquitination and degradation of fructose-1,6-bisphosphatase[50] (Fig. S11).

In response to 100 µg/mL escin, both WT and *erg6*Δ also upregulate genes encoding enzymes of the γ-aminobutyric acid (GABA) shunt pathway (Fig. S12) which degrades glutamate via GABA. In yeast, this pathway has been shown to be important for heat and oxidative stress tolerance[51].

The upregulated DEGs are also enriched in genes relating to cell wall organisation, including sporulation and chitin biosynthesis (Fig. S13). Crosstalk between the High Osmolarity Glycerol 1 (Hog1) and Cell Wall Integrity (CWI) mitogen-activated protein kinase (MAPK) pathways mean that it is difficult to dissect specific stresses which are initiating the upregulation of these genes, without utilising mutants which are defective in specific branches of these signalling pathways[52–54].

Many autophagy-related genes are upregulated in WT and *erg6*Δ in response to escin treatment (Fig. S14), including core phagosome components, and proteins involved in the cytoplasm-to-vacuole pathway, which selectively delivers hydrolases to the vacuole[55]. In response to 100 µg/mL escin, more autophagy-related genes are upregulated ≥ 2-fold in the *erg6*Δ strain than WT (11 vs. 7).

The *erg6*Δ strain also downregulates more genes than WT in response to 100 µg/mL escin (159 vs. 50), and these DEGs are enriched in genes relating to ribosome biogenesis and translation. These processes require substantial amounts of energy[56], and their downregulation is part of a general stress response, in which resources are diverted to stress resistance rather than cell proliferation[57,58].

If escin sequestered ergosterol from cells, or inhibited sterol sensing by interaction with either ergosterol or a sterol sensor, then we might expect to see a transcriptional change in sterol biosynthesis genes such as *ERG2* and *ERG11* in response to escin treatment. These genes are regulated by the sterol sensors and transcriptional activators Upc2 and Ecm22, in response to ergosterol content[59,60]. Differential expression of ergosterol biosynthesis genes is not observed (Fig. S6), although there is statistically significant but small upregulation of *UPC2* in each strain (1.3, 1.9 and 1.5-fold for WT, *erg6*Δ and *erg3*Δ respectively). A small number of genes related to sphingolipid supply are upregulated in response to escin in WT and *erg6*Δ (Fig. S7), although it should be noted that much of sphingolipid regulation is post-translational[31].

In contrast to the large transcriptome changes observed for the WT and *erg6*Δ strains, the *erg3*Δ strain upregulates only 19 genes in response to 100 µg/mL escin, and downregulates 4 (Fig. S15). Most of these DEGs are also differentially expressed in the WT and/or *erg6*Δ strain in response to escin treatment, with the exception of *HAP4* (encoding a regulator of respiration), *YOL163W* (considered non-functional), *YGL088W* (unknown function) and the cell wall mannoprotein genes *DAN1* and *DAN4*.

The *erg3*Δ transcriptome is not primed for the stress of escin treatment. In order to explore whether the escin response DEGs in the WT strain are already differentially expressed in *erg3*Δ under control conditions, potentially 'priming' *erg3*Δ for the stress of escin treatment, we compared DEGs in the comparisons WT 100 versus 0 µg/mL escin, and *erg3*Δ 0 µg/mL escin versus WT 0 µg/mL escin (Fig. S16a). Under control conditions, the *erg3*Δ strain has elevated expression of 18 genes which are also upregulated in WT in response to escin treatment, and lower expression of 5 genes which are downregulated in WT in response to escin treatment. A heatmap showing the expression levels of these overlapping genes is included in Fig. S16b. The majority of these genes are also differentially regulated in the *erg6*Δ strain under control conditions, and the *erg6*Δ strain does not exhibit the enhanced escin tolerance phenotype. The exceptions are *PAI3* (encoding a cytoplasmic proteinase A inhibitor), *SRL3* (encoding a cell cycle regulator), *HED1* (encoding a meiosis-specific protein), *MAL31* (encoding a maltose permease), *ARG3* (encoding ornithine carbamoyltransferase), *COS111* (encoding a mitochondrial protein), genes *YBR090C* and *YKR075C* of unknown function, and genes *YJR037W* and *YJL195C* which are unlikely to encode functional proteins.

Overall, this data shows that escin has no impact on growth and a negligible impact on the transcriptome of *erg3*Δ cells. This is not likely to be due to *erg3*Δ cells being already primed for the stresses induced by escin treatment, and is potentially attributable to the chemical composition of its membrane sterols.

Pre-mixing escin with ergosterol, but not brassicasterol, prevents escin-mediated growth inhibition. In order to explore the hypothesis that escin mediates toxicity by directly interacting with ergosterol, but not the altered sterols present in *erg3*Δ, we assessed the impact of treating WT cells with escin alone, or escin which had been pre-mixed with ergosterol in a 1:1 molar ratio. It was considered that if ergosterol interacts directly with escin, then an escin-ergosterol mixture would have reduced impact on WT growth than escin alone, due to reduced accessibility of the escin saponins. Notably, yeast cells do not import exogenous sterols under aerobic conditions[37].

The experiment was carried out using microplate cultures and complete supplement mixture (CSM) media, as opposed to YPD, as the exact content of CSM is defined, whereas YPD is a rich media containing complex molecules from yeast extract, which may also interact with escin and/or sterols. Previous studies have reported ergosta-7,22-dienol to be the predominant sterol in yeast lacking Erg3, with episterol and ergosta-7-enol also accumulating[31,43]. When sterol content was verified by Gas Chromatography-Mass Spectrometry (Figs. S2 and S3), the relative retention time of the largest sterol peak in the *erg3*Δ Total Ion Chromatogram corresponded to previous reports for ergosta-7,22-dienol, when the strain was grown in either YPD or CSM.

The MIC of escin in CSM media was determined to be 63 µg/mL for WT cells (Fig. 5b); 2.4-fold lower than in YPD. Meanwhile growth of the *erg3*Δ strain was uninhibited up to the highest concentration tested (500 µg/mL). When escin was pre-mixed with ergosterol in a 1:1 molar ratio, and the mixture added to cells, growth of the WT strain in the presence of 63 µg/mL escin was completely restored (Fig. 5c). Pre-mixing escin with ergosterol also restored the percentage of cells stained with the membrane impermeable dye propidium iodide to control treatment levels (Fig. S17), indicating decreased cell permeability and/or increased cell viability.

The sterols present in *erg3*Δ are of limited availability, and so for comparison we also assessed growth when escin was pre-mixed with the phytosterol brassicasterol, which also has one double bond in the B-ring, although the position of this is between C-5 and C-6 (Fig. 5a). In contrast to the restored growth observed when escin was pre-mixed with ergosterol, restoration of WT growth was not observed when escin was pre-mixed with brassicasterol in a 1:1 molar ratio (Fig. 5c).

This supports the hypotheses that escin interacts directly with ergosterol, and that small changes in sterol structure can have a large impact on the strength of sterol-saponin interactions.

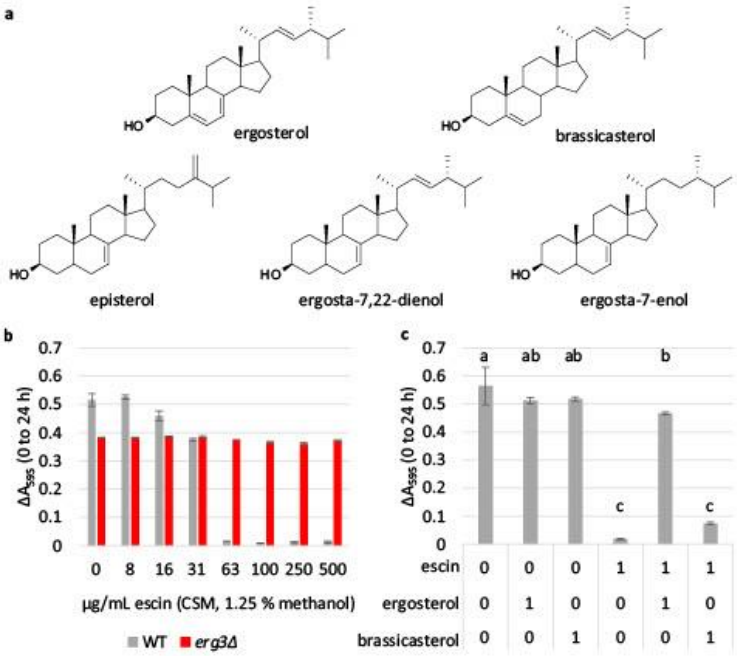

Figure 5. Restoration of growth when escin is pre-mixed with ergosterol, but not brassicasterol. (**a**) Structure of ergosterol (the predominant sterol in *S. cerevisiae* plasma membrane), brassicasterol (a plant sterol), and sterols which have been identified as accumulating in the *erg3*Δ strain (episterol, ergosta-7,22-dienol, ergosta-7-enol). (**b**) and (**c**), Growth in microplate cultures indicated by ΔA_{595} (0–24 h). Three biological replicates ± standard deviation (SD). In (**b**), the MIC of escin in CSM media is 63 µg/mL for WT, which is 2.4-fold lower than in rich complex medium. In (**c**), WT cells were grown in the presence of 0 or 63 µg/mL escin (1.25% methanol), alone or pre-mixed with ergosterol or brassicasterol in a 1:1 molar ratio. Ergosterol and brassicasterol only controls were included. Statistics: one-way ANOVA with post-hoc Tukey HSD test, conditions not connected by the same letter are significantly different ($p \leq 0.05$).

Discussion

Saponins are a diverse group of high-value plant natural products, with huge potential in many industries. A recent increase in the identification of plant genes involved in saponin biosynthesis has enabled the engineering of yeast for saponin production[61], however many saponins, including escin, are known to have antifungal activity and/or a lytic effect on red blood cells and synthetic membranes[9,23,25,62,63]. It is therefore likely that some saponins will inhibit yeast growth, particularly at high concentrations, which would limit productivity. Here, we explore the impact of the saponin mixture escin on yeast cells, as escin has potent therapeutic properties[4], and production of specific escin saponins in yeast would facilitate cost-effective biosynthesis and purification of bioactive components, at industrial scale.

We report that the MIC of escin to WT yeast is 150 µg/mL in rich undefined (YPD) medium and 63 µg/mL in synthetic defined (CSM) medium. In addition to the richer YPD medium containing complex precursors to many biosynthetic processes, these media differ in carbon content, buffering capacity and osmolarity[64]. These differences are likely to contribute to the difference in MIC observed.

In order to investigate the hypothesis that escin inhibits yeast growth via interaction with ergosterol, we assessed the impact of escin on the growth of mutants in ergosterol biosynthesis. We identified that escin has negligible impact on growth of the sterol C-5 desaturase mutant *erg3*Δ. There was also little impact on the transcriptome of *erg3*Δ cells in response to escin treatment. In contrast there are large transcriptome changes in WT and *erg6*Δ cells in response to escin treatment, and the upregulated processes correspond to those induced in response to osmotic, oxidative, temperature and starvation stress. Due to cross-over between stress signalling pathways[52–54], the specific initial perturbation which induces the transcriptome response cannot be pinpointed using transcriptome data alone. A comparison between genes which are differentially expressed in the WT strain in response to escin treatment, and genes which are differentially expressed in the *erg3*Δ strain compared to WT under control conditions, indicates that the *erg3*Δ transcriptome is not 'primed' for the stress of escin treatment.

The finding that pre-mixing escin with ergosterol in a 1:1 molar ratio alleviates the growth inhibitory impact of escin to WT cells, supports the hypothesis that the toxicity of escin to yeast is mediated by direct interaction between escin saponins and ergosterol.

Phenotypes of the viable ergosterol biosynthesis mutants, and relevance to yeast cell factories, have recently been reviewed[29]. Mutants in ergosterol biosynthesis are usually more susceptible to antifungal treatment than WT cells[29]. This has been attributed to increased membrane permeability, hyperpolarisation of the plasma membrane, and reduced activity of efflux pumps such as Pdr5p in the mutant cells, resulting in increased intracellular accumulation of the antifungal drugs[29]. An exception to this is the enhanced fluconazole tolerance of *Candida albicans* strains lacking the *C. albicans* Erg3 enzyme[29]. Fluconazole inhibits the lanosterol 14-α-demethylase enzyme Erg11, resulting in accumulation of 14α-methylergosta8-24(28)dienol in cells with functional Erg3, and 14α-methyl-fecosterol in cells lacking Erg3 activity. It has been hypothesised that 14α-methylergosta8-24(28) dienol is detrimental to *C. albicans* cells[65].

Ergosterol biosynthesis mutants also exhibit varying degrees of enhanced tolerance to the polyene antifungals nystatin and amphotericin B[29]. Nystatin binds ergosterol in synthetic liposomes, forming pores at high concentrations[66], whilst amphotericin B sequesters ergosterol into cell surface aggregates[67]. It is plausible that the sterols present in the mutant strains do not interact as strongly with nystatin and amphotericin B as ergosterol does. Additionally, *S. cerevisiae erg6*Δ cells exhibit increased tolerance to the steroidal glycoalkaloid α-tomatine, whilst *erg3*Δ cells exhibit enhanced tolerance to tomatidine (the aglycone of α-tomatine)[68]. The steroidal glycoalkaloid α-tomatine has been reported to increase the permeability of synthetic vesicles via interaction with sterols[69], and again, it is plausible that α-tomatine and tomatidine interact with the sterols present in *erg6*Δ and *erg3*Δ with lower affinity than ergosterol.

Recently, the impact of escin on synthetic model membranes has been studied using differential scanning calorimetry, wide-angle X-ray scattering, small-angle X-ray scattering and small angle neutron scattering. These studies indicate that escin increases the rigidity of 1,2-dimyristoyl-*sn*-glycero-3-phosphocholine (DMPC) phospholipid bilayers below the DMPC melting temperature, and increases the fluidity of DMPC bilayers above the DMPC melting temperature[17,62,63]. The membrane softening effect is likely due to headgroup interactions between the glycoside component of escin and the phosphocholine component of DMPC, whilst the stiffening effect is proposed to be due to incorporation of the rigid triterpenoid backbone of escin saponins into the lipid bilayer[17]. When cholesterol is included in DMPC bilayers, strong complexes form between cholesterol and escin saponins, reducing the amount of free escin available to interact with the phospholipid membrane, and resulting in deformation of small unilamellar vesicles[25]. It is plausible that escin saponins also interact with ergosterol, and similarly impact plasma membrane dynamics and organisation. This might induce pore formation, disrupt plasma membrane stability, and/or impact the lateral organisation and activity of plasma membrane lipids and proteins.

The finding that pre-mixing escin with ergosterol alleviates the inhibitory impact of escin, whilst pre-mixing with brassicasterol does not, and that *erg3*Δ mutants exhibit increased tolerance to escin treatment, whilst *erg2*Δ, *erg4*Δ, *erg5*Δ and *erg6*Δ do not, highlights that small changes in sterol and plausibly saponin structure can have a large impact on saponin bioactivity. The disruption of the C-5 desaturase gene *ERG3* is a promising engineering strategy for the production of escin saponins in engineered yeast. Strains with different lipidomes may exhibit enhanced tolerance to other saponin structures, and overall, this research demonstrates that screening the product tolerance of lipidome mutants should be a crucial prerequisite to the engineering of yeast strains for saponin production.

Methods

Yeast strains and media. This study used *Saccharomyces cerevisiae* BY4741 as the wild type background strain, and deletion mutants from the Yeast Deletion Collection[30]. YPD media; 10 g/L yeast extract, 20 g/L peptone, 20 g/L glucose. CSM media; 6.7 g/L yeast nitrogen base (Sigma Y0626), 790 mg/L Complete Supplement Mixture (Formedium DCS001), 20 g/L glucose.

Microplate cultures for growth studies. Cells from overnight cultures were washed in sterile water and inoculated into 96 well plates (Thermo Scientific #167008), in 100 µL culture volumes, with starting OD_{600} 0.2 (equivalent to A_{595} 0.04 in the plate reader). Plates were incubated in Tecan Sunrise plate readers at 30 °C, with 'normal' shaking level. To assess growth A_{595} was recorded, which correlates with cell density.

Extraction and analysis of yeast sterols. Yeast strains were inoculated into YPD or CSM media at OD_{600} 0.25 and incubated for 24 h (30 °C, 200 rpm). The cell density of each culture was then adjusted to OD_{600} 2.7, and approximately 36.9×10^6 cells (from 1.5 mL of culture) were collected by centrifugation, and lysed in 500 µL lysis buffer (20% KOH, 50% ethanol, 80 nM coprostanol) for 10 min (100 °C). Sterols were extracted into 500 µL hexane three times. Organic phases were pooled, and 1 mL evaporated to dryness using a GeneVac EZ-2 Elite evaporator. Samples were trimethylsilylated with 50 µL pyridine:N-methylsilyltrifluoroacetamine (1:4) directly prior to Gas Chromatography Time-Of-Flight Mass Spectrometry (GC/QTOF-MS). Full GC/QTOF-MS details are included in SI.

Transcriptome analysis. Overnight cultures in YPD media were used to inoculate 20 mL YPD in 100 mL conical flasks at OD_{600} 0.1. Cultures were grown (30 °C, 200 rpm shaking) to mid-log phase, and then treated with 0, 75 or 100 µg/mL escin in water for 60 min. Cell pellet samples of approximately 2×10^7 cells were frozen in liquid nitrogen and stored at − 80 °C prior to RNA extraction. For RNA extraction, sequencing and data analysis methods, see Supplementary Information. RNA sequencing was carried out at the University of Liverpool Centre for Genomic Research.

Propidium iodide (PI) assays. To prepare chambered slides (Ibidi 80807), 100 µL of 2 mg/mL concanavalin A (Sigma C2010) was pipetted into each well, incubated for 30 s, and aspirated off. Wells were then washed with water three times. Yeast was grown to OD_{600} 0.4 in CSM media, and 400 µL transferred to each well. After 5 min, the culture was aspirated off, wells were washed three times with treatment media (400 µL PBS 1.25% methanol, varying escin concentrations) and incubated for 1 h (30 °C, 200 rpm, dark). Cells were then washed three times with 400 µL of PBS containing 5 µg/mL PI (Invitrogen P3566), incubated for 20 min (30 °C, 200 rpm, dark), washed three times with 400 µL PBS and imaged on a Leica DMI8 inverted microscope (540-580/592-668 ex/em).

Data availability

Supplementary figures, methods and details of Differentially Expressed Genes and Gene Set Enrichment results are included in supplementary files. RNA sequencing data is available at the European Nucleotide Archive (Project Accession Number PRJEB61952).

Received: 10 May 2023; Accepted: 8 August 2023
Published online: 21 August 2023

References

1. Thimmappa, R., Geisler, K., Louveau, T., O'Maille, P. & Osbourn, A. Triterpene biosynthesis in plants. *Annu. Rev. Plant Biol.* 65, 225–257 (2014).
2. Vincken, J.-P., Heng, L., de Groot, A. & Gruppen, H. Saponins, classification and occurrence in the plant kingdom. *Phytochemistry* 68, 275–297 (2007).
3. Zhu, D. & Tuo, W. QS-21: A potent vaccine adjuvant. *Nat. Prod. Chem. Res.* 3, e113 (2016).
4. Gallelli, L. Escin: A review of its anti-edematous, anti-inflammatory, and venotonic properties. *Drug Des. Dev. Ther.* 13, 3425–3437 (2019).
5. den Brok, M. H. *et al.* Saponin-based adjuvants induce cross-presentation in dendritic cells by intracellular lipid body formation. *Nat. Commun.* 7, 13324 (2016).
6. Liao, Y. *et al.* Saponin surfactants used in drug delivery systems: A new application for natural medicine components. *Int. J. Pharm.* 603, 120709 (2021).
7. Zhang, X., Zhang, S., Yang, Y., Wang, D. & Gao, H. Natural barrigenol-like triterpenoids: A comprehensive review of their contributions to medicinal chemistry. *Phytochemistry* 161, 41–74 (2019).
8. Schreiner, T. B., Dias, M. M., Barreiro, M. F. & Pinho, S. P. Saponins as natural emulsifiers for nanoemulsions. *J. Agric. Food Chem.* 70, 6573–6590 (2022).
9. Augustin, J. M., Kuzina, V., Andersen, S. B. & Bak, S. Molecular activities, biosynthesis and evolution of triterpenoid saponins. *Phytochemistry* 72, 435–457 (2011).
10. Bouarab, K., Melton, R., Peart, J., Baulcombe, D. & Osbourn, A. A saponin-detoxifying enzyme mediates suppression of plant defences. *Nature* 418, 889–892 (2002).
11. Moses, T., Papadopoulou, K. K. & Osbourn, A. Metabolic and functional diversity of saponins, biosynthetic intermediates and semi-synthetic derivatives. *Crit. Rev. Biochem. Mol. Biol.* 49, 439–462 (2014).
12. Nakayasu, M., Yamazaki, S., Aoki, Y., Yazaki, K. & Sugiyama, A. Triterpenoid and steroidal saponins differentially influence soil bacterial genera. *Plants* 10, 2189 (2021).
13. Papadopoulou, K., Melton, R. E., Leggett, M., Daniels, M. J. & Osbourn, A. E. Compromised disease resistance in saponin-deficient plants. *Proc. Natl. Acad. Sci.* 96, 12923–12928 (1999).
14. Augustin, J. M. *et al.* UDP-glycosyltransferases from the UGT73C subfamily in *Barbarea vulgaris* catalyze sapogenin 3-*O*-glucosylation in saponin-mediated insect resistance. *Plant Physiol.* 160, 1881–1895 (2012).
15. Wang, C. *et al.* Metabolite profiling and transcriptome analysis explains difference in accumulation of bioactive constituents in licorice (*Glycyrrhiza uralensis*) under salt stress. *Front. Plant Sci.* 12, 727882 (2021).
16. Yendo, A. C. A., de Costa, F., Gosmann, G. & Fett-Neto, A. G. Production of plant bioactive triterpenoid saponins: Elicitation strategies and target genes to improve yields. *Mol. Biotechnol.* 46, 94–104 (2010).
17. Geisler, R., Dargel, C. & Hellweg, T. The biosurfactant β-aescin: A review on the physico-chemical properties and its interaction with lipid model membranes and Langmuir monolayers. *Molecules* 25, 117 (2019).
18. Domanski, D. *et al.* Molecular mechanism for cellular response to β-escin and its therapeutic implications. *PLoS ONE* 11, e0164365 (2016).
19. Sirtori, C. R. Aescin: Pharmacology, pharmacokinetics and therapeutic profile. *Pharmacol. Res.* 44, 183–193 (2001).
20. Du, Y., Song, Y., Zhang, L., Zhang, M. & Fu, F. Combined treatment with low dose prednisone and escin improves the anti-arthritic effect in experimental arthritis. *Int. Immunopharmacol.* 31, 257–265 (2016).
21. Zhang, L. *et al.* Network pharmacology based research on the combination mechanism between escin and low dose glucocorticoids in anti-rheumatoid arthritis. *Front. Pharmacol.* 10, 280 (2019).
22. Cheong, D. H. J. *et al.* Molecular targets and anti-cancer potential of escin. *Cancer Lett.* 422, 1–8 (2018).
23. Franiczek, R., Gleńsk, M., Krzyżanowska, B. & Włodarczyk, M. β-Aescin at subinhibitory concentration (sub-MIC) enhances susceptibility of *Candida glabrata* clinical isolates to nystatin. *Med. Mycol.* 53, 845–851 (2015).
24. Trdá, L. *et al.* Dual Mode of the saponin aescin in plant protection: Antifungal agent and plant defense elicitor. *Front. Plant Sci.* 10, 1448 (2019).
25. Sreij, R. *et al.* Aescin-cholesterol complexes in DMPC model membranes: A DSC and temperature-dependent scattering study. *Sci. Rep.* 9, 5542 (2019).
26. Zinser, E., Paltauf, F. & Daum, G. Sterol composition of yeast organelle membranes and subcellular distribution of enzymes involved in sterol metabolism. *J. Bacteriol.* 175, 2853–2858 (1993).
27. Ejsing, C. S. *et al.* Global analysis of the yeast lipidome by quantitative shotgun mass spectrometry. *Proc. Natl. Acad. Sci. U. S. A.* 106, 2136–2141 (2009).
28. Dufourc, E. J. Sterols and membrane dynamics. *J. Chem. Biol.* 1, 63–77 (2008).
29. Johnston, E. J., Moses, T. & Rosser, S. J. The wide-ranging phenotypes of ergosterol biosynthesis mutants, and implications for microbial cell factories. *Yeast* 37, 27–44 (2020).
30. Winzeler, E. A. *et al.* Functional characterization of the *S. cerevisiae* genome by gene deletion and parallel analysis. *Science* 285, 901–906 (1999).
31. Guan, X. L. *et al.* Functional interactions between sphingolipids and sterols in biological membranes regulating cell physiology. *Mol. Biol. Cell* 20, 2083–2095 (2009).

32. Galea, A. M. & Brown, A. J. Special relationship between sterols and oxygen: Were sterols an adaptation to aerobic life?. *Free Radic. Biol. Med.* **47**, 880–889 (2009).
33. Jordá, T. & Puig, S. Regulation of ergosterol biosynthesis in *Saccharomyces cerevisiae*. *Genes* **11**, 795 (2020).
34. Shakoury-Elizeh, M. *et al.* Metabolic response to iron deficiency in *Saccharomyces cerevisiae**. *J. Biol. Chem.* **285**, 14823–14833 (2010).
35. Kwast, K. E. *et al.* Genomic analyses of anaerobically induced genes in *Saccharomyces cerevisiae*: Functional roles of Rox1 and other factors in mediating the anoxic response. *J. Bacteriol.* **184**, 250–265 (2002).
36. Philpott, C. C., Protchenko, O., Kim, Y. W., Boretsky, Y. & Shakoury-Elizeh, M. The response to iron deprivation in *Saccharomyces cerevisiae*: Expression of siderophore-based systems of iron uptake. *Biochem. Soc. Trans.* **30**, 698–702 (2002).
37. Jordá, T., Rozès, N. & Puig, S. Sterol composition modulates the response of *Saccharomyces cerevisiae* to iron deficiency. *J. Fungi* **7**, 901 (2021).
38. Parks, L. W. S-ADENOSYLMETHIONINE AND ERGOSTEROL SYNTHESIS1. *J. Am. Chem. Soc.* **80**, 2023–2024 (1958).
39. Shobayashi, M., Mukai, N., Iwashita, K., Hiraga, Y. & Iefuji, H. A new method for isolation of S-adenosylmethionine (SAM)-accumulating yeast. *Appl. Microbiol. Biotechnol.* **69**, 704–710 (2006).
40. Aguilar, P. S. *et al.* Structure of sterol aliphatic chains affects yeast cell shape and cell fusion during mating. *Proc. Natl. Acad. Sci.* **107**, 4170–4175 (2010).
41. Jin, H., McCaffery, J. M. & Grote, E. Ergosterol promotes pheromone signaling and plasma membrane fusion in mating yeast. *J. Cell Biol.* **180**, 813–826 (2008).
42. Vaskovicova, K. *et al.* Plasma membrane protein Nce102 modulates morphology and function of the yeast vacuole. *Biomolecules* **10**, 1476 (2020).
43. Heese-Peck, A. *et al.* Multiple functions of sterols in yeast endocytosis. *Mol. Biol. Cell* **13**, 2664–2680 (2002).
44. Kato, M. & Wickner, W. Ergosterol is required for the Sec18/ATP-dependent priming step of homotypic vacuole fusion. *EMBO J.* **20**, 4035–4040 (2001).
45. Munn, A. L., Heese-Peck, A., Stevenson, B. J., Pichler, H. & Riezman, H. Specific Sterols required for the internalization step of endocytosis in yeast. *Mol. Biol. Cell* **10**, 3943–3957 (1999).
46. Wilson, W. A. *et al.* Regulation of glycogen metabolism in yeast and bacteria. *FEMS Microbiol. Rev.* **34**, 952–985 (2010).
47. François, J. & Parrou, J. L. Reserve carbohydrates metabolism in the yeast *Saccharomyces cerevisiae*. *FEMS Microbiol. Rev.* **25**, 125–145 (2001).
48. Brewster, J. L. & Gustin, M. C. Hog 1: 20 years of discovery and impact. *Sci. Signal.* **7**, re7 (2014).
49. Gasch, A. P. *et al.* Genomic expression programs in the response of yeast cells to environmental changes. *Mol. Biol. Cell* **11**, 4241–4257 (2000).
50. Santt, O. *et al.* The yeast GID complex, a novel ubiquitin ligase (E3) involved in the regulation of carbohydrate metabolism. *Mol. Biol. Cell* **19**, 3323–3333 (2008).
51. Cao, J., Barbosa, J. M., Singh, N. K. & Locy, R. D. GABA shunt mediates thermotolerance in *Saccharomyces cerevisiae* by reducing reactive oxygen production. *Yeast* **30**, 129–144 (2013).
52. Sanz, A. B., García, R., Rodríguez-Peña, J. M. & Arroyo, J. The CWI pathway: Regulation of the transcriptional adaptive response to cell wall stress in yeast. *J. Fungi* **4**, 1 (2018).
53. Chen, R. E. & Thorner, J. Function and regulation in MAPKsignaling pathways: Lessons learned from the yeast *Saccharomyces cerevisiae*. *Biochim. Biophys. Acta BBA Mol. Cell Res.* **1773**, 1311–1340 (2007).
54. Dunayevich, P. *et al.* Heat-stress triggers MAPK crosstalk to turn on the hyperosmotic response pathway. *Sci. Rep.* **8**, 15168 (2018).
55. Yamasaki, A. & Noda, N. N. Structural biology of the Cvt pathway. *J. Mol. Biol.* **429**, 531–542 (2017).
56. Warner, J. R. The economics of ribosome biosynthesis in yeast. *Trends Biochem. Sci.* **24**, 437–440 (1999).
57. Causton, H. C. *et al.* Remodeling of yeast genome expression in response to environmental changes. *Mol. Biol. Cell* **12**, 323–337 (2001).
58. Ho, Y.-H. & Gasch, A. P. Exploiting the yeast stress-activated signaling network to inform on stress biology and disease signaling. *Curr. Genet.* **61**, 503–511 (2015).
59. Vik, Å. & Rine, J. Upc2p and Ecm22p, dual regulators of sterol biosynthesis in *Saccharomyces cerevisiae*. *Mol. Cell Biol.* **21**, 6395–6405 (2001).
60. Davies, B. S. J., Wang, H. S. & Rine, J. Dual activators of the sterol biosynthetic pathway of *Saccharomyces cerevisiae*: Similar activation/regulatory domains but different response mechanisms. *Mol. Cell Biol.* **25**, 7375–7385 (2005).
61. Miettinen, K. *et al.* The TriForC database: A comprehensive up-to-date resource of plant triterpene biosynthesis. *Nucleic Acids Res.* **46**, D586–D594 (2018).
62. Sreij, R., Dargel, C., Moleiro, L. H., Monroy, F. & Hellweg, T. Aescin incorporation and nanodomain formation in DMPC model membranes. *Langmuir* **33**, 12351–12361 (2017).
63. Sreij, R. *et al.* DMPC vesicle structure and dynamics in the presence of low amounts of the saponin aescin. *Phys. Chem. Chem. Phys.* **20**, 9070–9083 (2018).
64. Hahn-Hägerdal, B. *et al.* Role of cultivation media in the development of yeast strains for large scale industrial use. *Microb. Cell Factories* **4**, 31 (2005).
65. Kelly, S. L., Lamb, D. C., Corran, A. J., Baldwin, B. C. & Kelly, D. E. Mode of action and resistance to azole antifungals associated with the formation of 14 alpha-methylergosta-8,24(28)-dien-3 beta,6 alpha-diol. *Biochem. Biophys. Res. Commun.* **207**, 910–915 (1995).
66. Coutinho, A., Silva, L., Fedorov, A. & Prieto, M. Cholesterol and ergosterol influence nystatin surface aggregation: Relation to pore formation. *Biophys. J.* **87**, 3264–3276 (2004).
67. Anderson, T. M. *et al.* Amphotericin forms an extramembranous and fungicidal sterol sponge. *Nat. Chem. Biol.* **10**, 400–406 (2014).
68. Simons, V. *et al.* Dual effects of plant steroidal alkaloids on *Saccharomyces cerevisiae*. *Antimicrob. Agents Chemotherapy* **50**, 2732–2740 (2006).
69. Keukens, E. A. J. *et al.* Dual specificity of sterol-mediated glycoalkaloid induced membrane disruption. *Biochim. Biophys. Acta BBA Biomembr.* **1110**, 127–136 (1992).

Acknowledgements

This work was funded by grants awarded by the Industrial Biotechnology Innovation Centre (IBioIC Project-2016-150) and the Biotechnology and Biological Sciences Research Council (BBSRC Project BB/S017712/1 and IBCatalyst Project No. 102297), and a BBSRC IBioIC Industrial CASE CSV Scholarship with Unilever. RNA sequencing was carried out at the University of Liverpool Centre for Genomic Research. The authors thank Dr Marcus Price (University of Edinburgh) and Prof. Klaus Suhling (King's College London) for comments on the manuscript.

Author contributions

E.J.J.: conceptualisation, investigation, data interpretation, manuscript preparation. J.T.: investigation, data interpretation. E.C.O.: data interpretation. T.M.: investigation, data interpretation, supervision. S.M.: investigation, data interpretation. SH: conceptualisation, data interpretation, supervision. S.J.R.: conceptualisation, data interpretation, supervision.

Competing interests

The authors declare no competing interests.

Additional information

Supplementary Information The online version contains supplementary material available at https://doi.org/10.1038/s41598-023-40308-0.

Correspondence and requests for materials should be addressed to E.J.J. or S.J.R.

Reprints and permissions information is available at www.nature.com/reprints.

Publisher's note Springer Nature remains neutral with regard to jurisdictional claims in published maps and institutional affiliations.

References

Abe, F., & Hiraki, T. (2009). Mechanistic role of ergosterol in membrane rigidity and cycloheximide resistance in *Saccharomyces cerevisiae*. *Biochimica et Biophysica Acta - Biomembranes*, *1788*(3), 743–752. https://doi.org/10.1016/j.bbamem.2008.12.002

Acton, N., & Roth1, R. J. (1992). On the Conversion of Dihydroartemisinic Acid into Artemisinin. In *J. Org. Chem* (Vol. 57). https://pubs.acs.org/sharingguidelines

Adel, M. M., & Sammour E. A. (2012). Effect of Sub-Lethal Dose of Natural Compound of Medicago Sativa (L., Leguminaceae) on the Hind Gut and Fatbody of Spodoptera littoralis (Lepidoptera, Noctuidae). In Journal of Applied Sciences Research, 8(3), 1398-1408.

Adel, M. M., Sehnal, F., & Jurzysta, M. (2000). Effects of alfalfa saponins on the moth Spodoptera littoralis. *Journal of Chemical Ecology*, *26*(4), 1065–1078. https://doi.org/10.1023/A:1005445217004

Agerbirk, N., Olsen, C. E., Bibby, B. M., Frandsen, H. O., Brown, L. D., Nielsen, J. K., Alan, J., & Renwick, A. (2003). A saponin correlated with variable resistance of Barnarea vulgaris to the diamondback moth Plutella xylostella. In *Journal of Chemical Ecology* (Vol. 29, Issue 6).

Aguilar, P. S., Heiman, M. G., Walther, T. C., Engel, A., Schwudke, D., Gushwa, N., Kurzchalia, T., & Walter, P. (2010). Structure of sterol aliphatic chains affects yeast cell shape and cell fusion during mating. *Proceedings of the National Academy of Sciences of the United States of America*, *107*(9), 4170–4175.

Ahmed, S. N., Brown, D. A., & London, E. (1997). *On the Origin of Sphingolipid/Cholesterol-Rich Detergent-Insoluble Cell Membranes: Physiological Concentrations of Cholesterol and Sphingolipid Induce Formation of a Detergent-Insoluble, Liquid-Ordered Lipid Phase in Model Membranes* (Vol. 36). https://pubs.acs.org/sharingguidelines

Alqathama, A., Shao, L., Bader, A., Khondkar, P., Gibbons, S., & Prieto, J. M. (2020). Differential anti-proliferative and anti-migratory activities of ursolic acid, 3-O-

acetylursolic acid and their combination treatments with quercetin on melanoma cells. *Biomolecules*, *10*(6), 1–14. https://doi.org/10.3390/biom10060894

Altmann, K., & Westermann, B. (2005). Role of essential genes in mitochondrial morphogenesis in *Saccharomyces cerevisiae*. *Molecular Biology of the Cell*, *16*(11), 5410–5417. https://doi.org/10.1091/mbc.E05-07-0678

Andre, C. M., Legay, S., Deleruelle, A., Nieuwenhuizen, N., Punter, M., Brendolise, C., Cooney, J. M., Lateur, M., Hausman, J. F., Larondelle, Y., & Laing, W. A. (2016). Multifunctional oxidosqualene cyclases and cytochrome P450 involved in the biosynthesis of apple fruit triterpenic acids. *The New Phytologist*, *211*(4), 1279–1294. https://doi.org/10.1111/nph.13996

Apel, A. R., D'Espaux, L., Wehrs, M., Sachs, D., Li, R. A., Tong, G. J., Garber, M., Nnadi, O., Zhuang, W., Hillson, N. J., Keasling, J. D., & Mukhopadhyay, A. (2017). A Cas9-based toolkit to program gene expression in *Saccharomyces cerevisiae*. *Nucleic Acids Research*, *45*(1), 496–508. https://doi.org/10.1093/nar/gkw1023

Appadurai, D., Gay, L., Moharir, A., Lang, M. J., Duncan, M. C., Schmidt, O., Teis, D., Vu, T. N., Silva, M., Jorgensen, E. M., & Babst, M. (2020). Plasma membrane tension regulates eisosome structure and function. *Molecular Biology of the Cell*, *31*(4), 287–303. https://doi.org/10.1091/mbc.E19-04-0218

Arendt, P., Miettinen, K., Pollier, J., De Rycke, R., Callewaert, N., & Goossens, A. (2017). An endoplasmic reticulum-engineered yeast platform for overproduction of triterpenoids. *Metabolic Engineering*, *40*, 165–175. https://doi.org/10.1016/j.ymben.2017.02.007

Ashour, M., Wink, M., & Gershenzon, J. (2010). Biochemistry of Terpenoids: Monoterpenes, Sesquiterpenes and Diterpenes. In *Biochemistry of Plant Secondary Metabolism: Second Edition* (Vol. 40, pp. 258–303). Wiley Blackwell. https://doi.org/10.1002/9781444320503.ch5

Augustin, J. M., Drok, S., Shinoda, T., Sanmiya, K., Nielsen, J. K., Khakimov, B., Olsen, C. E., Hansen, E. H., Kuzina, V., Ekstrøm, C. T., Hauser, T., & Bak, S. (2012). UDP-glycosyltransferases from the UGT73C subfamily in Barbarea vulgaris catalyse sapogenin 3-O-glucosylation in saponin-mediated insect resistance. *Plant Physiology*, *160*(4), 1881–1895. https://doi.org/10.1104/pp.112.202747

Augustin, J. M., Kuzina, V., Andersen, S. B., & Bak, S. (2011). Molecular activities, biosynthesis and evolution of triterpenoid saponins. In *Phytochemistry* (Vol. 72, Issue 6, pp. 435–457). https://doi.org/10.1016/j.phytochem.2011.01.015

Badenes-Perez, F. R., Gershenzon, J., & Heckel, D. G. (2014). Insect attraction versus plant defense: Young leaves high in glucosinolates stimulate oviposition by a specialist herbivore despite poor larval survival due to high saponin content. *PLoS ONE*, *9*(4). https://doi.org/10.1371/journal.pone.0095766

Baganz F, Hayes A, Marren D, Gardner DC, Oliver SG. Suitability of replacement markers for functional analysis studies in *Saccharomyces cerevisiae*. Yeast. 1997 Dec;13(16):1563-73. doi: 10.1002/(SICI)1097-0061(199712)13:16<1563::AID-YEA240>3.0.CO;2-6. PMID: 9509575.

Bagnat, M. (2000). Lipid rafts function in biosynthetic delivery of proteins to the cell surface in yeast. *Proceedings of the National Academy of Sciences*. https://doi.org/10.1073/pnas.060034697

Bahrami, Y., Franco, C. M. M., & Benkendorff, K. (2016). Acetylated triterpene glycosides and their biological activity from holothuroidea reported in the past six decades. In *Marine Drugs* (Vol. 14, Issue 8). MDPI AG. https://doi.org/10.3390/md14080147

Bak, S., Beisson, F., Bishop, G., Hamberger, B., Höfer, R., Paquette, S., & Werck-Reichhart, D. (2011). Cytochromes P450. *The Arabidopsis Book*, *9*, e0144. https://doi.org/10.1199/tab.0144

Baumann, N. A., Sullivan, D. P., Ohvo-Rekilä, H., Simonot, C., Pottekat, A., Klaassen, Z., Beh, C. T., & Menon, A. K. (2005). Transport of newly synthesized sterol to the sterol-enriched plasma membrane occurs via nonvesicular equilibration. *Biochemistry*, *44*(15), 5816–5826. https://doi.org/10.1021/bi048296z

Bean, T. P., Cools, H. J., Lucas, J. A., Hawkins, N. D., Ward, J. L., Shaw, M. W., & Fraaije, B. A. (2009). Sterol content analysis suggests altered eburicol 14α-demethylase (CYP51) activity in isolates of Mycosphaerella graminicola adapted to azole fungicides. *FEMS Microbiology Letters*, *296*(2), 266–273. https://doi.org/10.1111/j.1574-6968.2009.01645.x

Bhataya, A., Schmidt-Dannert, C., & Lee, P. C. (2009). Metabolic engineering of Pichia pastoris X-33 for lycopene production. *Process Biochemistry*, *44*(10), 1095–1102. https://doi.org/10.1016/j.procbio.2009.05.012

Bhutada, G., Kavšček, M., Hofer, F., Gogg-Fassolter, G., Schweiger, M., Darnhofer, B., Kordiš, D., Birner-Gruenberger, R., & Natter, K. (2018). Characterization of a lipid droplet protein from Yarrowia lipolytica that is required for its oleaginous phenotype. *Biochimica et Biophysica Acta - Molecular and Cell Biology of Lipids*, *1863*(10), 1193–1205. https://doi.org/10.1016/j.bbalip.2018.07.010

Bill, R. M. (2014). Playing catch-up with escherichia coli: Using yeast to increase success rates in recombinant protein production experiments. *Frontiers in Microbiology*, *5*(MAR). https://doi.org/10.3389/fmicb.2014.00085

Bontpart, T., Cheynier, V., Ageorges, A., & Terrier, N. (2015). BAHD or SCPL acyltransferase? What a dilemma for acylation in the world of plant phenolic compounds. In *New Phytologist* (Vol. 208, Issue 3, pp. 695–707). https://doi.org/10.1111/nph.13498

Bordbar, S., Anwar, F., & Saari, N. (2011). High-value components and bioactives from sea cucumbers for functional foods - A review. In *Marine Drugs* (Vol. 9, Issue 10, pp. 1761–1805). MDPI AG. https://doi.org/10.3390/md9101761

Böttger, S., & Melzig, M. F. (2013). The influence of saponins on cell membrane cholesterol. *Bioorganic and Medicinal Chemistry*, *21*(22), 7118–7124. https://doi.org/10.1016/j.bmc.2013.09.008

Bushra, R., & Aslam, N. (2010). An overview of clinical pharmacology of ibuprofen. In *Oman Medical Journal* (Vol. 25, Issue 3, pp. 155–161). Oman Medical Specialty Board. https://doi.org/10.5001/omj.2010.49

Callies, O., & Hernández Daranas, A. (2016). Application of isothermal titration calorimetry as a tool to study natural product interactions. In *Natural Product Reports* (Vol. 33, Issue 7, pp. 881–904). Royal Society of Chemistry. https://doi.org/10.1039/c5np00094g

Caloca, B., Navarro, A., Canales-Torres, M., Le, B., Rosas, C., Sero, Z., & Bachant, J. (2022). Comparison of concanavalin A and poly-l-lysine as cell adhesives for routine

yeast microscopy applications. *Yeast*, *39*(5), 312–322. https://doi.org/10.1002/yea.3686

Cárdenas, P. D., Almeida, A., & Bak, S. (2019). Evolution of Structural Diversity of Triterpenoids. In *Frontiers in Plant Science* (Vol. 10). Frontiers Media S.A. https://doi.org/10.3389/fpls.2019.01523

Cerqueira, N. M. F. S. A., Oliveira, E. F., Gesto, D. S., Santos-Martins, D., Moreira, C., Moorthy, H. N., Ramos, M. J., & Fernandes, P. A. (2016). Cholesterol Biosynthesis: A Mechanistic Overview. *Biochemistry*, *55*(39), 5483–5506. https://doi.org/10.1021/acs.biochem.6b00342

Chan, P. K. (2007). Acylation with diangeloyl groups at C21-22 positions in triterpenoid saponins is essential for cytotoxcity towards tumor cells. *Biochemical Pharmacology*, *73*(3), 341–350. https://doi.org/10.1016/j.bcp.2006.10.007

Cheeke, P. R. (2000). *Actual and potential applications of Yucca schidigera and Quillaja saponaria saponins in human and animal nutrition*. https://academic.oup.com/jas/article/77/suppl_E/1/4625613

Chen, C., Sun, R., Sun, Y., Chen, X., Li, F., Wen, X., Yuan, H., & Chen, D. (2020). Synthesis, biological evaluation and SAR studies of ursolic acid 3β-ester derivatives as novel CETP inhibitors. *Bioorganic and Medicinal Chemistry Letters*, *30*(2), 126824. https://doi.org/10.1016/j.bmcl.2019.126824

Chigurupati, H., Auddy, B., Biyani, M., & Stohs, S. J. (2016). Hepatoprotective Effects of a Proprietary Glycyrrhizin Product during Alcohol Consumption: A Randomized, Double-Blind, Placebo-Controlled, Crossover Study. *Phytotherapy Research*, *30*(12), 1943–1953. https://doi.org/10.1002/ptr.5699

Christensen, L. P. (2008). Chapter 1 Ginsenosides. Chemistry, Biosynthesis, Analysis, and Potential Health Effects. In *Advances in Food and Nutrition Research* (Vol. 55, pp. 1–99). https://doi.org/10.1016/S1043-4526(08)00401-4

Christianson, D. W. (2017). Structural and Chemical Biology of Terpenoid Cyclases. In *Chemical Reviews* (Vol. 117, Issue 17, pp. 11570–11648). American Chemical Society. https://doi.org/10.1021/acs.chemrev.7b00287

Chung, I. M., Lim, J. J., Ahn, M. S., Jeong, H. N., An, T. J., & Kim, S. H. (2016). Comparative phenolic compound profiles and antioxidative activity of the fruit, leaves, and roots of korean ginseng (Panax ginseng meyer) according to cultivation years. *Journal of Ginseng Research*, *40*(1), 68–75. https://doi.org/10.1016/j.jgr.2015.05.006

Chung, S. Y., Seki, H., Fujisawa, Y., Shimoda, Y., Hiraga, S., Nomura, Y., Saito, K., Ishimoto, M., & Muranaka, T. (2020). A cellulose synthase-derived enzyme catalyses 3-O-glucuronosylation in saponin biosynthesis. *Nature Communications*, *11*(1). https://doi.org/10.1038/s41467-020-19399-0

Coccia, M., Collignon, C., Hervé, C., Chalon, A., Welsby, I., Detienne, S., Van Helden, M. J., Dutta, S., Genito, C. J., Waters, N. C., Van Deun, K., Smilde, A. K., Van Den Berg, R. A., Franco, D., Bourguignon, P., Morel, S., Garçon, N., Lambrecht, B. N., Goriely, S., … Didierlaurent, A. M. (2017). Cellular and molecular synergy in AS01-adjuvanted vaccines results in an early IFNγ response promoting vaccine immunogenicity. *Npj Vaccines*, *2*(1). https://doi.org/10.1038/s41541-017-0027-3

Coelho, M. A. Z., Amaral, P. F. F., & Belo, I. (2010). *Yarrowia lipolytica: an industrial workhorse*.

Cohn, J. S., Kamili, A., Wat, E., Chung, R. W. S., & Tandy, S. (2010). Reduction in intestinal cholesterol absorption by various food components: Mechanisms and implications. *Atherosclerosis Supplements*, *11*(1), 45–48. https://doi.org/10.1016/j.atherosclerosissup.2010.04.004

Corey, E. J., Matsuda, S. P. T., & Bartelt, B. (1994). Molecular cloning, characterization, and overexpression of ERG7, the *Saccharomyces cerevisiae* gene encoding lanosterol synthase (sterol biosynthesis/2,3-epoxysqualene/gene cloning). In *Proc. Nati. Acad. Sci. USA* (Vol. 91). https://www.pnas.org

Cravotto, G., Beltramo, L., Sapino, S., Binello, A., & Carlotti, M. E. (2011). A new cyclodextrin-grafted viscose loaded with aescin formulations for a cosmeto-textile approach to chronic venous insufficiency. *Journal of Materials Science: Materials in Medicine*, *22*(10), 2387–2395. https://doi.org/10.1007/s10856-011-4399-z

Crissman, H. A., & Steinkamp, J. A. (1973). Rapid, simultaneous measurement of DNA, protein and cell volume in single cells from large mammalian cell populations.

Croteau, R., Kutchan, T. M., Lewix, N. G. (2000) Biochemistry and molecular biology of plants. Chapter 24 – Natural products (secondary metabolites). American Society of Plant Physiologist.

Czarnotta E, Dianat M, Korf M, Granica F, Merz J, Maury J, Baallal Jacobsen SA, Förster J, Ebert BE, Blank LM. Fermentation and purification strategies for the production of betulinic acid and its lupane-type precursors in *Saccharomyces cerevisiae*. Biotechnol Bioeng. 2017 Nov;114(11):2528-2538. doi: 10.1002/bit.26377. Epub 2017 Aug 17. PMID: 28688186.

Dale, M. P., Moses, T., Johnston, E. J., & Rosser, S. J. (2020). A systematic comparison of triterpenoid biosynthetic enzymes for the production of oleanolic acid in *Saccharomyces cerevisiae*. *PLoS ONE*, *15*(5). https://doi.org/10.1371/journal.pone.0231980

Dargel, C., Geisler, R., Hannappel, Y., Kemker, I., Sewald, N., & Hellweg, T. (2019). Self-assembly of the bio-surfactant aescin in solution: A small-angle x-ray scattering and fluorescence study. *Colloids and Interfaces*, *3*(2). https://doi.org/10.3390/colloids3020047

Davey HM, Hexley P. Red but not dead? Membranes of stressed *Saccharomyces cerevisiae* are permeable to propidium iodide. Environ Microbiol. 2011 Jan;13(1):163-171. doi: 10.1111/j.1462-2920.2010.02317.x. PMID: 21199254.

David Nes, W., Zhou, W., Dennis, A. L., Li, H., Jia, Z., Keith, R. A., Piser, T. M., & Furlong, S. T. (2002). Purification, characterization and catalytic properties of human sterol 8-isomerase. In *Biochem. J* (Vol. 367).

Dequin, S., Gloeckler, R., Herbert, C. J., & Boutelet, F. (1988). *Cloning, sequencing and analysis of the yeast S. uvarum ERGIO gene encoding acetoacetyl CoA thiolase 1" 9*

Ejsing CS, Sampaio JL, Surendranath V, Duchoslav E, Ekroos K, Klemm RW, Simons K, Shevchenko A. Global analysis of the yeast lipidome by quantitative shotgun mass spectrometry. Proc Natl Acad Sci U S A. 2009 Feb 17;106(7):2136-41. doi: 10.1073/pnas.0811700106. Epub 2009 Jan 27. PMID: 19174513; PMCID: PMC2650121.

Di Canito, A., Altomare, A., Fracassetti, D., Messina, N., Tirelli, A., Foschino, R., & Vigentini, I. (2023). The Riboflavin Metabolism in Four *Saccharomyces cerevisiae* Wine Strains: Assessment in Oenological Condition and Potential Implications with the Light-Struck Taste. *Journal of Fungi*, *9*(1). https://doi.org/10.3390/jof9010078

Dixit, V., Tewari, J., & Obendorf, S. K. (2010). Fungal growth inhibition of regenerated cellulose nanofibrous membranes containing quillaja saponin. *Archives of Environmental Contamination and Toxicology*, *59*(3), 417–423. https://doi.org/10.1007/s00244-010-9493-6

Doll, R., Hill, I, D., Hutton, C., Underwood, D, J., Clinical trial of a triterpenoid liquorice compound in gastric and duodenal ulcer, The Lancet, Volume 280, Issue 7260, 1962, Pages 793-796, ISSN 0140-6736, https://doi.org/10.1016/S0140-6736(62)92588-6.

Donald, K. A. G., Hampton, R. Y., & Fritz, I. B. (1997). Effects of overproduction of the catalytic domain of 3-hydroxy-3- methylglutaryl coenzyme A reductase on squalene synthesis in *Saccharomyces cerevisiae*. *Applied and Environmental Microbiology*.

Douglas, L. M., & Konopka, J. B. (2014). Fungal membrane organization: The eisosome concept. In *Annual Review of Microbiology* (Vol. 68, pp. 377–393). Annual Reviews Inc. https://doi.org/10.1146/annurev-micro-091313-103507

Du, X. W., Wills, R. B. H., & Stuart, D. L. (2004). Changes in neutral and malonyl ginsenosides in American ginseng (Panax quinquefolium) during drying, storage and ethanolic extraction. *Food Chemistry*, *86*(2), 155–159. https://doi.org/10.1016/j.foodchem.2003.11.003

Dufourc, E. J. (2008). The role of phytosterols in plant adaptation to temperature. In *Plant Signaling & Behavior* (Vol. 3, Issue 2). www.landesbioscience.com/journals/psb/article/5051

Ershov, P., Kaluzhskiy, L., Mezentsev, Y., Yablokov, E., Gnedenko, O., & Ivanov, A. (2021). Enzymes in the cholesterol synthesis pathway: Interactomics in the cancer context. *Biomedicines*, *9*(8). https://doi.org/10.3390/biomedicines9080895

Farhi M, Marhevka E, Masci T, Marcos E, Eyal Y, Ovadis M, Abeliovich H, Vainstein A. Harnessing yeast subcellular compartments for the production of plant terpenoids.

Metab Eng. 2011 Sep;13(5):474-81. doi: 10.1016/j.ymben.2011.05.001. Epub 2011 May 18. PMID: 21601648.

Farhi, M., Kozin, M., Duchin, S., & Vainstein, A. (2013). Metabolic engineering of plants for artemisinin synthesis. *Biotechnology and Genetic Engineering Reviews*, *29*(2), 135–148. https://doi.org/10.1080/02648725.2013.821283

Farhi, M., Marhevka, E., Masci, T., Marcos, E., Eyal, Y., Ovadis, M., Abeliovich, H., & Vainstein, A. (2011). Harnessing yeast subcellular compartments for the production of plant terpenoids. *Metabolic Engineering*, *13*(5), 474–481. https://doi.org/10.1016/j.ymben.2011.05.001

Fegueur, M., Richard, L., Charles, A. D., & Karst, E. (1991). Isolation and primary structure of the ERG9 gene of *Saccharomyces cerevisiae* encoding squalene synthetase. In *Curr Genet* (Vol. 20).

Feldmann, H. (2012). *Yeast*. Wiley-Blackwell.

Feng, M., Jin, Y., Yang, S., Joachim, A. M., Ning, Y., Mori-Quiroz, L. M., Fromm, J., Perera, C., Zhang, K., Werbovetz, K. A., & Wang, M. Z. (2022). Sterol profiling of Leishmania parasites using a new HPLC-tandem mass spectrometry-based method and antifungal azoles as chemical probes reveals a key intermediate sterol that supports a branched ergosterol biosynthetic pathway. *International Journal for Parasitology: Drugs and Drug Resistance*, *20*, 27–42. https://doi.org/10.1016/j.ijpddr.2022.07.003

Ferracini, C., Curir, P., Dolci, M., Lanzotti, V., & Alma, A. (2010). Aesculus pavia foliar saponins: Defensive role against the leafminer Cameraria ohridella. *Pest Management Science*, *66*(7), 767–772. https://doi.org/10.1002/ps.1940

Firenzuoli, F., & Gori, L. (2007). Herbal medicine today: Clinical and research issues. *Evidence-Based Complementary and Alternative Medicine*, *4*(SUPPL. 1), 37–40. https://doi.org/10.1093/ecam/nem096

Flagfeldt, D. B., Siewers, V., Huang, L., & Nielsen, J. (2009). Characterization of chromosomal integration sites for heterologous gene expression in *Saccharomyces cerevisiae*. *Yeast*, *26*(10), 545–551. https://doi.org/10.1002/yea.1705

Fleck, J. D., Betti, A. H., Pereira da Silva, F., Troian, E. A., Olivaro, C., Ferreira, F., & Verza, S. G. (2019). Saponins from Quillaja saponaria and Quillaja brasiliensis: Particular

chemical characteristics and biological activities. In *Molecules* (Vol. 24, Issue 1). MDPI AG. https://doi.org/10.3390/molecules24010171

Foresti, O., Ruggiano, A., Hannibal-Bach, H. K., Ejsing, C. S., & Carvalho, P. (2013). Sterol homeostasis requires regulated degradation of squalene monooxygenase by the ubiquitin ligase Doa10/Teb4. *ELife*, *2013*(2). https://doi.org/10.7554/eLife.00953

Francis, G., Kerem, Z., Makkar, H. P. S., & Becker, K. (2002). The biological action of saponins in animal systems: a review. *British Journal of Nutrition*, *88*(6), 587–605. https://doi.org/10.1079/bjn2002725

Freeman, E. G., Wisotsky, Z., & Dahanukar, A. (2014). Detection of sweet tastants by a conserved group of insect gustatory receptors. *Proceedings of the National Academy of Sciences of the United States of America*, *111*(4), 1598–1603. https://doi.org/10.1073/pnas.1311724111

Fu, Y., Zhou, E., Wei, Z., Song, X., Liu, Z., Wang, T., Wang, W., Zhang, N., Liu, G., & Yang, Z. (2014). Glycyrrhizin inhibits lipopolysaccharide-induced inflammatory response by reducing TLR4 recruitment into lipid rafts in RAW264.7 cells. *Biochimica et Biophysica Acta - General Subjects*, *1840*(6), 1755–1764. https://doi.org/10.1016/j.bbagen.2014.01.024

Fukushima EO, Seki H, Sawai S, Suzuki M, Ohyama K, Saito K, Muranaka T. Combinatorial biosynthesis of legume natural and rare triterpenoids in engineered yeast. Plant Cell Physiol. 2013 May;54(5):740-9. doi: 10.1093/pcp/pct015. Epub 2013 Jan 31. PMID: 23378447.

Gallelli, L., Cione, E., Wang, T., & Zhang, L. (2021). Glucocorticoid-like activity of escin: A new mechanism for an old drug. In *Drug Design, Development and Therapy* (Vol. 15, pp. 699–704). Dove Medical Press Ltd. https://doi.org/10.2147/DDDT.S297501

Gao, R., Liu, M., Chen, Y., Xia, C., Zhang, H., Xiong, Y., & Huang, S. (2016). Identification and characterization of human UDP-glucuronosyltransferases responsible for the in vitro glucuronidation of ursolic acid. *Drug Metabolism and Pharmacokinetics*, *31*(4), 261–268. https://doi.org/10.1016/j.dmpk.2015.11.010

Gao, S., Tong, Y., Zhu, L., Ge, M., Zhang, Y., Chen, D., Jiang, Y., & Yang, S. (2017). Iterative integration of multiple-copy pathway genes in Yarrowia lipolytica for heterologous β-

carotene production. *Metabolic Engineering*, *41*, 192–201. https://doi.org/10.1016/j.ymben.2017.04.004

Geisler, K., Hughes, R. K., Sainsbury, F., Lomonossoff, G. P., Rejzek, M., Fairhurst, S., Olsen, C. E., Motawia, M. S., Melton, R. E., Hemmings, A. M., Bak, S., & Osbourn, A. (2013). Biochemical analysis of a multifunctional cytochrome P450 (CYP51) enzyme required for synthesis of antimicrobial triterpenes in plants. *Proceedings of the National Academy of Sciences of the United States of America*, *110*(35). https://doi.org/10.1073/pnas.1309157110

Geisler, R., Dargel, C., & Hellweg, T. (2020). The biosurfactant β-aescin: A review on the physico-chemical properties and its interaction with lipid model membranes and langmuir monolayers. In *Molecules* (Vol. 25, Issue 1). MDPI AG. https://doi.org/10.3390/molecules25010117

Ghiulai, R., Roşca, O. J., Antal, D. S., Mioc, M., Mioc, A., Racoviceanu, R., Macaşoi, I., Olariu, T., Dehelean, C., Creţu, O. M., Voicu, M., & Şoica, C. (2020). Tetracyclic and pentacyclic triterpenes with high therapeutic efficiency in wound healing approaches. In *Molecules* (Vol. 25, Issue 23). MDPI AG. https://doi.org/10.3390/molecules25235557

Ghosh, S. (2017). Triterpene structural diversification by plant cytochrome P450 enzymes. *Frontiers in Plant Science*, *8*. https://doi.org/10.3389/fpls.2017.01886

Giaever, G., & Nislow, C. (2014). The yeast deletion collection: A decade of functional genomics. *Genetics*, *197*(2), 451–465. https://doi.org/10.1534/genetics.114.161620

Goodwin, P. H., & Best, M. A. (2023). Ginsenosides and Biotic Stress Responses of Ginseng. In *Plants* (Vol. 12, Issue 5). MDPI. https://doi.org/10.3390/plants12051091

Graebin, C. S. (2018). The Pharmacological Activities of Glycyrrhizinic Acid ("Glycyrrhizin") and Glycyrrhetinic Acid. In *Reference Series in Phytochemistry* (pp. 245–261). Springer Science and Business Media B.V. https://doi.org/10.1007/978-3-319-27027-2_15

Graham, S. E., & Peterson, J. A. (1999). *Minireview: How Similar Are P450s and What Can Their Differences Teach Us? 1*. http://www.idealibrary.com

Grossmann, G., Malinsky, J., Stahlschmidt, W., Loibl, M., Weig-Meckl, I., Frommer, W. B., Opekarová, M., & Tanner, W. (2008). Plasma membrane microdomains regulate turnover of transport proteins in yeast. *Journal of Cell Biology*, *183*(6), 1075–1088. https://doi.org/10.1083/jcb.200806035

Guclu-Ustundag, Ö., & Mazza, G. (2007). Saponins: Properties, applications and processing. *Critical Reviews in Food Science and Nutrition*, *47*(3), 231–258. https://doi.org/10.1080/10408390600698197

Hahn-Hägerdal, B., Karhumaa, K., Larsson, C. U., Gorwa-Grauslund, M., Görgens, J., & van Zyl, W. H. (2005). Role of cultivation media in the development of yeast strains for large scale industrial use. In *Microbial Cell Factories* (Vol. 4). https://doi.org/10.1186/1475-2859-4-31

Hamdane D, Zhang H, Hollenberg P. Oxygen activation by cytochrome P450 monooxygenase. Photosynth Res. 2008 Oct-Dec;98(1-3):657-66. doi: 10.1007/s11120-008-9322-1. Epub 2008 Jul 4. PMID: 18600471; PMCID: PMC2743973.

Hammer, S. K., & Avalos, J. L. (2017). Harnessing yeast organelles for metabolic engineering. *Nature Chemical Biology*, *13*(8), 823–832. https://doi.org/10.1038/nchembio.2429

Hampton, R., Dimster-Denk, D., & Rine, J. (1996). The biology of HMG-CoA reductase: The pros of contra-regulation. *Trends in Biochemical Sciences*, *21*(4), 140–145. https://doi.org/10.1016/S0968-0004(96)80168-X

Harju, S., Fedosyuk, H., & Peterson, K. R. (2004). *Rapid isolation of yeast genomic DNA: Bust n' Grab*. http://www.biomedcentral.com/1472-6750/4/8

He J, Chen Q, Xin P, Yuan J, Ma Y, Wang X, Xu M, Chu J, Peters RJ, Wang G. CYP72A enzymes catalyse 13-hydrolyzation of gibberellins. Nat Plants. 2019 Oct;5(10):1057-1065. doi: 10.1038/s41477-019-0511-z. Epub 2019 Sep 16. Erratum in: Nat Plants. 2019 Oct 3;: PMID: 31527846; PMCID: PMC7194175.

Heese-Peck, A., Pichler, H., Zanolari, B., Watanabe, R., Nther Daum, G., & Riezman, H. (2002). Multiple Functions of Sterols in Yeast Endocytosis. *Molecular Biology of the Cell*, *13*, 2664–2680. https://doi.org/10.1091/mbc.E02-04

Hibbs, J. (2006). Chemistry and Technology of surfactants. Chapter 4 – Anionic surfactants. Blackwell Publishing. 91-132.

Hill, R. A., & Connolly, J. D. (2013). Triterpenoids. In *Natural Product Reports* (Vol. 30, Issue 7, pp. 1028–1065). Royal Society of Chemistry. https://doi.org/10.1039/c3np70032a

Hill, R. A., & Connolly, J. D. (2020). Triterpenoids. In *Natural Product Reports* (Vol. 37, Issue 7, pp. 962–998). Royal Society of Chemistry. https://doi.org/10.1039/c9np00067d

Hillier, S. G., & Lathe, R. (2019). Terpenes, hormones and life: Isoprene rule revisited. In *Journal of Endocrinology* (Vol. 242, Issue 2, pp. R9–R22). BioScientifica Ltd. https://doi.org/10.1530/JOE-19-0084

Holtshausen, L., Chaves, A. V., Beauchemin, K. A., McGinn, S. M., McAllister, T. A., Odongo, N. E., Cheeke, P. R., & Benchaar, C. (2009). Feeding saponin-containing Yucca schidigera and Quillaja saponaria to decrease enteric methane production in dairy cows. *Journal of Dairy Science*, *92*(6), 2809–2821. https://doi.org/10.3168/jds.2008-1843

Honda, T. J., Yelwa, J. M., Amos, C., & Mshelia, A. D. (2019). *Production of bio-base surfactant Saponin from Cissuspopulnea plant leave International Journal of Advanced Chemistry Research Production of bio-base surfactant Saponin from Cissuspopulnea plant leave*. *December*, 3–8.

Hoshino, T. (2017). β-Amyrin biosynthesis: catalytic mechanism and substrate recognition. In *Organic and Biomolecular Chemistry* (Vol. 15, Issue 14, pp. 2869–2891). Royal Society of Chemistry. https://doi.org/10.1039/c7ob00238f

Hoshino, T., Chiba, A., & Abe, N. (2012). Lanosterol biosynthesis: The critical role of the methyl-29 group of 2,3-oxidosqualene for the correct folding of this substrate and for the construction of the five-membered D ring. *Chemistry - A European Journal*, *18*(41), 13108–13116. https://doi.org/10.1002/chem.201201779

Hu, K., Berenjian, S., Larsson, R., Gullbo, J., Nygren, P., Lövgren, T., & Morein, B. (2010). Nanoparticulate Quillaja saponin induces apoptosis in human leukemia cell lines with

a high therapeutic index. In *International Journal of Nanomedicine*. https://www.dovepress.com/

Huang, L., Li, J., Ye, H., Li, C., Wang, H., Liu, B., & Zhang, Y. (2012). Molecular characterization of the pentacyclic triterpenoid biosynthetic pathway in Catharanthus roseus. *Planta*, *236*(5), 1571–1581. https://doi.org/10.1007/s00425-012-1712-0

Hull, C. M., Loveridge, E. J., Rolley, N. J., Donnison, I. S., Kelly, S. L., & Kelly, D. E. (2014). Co-production of ethanol and squalene using a *Saccharomyces cerevisiae* ERG1 (squalene epoxidase) mutant and agro-industrial feedstock. *Biotechnology for Biofuels*, *7*(1). https://doi.org/10.1186/s13068-014-0133-7

Itkin, M., Davidovich-Rikanati, R., Cohen, S., Portnoy, V., Doron-Faigenboim, A., Oren, E., Freilich, S., Tzuri, G., Baranes, N., Shen, S., Petreikov, M., Sertchook, R., Ben-Dor, S., Gottlieb, H., Hernandez, A., Nelson, D. R., Paris, H. S., Tadmor, Y., Burger, Y., … Schaffer, A. (2016). The biosynthetic pathway of the nonsugar, high-intensity sweetener mogroside V from Siraitia grosvenorii. *Proceedings of the National Academy of Sciences of the United States of America*, *113*(47), E7619–E7628. https://doi.org/10.1073/pnas.1604828113

Ivanov,', E. L., Sugawara, N., White, C. I., Fabre, F., & Haberi, J. E. (1994). Mutations in XRS2 and RAD50 Delay but Do Not Prevent Mating-Type Switching in *Saccharomyces cerevisiae*. In *Molecular cell biology*.

Jain, S., Caforio, A., & Driessen, A. J. M. (2014). Biosynthesis of archaeal membrane ether lipids. In *Frontiers in Microbiology* (Vol. 5, Issue NOV). Frontiers Media S.A. https://doi.org/10.3389/fmicb.2014.00641

Jakočiūnas T, Pedersen LE, Lis AV, Jensen MK, Keasling JD. CasPER, a method for directed evolution in genomic contexts using mutagenesis and CRISPR/Cas9. Metab Eng. 2018 Jul;48:288-296. doi: 10.1016/j.ymben.2018.07.001. Epub 2018 Jul 5. PMID: 29981865.

Jandrositz, A., Turnowsky, F., & Hggenauer, C. (1991). The gene encoding squalene epoxidase from *Saccharomyces cerevisiae*: cloning and characterization (Recombinant DNA; terbinafine; sterol biosynthesis; antifungals; ERG1 gene). In *Gene* (Vol. 107).

Jan-Smith, E. (2022). The Biosynthesis of Aescin. Doctoral Thesis. University of East Anglia.

Jennings, S. M., Tsay, Y. H., Fisch, T. M., & Robinson, G. W. (1991). Molecular cloning and characterization of the yeast gene for squalene synthetase (isoprenoid pathway/ergosterol synthesis/cholesterol synthesis/*Saccharomyces cerevisiae*). In *Proc. Natl. Acad. Sci. USA* (Vol. 88). https://www.pnas.org

Jensen, R. H., Astvad, K. M. T., Silva, L. V., Sanglard, D., Jørgensen, R., Nielsen, K. F., Mathiasen, E. G., Doroudian, G., Perlin, D. S., & Arendrup, M. C. (2015). Stepwise emergence of azole, echinocandin and amphotericin B multidrug resistance in vivo in Candida albicans orchestrated by multiple genetic alterations. *Journal of Antimicrobial Chemotherapy*, *70*(9), 2551–2555. https://doi.org/10.1093/jac/dkv140

Jensen-Pergakes K, Guo Z, Giattina M, Sturley SL, Bard M. Transcriptional regulation of the two sterol esterification genes in the yeast *Saccharomyces cerevisiae*. J Bacteriol. 2001 Sep;183(17):4950-7. doi: 10.1128/JB.183.17.4950-4957.2001. PMID: 11489845; PMCID: PMC95368.

Jentsch, J. A., Kiburu, I., Pandey, K., Timme, M., Ramlall, T., Levkau, B., Wu, J., Eliezer, D., Boudker, O., & Menon, A. K. (2018). Structural basis of sterol binding and transport by a yeast StARkin domain. *Journal of Biological Chemistry*, *293*(15), 5522–5531. https://doi.org/10.1074/jbc.RA118.001881

Johnson, C. M. (2021). Protein-Ligand Interactions. Chapter 5 – Isothermal Titration Calorimetry. Human Press. 135-160.

Johnston, E. J., Moses, T., & Rosser, S. J. (2020). The wide-ranging phenotypes of ergosterol biosynthesis mutants, and implications for microbial cell factories. *Yeast*, *37*(1), 27–44. https://doi.org/10.1002/yea.3452

Johnston, E. J., Tallis, J., Cunningham-Oakes, E., Moses, T., Moore, S. J., Hosking, S., & Rosser, S. J. (2023). Yeast lacking the sterol C-5 desaturase Erg3 are tolerant to the anti-inflammatory triterpenoid saponin escin. *Scientific Reports*, *13*(1). https://doi.org/10.1038/s41598-023-40308-0

Jordá, T., & Puig, S. (2020). Regulation of ergosterol biosynthesis in *Saccharomyces cerevisiae*. In *Genes* (Vol. 11, Issue 7, pp. 1–18). MDPI AG. https://doi.org/10.3390/genes11070795

Kaneshiro, E. S., Johnston, L. Q., Nkinin, S. W., Romero, B. I., & Giner, J. L. (2015). Sterols of *Saccharomyces cerevisiae* erg6 knockout mutant expressing the Pneumocystis carinii S-adenosylmethionine:sterol C-24 methyltransferase. *Journal of Eukaryotic Microbiology*, *62*(3), 298–306. https://doi.org/10.1111/jeu.12181

Kar, T., Destain, J., Thonart, P., & Delvigne, F. (2012). Scale-down assessment of the sensitivity of Yarrowia lipolytica to oxygen transfer and foam management in bioreactors: Investigation of the underlying physiological mechanisms. *Journal of Industrial Microbiology and Biotechnology*, *39*(2), 337–346. https://doi.org/10.1007/s10295-011-1030-8

Karbalaei, M., Rezaee, S. A., & Farsiani, H. (2020). Pichia pastoris: A highly successful expression system for optimal synthesis of heterologous proteins. In *Journal of Cellular Physiology* (Vol. 235, Issue 9, pp. 5867–5881). Wiley-Liss Inc. https://doi.org/10.1002/jcp.29583

Karsa, D. (2006). Chemistry and Technology of surfactants. Chapter 1 – What are surfactants? Blackwell Publishing. 1-23.

Katano, H., Okamoto, N., Takakuwa, M., Taira, S., Kambe, T., & Takahashi, M. (2015). Simple and rapid separation of soyasaponin Bb from a soy extract. *Analytical Sciences*, *31*(2), 85–89. https://doi.org/10.2116/analsci.31.85

Kaushik, U., Aeri, V., & Mir, S. R. (2015). Cucurbitacins - An insight into medicinal leads from nature. In *Pharmacognosy Reviews* (Vol. 9, Issue 17, pp. 12–18). Medknow Publications. https://doi.org/10.4103/0973-7847.156314

Kemen, A. C., Honkanen, S., Melton, R. E., Findlay, K. C., Mugford, S. T., Hayashi, K., Haralampidis, K., Rosser, S. J., & Osbourn, A. (2014). Investigation of triterpene synthesis and regulation in oats reveals a role for β-amyrin in determining root epidermal cell patterning. *Proceedings of the National Academy of Sciences of the United States of America*, *111*(23), 8679–8684. https://doi.org/10.1073/pnas.1401553111

Kenny, P., & Wetzel, J. (1995). Letter: Fragmentation studies of ergosterol. The formation of the fragment ion at *m/z* 337. *Eur. Mass Spectrom*, *1*, 411.

Kim JE, Jang IS, Son SH, Ko YJ, Cho BK, Kim SC, Lee JY. Tailoring the *Saccharomyces cerevisiae* endoplasmic reticulum for functional assembly of terpene synthesis pathway. Metab Eng. 2019 Dec;56:50-59. doi: 10.1016/j.ymben.2019.08.013. Epub 2019 Aug 21. PMID: 31445083.

Kim, J. E., Jang, I. S., Son, S. H., Ko, Y. J., Cho, B. K., Kim, S. C., & Lee, J. Y. (2019). Tailoring the *Saccharomyces cerevisiae* endoplasmic reticulum for functional assembly of terpene synthesis pathway. *Metabolic Engineering*, *56*, 50–59. https://doi.org/10.1016/j.ymben.2019.08.013

Kirby J, Romanini DW, Paradise EM, Keasling JD. Engineering triterpene production in *Saccharomyces cerevisiae*-beta-amyrin synthase from Artemisia annua. FEBS J. 2008 Apr;275(8):1852-9. doi: 10.1111/j.1742-4658.2008.06343.x. Epub 2008 Mar 8. PMID: 18336574.

Kirby, J., & Keasling, J. D. (2009). Biosynthesis of plant isoprenoids: Perspectives for microbial engineering. *Annual Review of Plant Biology*, *60*, 335–355. https://doi.org/10.1146/annurev.arplant.043008.091955

Lacaille-Dubois1, M. A., & Wagner2, H. (1996). A review of the biological and pharmacological activities of saponins. In *Phytomedicine* (Vol. 2, Issue 4).

Lambert, E., Faizal, A., & Geelen, D. (2011). Modulation of triterpene saponin production: In vitro cultures, elicitation, and metabolic engineering. *Applied Biochemistry and Biotechnology*, *164*(2), 220–237. https://doi.org/10.1007/s12010-010-9129-3

Lange, B., & Turner, G. W. (2013). Terpenoid biosynthesis in trichomes-current status and future opportunities. In *Plant Biotechnology Journal* (Vol. 11, Issue 1, pp. 2–22). https://doi.org/10.1111/j.1467-7652.2012.00737.x

Larroude, M., Celinska, E., Back, A., Thomas, S., Nicaud, J. M., & Ledesma-Amaro, R. (2018). A synthetic biology approach to transform Yarrowia lipolytica into a competitive biotechnological producer of β-carotene. *Biotechnology and Bioengineering*, *115*(2), 464–472. https://doi.org/10.1002/bit.26473

Le, A., Parks, S., Nguyen, M., & Roach, P. (2018). Optimisation of the Microwave-Assisted Ethanol Extraction of Saponins from Gac (Momordica cochinchinensis Spreng.) Seeds. *Medicines*, *5*(3), 70. https://doi.org/10.3390/medicines5030070

Lee, M. E., DeLoache, W. C., Cervantes, B., & Dueber, J. E. (2015). A Highly Characterized Yeast Toolkit for Modular, Multipart Assembly. *ACS Synthetic Biology*, *4*(9), 975–986. https://doi.org/10.1021/sb500366v

Li Guan, X., Souza, C. M., Pichler, H., Dewhurst, G., Schaad, O., Kajiwara, K., Wakabayashi, H., Ivanova, T., Castillon, G. A., Piccolis, M., Abe, F., Loewith, R., Funato, K., Wenk, M. R., & Riezman, H. (2009). Functional Interactions between Sphingolipids and Sterols in Biological Membranes Regulating Cell Physiology. *Molecular Biology of the Cell*, *20*. https://doi.org/10.1091/mbc.E08

Li J, Zhang Y. Increase of betulinic acid production in *Saccharomyces cerevisiae* by balancing fatty acids and betulinic acid forming pathways. Appl Microbiol Biotechnol. 2014 Apr;98(7):3081-9. doi: 10.1007/s00253-013-5461-1. Epub 2014 Jan 5. PMID: 24389702.

Li, S. P., Lin, Z. X., Jiang, X. Y., & Yu, X. Y. (2018). Exosomal cargo-loading and synthetic exosome-mimics as potential therapeutic tools. In *Acta Pharmacologica Sinica* (Vol. 39, Issue 4, pp. 542–551). Nature Publishing Group. https://doi.org/10.1038/aps.2017.178

Liao, P., Hemmerlin, A., Bach, T. J., & Chye, M. L. (2016). The potential of the mevalonate pathway for enhanced isoprenoid production. In *Biotechnology Advances* (Vol. 34, Issue 5, pp. 697–713). Elsevier Inc. https://doi.org/10.1016/j.biotechadv.2016.03.005

Lichota, A., Gwozdzinski, L., & Gwozdzinski, K. (2019). Therapeutic potential of natural compounds in inflammation and chronic venous insufficiency. In *European Journal of Medicinal Chemistry* (Vol. 176, pp. 68–91). Elsevier Masson SAS. https://doi.org/10.1016/j.ejmech.2019.04.075

Lingwood, D., & Simons, K. (2010). *Lipid Rafts As a Membrane-Organizing Principle*. https://www.science.org

Liu, H. W., Li, J. K., Zhang, D. W., Zhang, J. C., Wang, N. L., Cai, G. P., & Yao, X. S. (2008). Two new steroidal compounds from starfish Asterias amurensis Lutken. *Journal of*

Asian Natural Products Research, *10*(6), 521–529. https://doi.org/10.1080/10286020801966674

Liu, H., Fan, J., Wang, C., Li, C., & Zhou, X. (2019). Enhanced β-Amyrin Synthesis in *Saccharomyces cerevisiae* by Coupling An Optimal Acetyl-CoA Supply Pathway. *Journal of Agricultural and Food Chemistry*, *67*(13), 3723–3732. https://doi.org/10.1021/acs.jafc.9b00653

Liu, J. F., Xia, J. J., Nie, K. L., Wang, F., & Deng, L. (2019). Outline of the biosynthesis and regulation of ergosterol in yeast. In *World Journal of Microbiology and Biotechnology* (Vol. 35, Issue 7). Springer Netherlands. https://doi.org/10.1007/s11274-019-2673-2

Liu, J., Ganapathy, K., Wywial, E., Bujnicki, J. M., Nwogwugwu, C. A., & Nes, W. D. (2011). Effect of substrate features and mutagenesis of active site tyrosine residues on the reaction course catalysed by Trypanosoma brucei sterol C-24-methyltransferase. *Biochemical Journal*, *439*(3), 413–422. https://doi.org/10.1042/BJ20110865

Liu, X. Bin, Liu, M., Tao, X. Y., Zhang, Z. X., Wang, F. Q., & Wei, D. Z. (2015). Metabolic engineering of Pichia pastoris for the production of dammarenediol-II. *Journal of Biotechnology*, *216*, 47–55. https://doi.org/10.1016/j.jbiotec.2015.10.005

Liu, X., Dong, J., Liang, Q., Wang, H. min D., Liu, Z., Xu, R., & Kang, W. (2019b). CoAgulant Effects and Mechanism of Schefflera heptaphylla (L.) Frodin. *Molecules*, *24*(24). https://doi.org/10.3390/molecules24244547

Lorenz, R. T., Rodriguez, R. J., Lewis,' And, T. A., & Parks', L. W. (1986). Characteristics of Sterol Uptake in *Saccharomyces cerevisiae*. In Journal of bacteriology (Vol. 167, Issue 3).

Loreto F, Pinelli P, Manes F, Kollist H. Impact of ozone on monoterpene emissions and evidence for an isoprene-like antioxidant action of monoterpenes emitted by Quercus ilex leaves. Tree Physiol. 2004 Apr;24(4):361-7. doi: 10.1093/treephys/24.4.361. PMID: 14757575.

Lu, Y., Zhu, J., Chen, X., Li, N., Fu, F., He, J., Wang, G., Zhang, L., Zheng, Y., Qiu, Z., Yu, X., Han, D., & Wu, L. (2009). 523 National Natural Science Foundation of China (No. 30472060) and 863 Hi-tech Program of China (No. 2007AA02Z171) 523. In *Drug Metab. Pharmacokinet* (Vol. 24, Issue 6). http://www.jstage.jst.go.jp/browse/dmpk

Ludwiczuk, A., Skalicka-Wozniak, K., & Georgiev, M. I. (2017). Pharacognosy. Fundamentals, Applications and Strategies. Chapter 11 - Terpenoids. Academic Press. 233-266.

Luo, J., Yang, H., & Song, B. L. (2020). Mechanisms and regulation of cholesterol homeostasis. In *Nature Reviews Molecular Cell Biology* (Vol. 21, Issue 4, pp. 225–245). Nature Research. https://doi.org/10.1038/s41580-019-0190-7

Lv, X., Wang, F., Zhou, P., Ye, L., Xie, W., Xu, H., & Yu, H. (2016). Dual regulation of cytoplasmic and mitochondrial acetyl-CoA utilization for improved isoprene production in *Saccharomyces cerevisiae*. *Nature Communications*, *7*. https://doi.org/10.1038/ncomms12851

Lv, Y., Koffas, M., Zhou, J., & Xu, P. (2019). Optimizing oleaginous yeast cell factories for flavonoids and hydroxylated flavonoids biosynthesis. *BioRxiv*. https://doi.org/10.1101/614099

Ma, T., Shi, B., Ye, Z., Li, X., Liu, M., Chen, Y., Xia, J., Nielsen, J., Deng, Z., & Liu, T. (2019). Lipid engineering combined with systematic metabolic engineering of *Saccharomyces cerevisiae* for high-yield production of lycopene. *Metabolic Engineering*, *52*, 134–142. https://doi.org/10.1016/j.ymben.2018.11.009

Mahmood, T., & Yang, P. C. (2012). Western blot: Technique, theory, and trouble shooting. *North American Journal of Medical Sciences*, *4*(9), 429–434. https://doi.org/10.4103/1947-2714.100998

Maicas, S. (2020). The role of yeasts in fermentation processes. In *Microorganisms* (Vol. 8, Issue 8, pp. 1–8). MDPI AG. https://doi.org/10.3390/microorganisms8081142

Malinowska, M. A., Sikora, E., Stalińska, J., Ogonowski, J., & Drukała, J. (2021). The effect of the new lupeol derivatives on human skin cells as potential agents in the treatment of wound healing. *Biomolecules*, *11*(6). https://doi.org/10.3390/biom11060774

Mallory, F. B., Gordon, J. T., & Conner, R. L. (1963). The isolation of a pentacyclic triterpenoid alcohol from a protozoan. In *Journal of the American Chemical Society*. https://doi.org/10.1021/ja00892a042

Maoka, T. (2020). Carotenoids as natural functional pigments. In *Journal of Natural Medicines* (Vol. 74, Issue 1). Springer. https://doi.org/10.1007/s11418-019-01364-x

Marie, C., Leyde, S., & White, T. C. (2008). Cytoplasmic localization of sterol transcription factors Upc2p and Ecm22p in *S. cerevisiae*. *Fungal Genetics and Biology*, *45*(10), 1430–1438. https://doi.org/10.1016/j.fgb.2008.07.004

Martel, C. M., Parker, J. E., Bader, O., Weig, M., Gross, U., Warrilow, A. G. S., Rolley, N., Kelly, D. E., & Kelly, S. L. (2010). Identification and characterization of four azole-resistant erg3 mutants of Candida albicans. *Antimicrobial Agents and Chemotherapy*, *54*(11), 4527–4533. https://doi.org/10.1128/AAC.00348-10

Martn, R. S., & Briones, R. (2000). Quality control of commercial quillaja (Quillaja saponaria Molina) extracts by reverse phase HPLC. *Journal of the Science of Food and Agriculture*, *80*(14), 2063–2068. https://doi.org/10.1002/1097-0010(200011)80:14<2063::AID-JSFA750>3.0.CO;2-2

Mary, W., Crombie, L., Crombie, L., Green, J. B., & Lucas, J. A. (1986). Pathogenicity of “take-all” fungus to oats: its relationship to the concentration and detoxification of the four avenacins. (Vol. 25, Issue 9).

Matthäus, F., Ketelhot, M., Gatter, M., & Barth, G. (2014). Production of lycopene in the non-carotenoid-producing yeast Yarrowia lipolytica. *Applied and Environmental Microbiology*, *80*(5), 1660–1669. https://doi.org/10.1128/AEM.03167-13

Merzendorfer, H., & Heinisch, J. J. (2013). Microcompartments within the yeast plasma membrane. In *Biological Chemistry* (Vol. 394, Issue 2, pp. 189–202). Walter de Gruyter GmbH. https://doi.org/10.1515/hsz-2012-0241

Micich, T. J., Foglia, T. A., & Holsinger, V. H. (1992). Polymer-Supported Saponins: An Approach to Cholesterol Removal from Butteroil. In *J. Agrie. FoodChem* (Vol. 40). https://pubs.acs.org/sharingguidelines

Miettinen, K., Iñigo, S., Kreft, L., Pollier, J., De Bo, C., Botzki, A., Coppens, F., Bak, S., & Goossens, A. (2018). The TriForC database: A comprehensive up-to-date resource of plant triterpene biosynthesis. *Nucleic Acids Research*. https://doi.org/10.1093/nar/gkx925

Milgate, J., & Roberts, D. C. K. (1995). The nutrional and biological significance of saponins. In *Nutrition Research* (Vol. 15, Issue 8).

Milkowski, C., & Strack, D. (2004). Serine carboxypeptidase-like acyltransferases. *Phytochemistry*, *65*(5), 517–524. https://doi.org/10.1016/j.phytochem.2003.12.018

Miziorko, H. M. (2011). Enzymes of the mevalonate pathway of isoprenoid biosynthesis. In *Archives of Biochemistry and Biophysics* (Vol. 505, Issue 2, pp. 131–143). https://doi.org/10.1016/j.abb.2010.09.028

Moretti-Almeida, G., Netto, L. E. S., & Monteiro, G. (2013). The essential gene YMR134W from *Saccharomyces cerevisiae* is important for appropriate mitochondrial iron utilization and the ergosterol biosynthetic pathway. *FEBS Letters*, *587*(18), 3008–3013. https://doi.org/10.1016/j.febslet.2013.07.024

Morrissey, J. P., & Osbourn, A. E. (1999). Fungal Resistance to Plant Antibiotics as a Mechanism of Pathogenesis. In Microbiology and molecular biology reviews (Vol. 63, Issue 3). https://journals.asm.org/journal/mmbr

Moses, T., Papadopoulou, K. K., & Osbourn, A. (2014b). Metabolic and functional diversity of saponins, biosynthetic intermediates and semi-synthetic derivatives. In *Critical Reviews in Biochemistry and Molecular Biology* (Vol. 49, Issue 6, pp. 439–462). Informa Healthcare. https://doi.org/10.3109/10409238.2014.953628

Moses, T., Pollier, J., Almagro, L., Buyst, D., Van Montagu, M., Pedreño, M. A., Martins, J. C., Thevelein, J. M., & Goossens, A. (2014). Combinatorial biosynthesis of sapogenins and saponins in *Saccharomyces cerevisiae* using a C-16α hydroxylase from Bupleurum falcatum. *Proceedings of the National Academy of Sciences of the United States of America*, *111*(4), 1634–1639. https://doi.org/10.1073/pnas.1323369111

Moses, T., Pollier, J., Faizal, A., Apers, S., Pieters, L., Thevelein, J. M., Geelen, D., & Goossens, A. (2015). Unraveling the triterpenoid saponin biosynthesis of the african shrub maesa lanceolata. *Molecular Plant*, *8*(1), 122–135. https://doi.org/10.1016/j.molp.2014.11.004

Moses, T., Pollier, J., Thevelein, J. M., & Goossens, A. (2013). Bioengineering of plant (tri)terpenoids: From metabolic engineering of plants to synthetic biology in vivo and in vitro. In *New Phytologist* (Vol. 200, Issue 1, pp. 27–43). https://doi.org/10.1111/nph.12325

Moses, T., Thevelein, J. M., Goossens, A., & Pollier, J. (2014c). Comparative analysis of CYP93E proteins for improved microbial synthesis of plant triterpenoids. *Phytochemistry*, *108*, 47–56. https://doi.org/10.1016/j.phytochem.2014.10.002

Mosquera, M. E. G., Jimenez, G., Tabernaero, V., Vinueza-Vaca, J., Garcia-Estrasa, C., Kosalkova, K., Sola-Landa, A., Monje, B., Acosta, C., Alonso, R., & Valera, M. A. (2021). Terpenes and terpenoids: building blocks to produce biopolymers. Sustain. Chem. 2, 467-492.

Nagegowda, D. A. (2010). Plant volatile terpenoid metabolism: Biosynthetic genes, transcriptional regulation and subcellular compartmentation. In *FEBS Letters* (Vol. 584, Issue 14, pp. 2965–2973). https://doi.org/10.1016/j.febslet.2010.05.045

Nakayasu, M., Yamazaki, S., Aoki, Y., Yazaki, K., & Sugiyama, A. (2021). Triterpenoid and steroidal saponins differentially influence soil bacterial genera. *Plants*, *10*(10). https://doi.org/10.3390/plants10102189

Nelson, D. R. (2011). Progress in tracing the evolutionary paths of cytochrome P450. *Biochimica et Biophysica Acta - Proteins and Proteomics*, *1814*(1), 14–18. https://doi.org/10.1016/j.bbapap.2010.08.008

Nelson, D. R. (2009). *The Cytochrome P450 Homepage*. http://drnelson.utmem.edu/

Nelson, D., & Werck-Reichhart, D. (2011). A P450-centric view of plant evolution. *Plant Journal*, *66*(1), 194–211. https://doi.org/10.1111/j.1365-313X.2011.04529.x

Nezil, F. A., & Bloom, M. (1992). *Combined influence of cholesterol and synthetic amphiphillic peptides upon bilayer thickness in model membranes*.

Nozzolillo, C., Arnason,', J. T., Campos, F., Donskov, N., & Jurzysta2, M. (1997). Alfalfa leaf saponins and insect resistance. In *Journal of Chemical Ecology* (Vol. 23, Issue 4).

Oka, T., & Jigami, Y. (2006). Reconstruction of de novo pathway for synthesis of UDP-glucuronic acid and UDP-xylose from intrinsic UDP-glucose in *Saccharomyces cerevisiae*. *FEBS Journal*, *273*(12), 2645–2657. https://doi.org/10.1111/j.1742-4658.2006.05281.x

Oleszek, W., Jurzysta, M., Ploszynski, M., Colquhoun, I. J., Price, K. R., & Fenwick8, G. R. (1992). Zahnic Acid Tridesmoside and Other Dominant Saponins from Alfalfa

(Medicago sativa L.) Aerial Parts. In *Food Chem* (Vol. 40). https://pubs.acs.org/sharingguidelines

Osbourn, A., Goss, R. J. M., & Field, R. A. (2011). The saponins-polar isoprenoids with important and diverse biological activities. In *Natural Product Reports* (Vol. 28, Issue 7, pp. 1261–1268). https://doi.org/10.1039/c1np00015b

Oulmouden, A., & Karst, F. (1990). Isolation of the ERGI2 gem of Saccharomyces cerevislae encoding mevalonate kinase (Recombinant DNA; yeast transformation; gene disruption). In *Oene* (Vol. 88).

Owatworakit, A., Townsend, B., Louveau, T., Jenner, H., Rejzek, M., Hughes, R. K., Saalbach, G., Qi, X., Bakht, S., Roy, A. D., Mugford, S. T., Goss, R. J. M., Field, R. A., & Osbourn, A. (2013). Glycosyltransferases from oat (Avena) implicated in the acylation of avenacins. *Journal of Biological Chemistry*, *288*(6), 3696–3704. https://doi.org/10.1074/jbc.M112.426155

Pączkowski, C., & Wojciechowski, Z. A. (1994). Glucosylation and galactosylation of diosgenin and solasodine by soluble glycosyltransferase(s) from Solanum melongena leaves. *Phytochemistry*. https://doi.org/10.1016/S0031-9422(00)86869-7

Paddon CJ, Keasling JD. Semi-synthetic artemisinin: a model for the use of synthetic biology in pharmaceutical development. Nat Rev Microbiol. 2014 May;12(5):355-67. doi: 10.1038/nrmicro3240. Epub 2014 Apr 1. PMID: 24686413.

Paddon, C. J., Westfall, P. J., Pitera, D. J., Benjamin, K., Fisher, K., McPhee, D., Leavell, M. D., Tai, A., Main, A., Eng, D., Polichuk, D. R., Teoh, K. H., Reed, D. W., Treynor, T., Lenihan, J., Jiang, H., Fleck, M., Bajad, S., Dang, G., … Newman, J. D. (2013). High-level semi-synthetic production of the potent antimalarial artemisinin. *Nature*, *496*(7446), 528–532. https://doi.org/10.1038/nature12051

Papadopoulou, K., Melton, R. E., Leggett, M., Daniels, M. J., & Osbourn, A. E. (1999). *Compromised disease resistance in saponin-deficient plants*. www.pnas.org

Park, Y. K., & Ledesma-Amaro, R. (2023). What makes Yarrowia lipolytica well suited for industry? In *Trends in Biotechnology* (Vol. 41, Issue 2, pp. 242–254). Elsevier Ltd. https://doi.org/10.1016/j.tibtech.2022.07.006

Phillips, D. R., Rasbery, J. M., Bartel, B., & Matsuda, S. P. (2006). Biosynthetic diversity in plant triterpene cyclization. In *Current Opinion in Plant Biology* (Vol. 9, Issue 3, pp. 305–314). https://doi.org/10.1016/j.pbi.2006.03.004

Pindado, S., Corriganh, O, I., O'Driscoll, C, M., Carbenoxolone Sodium, Editor(s): Harry G. Brittain, Analytical Profiles of Drug Substances and Excipients, Academic Press, Volume 24, 1996, Pages 1-43, ISSN 1075-6280, ISBN 9780122608247, https://doi.org/10.1016/S0099-5428(08)60690-5.

Pinkwart, K., Schneider, F., Lukoseviciute, M., Sauka-Spengler, T., Lyman, E., Eggeling, C., & Sezgin, E. (2019). Nanoscale dynamics of cholesterol in the cell membrane. *Journal of Biological Chemistry*, *294*(34), 12599–12609. https://doi.org/10.1074/jbc.RA119.009683

Polakowski, T., Bastl, R., Stahl, U., & Lang, C. (1999). *Enhanced sterol-acyl transferase activity promotes sterol accumulation in Saccharomyces cerevisiae*.

Porzoor, A., & Macreadie, I. G. (2015). Exogenous folates stimulate growth and budding of Candida glabrata. *Microbial Cell*, *2*(5), 163–167. https://doi.org/10.15698/mic2015.05.202

Pulendran, B., S. Arunachalam, P., & O'Hagan, D. T. (2021). Emerging concepts in the science of vaccine adjuvants. In *Nature Reviews Drug Discovery* (Vol. 20, Issue 6, pp. 454–475). Nature Research. https://doi.org/10.1038/s41573-021-00163-y

Quinn, P. J. (1985). A Lipid-Phase Separation Model of Low-Temperature Damage to Biological Membranes. In *Cryobiology* (Vol. 22).

Ragupathi, G., Gardner, J. R., Livingston, P. O., & Gin, D. Y. (2011). Natural and synthetic saponin adjuvant QS-21 for vaccines against cancer. In *Expert Review of Vaccines* (Vol. 10, Issue 4, pp. 463–470). https://doi.org/10.1586/erv.11.18

Rehan, M., Shafiullah, & Mir, S. A. (2020). Structural diversity, natural sources, and pharmacological potential of plant-based saponins with special focus on anticancer activity: a review. In *Medicinal Chemistry Research* (Vol. 29, Issue 10, pp. 1707–1722). Springer. https://doi.org/10.1007/s00044-020-02600-w

Ro, D. K., Paradise, E. M., Quellet, M., Fisher, K. J., Newman, K. L., Ndungu, J. M., Ho, K. A., Eachus, R. A., Ham, T. S., Kirby, J., Chang, M. C. Y., Withers, S. T., Shiba, Y.,

Sarpong, R., & Keasling, J. D. (2006). Production of the antimalarial drug precursor artemisinic acid in engineered yeast. *Nature*, *440*(7086), 940–943. https://doi.org/10.1038/nature04640

Roner, M. R., Sprayberry, J., Spinks, M., & Dhanji, S. (2007). Antiviral activity obtained from aqueous extracts of the Chilean soapbark tree (Quillaja saponaria Molina). *Journal of General Virology*, *88*(1), 275–285. https://doi.org/10.1099/vir.0.82321-0

Sáenz, J. P., Grosser, D., Bradley, A. S., Lagny, T. J., Lavrynenko, O., Broda, M., & Simons, K. (2015). Hopanoids as functional analogues of cholesterol in bacterial membranes. *Proceedings of the National Academy of Sciences of the United States of America*, *112*(38), 11971–11976. https://doi.org/10.1073/pnas.1515607112

Siddique, H, R. Saleem, M. Beneficial health effects of lupeol triterpene: A review of preclinical studies, Life Sciences, Volume 88, Issues 7–8, 2011, Pages 285-293, ISSN 0024-3205, https://doi.org/10.1016/j.lfs.2010.11.020.

Saleem, M., Alam, A., Arifin, S., Shah, M, S., Ahmed, B., Sultana, S., Lupeol, a triterpene, inhibits early responses of tumor promotion induced by benzoyl peroxide in murine skin, Pharmacological Research, Volume 43, Issue 2, 2001, Pages 127-134, ISSN 1043-6618, https://doi.org/10.1006/phrs.2000.0710.

Sanglard, D., Ischer, F., Parkinson, T., Falconer, D., & Bille, J. (2003). Candida albicans mutations in the ergosterol biosynthetic pathway and resistance to several antifungal agents. *Antimicrobial Agents and Chemotherapy*, *47*(8), 2404–2412. https://doi.org/10.1128/AAC.47.8.2404-2412.2003

Santivañez-Veliz, M., Moreno-Viguri, E., Pérez-Silanes, S., Varela, J., Cerecetto, H., González, M., & Lizarraga, E. (2017). *Development, validation and application of a GC-MS method for the simultaneous detection and quantification of neutral lipid species in Trypanosoma cruzi*.

Sato T, Yamaga H, Kashima S, Murata Y, Shinada T, Nakano C, Hoshino T. Identification of novel sesterterpene/triterpene synthase from Bacillus clausii. Chembiochem. 2013 May 10;14(7):822-5. doi: 10.1002/cbic.201300035. Epub 2013 Apr 3. PMID: 23554321.

Sato, T., Yoshida, S., Hoshino, H., Tanno, M., Nakajima, M., & Hoshino, T. (2011). Sesquarterpenes (C_{35} Terpenes) Biosynthesized via the Cyclization of a Linear C_{35} Isoprenoid by a Tetraprenyl-β-curcumene Synthase and a Tetraprenyl-β-curcumene Cyclase: Identification of a New Terpene Cyclase. Journal of the American Chemical Society *133* (25), 9734-9737. DOI: 10.1021/ja203779h

Savarino, P., Colson, E., André, J., & Gerbaux, P. (2023). Horse Chestnut Saponins–Escins, Isoescins, Transescins, and Desacylescins. *Molecules*, *28*(5). https://doi.org/10.3390/molecules28052087

Scheibel, J. J. (2004). The evolution of anionic surfactant technology to meet the requirements of the laundry detergent industry. In *Journal of Surfactants and Detergents*. https://doi.org/10.1007/s11743-004-0317-7

Schmitt, C., Grassl, B., Lespes, G., Desbrières, J., Pellerin, V., Reynaud, S., Gigault, J., & Hackley, V. A. (2014). Saponins: A renewable and biodegradable surfactant from its microwave-assisted extraction to the synthesis of monodisperse lattices. *Biomacromolecules*, *15*(3), 856–862. https://doi.org/10.1021/bm401708m

Schwartz, C., Shabbir-Hussain, M., Frogue, K., Blenner, M., & Wheeldon, I. (2017). Standardized Markerless Gene Integration for Pathway Engineering in Yarrowia lipolytica. *ACS Synthetic Biology*, *6*(3), 402–409. https://doi.org/10.1021/acssynbio.6b00285

Seki, H., Sawai, S., Ohyama, K., Mizutani, M., Ohnishi, T., Sudo, H., Fukushima, E. O., Akashi, T., Aoki, T., Saito, K., & Muranaka, T. (2011). Triterpene functional genomics in licorice for identification of CYP72A154 involved in the biosynthesis of glycyrrhizin. *Plant Cell*, *23*(11), 4112–4123. https://doi.org/10.1105/tpc.110.082685

Sen, S., Makkar, H. P. S., Muetzel, S., & Becker, K. (1998). Effect of Quillaja saponaria saponins and Yucca schidigera plant extract on growth of Escherichia coli. In *Letters in Applied Microbiology* (Vol. 27). https://academic.oup.com/lambio/article/27/1/35/6708134

Sezutsu, H., le Goff, G., & Feyereisen, R. (2013). Origins of P450 diversity. *Philosophical Transactions of the Royal Society B: Biological Sciences*, *368*(1612). https://doi.org/10.1098/rstb.2012.0428

Sharkey, T. D., & Yeh, S. (2001). Isoprene emission from plants. In *Annu. Rev. Plant Physiol. Plant Mol. Biol* (Vol. 52). www.annualreviews.org

Sheets ED, Holowka D, Baird B. Membrane organization in immunoglobulin E receptor signaling. Curr Opin Chem Biol. 1999 Feb;3(1):95-9. doi: 10.1016/s1367-5931(99)80017-9. PMID: 10021405.

Shi, W., Wang, Y., Li, J., Zhang, H., & Ding, L. (2007). Investigation of ginsenosides in different parts and ages of Panax ginseng. *Food Chemistry*, *102*(3), 664–668. https://doi.org/10.1016/j.foodchem.2006.05.053

Sim, E. S., Dharmarajan, H., Boorgu, D. S. S. K., Goyal, L., Weinstock, M., Whelan, R., Freiser, M. E., Corcoran, T. E., Jabbour, N., Wang, E., & Chi, D. H. (2021). Novel Use of Vitamin B2 as a Fluorescent Tracer in Aerosol and Droplet Contamination Models in Otolaryngology. *Annals of Otology, Rhinology and Laryngology*, *130*(3), 280–285. https://doi.org/10.1177/0003489420949588

Simons, V., Morrissey, J. P., Latijnhouwers, M., Csukai, M., Cleaver, A., Yarrow, C., & Osbourn, A. (2006). Dual effects of plant steroidal alkaloids on *Saccharomyces cerevisiae*. *Antimicrobial Agents and Chemotherapy*, *50*(8), 2732–2740. https://doi.org/10.1128/AAC.00289-06

Singh, B. (2006). A simple process for obtaining beta-aescin from indiain horse chestnut (Aesulus indica). Patent. EP 1 487 847 B1.

Sirtori, C. R. (2001). Aescin: Pharmacology, pharmacokinetics and therapeutic profile. *Pharmacological Research*, *44*(3), 183–193. https://doi.org/10.1006/phrs.2001.0847

Snopek, P., Nowak, D., Zieniuk, B., & Fabiszewska, A. (2021). Aeration and stirring in yarrowia lipolytica lipase biosynthesis during batch cultures with waste fish oil as a carbon source. *Fermentation*, *7*(2). https://doi.org/10.3390/fermentation7020088

Sokolov, S. S., Vorobeva, M. A., Smirnova, A. I., Smirnova, E. A., Trushina, N. I., Galkina, K. V., Severin, F. F., & Knorre, D. A. (2020). LAM Genes Contribute to Environmental Stress Tolerance but Sensibilize Yeast Cells to Azoles. *Frontiers in Microbiology*, *11*. https://doi.org/10.3389/fmicb.2020.00038

Song, S., Zhu, L., & Zhou, W. (2008). Simultaneous removal of phenanthrene and cadmium from contaminated soils by saponin, a plant-derived biosurfactant. *Environmental Pollution*, *156*(3), 1368–1370. https://doi.org/10.1016/j.envpol.2008.06.018

Spira, F., Mueller, N. S., Beck, G., Von Olshausen, P., Beig, J., & Wedlich-Söldner, R. (2012). Patchwork organization of the yeast plasma membrane into numerous coexisting domains. *Nature Cell Biology*, *14*(6), 640–648. https://doi.org/10.1038/ncb2487

Sprong H, van der Sluijs P, van Meer G. How proteins move lipids and lipids move proteins. Nat Rev Mol Cell Biol. 2001 Jul;2(7):504-13. doi: 10.1038/35080071. Erratum in: Nat Rev Mol Cell Biol 2001 Sep;2(9):698. PMID: 11433364.

Sreij, R., Dargel, C., Schweins, R., Prévost, S., Dattani, R., & Hellweg, T. (2019). Aescin-Cholesterol Complexes in DMPC Model Membranes: A DSC and Temperature-Dependent Scattering Study. *Scientific Reports*, *9*(1). https://doi.org/10.1038/s41598-019-41865-z

Srivastava, V. K., & Yadav, R. (2019). Isothermal titration calorimetry. In *Data Processing Handbook for Complex Biological Data Sources* (pp. 125–137). Elsevier. https://doi.org/10.1016/B978-0-12-816548-5.00009-5

Stella, V. J., & he, Q. (2008). Cyclodextrins. *Toxicologic Pathology*, *36*(1), 30–42. https://doi.org/10.1177/0192623307310945

Stocco, D. M., & Clark, B. J. (1996). Regulation of the Acute Production of Steroids in Steroidogenic Cells*. *Endocrine Reviews*. https://doi.org/10.1210/edrv-17-3-221

Strádalová, V., Stahlschmidt, W., Grossmann, G., Blažíková, M., Rachel, R., Tanner, W., & Malinsky, J. (2009). Furrow-like invaginations of the yeast plasma membrane correspond to membrane compartment of Can1. *Journal of Cell Science*, *122*(16), 2887–2894. https://doi.org/10.1242/jcs.051227

Sun, W., Qin, L., Xue, H., Yu, Y., Ma, Y., Wang, Y., & Li, C. (2019). Novel trends for producing plant triterpenoids in yeast. In *Critical Reviews in Biotechnology* (Vol. 39, Issue 5, pp. 618–632). Taylor and Francis Ltd. https://doi.org/10.1080/07388551.2019.1608503

Sun, X., Wang, W., Wang, K., Yu, X., Liu, J., Zhou, F., Xie, B., & Li, S. (2013). Sterol C-22 desaturase ERG5 mediates the sensitivity to antifungal azoles in neurospora crassa and Fusarium verticillioides. *Frontiers in Microbiology*, *4*(MAY). https://doi.org/10.3389/fmicb.2013.00127

Takase, S., Kera, K., Nagashima, Y., Mannen, K., Hosouchi, T., Shinpo, S., Kawashima, M., Kotake, Y., Yamada, H., Saga, Y., Otaka, J., Araya, H., Kotera, M., Suzuki, H., & Kushiro, T. (2019). Allylic hydroxylation of triterpenoids by a plant cytochrome P450 triggers key chemical transformations that produce a variety of bitter compounds. *Journal of Biological Chemistry*, *294*(49), 18662–18673. https://doi.org/10.1074/jbc.RA119.009944

Tam, K. I., & Roner, M. R. (2011). Characterization of in vivo anti-rotavirus activities of saponin extracts from Quillaja saponaria Molina. *Antiviral Research*, *90*(3), 231–241. https://doi.org/10.1016/j.antiviral.2011.04.004

Tang, Y., Zhao, Z. Z., Feng, T., Li, Z. H., Chen, H. P., & Liu, J. K. (2019). Triterpenes with unusual modifications from the fruiting bodies of the medicinal fungus Irpex lacteus. *Phytochemistry*, *162*, 21–28. https://doi.org/10.1016/j.phytochem.2019.02.017

Taylor, R. F. (1984). Bacterial Triterpenoids. In *Microbiological Reviews* (Vol. 48, Issue 3).

Thimmappa, R., Geisler, K., Louveau, T., O'Maille, P., & Osbourn, A. (2014). Triterpene biosynthesis in plants. In *Annual Review of Plant Biology* (Vol. 65, pp. 225–257). Annual Reviews Inc. https://doi.org/10.1146/annurev-arplant-050312-120229

Tholl, D. (2006). Terpene synthases and the regulation, diversity and biological roles of terpene metabolism. In *Current Opinion in Plant Biology* (Vol. 9, Issue 3, pp. 297–304). https://doi.org/10.1016/j.pbi.2006.03.014

Trombetta D, Castelli F, Sarpietro MG, Venuti V, Cristani M, Daniele C, Saija A, Mazzanti G, Bisignano G. Mechanisms of antibacterial action of three monoterpenes. Antimicrob Agents Chemother. 2005 Jun;49(6):2474-8. doi: 10.1128/AAC.49.6.2474-2478.2005. PMID: 15917549; PMCID: PMC1140516

Turner, E. M. C., (1960). An enzymatic basis for pathogenic specificity. *Nature*. Doi: 10.1038/186325a0

Tsay, Y. H., & Robinson, G. W. (1991). Cloning and Characterization of ERG8 an Essential Gene of *Saccharomyces cerevisiae* That Encodes Phosphomevalonate Kinase . *Molecular and Cellular Biology*, *11*(2), 620–631. https://doi.org/10.1128/mcb.11.2.620-631.1991

Tsyupka, D. V., Mordovina, E. A., Sindeeva, O. A., Sapelkin, A. V., Sukhorukov, G. B., & Goryacheva, I. Y. (2021). High-fluorescent product of folic acid photodegradation: Optical properties and cell effect. *Journal of Photochemistry and Photobiology A: Chemistry*, *407*. https://doi.org/10.1016/j.jphotochem.2020.113045

Welscher YM, Jones L, van Leeuwen MR, Dijksterhuis J, de Kruijff B, Eitzen G, Breukink E. Natamycin inhibits vacuole fusion at the priming phase via a specific interaction with ergosterol. Antimicrob Agents Chemother. 2010 Jun;54(6):2618-25. doi: 10.1128/AAC.01794-09. Epub 2010 Apr 12. PMID: 20385867; PMCID: PMC2876427.

United Nations Framework Convention on Climate Change. (2015). Paris Agreement. https://unfccc.int/documents/184656

V A L S A R A J , ⊥ A N D, | K T. (1997). *Soil Washing Potential of a Natural Surfactant*. https://pubs.acs.org/sharingguidelines

Van Der Rest, M. E., Kamminga, A. H., Nakano, A., Anraku, Y., Poolman, B., & Konings, W. N. (1995). The Plasma Membrane of *Saccharomyces cerevisiae*: Structure, Function, and Biogenesis. In *Microbiological Reviews* (Vol. 59, Issue 2).

Vik, Å., & Rine, J. (2001). Upc2p and Ecm22p, Dual Regulators of Sterol Biosynthesis in *Saccharomyces cerevisiae* . *Molecular and Cellular Biology*, *21*(19), 6395–6405. https://doi.org/10.1128/mcb.21.19.6395-6405.2001

Vincken, J. P., Heng, L., de Groot, A., & Gruppen, H. (2007). Saponins, classification and occurrence in the plant kingdom. In *Phytochemistry* (Vol. 68, Issue 3, pp. 275–297). https://doi.org/10.1016/j.phytochem.2006.10.008

Volkman, J. K. (2005). Sterols and other triterpenoids: Source specificity and evolution of biosynthetic pathways. *Organic Geochemistry*, *36*(2), 139–159. https://doi.org/10.1016/j.orggeochem.2004.06.013

Vongsangnak, W., Gua, J., Chauvatcharin, S., & Zhong, J. J. (2004). Towards efficient extraction of notoginseng saponins from cultured cells of Panax notoginseng.

Biochemical Engineering Journal, *18*(2), 115–120. https://doi.org/10.1016/S1369-703X(03)00197-9

Voshall, A., Christie, N. T. M., Rose, S. L., Khasin, M., Van Etten, J. L., Markham, J. E., Riekhof, W. R., & Nickerson, K. W. (2021). Sterol biosynthesis in four green algae: a bioinformatic analysis of the ergosterol versus phytosterol decision point 1. *J. Phycol*, *57*, 1199–1211. https://doi.org/10.1111/jpy.13164-20-064

Voth, W. P., Richards, J. D., Shaw, J. M., & Stillman, D. J. (2001). Yeast vectors for integration at the HO locus. In *Nucleic Acids Research* (Vol. 29, Issue 12).

Wagner, K. H., & Elmadfa, I. (2003). Biological relevance of terpenoids: Overview focusing on mono-, di- and tetraterpenes. In *Annals of Nutrition and Metabolism* (Vol. 47, Issues 3–4, pp. 95–106). https://doi.org/10.1159/000070030

Wattenberg, B. W., & Silbert, D. F. (1983). Sterol partitioning among intracellular membranes. Testing a model for cellular sterol distribution. *Journal of Biological Chemistry*, *258*(4), 2284–2289. https://doi.org/10.1016/s0021-9258(18)32920-x

Waugh, M. G., Lawson, D., & Hsuan, J. J. (1999). Epidermal growth factor receptor activation is localized within low-buoyant density, non-caveolar membrane domains. In *Biochem. J* (Vol. 337).

Weichert, M., Lichius, A., Priegnitz, B. E., Brandt, U., Gottschalk, J., Nawrath, T., Groenhagen, U., Read, N. D., Schulz, S., & Fleißner, A. (2016). Accumulation of specific sterol precursors targets a MAP kinase cascade mediating cell-cell recognition and fusion. *Proceedings of the National Academy of Sciences of the United States of America*, *113*(42), 11877–11882. https://doi.org/10.1073/pnas.1610527113

Werck-Reichhart, D., & Feyereisen, R. (2011). *Protein family review Cytochromes P450: a success story*. http://genomebiology.com/2000/1/6/reviews/3003.1

Wilkinson, J. A., & Brown, A. M. G. (1999). Horse chestnut - Aesculus hippocastanum: Potential applications in cosmetic skin-care products. *International Journal of Cosmetic Science*, *21*(6), 437–447. https://doi.org/10.1046/j.1467-2494.1999.234192.x

Williams, J. R., & Gong, H. (2007). Biological activities and syntheses of steroidal saponins: The shark-repelling pavoninins. *Lipids*, *42*(1), 77–86. https://doi.org/10.1007/s11745-006-1002-3

Wong, L. H., Gatta, A. T., & Levine, T. P. (2019). Lipid transfer proteins: the lipid commute via shuttles, bridges and tubes. In *Nature Reviews Molecular Cell Biology* (Vol. 20, Issue 2, pp. 85–101). Nature Publishing Group. https://doi.org/10.1038/s41580-018-0071-5

Woods, K., & Höfken, T. (2016). The zinc cluster proteins Upc2 and Ecm22 promote filamentation in *Saccharomyces cerevisiae* by sterol biosynthesis-dependent and -independent pathways. *Molecular Microbiology*, *99*(3), 512–527. https://doi.org/10.1111/mmi.13244

Wu X, Liu L, Zhang M, Wu D, Wang Y, Sun Y, Fawcett JP, Gu J, Zhang J. Simultaneous analysis of isomers of escin saponins in human plasma by liquid chromatography-tandem mass spectrometry: application to a pharmacokinetic study after oral administration. J Chromatogr B Analyt Technol Biomed Life Sci. 2010 Apr 1;878(11-12):861-7. doi: 10.1016/j.jchromb.2010.02.002. Epub 2010 Feb 6. PMID: 20185376.

Wu, J., Lin, L., & Chau, F.-T. (2001). *Ultrasound-assisted extraction of ginseng saponins from ginseng roots and cultured ginseng cells*. www.elsevier.com/locate/ultsonch

Xu, F., Rychnovsky, S. D., Belani, J. D., Hobbs, H. H., Cohen, J. C., & Rawson, R. B. (2005). Dual roles for cholesterol in mammalian cells. *Proceedings of the National Academy of Sciences of the United States of America*, *102*(41), 14551–14556. https://doi.org/10.1073/pnas.0503590102

Yamane, S., Yamaoka, M., Yamamoto, M., Maruki, T., Matsuzaki, H., Hatano, T., & Fukui, S. (1998). Region specificity of chromosome III on gene expression in the yeast *Saccharomyces cerevisiae*. In *J. Gen. Appl. Microbiol* (Vol. 44).

Yan X, Fan Y, Wei W, Wang P, Liu Q, Wei Y, Zhang L, Zhao G, Yue J, Zhou Z. Production of bioactive ginsenoside compound K in metabolically engineered yeast. Cell Res. 2014 Jun;24(6):770-3. doi: 10.1038/cr.2014.28. Epub 2014 Mar 7. PMID: 24603359; PMCID: PMC4042165.

Yang, H., Tong, J., Lee, C. W., Ha, S., Eom, S. H., & Im, Y. J. (2015). Structural mechanism of ergosterol regulation by fungal sterol transcription factor Upc2. *Nature Communications*, *6*. https://doi.org/10.1038/ncomms7129

Yang Y, Wei Y, Guo X, Qi P, Zhu H, Tang W. Glycyrrhetic acid monoglucuronide: sweetness concentration-response and molecular mechanism as a naturally high-potency sweetener. Food Sci Biotechnol. 2019 Feb 6;28(4):1187-1193. doi: 10.1007/s10068-019-00559-y. PMID: 31275719; PMCID: PMC6595034.

Yang, X. W., Zhao, J., Cui, Y. X., Liu, X. H., Ma, C. M., Hattori, M., & Zhang, L. H. (1999). Anti-HIV-1 protease triterpenoid saponins from the seeds of Aesculus chinensis. *Journal of Natural Products*, *62*(11), 1510–1513. https://doi.org/10.1021/np990180u

Yano, R., Takagi, K., Takada, Y., Mukaiyama, K., Tsukamoto, C., Sayama, T., Kaga, A., Anai, T., Sawai, S., Ohyama, K., Saito, K., & Ishimoto, M. (2017). Metabolic switching of astringent and beneficial triterpenoid saponins in soybean is achieved by a loss-of-function mutation in cytochrome P450 72A69. *Plant Journal*, *89*(3), 527–539. https://doi.org/10.1111/tpj.13403

Yasumoto, S., Fukushima, E. O., Seki, H., & Muranaka, T. (2016). Novel triterpene oxidizing activity of Arabidopsis thaliana CYP716A subfamily enzymes. *FEBS Letters*, *590*(4), 533–540. https://doi.org/10.1002/1873-3468.12074

Yu, Z., & Su, P. (2013). Effect of β-aescin extract from Chinese Buckeye Seed on chronic venous insufficiency. *Pharmazie*, *68*(6), 428–430. https://doi.org/10.1691/ph.2013.2886

Yuan J, Ching CB. Mitochondrial acetyl-CoA utilization pathway for terpenoid productions. Metab Eng. 2016 Nov;38:303-309. doi: 10.1016/j.ymben.2016.07.008. Epub 2016 Jul 26. PMID: 27471067.

Zhang, G., Cao, Q., Liu, J., Liu, B., Li, J. and Li, C. (2015), Refactoring β-amyrin synthesis in *Saccharomyces cerevisiae*. AIChE J., 61: 3172-3179. https://doi.org/10.1002/aic.14950

Zhang, J. L., Bai, Q. Y., Peng, Y. Z., Fan, J., Jin, C. C., Cao, Y. X., & Yuan, Y. J. (2020). High production of triterpenoids in Yarrowia lipolytica through manipulation of lipid

components. *Biotechnology for Biofuels*, *13*(1). https://doi.org/10.1186/s13068-020-01773-1

Zhang, N., Fan, Y., Li, C., Wang, Q., Leksawasdi, N., Li, F., & Wang, S. (2018). Cell permeability and nuclear DNA staining by propidium iodide in basidiomycetous yeasts. *Applied Microbiology and Biotechnology*, *102*(9), 4183–4191. https://doi.org/10.1007/s00253-018-8906-8

Zhang, T., Lei, J., Yang, H., Xu, K., Wang, R., & Zhang, Z. (2011). An improved method for whole protein extraction from yeast *Saccharomyces cerevisiae*. *Yeast*, *28*(11), 795–798. https://doi.org/10.1002/yea.1905

Zhang, X., Wang, D., Duan, Y., Zheng, X., Lin, Y., & Liang, S. (2020). Production of lycopene by metabolically engineered Pichia pastoris. *Bioscience, Biotechnology and Biochemistry*, *84*(3), 463–470. https://doi.org/10.1080/09168451.2019.1693250

Zhang, Z., Li, S., & Lian, X.-Y. (2010). An Overview of Genus Aesculus L.: Ethnobotany, Phytochemistry, and Pharmacological Activities. In *Pharmaceutical Crops* (Vol. 1).

Zhao Y, Fan J, Wang C, Feng X, Li C. Enhancing oleanolic acid production in engineered *Saccharomyces cerevisiae*. Bioresour Technol. 2018 Jun;257:339-343. doi: 10.1016/j.biortech.2018.02.096. Epub 2018 Feb 23. PMID: 29526355.

Zhu, C., Tang, P., & Yu, B. (2008). Total synthesis of lobatoside E, A potent antitumor cyclic triterpene saponin. *Journal of the American Chemical Society*, *130*(18), 5872–5873. https://doi.org/10.1021/ja801669r

Zinser, E., Paltauf, F., & Daum, G. (1993). Sterol Composition of Yeast Organelle Membranes and Subcellular Distribution of Enzymes Involved in Sterol Metabolism. In *Journal of Bacteriology* (Vol. 175, Issue 10).

Zweytick, D., Leitner, E., Kohlwein, S. D., Yu, C., Rothblatt, J., & Daum, G. (2000). Contribution of Are1p and Are2p to steryl ester synthesis in the yeast *Saccharomyces cerevisiae*. *European Journal of Biochemistry*, *267*(4), 1075–1082. https://doi.org/10.1046/j.1432-1327.2000.01103.x